



UNIVERSITAT DE
BARCELONA

RANK-RANKL signaling in breast cancer. Therapeutic applications of RANKL inhibition in breast cancer

Marina Ciscar García

ADVERTIMENT. La consulta d'aquesta tesi queda condicionada a l'acceptació de les següents condicions d'ús: La difusió d'aquesta tesi per mitjà del servei TDX (www.tdx.cat) i a través del Dipòsit Digital de la UB (diposit.ub.edu) ha estat autoritzada pels titulars dels drets de propietat intel·lectual únicament per a usos privats emmarcats en activitats d'investigació i docència. No s'autoritza la seva reproducció amb finalitats de lucre ni la seva difusió i posada a disposició des d'un lloc aliè al servei TDX ni al Dipòsit Digital de la UB. No s'autoritza la presentació del seu contingut en una finestra o marc aliè a TDX o al Dipòsit Digital de la UB (framing). Aquesta reserva de drets afecta tant al resum de presentació de la tesi com als seus continguts. En la utilització o cita de parts de la tesi és obligat indicar el nom de la persona autora.

ADVERTENCIA. La consulta de esta tesis queda condicionada a la aceptación de las siguientes condiciones de uso: La difusión de esta tesis por medio del servicio TDR (www.tdx.cat) y a través del Repositorio Digital de la UB (diposit.ub.edu) ha sido autorizada por los titulares de los derechos de propiedad intelectual únicamente para usos privados enmarcados en actividades de investigación y docencia. No se autoriza su reproducción con finalidades de lucro ni su difusión y puesta a disposición desde un sitio ajeno al servicio TDR o al Repositorio Digital de la UB. No se autoriza la presentación de su contenido en una ventana o marco ajeno a TDR o al Repositorio Digital de la UB (framing). Esta reserva de derechos afecta tanto al resumen de presentación de la tesis como a sus contenidos. En la utilización o cita de partes de la tesis es obligado indicar el nombre de la persona autora.

WARNING. On having consulted this thesis you're accepting the following use conditions: Spreading this thesis by the TDX (www.tdx.cat) service and by the UB Digital Repository (diposit.ub.edu) has been authorized by the titular of the intellectual property rights only for private uses placed in investigation and teaching activities. Reproduction with lucrative aims is not authorized nor its spreading and availability from a site foreign to the TDX service or to the UB Digital Repository. Introducing its content in a window or frame foreign to the TDX service or to the UB Digital Repository is not authorized (framing). Those rights affect to the presentation summary of the thesis as well as to its contents. In the using or citation of parts of the thesis it's obliged to indicate the name of the author.



UNIVERSITAT DE
BARCELONA

University of Barcelona

Faculty of Medicine and Health Science

Biomedicine PhD program

“RANK-RANKL signaling in breast cancer. Therapeutic applications of RANKL inhibition in breast cancer”

Doctoral thesis report presented by Marina Císcar García to obtain the title of doctor by University of Barcelona.

Doctoral Thesis performed at:

Institut d'Investigació Biomèdica de Bellvitge (IDIBELL), L'Hospitalet d'Llobregat and Centro Nacional de Investigaciones Oncológicas (CNIO), Madrid.

Thesis director: Eva González Suárez

A blue ink signature of Eva González Suárez, consisting of a large, stylized 'S'.

Thesis tutor: Francesc Ventura Pujol

Signat per Francesc Ventura

PhD candidate: Marina Císcar García

A black ink signature of Marina Císcar García, written in a cursive style.

Signat per Francesc Ventura

MAYO, 2022

*A ti,
que decidiste ir por el lado colorido de la vida.
Te voy a querer siempre.*

INDEX

ACKNOWLEDGMENTS	7
ABBREVIATIONS LIST	10
CLINICAL GLOSSARY	16
INTRODUCTION	18
Breast cancer	19
Definition	19
Incidence	19
Classification	19
- Morphological classification	19
- Histological grading	21
- Pathological stage	22
- ER/PR and HER2 IHC classification	23
- Molecular intrinsic classification	23
- Surrogate molecular classification	26
Hereditary breast cancer.....	27
Treatment	27
- Surgery.....	27
- Radiotherapy	27
- Chemotherapy	28
- Hormonal therapy	28
- Targeted therapy	29
- Immunotherapy.....	29
Impact of menopause	31
RANK-RANKL signaling pathway.....	32
Components	32
- RANK	32
- RANKL	33
- OPG	36
- LGR4.....	37

RANKL reverse signaling.....	37
Bone metabolism.....	38
Immunity.....	39
Mammary gland development.....	40
Breast cancer.....	42
- Models of mammary gland tumorigenesis.....	42
- Clinical breast cancer.....	44
Clinical applications of RANK-RANKL signaling inhibition.....	46
- Anti-RANKL drugs.....	46
- Denosumab: clinical trials.....	48
Patient-derived xenograft (PDXs).....	50
Relevance of PDX models.....	50
Breast cancer PDX models.....	52
OBJECTIVES.....	53
METHODS.....	55
Samples.....	56
Clinical samples: Tissue Microarrays (TMAs) staining and scoring.....	56
PDX samples. Generation.....	57
Cell lines. Lentiviral transduction, infection and culture.....	58
Mouse models.....	59
Genetically modified mouse models and immune-deficient strains.....	59
<i>In vivo</i> treatments.....	59
Tumor analyses.....	60
Tissue collection and processing.....	60
Tissue cell isolation.....	60
<i>In vitro</i> assays.....	60
<i>In vivo</i> assays.....	61
Flow cytometry.....	61
Enzyme-linked immunosorbent assay (ELISA).....	62

Tissue histology and immunostaining	62
Quantitative Reverse Transcription Polymerase Chain Reaction (Q-RT-PCR)...	63
Western Blot	64
RNA sequencing.....	65
Statistical analyses	66
RESULTS.....	67
CHAPTER 1: RANK is an independent biomarker of poor prognosis in estrogen receptor-negative breast cancer and a therapeutic target in patients-derived xenografts	68
1.1. RANK expression in tumor cells associates with ER ⁻ tumors and predicts poor survival in postmenopausal patients	70
1.2. In ER ⁺ BC, RANK expression does not associate with survival and tmRANKL expression associates with younger patients	72
1.3. RANK expression in ER ⁻ tumors associates with poor response to chemotherapy and poor survival in postmenopausal patients	73
1.4. Distinct RANK biology according to ER expression and menopause	75
1.5. RANK is expressed and functional in ER ⁻ BC PDXs	76
1.6. RANK pathway promotes tumor cell proliferation and stemness in ER- BC PDXs	78
1.7. RANKL inhibitors improve the response to docetaxel in ER ⁻ BC PDXs	78
1.8. RANK signaling in BC PDXs regulates pathways involved in cell proliferation, metabolism, stemness, and immunity	80
Supplementary figures	83
Supplementary tables	97
CHAPTER 2: The role of RANKL in Breast Cancer	98
2.1. An intracellular form of RANKL is associated with ER ⁻ BC	99
2.2. RANKL3, unlike RANKL2, is evolutionary conserved, indicating functionality	101
2.3. RANKL3 is confined to the cytoplasm of BC cells	102
2.4. RANKL1 and RANKL3 overexpression in BC do not influence proliferation <i>in vitro</i>	104

2.5. RANKL1 and RANKL3 overexpression promote tumor aggressiveness in immune-deficient mice	106
2.6. Denosumab attenuates the growth of RL1-OE tumors in nude but not in NSG mice	110
2.7. Therapeutic benefit of RANKL inhibition is observed in RANKL1-expressing BC PDX	113
2.8. RL1-OE E0771 cells give rise to tumors with shorter latency and faster tumor growth regardless of the immune system	115
2.9. Non-tumoral RANK promotes the initiation and contributes to the progression of RL1-OE E0771 tumors	118
2.10. The earlier onset and faster growth of RL1-OE E0771 tumors are not affected by RANK-expressing TAMs	118
2.11. RANKL blockade delays the tumor onset of RL1-OE tumors in immune-competent mice.....	120
2.12. The overexpression of RANKL1 and RANKL3 triggers a similar gene expression profile.....	121
Tables.....	127
DISCUSSION	145
CONCLUSIONS	157
REFERENCES	159
LIST OF FIGURES	194
LIST OF TABLES.....	198
APPENDIX	201

Inhibition of RANK signaling in breast cancer induces an anti-tumor immune response orchestrated by CD8⁺ T cells.

RANK signaling increases after anti-HER2 therapy contributing to the emergence of resistance in HER2-positive breast cancer.

ACKNOWLEDGEMENTS

Ha sido un viaje emocionante, agotador, a veces frustrante pero gratificante, muy gratificante. Gracias a todos y cada uno de vosotros por haberme acompañado en esta aventura. Sin vosotros, nada hubiese sido igual.

En primer lugar, gracias, Eva, por abrirme las puertas de tu laboratorio, permitirme conocer a una gran familia de científicos y acabar la tesis en uno de los mejores centros de investigación del mundo. Gracias a esa “Old School” que me acogió desde el minuto cero y a los que llegaron cuando yo ya era una más: Jorge, Guille, Adrián, EvaT, Sandra, Clara, Adriá, Laura, Marta, Joan, Fran, María, Bea, Enrique, Ilaria, Ana, Andrea y Kim. No me olvido de Porfi y Álvaro. GRACIAS a cada uno de vosotros, por enseñarme ciencia de laboratorio (¡y de la vida, en general!), por el sentido del humor que TANTO amenizó los amaneceres duros de FACS, atardeceres y muchos más anocheceres at PEBC6-IDIBELL. Inolvidables (y necesarias) las excursiones extraescolares: esas cimbras que alcanzamos, los aviones que cogimos, movimientos-mochila, clases de gym (o non-gym), bravas y Foster. Mención especial a una científica increíble, mi super griega-catalana Maraki. Gracias por ser un pilar fundamental, dentro y fuera del laboratorio, por los honest-green (que tantas toxinas han eliminado) y por nuestras conversaciones intentando arreglar un poco nuestro mundo.

Gracias a mi familia científica madrileña, que ha tenido que lidiar con los subi-bajones correspondientes a la última etapa de la tesis. Gracias Mía, por cuidarme en todos los sentidos, por tu carisma de mami, tus sugerencias y por estar siempre que te he necesitado (y sin necesitarte, también). Gracias Gema y Patricia, por vuestra infinita paciencia e implicación en todo lo que he necesitado (¡qué sería de este libro sin vosotras!). Sin duda alguna, sois los tres cimientos de nuestra casa. Y qué decir de mis “compañeros de pupitre”: Hembrix, Machi, Jaime, Sergi, Víctor, Josito, Pedro, Teresa, Pablo, Isa, Thelma, de los nuevos fichajes Sara, Angélica y Lucía y de nuestro super limpiador Ángel. Gracias por cada palabra de motivación, por ser tan buenos compañeros y unos científicos acojonantes. Gracias especiales a un equipo espacial: Mía, Gema, Sergi y Víctor. Este trabajo también es vuestro. Solo un buen desayuno ha podido arreglar bonitos amaneceres desde la sala de necropsias. Mención especial también para mi doctor favorito. Gracias Josi por aparecer justo a tiempo y llegar (casi) juntos a la meta surfeando adversidades. No dudes que conseguirás todo lo que te propongas. Yo espero estar muy cerquita para verlo.

Y además de compañeros de trabajo... GRACIAS a mis dos compañeros de vida estos tres años. Honestamente, casi no recuerdo vuestro nombre real... porque para mí sois y seréis Hembrix (Tasia Dearandel Thysencrup Caleruega Amanzorada Mirtuosa) and

Machi (Bambuino II de la Palma del Nevat Kiaudi Somontirirín) forever, como pin y pon, como la dama y el vagabundo, un pack invencible e indestructible. Juntos hemos hecho rico a Amazon, a Glovo, a Uber (tanto en el sector comida como carruaje), a Antonio Rodilla, Gym Yoofit y a MitelePlus. Hemos superado una pandemia y un 2021 aún peor... Pero aquí estamos y ya no hay nada que se nos resista. Sois unos compañeros y amigos excepcionales, en casa, en el trabajo, de vacaciones and repeat. ¡Os quiero!

Gracias también a la pandilla del pueblo por animarme siempre, a mis biomedic-girls por sacarme del bucle del trabajo y a mis máster-friends por entenderme en cada momento. Grazie Alessia, Köszönöm Melinda por aparecer, por quedaros y por estar siempre cerca a pesar de la distancia. ¡¡Nos quedan infinitas aventuras!! Y GRACIAS INMENSAS a mis diamantes, Marti y Lala. Siendo tremenda suerte de teneros porque no ha debido de ser fácil escuchar mis quejas en bucle durante tantos años. Gracias a ambas por cuidarme y animarme siempre con palabras sinceras que curan, alientan y enseñan. Gracias por China, Tailandia, País Vasco, Valladolid, Segovia, Canals o Calasparra. Juntas a cada paso. Os adoro.

Y como no, gracias a ti Ono, por ser mi mensaje positivo cada día, por sacarme carcajadas de las que te duele la barriga, pero, sobre todo, por llenarme la vida de "música". Ya no quiero vivir sin ella.

Y por último, INFINITAS GRACIAS a mi familia, mi clan, mi motor. Gracias abu, por la fuerza que me has dado con tus comidas, pero, sobre todo, con tus palabras de sabia y tus lecciones. Eres la abu más increíble del mundo. Gracias Nancy, por cuidar de ella con tanto amor y ser parte de nuestra familia. Gracias a mis tíos, por darme los mejores primos que una quisiera tener. Y a mi hermana y a mis padres... que lo sois todo para mí. Mana, ahora entiendo cuando la mamá nos decía: no sabéis la suerte que tenéis de teneros. Hace tiempo que lo sé, pero echando la vista atrás, te aseguro que, sin ti, no hubiese podido. Porque ya sabrás bien que el mundo y yo... te queremos de veras, pero yo siempre, un poquito más que el mundo. Mamá y papá, las gracias se me quedan cortas por vuestro apoyo, por ser mi ejemplo, por darme **TODO** y mucho más. Especialmente, gracias por enseñarme a disfrutar del camino y a enfrentarme a las adversidades con la mejor actitud posible (sin dejarnos la salud por el camino). Sois los mejores padres del universo.

Me gustaría dedicar todo el trabajo de estos años a los que están, pero, sobre todo, a los que "no estando" han iluminado mi camino con su luz y su recuerdo, especialmente a mi tía Paqui y a mis super abus Diego y Pepita. Sé que nos volveremos a reencontrar cualquier día de julio comiendo gambas y bebiendo cerveza Estrella Levante. Os adoro.

ABBREVIATIONS LIST

Abbreviation	Definition
5-FU	5-fluorouracil
ABs	Apoptotic bodies
AC	Doxorubicin, cyclophosphamide
ADAM	A disintegrin and metalloprotease
AIs	Aromatase inhibitors
AJCC	American Joint Committee on Cancer
ALDH	aldehyde dehydrogenase
AP1	Activator protein 1
ATCC	American Type Culture Collection
BC	Breast Cancer
BCSS	Breast Cancer-Specific Survival
BM	Bone metastasis
BMD	Bone mineral density
BMFS	Bone metastasis-free survival
BRCA1	Breast Cancer gene 1
BRCA2	Breast Cancer gene 2
BSA	Bovine Serum Albumin
CD40L	CD40 ligand
CIS	Carcinoma in situ
CMF	Cyclophosphamide, methotrexate, 5-FU
CNA	Copy Number Aberrations
CRDs	Cysteine-rich domains
CSCs	Cancer Stem Cells
CSF1	Colony-stimulating factor 1
DCIS	Ductal carcinoma in situ
DCs	Dendritic Cells
DD	Death domain
DFS	Disease-Free Survival
DMFS	Distant Metastasis-Free Survival
DMEM	Dulbecco's modified Eagle's medium
DNS	Denosumab
E1	Estrone
E2	Estradiol
E3	Estriol
EC	Epirubicin, Cyclophosphamide
EGFR	Epidermal growth factor receptor
ELDA	Extreme Limiting Dilution Analysis
ELISA	Enzyme-linked immunosorbent assay
EMT	Epithelial-Mesenchymal transition
ER	Estrogen receptor
ESR1	Estrogen Receptor 1
EVs	Extracellular vesicles
FAC	5-FU, doxorubicin, cyclophosphamide
FBS	Fetal Bovine Serum
FC	Fold Change

FDA	Food and Drug Administration
FDCR-1	Follicular DC-derived receptor-1
FDR	False Discovery Rate
FEC	5-FU, epirubicin, cyclophosphamide
FHL2	Four-and-a-half LIM domain 2
Fig	Figure
G	grade
Gab2	Grb2-associated binding protein 2
GAGs	Glycosaminoglycans
GEP	Gene expression profiling
GFR	Growth Factor Reduced
GPR48	G protein-coupled receptor 48
GSEA	Gene set enrichment analysis
h	Hour
H	H-Score
HER2	Human epidermal growth factor receptor 2
HR	Hormone receptors
HRT	Hormone replacement therapy
IC	Invasive carcinoma
ICC	Invasive cribriform carcinoma
ICO	Catalan Institute of Oncology
icRANKL	RANKL intracellular staining
IDB	IDIBELL dataset
IDC	Invasive ductal carcinoma
IHC	Immunohistochemical
ILC	Invasive lobular carcinoma
IPC	Intracystic papillary carcinoma
ITC	Invasive tubular carcinoma
LCIS	Lobular carcinoma in situ
LDA	Limiting dilution assay
LECs	Luminal epithelial cells
LGR4	Leucin-rich repeats containing G protein-coupled receptor 4
LHRH	Luteinizing Hormone-releasing hormone
LTA	Lymphotoxin alpha
RANK^{LysMΔ/Δ}	LysM-Cre-RANK ^{flox/flox}
MALT	Mucosa-associated tissues
MAPK	Mitogen-activated protein Kinase
MaSCs	Mammary stem cells
MC	Mucinous carcinoma
MECs	Myoepithelial cells
min	Minutes
MMPs	Matrix metalloproteinases
MMTV	Mouse mammary tumor virus
MOc	Mature Osteoclasts
MØs	Macrophages
MPC	Micropapillary carcinoma

NES	Normalized Enrichment Score
NFATc1	Nuclear Factor of activated T cells 1
NF-kB	Nuclear Factor Kappa-B
NHSB	Nottingham Health Science Biobank
NK	Natural Killer
NPI	Nottingham Primary Index
NPS	Nottingham Primary Series
NSG	NOD scid gamma mouse
nude	Athymic nude Foxn1nu
o/n	Overnight
OCIF	Osteoclastogenesis inhibitory factor
ODAR	Osteoclast differentiation and activation receptor
ODF	Osteoclast differentiation factor
OE	Overexpression
OPG	Osteoprotegerin
OPGL	Osteoprotegerin ligand
OS	Overall Survival
p	p-value
PCA	Principal Component Analysis
pCR	pathological complete response
PDXs	Patient-derived xenografts
PFA	Paraformaldehyde
PFS	Progression-free survival
pMØs	Peritoneal macrophages
PR	Progesterone receptor
PTHrP	Parathyroid hormone-related
PyMT	Polyoma middle-T
Q-RT-PCR/qPCR	Quantitative Reverse Transcription Polymerase Chain Reaction
RANK	Receptor activator of nuclear factor kappa-B
RANKL	Receptor activator of nuclear factor kappa-B ligand
RANKL1	RANKL isoform 1
RANKL2	RANKL isoform 2
RANKL3	RANKL isoform 3
RGS10	Regulator of G-protein signaling 10
RL1	RANKL1
RL3	RANKL3
RSPOs	R-spondins
SDFS	Skeletal disease-free survival
SERD	Selective Estrogen Receptor Degradar
SERM	Selective Estrogen Receptor Modulator
SREs	Skeletal-related events
sRANKL	soluble RANKL
TAC	Docetaxel, doxorubicin, cyclophosphamide
TAMs	Tumor-associated macrophages
TANK	TRAF family member-associated NF-kB activator

TC	Docetaxel, cyclophosphamide
TEBs	Terminal End buds
TILs	Tumor-associated lymphocytes
TMA s	Tissue Microarrays
tmRANKL	transmembrane RANKL
TNBC	Triple Negative Breast Cancer
TNF	Tumor Necrosis Factor
TNFR	Tumor Necrosis Factor Receptor
TNFRSF11A	TNFR superfamily member 11A
TNFRSF11B	Tumor necrosis factor receptor superfamily member 11 B
TNFSF11	TNF superfamily member 11
TR1	TNF receptor-like molecule 1
TRAIL	Tumor necrosis factor-related apoptosis-inducing ligand
TRANCE	TNF-related activation-induced cytokine
TRANCE-R	TNF-related activation-induced cytokine receptor
TRAP 5b	Tartrate-resistant acid phosphatase 5b
UICC	Union for International Cancer Control
WHO	World Health Organization
α-RL	anti-murine RANKL

CLINICAL GLOSSARY

The following clinical terms have been obtained from National Cancer Institute (<https://www.cancer.gov/>) and Ontology Search (<https://www.ebi.ac.uk/ols/index>).

Breast Cancer-Specific Survival: Percentage of people who have not died from breast cancer over a certain period after diagnosis.

Bone Metastasis-Free Survival: Time from the start of treatment for cancer that a patient is still alive and cancer has not spread to the bone.

Disease-Free Survival: Time after primary treatment for cancer ends that the patient survives without any signs or symptoms of that cancer.

Distant Metastasis-Free Survival: Time from the start of treatment for cancer to the appearance of distant metastasis. Distant Metastasis refers to cancer that has spread from the primary tumor to distant organs or distant lymph nodes.

Overall Survival: Time from the start of treatment (cancer) that patients diagnosed with the disease are still alive.

Progression-Free Survival: Time from the date of the first diagnosis of cancer and the date of the first documented evidence of disease progression and death.

INTRODUCTION

Breast cancer

Definition

Breast cancer (BC) is a malignant tumor arising from the breast tissue when cells grow out of control. The malignant cells occur in the lining cells (epithelium) of the ducts or lobules in the glandular tissue of the breast (*Breast Cancer Facts and Statistics*, WHO).

Incidence

According to the latest statistics from the World Health Organization (WHO), BC accounts for 10% of all types of cancers (Bray *et al.*, 2018). Female BC is the most commonly diagnosed cancer in 2020, representing 11.7% of all cancer cases, and it is the fifth leading cause of cancer mortality worldwide (6.9%). BC is the leading cause of cancer death among women, accounting for 15.5% of cancer deaths in 2020. The global cancer burden is expected to increase by more than 47% by 2040, according to the GLOBOCAN Cancer prediction tool (Bray *et al.*, 2018; Sung *et al.*, 2021).

Over the recent years, the BC incidence rate has been rising in most countries, being higher in developed countries compared to less developed countries. This fact reflects the degree of economic growth and social and lifestyle components that have an essential impact on the prevalence of risk factors, including, for example, the delay of motherhood ('Health Effects of Overweight and Obesity in 195 Countries over 25 Years', 2017; Park *et al.*, 2021). In contrast, the BC death rate continues to decline due to the introduction of population-based screening using early-detection techniques, the systemic use of adjuvant therapies, and regular physical activity (Rossouw *et al.*, 2002a; Ravdin *et al.*, 2007; Oberaigner *et al.*, 2010; Youlden *et al.*, 2012; Bray *et al.*, 2018; DeSantis *et al.*, 2019).

Classification

To carry out the assessment of diagnosis and prognosis and to facilitate treatment decisions for patients, different classifications of BC have become necessary:

Morphological classification. BC can be divided into carcinoma, adenocarcinoma, and sarcoma, depending on the cell of origin. **Carcinomas** are tumors developed from breast epithelial cells, **adenocarcinomas** arise out of glandular epithelial cells, and **sarcomas** can be originated from muscle cells, fat or connective tissue located in the breast supporting the ducts and lobules.

Attending to the expansion of the tumor, BC can be broadly categorized as *in situ* (CIS) or **invasive** (IC). Breast carcinoma *in situ* is formed by abnormal epithelial cells entirely confined within breast ducts and lobules. Moreover, this type of carcinoma is sub-classified as ductal (DCIS, originated in breast ductal cells) or lobular (LCIS, originated in breast lobular or alveolar cells). While LCIS tumors have low histological variation, DCIS is more common and encompasses a heterogeneous tumor group. Breast invasive carcinoma is a heterogeneous group of epithelial tumors characterized by the rupture of the lobule where they began, invasion of adjacent tissues, and a high tendency to metastasize to distant organs. These tumors are divided into histological subtypes (Table 1) (*Breast Disease: Diagnosis and Pathology*).

Frequency	Description
80%	Invasive ductal carcinoma (IDC) starts growing in a milk duct and invades the fibrous or fatty tissue of the breast outside of the duct.
5-10%	Invasive lobular carcinoma (ILC) starts in the breast's milk-producing lobules. It is a carcinoma composed of non-cohesive cells that are individually dispersed in a single-file linear pattern in a fibrous stroma.
1-4%	Invasive tubular carcinoma (ITC) is a subtype of IDC. ITCs are usually small, well-differentiated, and made up of tubule-shaped structures called "tubules". They have an excellent prognosis.
3-5%	Mucinous carcinoma (MC) is a subtype of IDC. They are well-circumscribed carcinomas composed of poorly differentiated cells without glandular structures, scant stroma, and prominent lymphoid infiltration.
1-6%	Invasive cribriform carcinoma (ICC) is a subtype of IDC. Cancer cells invade the stroma in nest-like formations between the ducts and lobules in this subtype. ICCs are usually low-grade tumors.
2-3%	Micropapillary carcinoma (MPC) is a subtype of IDC. The tumor cells are arranged in micropapillary or tubule-alveolar clusters surrounded by lacunae or clear space. Due to its lymphotropic nature, MPC carries an unfavorable prognosis.
1-2%	Intracystic papillary carcinoma (IPC) is a subtype of IDC. These tumors have a well-defined border and are composed of small, finger-like projections. This is an excellent prognosis BC.

0.1%	Neuroendocrine carcinomas are defined by the expression of neuroendocrine markers along with the presence of morphological neuroendocrine characteristics. These tumors are generally low-grade with a favorable prognosis.
1%	Apocrine carcinoma is a rare subtype of IDC. Tumors are constituted by the cytological and immunohistochemical features of the apocrine cells in more than 90% of the tumor cells.
1%	Metaplastic carcinomas are adenocarcinomas with areas of spindle cells, squamous cells, and/or mesenchymal differentiation. Fusiform cells and squamous cells may also appear without any variety of adenocarcinoma. These tumor cells are often found to be high grade, which means that they look very different from normal cells and are dividing rapidly.

Table 1. Main subtypes of invasive breast carcinomas.

Other rare types of breast tumors are Paget's disease and inflammatory BC. In Paget's disease (1-5%), cancer starts in the ducts of the nipple and then extends to the nipple surface, the areola, and other areas of the breast. The nipple and areola often become scaly, red, itchy, and irritated. Inflammatory BC (1%) is a very aggressive form of BC. These tumors start with the reddening and swelling of the breast and grow and spread quickly (*Paget Disease of the Breast - National Cancer Institute; Types of Breast Cancer - National Breast Cancer Foundation*).

Histological grading. Currently, it is well known that BC is a disease with high intra-tumoral and inter-tumoral heterogeneity. Therefore, pathologists have attempted to develop new grading systems to allow clinicians to monitor their patients better. The histological grade is reported using the "Blood-Richardson-Elston Scale" (also called "Nottingham Histologic Score System"). It describes the degree of differentiation, which reflects the resemblance of tumor cells to normal breast cells by the evaluation of the degree of tumor differentiation (tubule formation), nuclear pleomorphism (nuclear size and shape), and proliferation (mitosis rate).

- Tubule formation: Percentage of cancer composed of tubular structures.
- Nuclear pleomorphism: Degree of variation (size and shape) of the nucleus of tumor cells.
- Mitotic rate: Rate of cell division.

Each of these features is assigned a score ranging from 1 to 3; the values are summated, resulting in a total score of between 3 and 9, and then categorized into a final grade (G). Scores 3-5 represent G1 (well-differentiated tumors, good prognosis), scores 6-7 represent G2 (moderately differentiated, intermediate prognosis), and scores 8-9 represent G3 (poorly differentiated, poor prognosis) (van Dooijeweert, van Diest and Ellis, 2021).

Pathological stage. The most common tool for staging BC is the TNM staging system published by the American Joint Committee on Cancer (AJCC) and the Union for International Cancer Control (UICC). This system provides information about the extent of cancer at the primary site (**T**umor), at the regional lymph nodes (**N**odes), and distant metastatic sites (**M**etastases):

- **Tumor** (T: T0, T1, T2, T3, T4). It refers to the size and location of the primary tumor. Higher T numbers mean a larger tumor and/or broader spread to nearby tissues. T0 means no evidence of cancer in the breast. **T1** means the cancer is 20 millimeters (mm) or smaller. **T2** means the tumor is larger than 20 mm but smaller than 50 mm. **T3** means the tumor is larger than 50 mm. **T4** means the tumor has grown into the chest wall, into the skin, into the wall and the skin, or it is inflammatory BC.
- **Nodes** (N: N0, N1, N2, or N3). It stands for spread to nearby lymph nodes and, if so, how many lymph nodes are affected. Higher numbers after the N indicate more affected nodes.
- **Metastasis** (M: M0, M1). It describes the spreading of tumor cells to distant parts of the body.

The **stage** of the cancer is assigned by combining the T, N, and M classifications, the tumor grade, and the results of estrogen receptor (ER), progesterone receptor (PR), and human epidermal growth factor receptor 2 (HER2) test. The stage defines the prognosis of cancer. There are five stages (stages 0-IV) where stage I to stage IIA is referred to as “early-stage” while stage IIB to stage III is referred to as “locally advanced”.

- **Stage 0 (Tis, N0, M0):** The tumor is located in the ducts of the breast tissue, and it has not spread to the surrounding tissue.
- **Stage IA (T1, N0, M0):** The tumor is small and invasive but has not spread to the lymph nodes.
- **Stage IB (T0/T1, N1, M0):** The cancer cells have spread to the lymph nodes, but the size is less than 2 mm in size.

- Stage IIA (T0/T1/T2, N1, M0): The tumor is 20 mm or smaller and it has spread to 1 to 3 axillary lymph nodes, or the tumor is larger than 20 mm but smaller than 50 mm, and it has not spread to the axillary lymph nodes.
- Stage IIB (T2/T3, N0/N1, M0): The tumor is smaller than 50 mm and has spread to 1 to 3 axillary lymph nodes, or the tumor is larger than 50 mm but is not spread to the axillary lymph nodes.
- Stage IIIA (T0/T1/T2/T3, N1/N2, M0): The tumor is larger than 50 mm, and it has spread to 1 to 3 axillary lymph nodes or 4 to 9 axillary or internal mammary lymph nodes.
- Stage IIIB (T4, N0/N1/N2, M0): The cancer cells have spread to 9 axillary or internal mammary lymph nodes, chest wall, or caused swelling or ulceration (including inflammatory BC).
- Stage IIIC (any T, N3, M0): When the tumor, of any size, has spread to 10 or more axillary, mammary, and under collarbone lymph nodes.
- Stage IV or metastatic (any T, any N, M1): Cancer has spread to other organs.

ER/PR and HER2 Immunohistochemical (IHC) classification. Information about ER, PR, and HER2 is routinely available in breast cancer specimens, inexpensive, and useful for therapeutic decision making. Clinicians still rely on these pathological tumor markers, and based on them, four subgroups have been described (Onitilo *et al.*; Parise and Caggiano, 2014):

- **Luminal-HER2⁺ subtype: ER/PR⁺, HER2⁺** (ER⁺/PR⁺, HER2⁺; ER⁺/PR⁻, HER2⁺).
- **Luminal subtype: ER/PR⁺, HER2⁻** (ER⁺/PR⁺, HER2⁻; ER⁺/PR⁻, HER2⁻).
- **HER2⁺ subtype: ER/PR⁻, HER2⁺** (ER⁻/PR⁻, HER2⁺).
- **Triple Negative BC subtype (TNBC): ER/PR⁻, HER2⁻** (ER⁻/PR⁻, HER2⁻).

Molecular intrinsic classification. In the last two decades, significant efforts to complement the morphological type of BC with molecular parameters have been made. Gene expression profiling (GEP) has given us insight into the molecular complexity of breast tumors and their evolution, improving the strategies for generating the prognosis. Many different GEP tests have been developed; however, they are only applicable to clinically defined subgroups of BCs (Azim *et al.*, 2013). Molecular subtyping may be helpful to understand underlying factors specific to biological pathways and how behavioral and lifestyle risk factors differ by molecular subgroup. Studies conducted by Sørлие *et al.* demonstrated that BC presents a distinctive “molecular portrait”, according to which tumors can be classified into five intrinsic subtypes with different clinical outcomes (Perou *et al.*, 2000; Sørлие *et al.*, 2001; Bernard *et al.*, 2009a).

- **Luminal tumors.** They are the most common type of BC (60-80% of all tumors), characterized by the genetic expression of hormone receptors (HR). The name “luminal” is relative to the similarity between genes expressed by these tumors and those expressed by luminal epithelial cells of the breast (Perou *et al.*, 2000). The luminal subtype is divided into two groups (Sørlie *et al.*, 2001, 2003; Sørlie, 2004) based on gene expression patterns and clinical prognosis differences: Luminal A tumors (40% of all tumors) and luminal B tumors (20% of all tumors). Compared with the luminal B subtype, luminal A tumors show higher expression of *ESR1* (*Estrogen Receptor 1*), *GATA3*, *HNF3α*, *PIK3CA*, and *MAP3K1*. Luminal B tumors are less well-differentiated and typically of higher grade (Vuong *et al.*, 2014). Moreover, these tumors show higher expression of proliferative or cell-cycle genes such as *MKI67*, *FOXA1*, and *ESR1* (the latter is similarly expressed in luminal A) and lower expression of *PR* (progesterone receptor) (Prat *et al.*, 2015). Luminal B tumors, unlike luminal A, are associated with a high frequency of p53 mutations (Tang and Tse, 2016). Related to the clinical course, patients with luminal B tumors have significantly shorter overall survival (OS) and disease-free survival (DFS) compared to patients with luminal A adenocarcinomas. Luminal A tumors have the best prognosis within all the BC subtypes (Sørlie *et al.*, 2003; Sørlie, 2004; Loi, 2008).
- **Human epidermal growth factor receptor 2 (HER2)-enriched tumors** (12-20% of all tumors). They are characterized by amplification and overexpression of HER2/neu pathway genes (*HER2* and *GRB7*), intermediate levels of luminal genes (*ESR1* and *PGR*), and low expression of basal genes (*KRT5* and *FOXC1*) (Perou *et al.*, 2000; Prat *et al.*, 2015). *HER2* gene encodes a transmembrane tyrosine kinase receptor that binds to its extracellular signal triggering a cascade that mediates cell proliferation, differentiation, and survival. Moreover, it is a well-known prognostic marker of BC associated with aggressive tumor growth and poorer clinical outcomes than luminal cancers (Sørlie *et al.*, 2001, 2003; Tang and Tse, 2016).
- **Basal tumors** (15% of all tumors). They express many of the same genes found in the basal myoepithelial cells, including *KRT5*, *KRT14*, and *KRT17*, and show high expression of proliferation-related genes (*MKI67*) and mutations of *TP53* and *PIK3CA* genes. They fail to express *ESR1* and associated genes (Perou *et al.*, 2000; Sørlie *et al.*, 2001, 2003; Sørlie, 2004; Tang and Tse, 2016). Basal-like BCs are frequently high-grade, large, and have a high rate of local and distant recurrence (Tang and Tse, 2016). The basal-like subtype represents 70-80% of all TNBC (Prat *et al.*, 2015; Tang and Tse, 2016). TNBC has been subdivided into six different subgroups: *basal-like 1*

(loss of cell-cycle checkpoint genes, increase in proliferation pathways, and DNA damage response genes); *basal-like 2* (enriched in growth factor-, glycolysis- and gluconeogenesis-related genes); *immunomodulatory* (enriched in genes associated with immune cell processes); *luminal androgen receptor* (enriched in hormonally-regulated pathways, including steroid synthesis, porphyrin metabolism and androgen/estrogen metabolism); *mesenchymal* (enriched in pathways involved in cell motility and cell differentiation pathways) and *mesenchymal stem-like* (similar to mesenchymal subtype but they are also enriched in genes representing processes linked to growth factor signaling pathways, angiogenesis, and immune signaling) (Lehmann *et al.*, 2011; Wang *et al.*, 2019). Basal-like BC shares the fewest similarities with the other groups and has the most extraordinary intrinsic diversity. These patients have a poor prognosis, and almost 40% of them experience a relapse within five years after diagnosis (*Molecular Subtypes of Breast Cancer: A Review for Breast Radiologists* Karen S. Johnson, MD,1, * Emily F. Conant, MD,2 Mary Scott Soo, MD; Fulford *et al.*, 2007).

- **Claudin-low** (2-14% of all tumors). These tumors are characterized by the low expression of critical cell-cell adhesion molecules, high expression of epithelial-mesenchymal transition (EMT) genes, and stem cell-like differentiated gene expression patterns. Claudin-low tumors have marked immune and stromal cell infiltration (Prat *et al.*, 2010; Dias *et al.*, 2017). They have greater variation in mutational burden and copy number aberrations (CNA) than in other subtypes (Fougner *et al.*, 2019). Claudin-low breast tumors are reported to be mostly ER⁻, PR⁻ and HER2⁻ and are associated with poor prognosis (Prat *et al.*, 2010).
- **Normal-like** (5-8% of all tumors). Some studies have questioned the existence of this subtype based on the small number of breast tumors that fall into the normal-like subtype (Smid *et al.*, 2008; Prat and Perou, 2011). These tumors represent samples with low tumor cell content and more normal tissue components (Eliyatkin *et al.*, 2015). They are defined by the expression of many genes expressed in adipose tissue and other types of non-epithelial cells. Additionally, they show high levels of basal genes and low luminal genes (Sørliie *et al.*, 2001). Patients harboring these tumors present an intermediate clinical prognosis.

In the last two decades, many different GEP tests have been developed. However, there is controversy about the value that such assays add to clinic-pathological characteristics and patients' treatment decisions (Azim *et al.*, 2013). The following Table 2 shows some

of the most representative BC genomic tests (*Prosigna Breast Cancer Prognostic Gene Signature Assay* | *Breastcancer.org*; Bernard *et al.*, 2009b; Pourteimoor, Mohammadi-Yeganeh and Paryan, 2016):

Genomic test	Risk measurement	Patient requirements
PAM50	Distant recurrence	Postmenopausal women, early-stage, HR ⁺ disease with up to three positive lymph nodes after five years of hormonal therapy treatment.
Oncotype DX Breast Recurrence Score Test	Distant recurrence Benefit from chemotherapy	Early-stage, HR ⁺ , HER2 ⁻ BC.
MammaPrint	Recurrence within ten years	Patients with stage I or stage II HR ⁺ or HR ⁻ .
EndoPredict	Distant recurrence	Early-stage, HR ⁺ , HER2 ⁻ BC with node-negative or up to three positive lymph nodes.

Table 2. Representative BC genomic tests.

Surrogate molecular classification. Gene expression profiles are difficult to integrate into daily clinical practice due to the high economic cost. For that, a surrogate molecular classification has been elaborated based on immune-histochemical studies (based on the expression of ER, PR, HER2, and the proliferation marker Ki-67) applied routinely in managing tumor samples in the clinic. (Lundgren *et al.*, 2019; Gómez-Acebo *et al.*, 2021). Table 3 shows the main surrogate molecular subtypes (Gomes Do Nascimento and Otoni, 2020):

Subtype	ER	PR	HER2	Ki67	Histological grade	Clinical Prognosis	Frequency
Luminal A-like	+	+	-	Low	Well-differentiated	Good	40-50%
Luminal B-like HER2⁻	+	-	-	High	Moderately differentiated	Intermediate	20-30%
Luminal B-like HER2⁺	+	-/+	+	Low/High	Moderately differentiated	Intermediate	
HER2⁺	-	-	+	High	Poorly differentiated	Poor	15-20%
TNBC	-	-	-	High	Poorly differentiated	Poor	10-20%

Table 3. Classification of molecular subtypes of BC, prognosis and therapies.

Treatment decisions are mainly based on that clinical classification and take into account other clinic-pathological factors previously mentioned, including age, tumor size, histological grade, lymph node metastases, and vascular invasion. These parameters

have been consolidated into different guidelines (*Guidelines Detail*; Galea *et al.*, 1992; Gómez-Acebo *et al.*, 2021).

Hereditary breast cancer

A crucial factor in the management of BC is genetics (Haffty, Euhus and Pierce, 2020). About 5-10% of all BC cases are hereditary, and this type of tumor has some distinctive clinical features compared with sporadic BC (Yang and Lippman, 1999). These characteristics include early onset of disease, excess of bilateral disease, high risk of developing a second primary cancer (ovarian, colon, and prostate cancer), and transmission of the disease through successive generations in an autosomal dominant pattern (Claus, Risch and Thompson, 1990). Among the gene mutations associated with BC, the primary genes affected are *BRCA1* (**BR**east **CA**ncer gene **1**) and *BRCA2* (**BR**east **CA**ncer gene **2**), representing 25-28% of all hereditary BC cases. BC risks are at 40-87% for *BRCA1* mutation carriers and 18-88% for *BRCA2* mutation carriers (Engel and Fischer, 2015). In addition to *BRCA1* and *BRCA2*, mutations in other seven genes are associated with the risk of developing BC: *ATM*, *CDH1*, *CHEK2*, *NF1*, *PALB2*, *PTEN*, and *TP53* (Pharoah, Guilford and Caldas, 2001; Finkel, 2002; Weischer *et al.*, 2012; Yang *et al.*, 2018; Carbognin *et al.*, 2019; Maani *et al.*, 2019; Bergstrom *et al.*, 2020; Yi *et al.*, 2020).

Treatment

The different types of treatments are classified according to the localization and administration time. According to the localization, they can be divided into local (the place where the tumor is) or systemic (the entire body) treatments, and considering the administration time into adjuvant (after prophylactic surgery) or neoadjuvant (before surgery) treatments.

- **Surgery**: There are two types of surgery for BC: lumpectomy and mastectomy. Lumpectomy is a surgery in which only the part of the breast containing cancer and surrounding normal tissue is removed. In a mastectomy, the entire breast is removed, including all breast tissue and sometimes other nearby tissues. To determine whether cancer cells have spread to the lymph nodes, it is necessary to evaluate the presence of cancer cells in breast lymph nodes by the sentinel lymph node biopsy or axillary lymph node dissection (Burstein *et al.*, 2019).
- **Radiotherapy**: It uses high-energy X-rays or another particle to damage the DNA of cancer cells. The treatment area may include the breast area, lymph nodes, or

another part of the body whether cancer has spread. There are several types of radiation therapy: External-beam radiation (the most common type of radiotherapy, it is given by a linear accelerator) and brachytherapy or internal radiation (radioactive substance sealed in seeds or catheters placed inside of the body or directly into cancer where the cancer is located). Other types of radiation are intraoperative radiation therapy, systemic radiation therapy, radioimmunotherapy, and radiosensitizers or radioprotectors (*Radiation Therapy for Breast Cancer Treatment: Types, Side Effects and More*; Burstein *et al.*, 2019). Adjuvant radiation therapy is given after surgery (most commonly after a lumpectomy), but sometimes it is provided as a neoadjuvant therapy before the surgery to reduce a large tumor, making it easier to remove.

Chemotherapy: Is the use of antineoplastic agents which kill the cancer cells interfering with their ability to grow and divide. Chemotherapy remains an essential treatment for preventing recurrence in many patients with stage I-III BC (Loibl *et al.*, 2021). It is the only systemic therapy with demonstrated efficacy in TNBC and an essential adjunct to endocrine therapy or HER2-directed therapy in patients with HR⁺/HER2⁻ or HER2⁺ BC, respectively (Waks and Winer, 2019). In most cases, chemotherapy is most effective by using different combinations of drugs. Before surgery, it may be given to shrink a large tumor and make surgery more accessible, or after surgery to reduce the risk of recurrence. The most common chemotherapy combinations are AC (doxorubicin, cyclophosphamide), EC (epirubicin, cyclophosphamide), paclitaxel or docetaxel after AC/EC, FAC (5-FU (5-fluorouracil), doxorubicin, cyclophosphamide), FEC (5-FU, epirubicin, cyclophosphamide), CMF (cyclophosphamide, methotrexate, 5-FU), TAC (docetaxel, doxorubicin, cyclophosphamide), and TC (docetaxel, cyclophosphamide). In Table 4, the most commonly used chemotherapeutic agents are shown.

- **Hormonal/Endocrine therapy:** it was the first systemic treatment directed against a specific target. The molecules used in endocrine therapy work by blocking hormone actions or decreasing hormone levels in the body. It is an effective treatment for tumors positive for ER or PR. Blocking hormones are used by the tumor to stimulate its growth, can help prevent cancer recurrence and increase patients' survival. The standard hormonal treatment during the last two decades has been tamoxifen. Tamoxifen is a selective ER **modulator** (SERM) that binds to the estrogen receptor, blocking their effects. It is effective for treating

pre- and postmenopausal women with HR⁺ BC. Fulvestrant is a selective estrogen receptor **degrader** (SERD) approved to treat patients with ER⁺ advanced BC (Soleja, Raj and Unni, 2019). Other hormonal therapies block estrogen production, such as aromatase inhibitors (AIs). Although the ovary does not produce estrogen in postmenopausal women, a small amount of this hormone is still produced by the adipose tissue by the aromatase enzyme. AIs (anastrozole, exemestane, and letrozole) block the aromatase enzyme decreasing the amount of estrogen produced and are helpful in postmenopausal women. Nevertheless, AIs can also be used in premenopausal women only in combination with ovarian suppression. Another way to block the estrogen production in premenopausal patients is ovarian ablation (ovary removal) or ovarian suppression (shutting down). Oophorectomy (a surgical procedure to remove the ovaries), luteinizing hormone-releasing hormone (LHRH) agonists (drugs that stop the signal that the body sends to the ovaries to make estrogen), and chemotherapy drugs (drugs that damage the ovaries so they no longer produce estrogen) are different ways to remove or shut down the ovaries to treat BC in premenopausal women.

- **Targeted therapy:** In addition to the targeted therapies against the HR⁺ tumors, newer and more effective treatments that attack cancer-specific genes and proteins and the tissue environment that contributes to the growth and survival of cancer cells have been developed. Importantly, this type of treatment avoids damage to the normal cells and has less severe side effects than standard drugs. Targeted therapy is currently being used in combination with traditional chemotherapy. The most common targeted therapies are mononuclear antibodies and small-molecule drugs against tyrosine kinases, mTOR, Pi3K, PARP, CDK4/6, or angiogenesis inhibitors. (Masoud and Pagès, 2017). The development of humanized monoclonal antibodies binding to the extracellular domain of HER2 (e.g. trastuzumab), EGFR-HER2 small molecule kinase inhibitors (e.g. lapatinib), and antibody-drug conjugates (e.g. T-DXd) have revolutionized HER2⁺ BC treatment (Pernas and Tolaney, 2019; Cortés *et al.*, 2022).
- **Immunotherapy/Immuno-oncology:** It is a form of treatment that uses the immune system of the own patient to prevent, control, and eliminate cancer. It is also called biotherapy because it uses living organisms or substances derived from living organisms to fight disease. Cancer immunotherapy comes in various forms, including targeted monoclonal antibodies, cancer vaccines, adoptive cell

therapies, oncolytic viruses, immune checkpoint inhibitors, cytokines, and adjuvants (*What is Immunotherapy - Cancer Research Institute (CRI)*, no date).

Independently of the BC subtype, surgery is usually the first type of treatment for BC. Subsequently, surgery is followed by other treatments such as chemotherapy, radiotherapy, or hormone/targeted therapies depending on the subtype and stage of the BC.

Drug family	Subgroup	Mechanism of action	Drug name
Antimetabolites	Antifolates	Block the activity of folic acid, resulting in inhibition of cell division, DNA and RNA synthesis and repair, and protein synthesis.	Methotrexate
	Pyrimidine antagonists	Mimic the structure of metabolic pyrimidines and inhibit enzymes involved in DNA synthesis through competitive antagonism.	5-FU
			Capecitabine
Alkylating agents	Oxazaphosphorines	Induce cross-linking at guanine.	Cyclophosphamide
	Platinum-based agents	Cross-link between DNA strands, thus decreasing DNA replication.	Cisplatin
			Carboplatin
Mitotic inhibitors	Vinca alkaloids	Bind to β -tubulin and inhibit polymerization into microtubules to prevent mitotic spindle formation, thus arresting the cell cycle in M-phase.	Vinorelbine
	Taxanes	Stabilize polymerized microtubules of the mitotic spindle to stop mitosis and thereby the process of cell division.	Docetaxel
			Paclitaxel
	Nontaxane microtubule inhibitors	Inhibit microtubule stability by blocking mitotic spindles without affecting depolymerization and thereby stops the process of cell division.	Eribulin
			Ixabepilone
Epothilone			

Antibiotics	Anthracyclines	They have multiple mechanisms of action including the inhibition of topoisomerase II, the inhibition of DNA and RNA synthesis by intercalation with DNA, DNA strand excision, and generation of free radicals.	Doxorubicin
			Epirubicin

Table 4. Classification of the chemotherapeutic agents and their mechanism of action. Data obtained from the American Cancer Society (<https://www.cancer.org/cancer/breast-cancer/treatment.html>).

Impact of menopause

After menopause, there is a physiological withdrawal of ovarian sex steroids, responsible for metabolic control and homeostasis. The metabolism modification in combination with limited physical activity and a high-fat diet gives rise to some lipid metabolic disorders, affecting the body fat mass, fatty acid metabolism, adiposity, and obesity (Ko and Kim, 2020).

One of the main ovarian sex hormones is estrogen which is three types: Estrone (E1), Estradiol (E2), and Estriol (E3). Aromatase is a critical enzyme for estrogen production. Ten alternative tissue-specific promoters have been described, regulating the aromatase expression in gonads, fatty tissues, skin, and placenta (Zhao *et al.*, 2016). E1 is produced in the skin and adipose tissues from circulating androstenedione of adrenal origin (*Menopause*, no date). The ovarian follicle produces E2 during the monthly menstrual cycle, and E3 is synthesized in the placenta (Zhao *et al.*, 2016). The sources of estrogen production differ between premenopausal and postmenopausal women. In premenopausal patients, the central tissue involved in the ovary, whereas in postmenopausal is the extra-ovarian sites (adipose tissue and skin). In premenopausal women, the ovarian follicles are composed of an oocyte surrounded by granulosa cells and a layer of theca cells. Granulosa cells are responsible for synthesizing E2 in the ovary by converting androgen into E2 by aromatase activity. E1 is the primary form of estrogen in postmenopausal, and despite deficient levels, E2 is also biologically active (Shozu *et al.*, 2003).

Some studies have reported that higher estrogen production from fat and skin correlated with obese postmenopausal women. In turn, overweight postmenopausal women showed a higher risk for developing BC than normal-weight postmenopausal women

(Cleary and Grossmann, 2009; Brown and Simpson, 2010; Bulun *et al.*, 2012; Zhao *et al.*, 2016). Overweight postmenopausal women have an increased risk to develop ER⁺ BC disease (Rosenberg *et al.*, 2006; Neuhouser *et al.*, 2015). Even if the potential mechanisms that could explain the relationship between metabolism, obesity, and higher risk of developing BC are not clear enough, there are three main hypotheses: (1) In overweight postmenopausal patients, the levels of circulating estrogens are higher than in slim postmenopausal patients. (2) Obesity is highly associated with increased circulating levels of insulin and insulin-like growth factor (IGF), which stimulate BC growth. (3) The adipose tissue produces hormones, cytokines, and growth factors that stimulate BC growth (MacCìò and Madeddu, 2011).

RANK-RANKL signaling pathway

Components

The receptor activator of nuclear factor kappa-B (NF- κ B) ligand (RANKL), the receptor activator of NF κ B (RANK), and the decoy receptor osteoprotegerin (OPG) were described in the late 1990s (Nakashima, Hayashi and Takayanagi, 2012) and are known as the RANKL/RANK/OPG system. RANKL belongs to the tumor necrosis factor (TNF) superfamily, and RANK and OPG to the TNF receptor (TNFR) superfamily. Members of both super-families are broadly expressed in various tissues and organ systems.

RANK: It is alternatively named TNF-related activation-induced cytokine receptor (TRANCE-R) (Wong *et al.*, 1998), osteoclast differentiation and activation receptor (ODAR) (Hofbauer *et al.*, 2000), or TNFR superfamily member 11 A (TNFRSF11A). TNFR superfamily can be subdivided into three families depending on their signal transduction mechanisms (Figure 1). All the members of this family harbor an extracellular domain with varying numbers of cysteine-rich domains (CRDs) that act as ligand binding sites. The “Death receptor” family carries a death domain (DD) in their cytoplasmic part. After an apoptotic input, the cytoplasmic DD recruits apoptosis-related factors activating downstream caspases and inducing apoptosis. The “TRAF-interacting receptor” family is negative for DD and can activate NF- κ B transcription factor family members and mitogen-activated protein kinase (MAPK) pathways. The “Decoy receptor” family is composed of four decoy molecules that are cell surface or soluble proteins.

As we observe in Figure 1, RANK belongs to the TRAF-interacting receptor family. It encodes a type I homo-trimerizing transmembrane glycoprotein composed of 625 amino acids in mice and 616 amino acids in humans. Both murine and human RANK are composed of extracellular, transmembrane, and intracellular domains. RANK contains

four CRDs at the amino-terminus (or extracellular domain) and three TRAF-binding domains at the carboxyl-terminus or cytosolic domain (Nakashima, Hayashi and Takayanagi, 2012; Okamoto *et al.*, 2017). Human and mouse RANK share 66% identity in their amino acid sequences. It is expressed on the surface of various cells such as osteoclast precursors, mature osteoclasts, dendritic cells, mammary gland epithelial cells, BC cells, and prostate cancer cells (Anderson *et al.*, 1997a; Kong *et al.*, 1999; Fata *et al.*, 2000; Hofbauer and Heufelder, 2001; Mosheimer *et al.*, 2005; Chen *et al.*, 2006; Kim *et al.*, 2006). In addition to the canonical isoform of human RANK, a brief description of additional variants resulting from alternative splicing has been reported (Papanastasiou, Sirinian and Kalofonos, 2012).

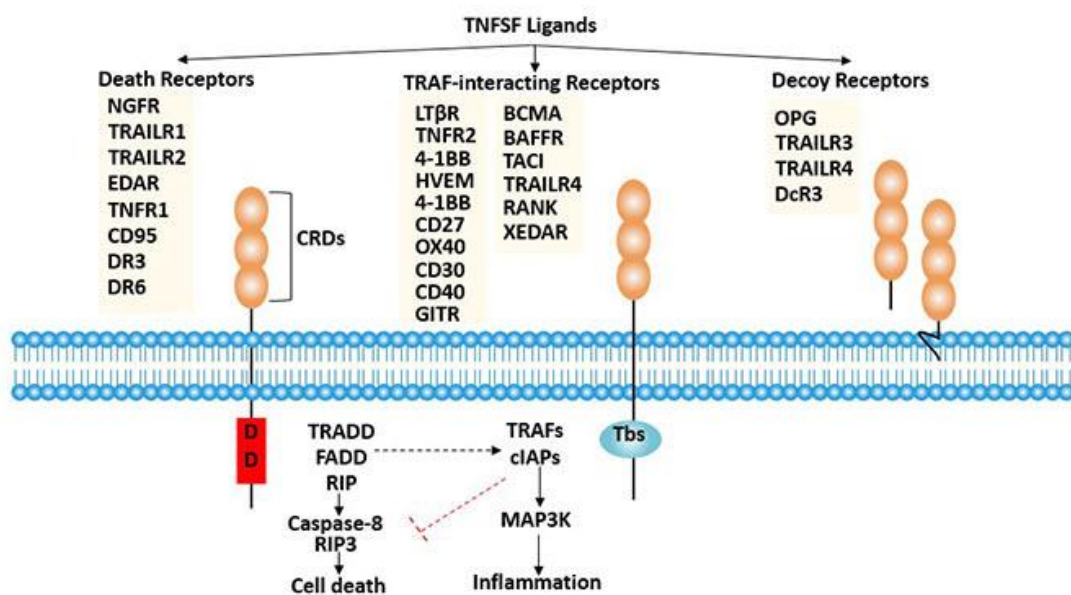


Figure 1. Members and classification of the TNFR superfamily. Figure obtained from <https://www.cusabio.com/c-20948.html>

RANKL: Four research groups independently isolated the type II transmembrane protein TNF superfamily 11 (TNFSF11) using different experimental systems and gave it other names: TNF-related activation-induced cytokine (TRANCE) (Wong, Josien, *et al.*, 1997), RANKL (Anderson *et al.*, 1997b), osteoprotegerin ligand (OPGL) (Lacey *et al.*, 1998) and osteoclast differentiation factor (ODF) (Yasuda *et al.*, 1998). While TRANCE and RANKL were isolated as a factor playing a role in the survival and activation of dendritic or T cells, OPGL and ODF were isolated from myelomonocytic and bone marrow stromal cell lines as a factor of osteoclastogenesis. It has been described that different cell types in bone express RANKL (Eghbali-Fatourechi *et al.*, 2003; Bord *et al.*, 2004; Hofbauer and Schoppet, 2004) and various osteoactive factors, such as glucocorticoids, Vitamin D3 and TNF- α , among others, regulate its expression (Gao *et al.*, 1998; Yasuda *et al.*, 1998;

Hofbauer *et al.*, 1999). Furthermore, RANKL is essential as a paracrine mediator of progesterone-induced proliferation in the adult mouse mammary gland (Beleut *et al.*, 2010). Binding studies have demonstrated that RANKL can bind to the functional receptor RANK and the decoy receptor OPG (Anderson *et al.*, 1997a; Yasuda *et al.*, 1998).

Three distinct isoforms of RANKL have been identified in both mice and humans. According to mouse RANKL, in addition to the canonical protein (RANKL1) composed of 316 amino acids, two new isoforms were detected: RANKL2 (287 amino acids) and RANKL3 (199 amino acids). RANKL1 is a transmembrane protein (tmRANKL1) with an extracellular domain at the carboxyl-terminus (Nakashima, Hayashi and Takayanagi, 2012; Okamoto *et al.*, 2017) bearing close homology to other TNFSF members such as TRAIL, FasL, and TNF- α (Wong, Rho, *et al.*, 1997). The extracellular ectodomain is cleaved by enzymes to produce a soluble form (sRANKL1), released into the extracellular environment. It has been proposed that the soluble form of RANKL has a more potent activity (Wada *et al.*, 2006). The proteolytic cleavage of RANKL requires members of the disintegrin and metalloprotease domain (ADAM) family and matrix metalloproteinases (MMPs). For example, ADAM17 (also named TACE) and ADAM19 have been shown to cleave RANKL *in vitro* (J, L and CP, 2001; V *et al.*, 2003). RANKL2 has a shorter intracellular domain than the original RANKL1, and RANKL3 lacks a transmembrane domain.

RANKL1 is detected in the endoplasmic reticulum, Golgi network, and cytoplasmic and membrane regions. RANKL2 is predominantly detected in the endoplasmic reticulum and Golgi networks. RANKL3 protein is diffusely seen in the cytoplasmic region of the cells and the endoplasmic reticulum, and Golgi networks (Ikeda *et al.*, 2001). Further studies suggested that RANKL3 could not be transported and secreted adequately being accumulated in the cytoplasmic region (Ikeda *et al.*, 2003).

Human RANKL1, RANKL2, and RANKL3 are composed of 317, 270, and 244 amino acids, respectively (Figure 2). As in mouse, whereas RANKL1 possess intracellular, transmembrane, and extracellular domains, RANKL3 contains only the extracellular domain. In the case of RANKL2, the sequence which encodes the intracellular domain is completely deleted. Electron microscopy revealed that, unlike RANKL2 and RANKL3, RANKL1 is detected in the membrane of human cells (Suzuki *et al.*, 2004).

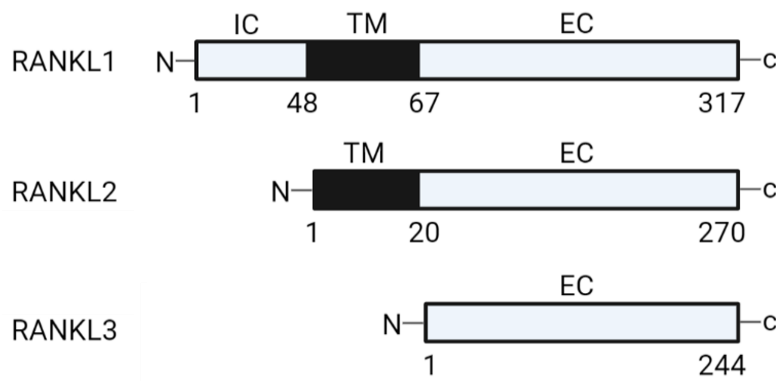


Figure 2. Human RANKL isoforms. Numbers show the amino acid position. Picture adapted from (Suzuki *et al.*, 2004).

Human and mouse RANKL proteins share 85% identity in their amino acid sequences allowing crosstalk between human and murine RANKL and their receptors (Cheng *et al.*, 2009). Moreover, like other members of the TNF family, the extracellular domain of RANKL forms homotrimeric structures suggesting that there are multiple trimeric structures of different RANKL isoforms showing distinct biological functions (Ito *et al.*, 2002; Ikeda *et al.*, 2003).

The binding of RANKL to RANK triggers the activation of the receptor, transducing the signal by recruiting TRAFs, mainly TRAF6 (Darnay *et al.*, 1998; Galibert *et al.*, 1998; Armstrong *et al.*, 2002), which activates MAPKs p38 and JNK and the transcription factors NF- κ B and activator protein 1 (AP1) (Darnay *et al.*, 1999). NF- κ B activation induces the nuclear factor of activated T cells 1 (NFATc1), a crucial factor for osteoclastogenesis regulation. Other interacting factors that may modulate RANK signaling include Grb2-associated binding protein 2 (Gab2) (Wada *et al.*, 2005), epidermal growth factor receptor (EGFR) (Yi *et al.*, 2008), four-and-a-half LIM domain 2 (FHL2) (Bai *et al.*, 2005), Lyn (H. J. Kim *et al.*, 2009), CYLD (Jin *et al.*, 2008) de-ubiquitinase and TRAF family member-associated NF- κ B activator (TANK) (Maruyama *et al.*, 2012). RANK also regulates calcium oscillation through downstream activation of the regulator of G-protein signaling 10 (RGS10) (Yang and Li, 2007) and activates Src family kinase signaling leading to Akt/PKB activation (Wong *et al.*, 1999). Two different NF- κ B pathways have been reported: the canonical and non-canonical signaling pathways. The classical pathway is activated when inflammatory cytokines, such as TNF- α and IL-1, among others, bind to the receptor. Subsequently, I κ B is phosphorylated by the I κ B kinase complex (IKK α , IKK β , NEMO) being ubiquitinated and degraded by the ubiquitin-proteasome system. Free NF- κ B translocates to the nucleus regulating the expression of target genes. The non-canonical pathway is independent of I κ B degradation and is activated by agonists involved in secondary lymphoid organogenesis,

mature B cell function, and adaptive immunity. In that case, the C-terminal end of p100 is degraded (Jimi *et al.*, 2019) (Figure 3).

OPG: It is alternatively named osteoclastogenesis inhibitory factor (OCIF) (Tsuda *et al.*, 1997), TNF receptor-like molecule 1 (TR1), follicular DC-derived receptor-1 (FDCR-1) (Kwon *et al.*, 1998) or tumor necrosis factor receptor superfamily member 11 B (TNFRSF11B), encodes a full-length protein of 401 amino acids. It is cleaved by signal peptidase to a 380 amino acid form containing four cysteine-rich at the amino-terminus and two death domains at the carboxyl-terminus. OPG is exported to the extracellular space as a soluble decoy receptor by mesenchymal-derived cells such as osteoblasts and bone marrow stromal cells (Walsh and Choi, 2003; Kondo *et al.*, 2004; Nakashima, Hayashi and Takayanagi, 2012; Okamoto *et al.*, 2017). Human and mouse OPG proteins share 85% identity in their amino acid sequences. OPG binds to RANKL with high affinity, but it has also been shown to bind with lower affinity to lymphotoxin alpha (LTA) and tumor necrosis factor-related apoptosis-inducing ligand (TRAIL). Other ligands for OPG are syndecan-1, glycosaminoglycans (GAGs), von Willebrand Factor, and Factor VIII von Willebrand Factor Complex (Baud'huin *et al.*, 2013).

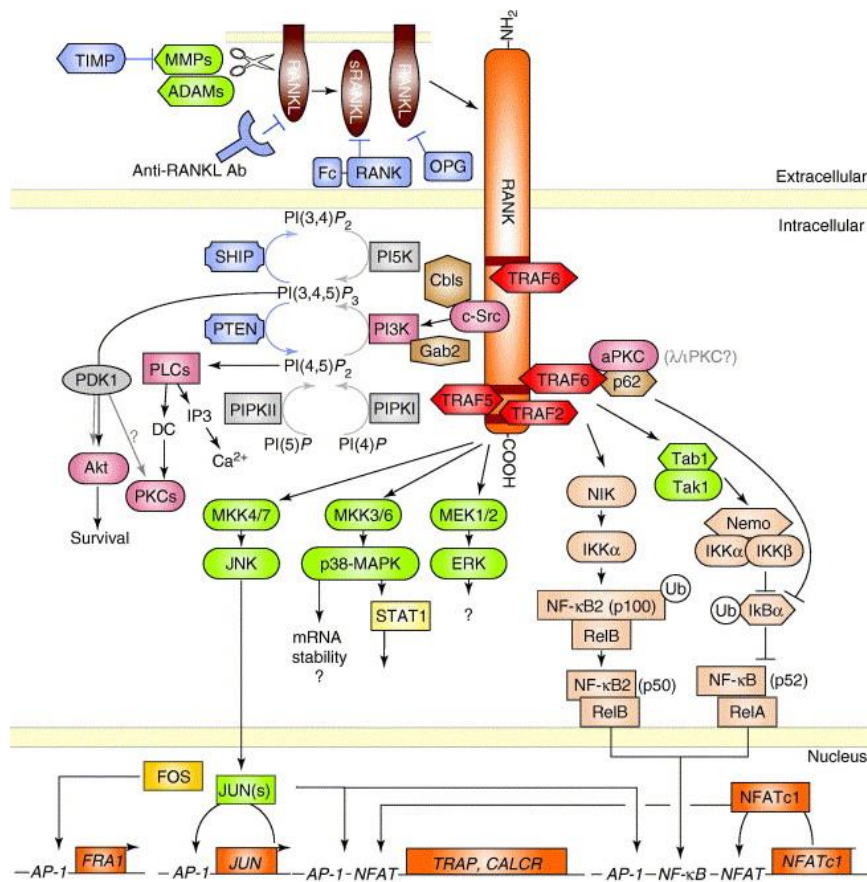


Figure 3. Schematic diagram of the RANKL-RANK-induced signaling cascades. Figure obtained from (Wada *et al.*, 2006).

LGR4: Leucine-rich repeats containing G protein-coupled receptor 4 (LGR4), also named G protein-coupled receptor 48 (GPR48), is a 951-amino acid transmembrane receptor belonging to the group B of the LGR family. LGR4 has been detected in several tissues, including the mammary gland, bone, prostate, skin, pancreas, and ovary. It is commonly activated by R-spondins (RSPOs), Norrin, and circLGR4 modulating signaling pathways associated with physiological and developmental processes such as mammary gland development and mammary stem cell biology (Hsu, Liang and Hsueh, 1998; Loh *et al.*, 2000; Loh, Broussard and Kolakowski, 2001; Sigl, Jones and Penninger, 2016). Furthermore, although the information is very reduced, LGR4 has been described as a novel receptor for RANKL, competing with RANK and suppressing canonical RANK signaling during osteoclast differentiation (Luo *et al.*, 2016). However, further studies are needed to validate this interaction.

RANKL reverse signaling

Most ligands of the TNF superfamily exist as soluble cytokines and as transmembrane proteins. Both forms have bioactivity, although some functions are different. In 1994, Smith *et al.* suggested that transmembrane ligands of the TNF superfamily had the potential to trigger bidirectional signals since the cytoplasmic parts of the molecules are highly conserved across species (Kisikwa *et al.*, 2013). This reverse signaling has been demonstrated mainly in the immune system and within the TNF superfamily (Eissner, Kolch and Scheurich, 2004a). The cytoplasmic domains of the different transmembrane forms of the TNF family ligands do not possess any apparent enzymatic function and, therefore probably signal through associated proteins (Eissner, Kolch and Scheurich, 2004a), promoting different signal transduction pathways. RANKL, as a member of the TNF superfamily, may receive signals, subsequently acting as a receptor, to transmit positive and negative feedback signals into the ligand-bearing cell.

Recently, it has been observed that the vesicular RANK secreted from osteoclasts induces osteoblastogenesis via RANK-RANKL reverse signaling (Ikebuchi *et al.*, 2018). The average lifespan of human osteoclasts is two weeks, and then they undergo apoptosis, releasing apoptotic bodies (ABs), which are the main class of extracellular vesicles (EVs) produced in this process. The vesicular RANK secreted from mature osteoclasts binds to RANKL expressed in osteoblasts and promotes osteoblastogenesis by activating *Runx2*. This activation via RANK-RANKL reverse signaling also increases the mineralization of osteoblasts (Ikebuchi *et al.*, 2018). Moreover, Ma *et al.* have also described that mature osteoclasts-ABs show the highest osteogenic potency among

osteoclast-derived EVs by activating PI3K/Akt/mechanistic target of rapamycin (mTOR)/ribosomal protein S6 kinase signaling (Ma *et al.*, 2019a).

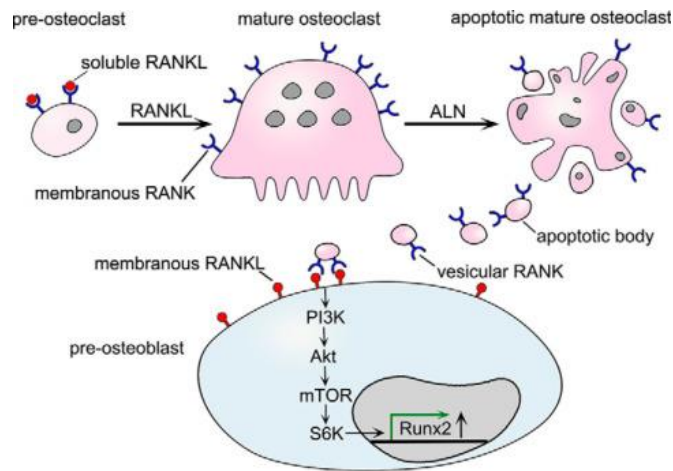


Figure 4. Schematic of RANKL reverse signaling activation by mature osteoclasts-ABs. Obtained from (Ma *et al.*, 2019b).

Bone metabolism

Bone is a dynamic tissue undergoing continuous formation and resorption processes in response to a considerable number of signals. During bone turnover, osteoclasts, differentiated from hematopoietic precursors of the monocyte/macrophage lineage, demineralize and resorb the older bone. In contrast, osteoblasts, differentiated from mesenchymal stem cells, deposit new bone to maintain a bone mass appropriate (Ito *et al.*, 2002). Any variation in the process of bone turnover may alter bone mineral density (BMD), bone strength, and bone micro-architecture. The osteoblasts produce colony-stimulating factor 1 (CSF1), a cytokine that promotes the proliferation and expression of RANK in osteoclast precursors. On the other hand, locally acting factors induce RANKL on osteoblasts attracting osteoclast precursors. Interaction of RANKL from osteoblasts and RANK on the surface of osteoclast precursors gives rise to the bone-remodeling unit in which osteoclast precursors fuse and attach to the bone surface as resorbing osteoclasts. Additionally, the osteoblast lineage also produces OPG, preventing RANKL from binding to RANK, inhibiting RANK activation, and impeding osteoclast recruitment and differentiation (Kearns, Khosla and Kostenuik, 2008; Wright *et al.*, 2009).

Bone remodeling depends ultimately on the delicate balance between RANKL and OPG, which, in turn, are influenced by different factors. Therefore, an increase in the OPG/RANKL ratio leads to a decrease in bone resorption and an increase in bone mass, whereas a reduction of the OPG/RANKL ratio shows the opposite effects (Kearns, Khosla and Kostenuik, 2008). The increase in osteoclast activity promotes bone

resorption resulting in diminished bone density and architectural deterioration of bone tissue, which drives osteoporosis (Wright *et al.*, 2009).

Immunity

The RANKL/RANK/OPG molecular triad constitutes a cross-talk between bone metabolism and the immune response denominated osteoimmunology (Theoleyre *et al.*, 2004; Walsh *et al.*, 2006).

The first line of defense against foreign pathogens is the innate immune response. It encompasses physical and chemical barriers and cellular protection. These non-specific cells involved in immediate and independent antigen responses are natural killer cells (NKs), macrophages, neutrophils, dendritic cells (DCs), mast cells, basophils, and eosinophils. The second line of defense is the acquired immunity, specific to the antigen presented. This adaptive immunity is marked by clonal expansion of T and B lymphocytes, releasing many antibodies to neutralize their target antigen (Charles A Janeway *et al.*, 2001). Based on the production and maturation of the cells, primary lymphoid organs (red bone marrow and thymus) are the responsible for immune cell production, while the secondary lymphoid organs (lymph nodes, spleen, and mucosa-associated tissues (MALT)) are the responsible for recognizing foreign antigens and offering defensive response and also for maintaining the mature naïve lymphocytes. It has been described RANKL as a maintainer of the bone marrow and its indwelling immune cells (Ono *et al.*, 2020). Moreover, both RANK and RANKL are involved in the central tolerance occurred in the thymus to prevent the development of autoimmune diseases (Rossi *et al.*, 2007; Hikosaka *et al.*, 2008; Roberts *et al.*, 2012; White *et al.*, 2014) and have a central role in the organogenesis of those secondary lymphatic organs (Yoshida *et al.*, 2002; Cupedo and Mebius, 2005; Mueller and Hess, 2012; Sugiyama *et al.*, 2012).

Mature hematopoietic cells are traditionally categorized into two different lineages: lymphoid lineage (T, B, and NKs) and myeloid lineage, which includes granulocytes (neutrophils, eosinophils, and basophils), monocytes-macrophages, erythrocytes, megakaryocytes and mast cells (Iwasaki and Akashi, 2007). The immune populations that are relevant to this doctoral thesis will be discussed below.

NKs: Natural Killer cells are derived from lymphoid progenitors but are part of the innate immune system, unlike T and B cells. NK cells recognize virus-infected, aberrant, or transformed cells using a sophisticated array of activating, costimulatory, and inhibitory

receptors (Miller and Lanier, 2019). NKs derived from bone marrow and blood have been described to express RANK in the presence of IL-10 (Atkins *et al.*, 2006).

Monocyte/Macrophages: Monocytes are derived from myeloid lineage and are released from the bone marrow into the bloodstream where, upon inflammatory signals, they migrate into the affected tissue and differentiate into different macrophage (M \emptyset) subsets or DCs, depending on the cytokine environment (Fang *et al.*, 2018). The **macrophages** are phagocytic cells involved in the different biological processes such as development, homeostasis, and immune response to pathogens. They have been described as plastic cells that transit through a gradient of pro-inflammatory to anti-inflammatory phenotypes, classified as M1 and M2 subpopulations, respectively. The effect of the RANK pathway on monocytes' and macrophages' function is context-dependent. *In vitro* experiments where were cultured unfractionated peripheral blood monocytes with RANKL in combination with other cytokines revealed to be sufficient to induce differentiation into osteoclasts and maintain bone homeostasis (Zheng *et al.*, 2006; Italiani and Boraschi, 2014). Interestingly, RANKL could trigger M1 macrophages, actively involved in bone formation (Huang *et al.*, 2017). However, Fujimura and colleagues revealed that the treatment of RANKL induced abundant cytokine expression changes in the M2 phenotype. Notably, the cytokine release was validated on the targets identified on M2 macrophages, and CCL5, CCL17, and CXCL10 production were increased upon RANKL stimulation (Fujimura *et al.*, 2016). Apart from polarization to M1-like phenotype, depending on the tissue environment, RANKL also might induce M2 macrophages, playing an immuno-regulatory effect *in vivo* (Meng *et al.*, 2017).

Mammary gland development

The mammary gland comprises multiple cell types that can be grouped into two cellular compartments: the epithelium (derived from ectoderm) and the surrounding stroma (derived from mesoderm). The development of this organ, which finishes after birth, is defined in different stages in response to hormones and growth factors: embryonic, pubertal, pregnancy, lactation, and involution.

The epithelium consists of a branching structure composed of ducts (developed during puberty) and alveoli (developed during pregnancy). The mammary epithelium compartment consists of two differentiated cell types organized into two main layers: an inner luminal epithelial cells (LECs) with the function of secreting milk during pregnancy and an outer layer of myoepithelial cells (MECs) adjacent to a basement membrane that separates it from the underlying mammary stroma and is then responsible for the

contraction of the alveoli and milk secretion (Cristea and Polyak, no date; McNally and Stein, no date). At the embryonic stage, the mammary gland is formed by a small branched epithelial tree connected to the nipple after the invasion of epithelial mammary buds into the fat pad under hormonal stimulation. From birth to puberty, the mammary epithelium remains quiescent. However, at the puberty stage, the estrogen signal induces the complete invasion of the ductal tree and the fat pad. At the end of the ducts, there are unique structures named terminal end buds (TEBs) composed of high proliferative cells responsible for the elongation of the ductal tree. In adulthood, the mammary epithelium of the virgin female mice proliferates and involutes depending on the levels during the estrous cycle. During the first phase of pregnancy, the circulating hormones, such as the progesterone, induce a massive proliferation of ductal branches and alveolar buds. After that, progesterone, prolactin, and parathyroid hormone-related peptide (PTHrP) trigger the alveolar buds' differentiation into a milk-secreting phenotype. Additionally, the myoepithelial layer acquires contractility to stimulate milk secretion by oxytocin production. The involution occurs after lactation when the milk demand is reduced and pups are weaned. Then, the mammary gland reverts to its initial stage by apoptosis, development of the adipose tissue, and remodeling of the mammary gland before pregnancy (Figure 5) (Brisken and Ataca, 2015; Fu *et al.*, 2020).

Based on the hormone receptor expression, the luminal layer is classified into two different groups: HR⁺ cells expressing ER and PR and HR⁻ cells. HR⁺ cells are considered mature luminal cells with a low proliferation rate. Opposite, HR⁻ cells are considered luminal progenitors with a high proliferation rate (Fu *et al.*, 2020).

RANK signaling pathway has been widely studied in the mammary gland. In the murine virgin mammary gland, RANK and RANKL expression are maintained relatively low with variations during pregnancy and involution. RANKL is the main mediator of progesterone signaling in the mammary epithelium. Progesterone has mitogenic effects on MECs through two waves of proliferation: Progesterone induces the first wave of proliferation in PR⁺ luminal cells and up-regulation of Wnt4 and RANKL (Joshi *et al.*, 2010). This first wave is faster and weaker than the second and requires Cyclin D1. The second wave, which takes place 72 hours after progesterone stimuli, is longer and more intense than the first wave. Moreover, it affects the HR-luminal progenitors and myoepithelial cells when in a paracrine manner, RANKL previously regulated activate the RANK pathway leading to their proliferation. In this second wave, the proliferation is independent of Cyclin D1. (Hennighausen and Robinson, 2001; Gonzalez-Suarez *et al.*, 2007; Asselin-Labat *et al.*, 2010; Joshi *et al.*, 2010). It has also been reported that the RANKL/RANK system controls the mammary stem cell (MaSC) pool. MaSCs are actively cycling during

women's whole reproductive period, and their numbers change during aging, pregnancy, and the menstrual cycle (Asselin-Labat *et al.*, 2010; Joshi *et al.*, 2010). Progesterone acts on luminal epithelial cells inducing RANKL expression, which increases the pool of MaSCs by interacting with RANK-expressing basal epithelial cells in a paracrine manner (Rao *et al.*, 2018).

Importantly, diverse impairments have been described in *rankl*^{-/-}, *rank*^{-/-} or *lgr4*^{-/-} mice. Mice deficient in *rank* or *rankl* show a severe defect in MECs differentiation and survival during gestation. Then, the formation of the structures responsible for the milk secretion during pregnancy is blocked (Fata *et al.*, 2000). However, they usually develop after birth and puberty (Fata *et al.*, 2000). Moreover, RANK overexpression under the mouse mammary tumor virus (MMTV) promoter shows hyper-proliferative mammary glands and a complete blockage in the differentiation of lobulo-alveolar structures, and impaired lactogenesis leading to tumorigenesis after multiple pregnancies (Gonzalez-Suarez *et al.*, 2007; Pasquale *et al.*, 2013).

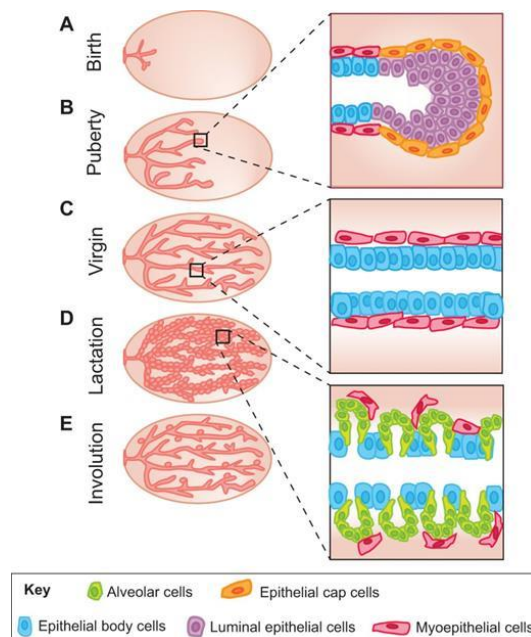


Figure 5. The mammary gland development is multistage. Picture obtained from (Inman *et al.*, 2015)

Breast cancer

Models of mammary gland tumorigenesis: RANK and RANKL also play an essential role in the development of BC due to their function regulating proliferation, stemness, differentiation of mammary epithelial, and its interaction with the immune system. Studies with preclinical models, both genetic and carcinogen+hormonal-induced, revealed that RANK signaling plays a crucial role in tumor initiation (Gonzalez-Suarez *et al.*, 2010;

Schramek *et al.*, 2010a; Yoldi *et al.*, 2016). The genetic loss of either RANK or RANKL in several models of tumorigenesis and the pharmacological inhibition of RANKL promoted longer tumor latency (Gonzalez-Suarez *et al.*, 2010; Schramek *et al.*, 2010a; Nolan *et al.*, 2016; Yoldi *et al.*, 2016). On the other hand, RANK overexpression under the MMTV promoter increased tumorigenesis of breast tissue induced by carcinogens and progesterone (Gonzalez-Suarez *et al.*, 2010). Further experiments using RANKL inhibitors prevented tumor formation in WT mice or delayed it in RANK-overexpressing mice (Gonzalez-Suarez *et al.*, 2010). Moreover, the genetic deletion of RANK in breast tissue showed attenuation of progestin-driven tumorigenesis, tumor growth, and stem cell expansion (Schramek *et al.*, 2010b), indicating that RANK-RANKL signaling is the main mediator of the oncogenic role of progesterone in the mammary gland.

In murine breast tumor models driven by the expression of an activated rat c-neu oncogene (ErbB2), homologue of HER2 (also called Neu) under the direction of the MMTV promoter, mammary-gland specific deletion of RANK did not alter the incidence or development of mammary cancer (Schramek *et al.*, 2010a). However, pharmacological inhibition of RANKL in mice overexpressing-her2 decreased tumorigenesis and metastatic burden (Gonzalez-Suarez *et al.*, 2010). In the same line, heterozygous RANK deletion decreased lung metastases in MMTV-ErbB mice compared to RANK WT (Tan *et al.*, 2011). In a whole-body RANK knockout mouse model, tumors driven by Polyoma middle-T (PyMT) expression in the mammary gland showed significantly lower tumor-initiating and metastatic ability (Yoldi *et al.*, 2016). Additional studies revealed that RANK activation in mammary epithelial cells enhanced proliferation and induced the accumulation of MaSCs and progenitors (Gonzalez-Suarez *et al.*, 2007; Palafox *et al.*, 2012; Pasquale *et al.*, 2013).

Besides, the inhibition of RANKL in a Brca1-deficient mouse model reduced mammary tumorigenesis and attenuated progesterone-induced proliferation in three-dimensional human breast organoids derived from pre-neoplastic BRCA1 mutated tissue (Nolan *et al.*, 2016). From normal tissue of BRCA1-mutation carriers, RANK⁺ and RANK⁻ luminal progenitors were identified, showing that RANK⁺ cells were highly proliferative, bearing aberrant DNA repair and a molecular signature similar to the basal-like BC (Nolan *et al.*, 2016). The genetic inhibition of RANK in the mammary epithelium markedly delayed onset and reduced incidence of Brca1;p53 mutation-driven mammary cancer (Sigl *et al.*, 2016). Furthermore, pharmacological inhibition of RANKL in mice abolished the occurrence of Brca1 mutation-driven pre-neoplastic lesions (Sigl *et al.*, 2016). In human BC cell lines with non-functional BRCA1, RANK overexpression increased the frequency

of CD44⁺/CD24^{low/-}, a subpopulation ascribed to breast cancer stem cells (CSCs), characterized by both self-renewal and differentiation capacities (Palafox *et al.*, 2012).

Based on pharmacological and genetic evidence that inhibition of the RANKL-RANK signaling pathway prevents BC development in mouse models, BRCA-D clinical trial (ACTRN12614000694617) is currently ongoing (*TransBCR | Clinical Trial - BRCA-D*, no date). BRCA-D trial is a pre-operative window study evaluating the biological effects of denosumab (DNS). This fully human IgG2 monoclonal antibody binds to human soluble and membrane RANKL with high affinity and specificity (Sordillo and Pearse, 2003; McClung *et al.*, 2006) on normal breast tissue from BRCA1 mutation carriers and high-risk non-carriers.

In 2003 the Million Women Study and the Women Health Initiative Study reported that women using combined estrogen and progesterone hormone replacement therapy (HRT) developed BC more frequently than women using estrogen-only HRT (Rossouw *et al.*, 2002b; Banks *et al.*, 2003). These results were confirmed in 2013 (Manson *et al.*, 2013). The hormones used as HRT induce RANKL expression in mammary epithelial cells, increasing the proliferation of these cells and MaSCs.

Not only in initiation but also in tumor progression and metastasis RANKL-RANKL signaling pathway has been reported (de Groot *et al.*, 2018; Peters *et al.*, 2019). It has been described that RANKL treatment-induced de-differentiation of established tumors from the MMTV-PyMT mouse model and promoted the growth of tumor transplant derived from PyMT in syngeneic hosts (Yoldi *et al.*, 2016). In the same line, pharmacological inhibition of the RANK signaling pathway reduced CSCs in these aggressive tumors, decreasing recurrence and metastasis and inducing tumor cell differentiation (Yoldi *et al.*, 2016). The transplantation of RANK null tumor cells into the mammary gland of WT hosts impaired tumor and metastasis initiation ability demonstrating that tumor cell-intrinsic mechanism mediated the reduction in CSCs (Yoldi *et al.*, 2016).

Clinical breast cancer: Clinical data analysis revealed high levels of RANK mRNA in HR⁻ primary breast adenocarcinomas and TNBC subtype, and progressively increased with bad clinic-pathological markers such as higher grade and proliferative index due to these tumors are the more aggressive (Palafox *et al.*, 2012). These results are also supported by the longer DFS found in BC patients with lower RANK levels (Santini, Schiavon, *et al.*, 2011) and the association of RANK with worse OS (Park *et al.*, 2014), worse disease-free survival (DFS), and risk of bone metastasis (BM) (Vidula *et al.*, 2017). Importantly, Pfitzner and collaborators described an association of RANK with the most

aggressive BC samples in the neoadjuvant GeparTrio trial. RANK was also found in tumor-associated macrophages (TAMs), previously described in other works (Palafox *et al.*, 2012). Besides, RANK expression in the primary tumor was associated with higher sensitivity to chemotherapy. However, all this prognostic and predictive information was not an independent parameter for BC patients (Pfitzner *et al.*, 2014). Recently we published that, not only in TNBC but also in HER2⁺ BC samples, RANK was expressed (Sanz-Moreno *et al.*, 2021). Moreover, our results revealed that both anti-HER2 treatment and resistance to anti-HER2 therapy increased RANK expression and that enhanced RANK signaling led to increased anti-HER2 resistance (Sanz-Moreno *et al.*, 2021). Furthermore, we demonstrated a physical and functional interaction between RANK and HER2, suggesting a RANK/HER2 crosstalk (Sanz-Moreno *et al.*, 2021).

According to RANKL expression in BC, contradictory data has been published. Analysis of clinical BC samples revealed RANKL detection in 62% and 41% of the non-metastatic and metastatic samples, respectively (Bhatia, Sanders and Hansen, 2005). That results were validated in another study in which RANKL was found in 60% of a heterogeneous BC dataset (Van Poznak *et al.*, 2006a). However, in Pfitzner's study, RANKL expression was found only in 6% of the BC samples using the Amgen anti-RANKL antibody (Pfitzner *et al.*, 2014). RANKL, detected in normal breast, pre-invasive and invasive lesions (Gonzalez-Suarez *et al.*, 2010), has been significantly associated with luminal A-like tumors. Moreover, a positive correlation has been reported between RANKL and PR (Azim *et al.*, 2015). Although RANKL has been detected, its role is still undeciphered in BC.

Although the prognosis of BC patients is generally favorable, 20-30% of patients still develop distant metastases (Eckhardt *et al.*, 2012), and metastasis is responsible for most cancer deaths rather than primary tumors. Data from different studies suggest that the expression of RANK in BC determines whether tumors predominantly migrate into bone (Jones *et al.*, 2006a; Santini, Schiavon, *et al.*, 2011) despite BC also metastasizing to other tissues such as the liver, lung, and brain (Kennecke *et al.*, 2010; Gerratana *et al.*, 2015; Wu *et al.*, 2016, 2017). Due to RANKL being highly expressed in the bone marrow environment, it could be one of the factors that facilitates metastasis of human malignant epithelial cells expressing RANK to bone, triggering cytoskeletal changes and migration (Jones *et al.*, 2006a). Disseminated breast tumor cells can be frequently detected in the bone marrow of patients with malignant tumors in the so-called "micrometastases niches". These niches form a favorable microenvironment for the development of metastatic spread and allow the tumor cells to escape immune surveillance (Terpos and Dimopoulos, 2011; Ming, Cronin and Penninger, 2020). The

tumor microenvironment of the bone tissue includes immune, tumor, and resident bone cells (osteoblasts, osteoclasts, and osteocytes). All of them participate in a “vicious cycle” that increases osteolysis and cancer cell proliferation (Croucher, McDonald and Martin, 2016; Renema *et al.*, 2016). BC cells increase RANKL expression in osteoclasts by secreting PTHrP (Kamalakar *et al.*, 2017; Ricarte *et al.*, 2018), which secrete cytokines that promote osteoclast differentiation and survival, resulting in osteolysis and metastasis (Ming, Cronin and Penninger, 2020).

Although most BCs exhibit low immune infiltration, accumulative evidence suggests that RANK-RANKL interactions between tumor cells and the specific immune populations from the tumor microenvironment could be enough to develop metastasis such as the RANKL-expressing tumor-infiltrating regulatory (Tan *et al.*, 2011; Rachner *et al.*, 2019). Recently, we published that the loss of RANK signaling in mouse tumor cells increases tumor-associated lymphocytes (TILs) and CD8⁺ T-cell infiltration and attenuates tumor growth while reducing the infiltration of TAMs and neutrophils into the tumor. Furthermore, in RANK-expressing tumors, we demonstrated higher survival and activation of the neutrophils inducing an immunosuppressive environment, which could restrict the cytotoxic T-cell response (Gómez-Aleza *et al.*, 2020). Anti-RANKL treatment in pre-operative premenopausal early-stage BC patients (D-BEYOND, NCT01864798) increased tumor-infiltrating lymphocytes and CD8⁺T cells, in line with our preclinical results (Gómez-Aleza *et al.*, 2020). Other studies reported that M2 macrophages-expressing RANK were attracted by RANKL, produced by the tumor microenvironment, regulating the production of chemokines and the activation of T-regulatory lymphocytes, supporting the immunosuppressive state within the tumor microenvironment (Fujimura *et al.*, 2015).

Clinical applications of RANK-RANKL signaling inhibition

Identifying the key role of the RANK/RANKL pathway in bone remodeling opened up the possibility of developing novel agents able to reduce osteoclastic bone resorption by inhibiting RANKL.

Anti-RANKL drugs: The effect of RANKL inhibition was first evaluated in preclinical and clinical studies using Fc fusion proteins (Simonet *et al.*, 1997; Bekker *et al.*, 2001; Ominsky *et al.*, 2007). With OPG-Fc, the residues 22-194 of human OPG were fused to the Fc domain of human immunoglobulin G1 (IgG1), resulting in 200 times more active than full-length OPG, demonstrated in an *in vivo* mouse bone density assay (Bekker *et al.*, 2001; Body *et al.*, 2003; Ominsky *et al.*, 2007). Human RANK-Fc originated by fusing

the four extracellular CRDs of RANK (22-201 amino acids) and the Fc region of human IgG1. It selectively binds to RANKL but not to other TNF ligands and strongly inhibits bone resorption in preclinical models (Sordillo and Pearse, 2003). In both cases, the Fc domain allowed the dimerization required for high affinity to trimeric RANKL, facilitated large-scale purification through column chromatography, and dramatically increased biodistribution and pharmacokinetics of the recombinant proteins *in vivo* (Schwarz and Ritchlin, 2007).

Subsequent studies explored the effect of DNS, a fully human IgG2 monoclonal antibody that binds to human soluble and membrane RANKL with high affinity and specificity but fails to recognize rodent RANKL (Sordillo and Pearse, 2003; McClung *et al.*, 2006). Importantly, DNS had several advantages over the other molecules:

- 1) DNS does not bind to TRAIL or other TNF family members, including CD40 ligand (CD40L), TNF- α , and TNF- β (Sordillo and Pearse, 2003), whereas TRAIL binding has been observed with OPG-Fc (Emery *et al.*, 1998; Kostenuik *et al.*, 2009).
- 2) The fully monoclonal antibody has a half-life longer than the OPG-Fc and RANK-Fc constructs due to its molecular mass.
- 3) Neutralizing antibodies against OPG-Fc could have neutralizing effects on both the drug and natural OPG, which would not be expected with DNS (*Amgen Europe BV. Prolia™ (denosumab) European Union summary of product characteristics. <http://www.ema.europa.eu>*).
- 4) The binding of OPG-Fc to TRAIL, unlike DNS, could block its role in tumor surveillance (Wiley *et al.*, 1995).

In 2010 DNS was approved by the United States Food and Drug Administration (FDA) to treat osteoporosis and other diseases (Figure 6). According to data presented at the ENDO annual meeting, DNS is the second drug most used after alendronate for SREs.

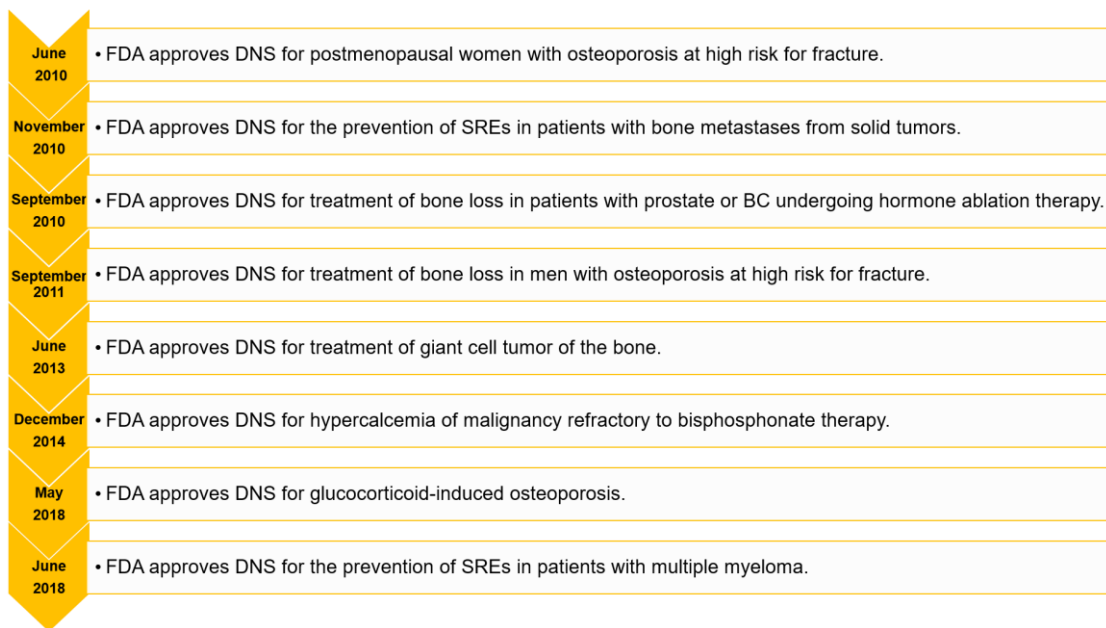


Figure 6. The approvals in clinics for denosumab by FDA. (<https://www.fda.gov/>)

Denosumab: clinical trials: According to ClinicalTrial.gov, until May 2022, DNS has been included in 276 clinical trials; 95 of them are involved patients with cancer and 32 with breast cancer. More than half of the clinical trials approved for DNS aimed to study its therapeutic potential in osteoporosis, bone metastases, and other bone-related diseases.

The efficacy of DNS in preventing vertebral and non-vertebral fractures in postmenopausal patients with osteoporosis has already been demonstrated for up to ten years, as reported in the FREEDOM clinical trial (Bell and Bell, 2011; Bone *et al.*, 2017) [ClinicalTrials.gov Identifier: NCT00089791]. Moreover, published results of phase III clinical trials confirmed that DNS was more effective than zoledronic acid in delaying time to first on-study skeletal-related events (SREs) and had a favorable safety in patients with bone metastasis from advanced cancers (Lipton *et al.*, 2012) [ClinicalTrials.gov Identifier: NCT00321464; NCT00321620; NCT00330759].

Furthermore, the ABC SG-18 trial [ClinicalTrials.gov Identifier: NCT00556374] investigated the effects of DNS in postmenopausal patients with early-stage HR⁺ BC treated with AIs adjuvant therapy. This study was the first trial showing that DNS can successfully prevent fractures by increasing bone mineral density in patients with BC. Moreover, it improved bone health, led to a moderate increase in DFS, and can be administered without added toxicity in postmenopausal women with BC receiving AIs (Gnant *et al.*, 2018). The D-CARE clinical trial [ClinicalTrials.gov Identifier:

NCT01077154] was designed to test whether DNS and the standard of care would increase bone metastasis-free survival (BMFS) in women with high-risk early BC. Despite preclinical evidence suggesting RANKL inhibition might delay bone metastasis or disease recurrence in patients with BC (Coleman *et al.*, 2020), in this clinical trial, DNS did not improve either BMFS or DFS in women with early-stage high-risk BC *versus* placebo. Furthermore, no subgroup (Table 5) was identified that experienced a BMFS or DFS improvement after DNS treatment (Coleman *et al.*, 2020). However, the effects of DNS on the incidence and timing of first fractures were similar to those observed in the ABCSG-18 study. Although both ABCSG-18 and D-CARE trials were carried out in an adjuvant setting, differences in patient cohorts and treatment schedules may explain the conflicting results. The patients enrolled in the D-CARE trial were unselected and heterogeneous in terms of tumor biology, RANK/RANKL expression levels, tumor type, or menopausal status. The high proportion of patients who withdrew their consent (>10%) and the lower number of patients to reach the endpoints efficiently might have biased the clinical outcome.

In a neoadjuvant setting GeparX trial (*GeparX (GBG 88) - GBG*) [ClinicalTrials.gov Identifier: NCT02682693], a multicenter, prospective, 2x2 randomized, open-label phase IIb study was performed. It examined the pathological complete response (pCR) to study the benefit of adding DNS to two different Paclitaxel regimens in combination with either Trastuzumab and Pertuzumab (for HER2⁺ patients) or Carboplatin (for TNBC patients) and an Epirubicin + Cyclophosphamide regimen (combined with HER2 inhibitors for HER2⁺ patients). Interestingly, although RANK expression resulted in a significantly higher pCR rate than RANK low, mainly because of the higher RANK frequency in ER⁻ tumors which are the more sensitive to chemotherapy due to their high rate of proliferation, the clinical benefit of DNS concerning RANK expression was not clear. Recently we published the data of the D-BEYOND trial (Gómez-Aleza *et al.*, 2020) [ClinicalTrials.gov Identifier: NCT01864798], a preoperative single-agent DNS for premenopausal early-stage BC patients. Despite both primary (tumor cell proliferation) and secondary endpoints were not observed, an increase of tumor-infiltrating lymphocytes and CD8⁺ T cells after RANK pathway inhibition was demonstrated. Moreover, higher RANK signaling activation in tumors and RANKL levels in serum at baseline predicted these immune-modulatory effects. Our results clinically support the use of DNS to lead luminal BC for immunotherapy. However, further explorative analyses in new clinical trials are necessary to decipher the best setting in which DNS has the potential benefit.

Breast cancer therapy and lymph node status
Neoadjuvant therapy and any lymph node status
Adjuvant therapy and lymph node-negative
Adjuvant therapy and lymph node-positive
Menopausal status
Premenopausal
Postmenopausal
Age (years)
<50
≥50
Hormone receptor status
ER or PR ⁺
ER or PR ⁻
HER2 status
HER2 ⁺
HER2 ⁻
Molecular subtypes of breast cancer
HR ⁺ and HER2 ⁺
HR ⁺ and HER2 ⁻
HR ⁻ and HER2 ⁺
HR ⁻ and HER2 ⁻

Table 5. Subgroups of patients enrolled in the D-CARE clinical trial. Data obtained from (Coleman *et al.*, 2020).

Patient-derived xenografts (PDXs)

Relevance of PDX models

In the last four decades, many studies have established basic methodology and systemic approaches for preclinical experiments both *in vivo* and *in vitro* (Shoemaker, Wolpert-DeFilippes and Venditti, 1984; Pagé, 1997). Human cancer-derived cell line panels represent the best characterized and most frequent collections of human cancer models to study the biology of cancer and test new treatments (Abaan *et al.*, 2013). The NCI-60 human tumor cell line panel is the collection of human cancer cell lines most commonly used in the last twenty years. A vast number of pharmacological, genomic, biochemical, and molecular datasets have been obtained (Shoemaker, 2006; Weinstein, 2012). However, these cells have important limitations in preclinical studies because they have been adapted to grow indefinitely in artificial culture conditions, suffering irreversible alterations in biological properties and lacking the predictive value (Gillet *et al.*, 2011). In addition, cell line models are not representative of the clinic's complex heterogeneity and

do not possess the tissue architecture of the original tumor (Yiu *et al.*, 2014; Davies, Wang and Zoubeidi, 2018). For all these reasons, establishing cancer cell lines is not an appropriate strategy for personalized medicine applications. Developing and characterizing better preclinical models is critical for translational cancer research. Novel models such as short-term primary cultures or organoids are being developed, although critical validation studies are still required before future applications in preclinical screening projects. For that, PDX models have emerged as valuable models for translational research to facilitate individualized medicine.

In the 1980s, the use of lung PDX models to test cytotoxic therapies showed the initial successful results (Fiebig *et al.*, 1985). Although in the first xenograft experiments, the success of engrafting rates was low (Naundorf *et al.*, 1992), currently, with newly-developed immunodeficient host mouse models (Shultz, Ishikawa and Greiner, 2007) and modified transplantation conditions, the success of transplant rate has increased (Al-Hajj *et al.*, 2003; Ding *et al.*, 2010; Shen *et al.*, 2013; Zhang and Lewis, 2013). Since their development, PDXs have been the standard model for preclinical research, expanding their use in translational research. Most PDXs show their donor tumor's main histologic and genetic characteristics and remain stable across passages. Moreover, PDX mouse models have emerged as a research platform to study tumor progression, drug response, and resistance, identify new biomarkers, and develop chemotherapeutic approaches for individual patients (Kelland, 2004; Hidalgo *et al.*, 2014). In recent years, there has been a renewed interest in developing PDX models for different tumor types (M. P. Kim *et al.*, 2009; Calles, Rubio-Viqueira and Hidalgo, 2013; Byrne *et al.*, 2017). Nowadays, several collections of characterized PDX models represent the complexity of clinical tumor heterogeneity and molecular diversity of human cancers (Conte *et al.*, 2019).

Despite the advantages of using PDX, fundamental limitations for their use in translational cancer research have been described (Hidalgo *et al.*, 2014; Kumar, Bajaj and Bodla, 2016): (I) Defining the best strategy of engraftment in mice (subcutaneous vs. orthotopic); (II) Delay between engraftment time in mice and clinical schedules for patient's treatment; (III) Limitation of the study in the involvement of the immune system or immunotherapy since the mice have partial (immune-compromised) or no immune system (immune-suppressed). (IV) Engraftment failure, which is still high for some tumor types; (V) Rapid replacement of human cancer stroma included in the tumor pieces by murine stroma; (VI) The use of xenografts is relatively time-consuming and expensive, raises animal ethical issues, and in some cases, the model is inappropriate as a likely

predictor of clinical outcome (Kelland, 2004; Hidalgo *et al.*, 2014; Cassidy, Caldas and Bruna, 2015).

Breast Cancer PDX models

The use of PDXs for the study of translational BC research becomes particularly important since these models can represent the full spectrum of heterogeneity of BC (Dobrolecki *et al.*, 2016). BC PDX models share most architectural, biological, and molecular features with their originating patient tumor sample, preserving the intra-tumor heterogeneity. These grafts maintain critical features of the original tumors, including histopathology, clinical markers, gene expression profiles, or copy number variants (Derose *et al.*, 2011; Eirew *et al.*, 2015).

ER⁺ subtype has historically been more difficult to grow in immune-deficient mice successfully. The observation that tumor take is significantly lower in ER⁺ than in ER⁻ tumors suggested that the hormone dependence of these tumors is the major limiting factor (Marangoni *et al.*, 2007; Cottu *et al.*, 2012; Moon *et al.*, 2015). However, the relationship between tumor characteristics and *in vivo* engraftment is controversial (Visonneau *et al.*, 1998; Derose *et al.*, 2011; Dobrolecki *et al.*, 2016; Gomez-Miragaya and González-Suárez, 2017).

PDXs have acquired high importance in preclinical trials and personalized medicine despite their limitations. For that, the scientific community involved in the field has generated consortiums such as EurOPDX (<https://www.europdx.eu/>) or PDXnet (<https://portal.pdxnetwork.org/>) to mutualize efforts and exchange models and expertise, allowing, among other things, to elucidate standard procedures and harmonize working practices.

OBJECTIVES

The overall objectives of this doctoral thesis are:

1. Investigate the biology of RANK signaling in human breast adenocarcinomas and its clinical implications by:

- 1.1 The analysis of RANK and RANKL protein expression patterns in large clinical collections of BC samples.
- 1.2 The study of putative associations between RANK and RANKL expression with clinic-pathological and survival parameters.
- 1.3 The functional modulation of RANK signaling in RANK⁺ BC PDXs.

2. Elucidate the role of RANKL in breast cancer by:

- 2.1 The evaluation of the functionality of RANKL (canonical RANKL1 and the non-canonical RANKL3 isoforms) on tumor cells.
- 2.2 The therapeutic effect of RANKL inhibition in RANKL⁺ BC cell lines and PDXs.

METHODS

Samples

Clinical samples: Tissue Microarrays (TMAs) staining and scoring

RANK and tmRANKL expressions were evaluated in TMAs from five different cohorts of BC patients. The *IDB* TMA (generated by A. Sierra (IDIBELL, Spain)) consists of 318 samples from patients diagnosed between 1989 and 2009 in three hospitals: 252 samples from the Catalan Institute of Oncology (ICO)-Hospital Duran i Reynals and the Hospital Universitari de Bellvitge (L'Hospitalet de Llobregat, Spain), 24 samples from the Consorci Hospitalari Parc Taulí (Sabadell, Spain), and 42 samples from ICO-Hospital Universitari Germans Trias i Pujol (Badalona, Spain). Clinic-pathologic information was available from 314 of them. The patients were between 24-88 years old at diagnosis, and 61% were diagnosed when in/older than their fifties (mean: 55 years). Follow-ups ranged from 8 to 146 months (mean: 76.6 months). Metastasis relapse occurred in 43.4% (138/318) of patients; of these, 84 patients (60.9%) developed brain metastasis, 47 (34.1%) lung metastasis, 54 (39.1%) liver metastasis, 40 (29.0%) non-regional lymph node metastasis and 89 (64.5%) bone metastasis. Just over half (56.6%, 180/318) of the patients had no metastatic progression after a minimum follow-up of 5 years. The *NPS* TMA is a well-characterized cohort of unselected early-stage (I-III) primary operable invasive BC from patients aged 70 years or younger enrolled in the Nottingham Tenovus Primary Breast Carcinoma Series between 1990 and 1997 (n=1.597) and managed by a uniform protocol. A subset of cases from this collection (n=298) was included in the *METABRIC* study (Curtis *et al.*, 2012), where gene expression data is available. Outcome data include survival status, survival time, cause of death, development, and time to locoregional recurrence and distant metastasis (DM). Treatments include chemotherapy (CMF) or endocrine therapy. At that time, patients with HER2⁺ tumors had no access to trastuzumab. HR⁺ status was defined as > 1% of tumor cells expressing estrogen receptors. HER2⁺ status was defined using immunohistochemistry as HER2 3+.

Two other collections of ER⁻ tumors were analyzed, the Nottingham *ER-NEGATIVE ONLY* cohort (1998 to 2006), which contains 396 samples, and the *CNIO TNBC*, a small collection of 66 patients with TNBC with 40-50% of relapse, generated by Dr. M. Quintela-Fandino (CNIO, Spain) and approved by the corresponding institutional review board (Hospital Universitario 12 de Octubre, number 11/137).

Histological grade was assessed based on the Nottingham Grading System (ELSTON and ELLIS, 1991; Rakha *et al.*, 2008). Other clinic-pathologic factors such as ER, PR, and/or HER2 expression, proliferation rate (Ki-67 expression or mitosis), vascular

invasion as well as patient age and survival analysis (BCSS, DFS, and DMFS) were analyzed before including the samples in the TMAs, prepared as previously described (Abd El-Rehim *et al.*, 2005). This work obtained ethics approval to use the human tissue samples by the Northwest-Greater Manchester Central Research Ethics Committee under the title Nottingham Health Science Biobank (NHSB), reference number 15/NW/0685. Before surgery, all individuals obtained informed consent to use their tissue materials in research.

RANK or tmRANKL staining was scored for intensity (on a scale of 0 to 3: 0 = no staining, 1 = weak, 2 = moderate, 3 = intense) and positive cell percentage (on a scale of 0 to 100%) within tumor cells or surrounding stroma for each TMA core sample. The sum of multiplying staining intensity by positive area is in the H-Score (H) value, ranging from 0 to 300. TMA cores were discarded whether the representative tissue was < 30% of the total TMA core area. Patients were stratified according to RANK or tmRANKL H-Score as being protein-positive (H-Score \geq 1) or protein-negative (H-Score = 0). As TMA samples are enriched in tumor cells, the stroma content was not always present or representative. Thus, we did not calculate an H-Score for the stroma. The total number of scorable samples for each of the collections and stainings is:

IDB: 318 samples (338 RANK_T, 307 RANK_S; 367 RANKL_T, 353 RANKL_S). *NPS*: 1597 samples (1149 RANK_T, 1097 RANK_S; 1089 RANKL_T, 984 RANKL_S). *METABRIC*: 298 samples (229 RANK_T, 229 RANK_S, 213 RANKL_T, 213 RANKL_S). *ER-NEGATIVE ONLY*: 359 RANK_T, 360 RANK_S; 300 RANKL_T, 293 RANKL_S. *CNIO TNBC*: 66 RANK_T, 66 RANK_S; 59 RANKL_T, 59 RANKL_S.

PDX samples. Generation

All human samples were obtained following institutional guidelines. Written informed consent for PDX generation was obtained from all subjects, and the study received approval from the corresponding institutional Ethics Committee by the declaration of Helsinki. IDB PDX (IDB-01, 02, 03, 04, 05, 06, 08, 09, 10, and 11) were generated by orthotopic transplantation of human fresh tumor tissue or injection of metastatic cancer cells isolated from pleural effusions into the cleared mammary fat pad of immune-deficient mice, as described previously (Derose *et al.*, 2011; Gómez-Miragaya *et al.*, 2017). The rest of the PDXs were obtained through collaboration with Dr. V. Serra and Dr. J Arribas (Vall d' Hebron Institute of Oncology), Dr. A. Welm (Huntsman Cancer Institute), Dr. MT Lewis (Baylor College of Medicine), Dr. A Bruna and C. Caldas (Cancer Research UK Cambridge Institute) and Dr. R. Clarke (Manchester Breast Centre). PDXs were maintained by consecutive rounds of transplantation with tumor pieces.

Cell lines. Lentiviral transduction, infection and culture

The human breast cancer cell lines KPL1, MCF7, MDA-MB-468, MDA-MB-231, and the murine breast cancer cell line E0771 were purchased from the American Type Culture Collection (ATCC). ATCC provides molecular authentication in support of their collection through their genomics, immunology, and proteomic cores, as described, by using DNA barcoding and species identification, quantitative gene expression, and transcriptomic analyses (ATCC Bulletin, 2010). The Genomic Unit from CNIO performed further authentication in all cell lines. The human cell lines were cultured in DMEM high glucose, supplemented with 10% fetal bovine serum (FBS, Gibco), 2 mM L-glutamine, 100 U/ml penicillin, and 100 µg/ml streptomycin (Gibco). The E0771 cell line was cultured in RPMI supplemented with 2 mM L-glutamine, 100 U/ml penicillin, 100 µg/ml streptomycin, and 1% HEPES (Sigma). All cells were cultured at 37 °C in the presence of 5% CO₂ in humidified incubators and tested for mycoplasma's absence.

To ectopically express mouse RANKL1 (NM_011613.3, ENSEMBL), human RANKL1 (NM_003701, ENSEMBL), and human RANKL3 (NM_033012.3, ENSEMBL), the corresponding genes (Mm30224, GC-N0083, GC-T2144 GeneCopoeia) were cloned in lentiviral vectors with different strength promoters to achieve different levels of *RANKL*/*RANKL* expression. The lentiviral vectors used were pwpi-GW (EF1a promoter with GFP, modified from the original Addgene plasmid #12254 to insert the gateway cassette by H. Kendrick and M. Smalley) and pSD69 (PGK promoter with puromycin selection, generously donated by Drs. S. Duss and M. Bentires-Alj) using Gateway® cloning system strategy, following manufacture's instructions (Katzen, 2007). The expression plasmids were verified by digestion with restriction enzymes and Sanger sequencing analyses. As controls, we used empty pwpi or pSD69-lacZ plasmids. Lentiviruses were prepared in HEK293T cells with packaging and envelope plasmids psPAX2 (12260, Addgene) and pMD2.G (12259, Addgene) by the calcium phosphate method. After 16 h, 25 mM HEPES was added. Virus-containing supernatants were centrifuged at 300 g for 5 min and filtered using 0.22 µm filters (Millipore). Human and mouse cell lines at roughly 40% confluence were infected in a ratio of 1:4 of the virus with a fresh growth medium and 8 µg/ml of polybrene (Millipore). Plates were centrifuged for 1 h at 600 g at 32 °C to improve infection, and infected cells were selected by sorter (pwpi) or puromycin (pSD69). Infected E0771 cells with pSD69 lentiviral particles were selected with 1 µg/ml puromycin starting 3 days after infection. Subsequently, puromycin was maintained at half of the selection concentration.

Mouse Models

Genetically modified mouse models and immune-deficient strains

All research involving animals has been performed at the IDIBELL and CNIO animal facility in compliance with protocols approved by the IDIBELL and CNIO Committee on Animal Care and following national and European Union regulations. Cages, bedding, food, and water were all autoclaved. Mice were kept in individually ventilated, and open cages, and food and water were provided ad libitum.

The athymic nude *Foxn1*^{nu} (nude) mice were obtained from Envigo. NOD scid gamma mouse (NOD.Cg-Prkdcscid;Il2rgtm1Wjl/SzJ) immune-deficient mice (NSG) and (C57BL/6J.OlaHsd) immune-competent mice (C57BL/6) were bred at IDIBELL and CNIO's animal facilities. RANK^{flox/flox} mice (MGI: 4415802) in the C57BL/6 background were provided by Dr. J. Penninger (Hanada *et al.*, 2009). When the Cre-recombinase is active in RANK^{flox/flox} mice, the loxP-flanked *Tnfrsf11a* exons 2 and 3 are excised, resulting in a frameshift, which leads to a premature stop codon. LysMCre mice (MGI: 1934631) in C57BL/6 were received from Dr. A. Nebreda. All the mice used for experiments were between 10 to 12 weeks old.

In vivo treatments

The treatments upon PDXs transplantation started when tumors reached 5 x 5 mm in diameter. Mice were randomized for Mock, human-RANKL (0.75 mg/Kg, twice per week; Amgen Inc), human-RANK-Fc (10 mg/Kg, 3 times per week; Amgen Inc), OPG (10 mg/Kg, 3 times per week, Amgen Inc), and DNS (10 mg/Kg, 3 times per week, XGEVA®). Docetaxel (20 mg/Kg, Hospira/Actavis, once per week) was administered once per week, together with dexamethasone (0.132 mg/Kg, Merck) to reduce the inflammation caused for the chemotherapy treatment. Upon human cell line transplantation, the treatments started when tumors reached 3 x 3 mm of diameter. Mice were randomized for Mock, DNS (10 mg/Kg, 3 times per week, XGEVA®). Upon E0771 cell line transplantation, the treatments started immediately after cell injection (day 0). Mice were randomized for Mock (isotype control rat IgG_{2a}, 200 µg, clone 2A3 from BioXCell) and anti-RANKL (α-RL) (200 µg, 3 times per week; clone IK22/5 from BioXCell). All the drugs were intraperitoneally injected, and the treatments were maintained until sacrifice. Tumor development was monitored by caliper measurement once per week. In all cases, mice were sacrificed before tumors exceeded 10 x 10 mm. Euthanasia was performed by CO₂ inhalation.

Tumor analyses

Tissue collection and processing

Tissue pieces were snap-frozen freshly upon collection and stored at -80 °C for further analysis. For histological samples, tissue was fixed overnight (o/n) in 37% formaldehyde. Then, the samples were gradually dehydrated by subsequent immersion in 70, 80, 96, and 100% ethanol, followed by incubation in xylol for 1 hour (h) to be finally embedded in paraffin. Blood samples were collected in Vacutainer blood collection tubes (BD) by intra-cardiac puncture at the endpoint and centrifuged for 90 seconds for 10,000 x g to obtain the serum.

Tissue cell isolation

As described previously (Smalley, 2010), single cells were isolated from tumors. Briefly, fresh tissues were mechanically dissected with a McIlwain tissue chopper and enzymatically digested with an appropriate medium (Dulbecco's modified Eagle's medium (DMEM) F-12, 0.3% collagenase A, 2.5 U/ml dispase, 20 mM HEPES, and penicillin/streptomycin) for 60 minutes (min) at 37 °C. Samples were washed with Leibowitz L15 medium/10% FBS between each step. Erythrocytes were eliminated by treating samples with hypotonic lysis buffer, and fibroblasts were excluded by incubation with DMEM F-12/10% FBS for 1 h at 37 °C. Single epithelial cells were isolated by treating with trypsin for 2 min at 37 °C. The cell suspension was finally filtered with 40- μ m filters and counted.

In vitro assays

For tumorsphere assays, primary tumorspheres were derived by plating 100.000 tumor cells/ml in 2 ml of medium, containing EGF (10 ng/ml), FGF (10 ng/ml), 1X B27, heparin (4 mg/ml), and 1% penicillin/streptomycin in ultra-low attachment plates (Corning® Costar®). After 14 days, single tumors were isolated by incubating with PBS/1 mM EDTA for 5 min and then with trypsin for 5 minutes at 37 °C and plated for secondary tumorsphere formation at a concentration of 10.000 cells/ml in triplicates. Tumorsphere number and size were analyzed 14 to 21 days later. The medium was weekly refreshed including the stimuli (RANKL (500 ng/ml; Amgen Inc) or RANK-Fc (1 μ g/ml; Amgen Inc)) as needed. For the analysis, three different pictures were taken for each well and the diameter of the tumorspheres was measured with the Fiji software (Schindelin *et al.*, 2012).

For RANKL stimulation, single tumor cells from PDXs were embedded in Corning™ Matrigel™ Growth Factor Reduced Basement Membrane Matrix (Corning™), plated in a medium containing 1X B27 (Gibco), EGF (10 ng/ml), hydrocortisone (0.5 µg/ml), insulin (5 µg/ml), cholera toxin (100 ng/ml), and 1% penicillin/streptomycin. Cells were stimulated, with mock or human-RANKL (500 ng/ml; Amgen Inc) for 24 h, and tumor cells were collected for gene expression analyses.

In vivo assays

For tumor-limiting dilution assays (LDAs), single tumor cells from PDXs were mixed 1:1 with Matrigel Basement Membrane (BD Biosciences) and orthotopically implanted in the inguinal mammary gland of NSG mice. Tumor development was monitored once per week for a maximum of 25 weeks. The tumor-initiating potential was defined as the ability to form palpable, growing tumors of ≥ 3 mm in diameter. Results were analyzed by Extreme Limiting Dilution Analysis (ELDA) (<http://bioinf.wehi.edu.au/software/limdil>; Hu, Y, and Smyth, GK, 2009).

Flow cytometry

Surface markers: Single tumor cells were resuspended and incubated in a blocking solution (human cells were blocked using buffer solution containing 2% FBS, 2 mM EDTA, and IgG blocking reagent (SIGMA) in PBS. Murine cells were blocked with 2% FBS, 2 mM EDTA, 2% Bovine Serum Albumin (BSA) and FcR blocking reagent (Miltenyi Biotec)) for 10 min on ice. Then, cells were labeled with fluorophore-conjugated antibodies against the different surface molecules indicated in Table 1 and incubated for 30 min on ice in the dark. For extracellular human RANKL staining, the cells were stained with a primary antibody mouse anti-human RANKL for 1 h on ice. Then, a secondary antibody, goat anti-mouse-AF647 (1:1500; Biolegend), was used. To discern between human and murine cells, the H2kD marker was used. The manufacturer's procedures assessed single tumor cells for their aldehyde dehydrogenase (ALDH) activity using the ALDEFLUOR™ Kit (STEMCELL Technologies). DAPI was used to exclude dead cells.

Intracellular RANKL: For intracellular human RANKL detection, single-cell suspensions were stimulated for 4 h at 37 °C in their medium containing brefeldin A (5 µg/ml). Then, cells were fixed using paraformaldehyde (PFA) 4% and permeabilized using Permeabilization Buffer (eBioscience). Next, the cells were stained as described in "extracellular markers". Zombie was used to exclude dead cells.

For the all flow cytometry assays, the gating strategy was based on “Fluorescence Minus One” controls. A population of 10.000 living cells was acquired. The Gallios flow cytometer (Beckman Coulter) was used. Data were analyzed using the FlowJo software. For sorting experiments, cells were sorted using the MoFlo XDP High-Speed Cell Sorter System (Beckman Coulter) at 25 psi with a 100- μ m tip.

Human markers					
Marker	Fluorophore-conjugated	Clone	Brand	Concentration/Dilution	Blocking buffer
CD24	PE	ML5	BD Pharmingen	1:1000	IgG blocking reagent
CD44	APC	G44-26	BD Pharmingen	1:1000	IgG blocking reagent
EpCAM	APC	EBA-1	BD Pharmingen	1:1000	IgG blocking reagent
CD10	PE-cyanine5	HI10a	BD Pharmingen	1:1000	IgG blocking reagent
CD49f	AF647	GoH3	BD Pharmingen	1:1000	IgG blocking reagent
CD133/1	PE	AC133	Miltenyi Biotec	1:1000	IgG blocking reagent
RANKL	-	M366	Amgen	4 μ g/mL	IgG blocking reagent
Mouse markers					
Marker	Fluorophore-conjugated	Clone	Brand	Concentration	Blocking buffer
H2kD	PE-cyanine7	SF1-1.1	BioLegend	1 μ g/mL	IgG blocking reagent
CD45	APC-cyanine7	30-F11	BioLegend	0.125 μ g/mL	FcR blocking reagent
CD11b	APC	M1/70	BioLegend	2.5 μ g/mL	FcR blocking reagent
F4/80	PE	BM8	BioLegend	1.25 μ g/mL	FcR blocking reagent
CD3	APC	145-2C11	BioLegend	3.2 μ g/mL	FcR blocking reagent
NK1.1	PE	PK136	BioLegend	2.5 μ g/mL	FcR blocking reagent
Viability Dyes					
Marker	Brand		Concentration/Dilution		
DAPI	ThermoFisher		2 μ g/mL		
Zombie Violet	BioLegend		1:1000		

Table 1: Antibodies employed for flow cytometry.

Enzyme-linked immunosorbent assay (ELISA)

Human or mouse soluble RANKL levels (sRANKL) were measured using the DuoSet enzyme-linked immune-sorbent assay kit (R&D System). Tartrate-resistant acid phosphatase 5b (TRAP 5b) activity was measured in mouse serum samples according to the manufacturer’s instructions (IDS).

Tissue histology and immunostaining

Three-micrometer sections were cut, and immunohistochemistry of human RANK and RANKL was performed as previously described (Gonzalez-Suarez *et al.*, 2010). Antigen retrieval was carried out with the Diva Decloaker solution (Biocare Medical) in a water bath at 90 °C during 14–16 h for RANK staining. Sodium citrate buffer (0.01 M, pH = 6) was used for RANKL staining. Anti-human RANK monoclonal antibody (Amgen, N-1H8; 5 μ g/ml) and anti-human RANKL monoclonal antibody (Amgen, M366; 1.85 μ g/ml) were

used. Protein block was done with TNB Blocking Buffer (PerkinElmer) for both. Antibodies were used to evaluate the proliferation and death anti-Ki67 (SP6, Abcam) and anti-cleaved caspase-3 (Asp175, Cell Signaling). VECTASTAIN® Elite® ABC-HRP Kit (Vector Laboratories) was used to amplify the RANK, RANKL, and cleaved caspase-3 staining. Images were analyzed with the FIJI software.

Quantitative Reverse Transcription Polymerase Chain Reaction (Q-RT-PCR)

Total RNA was isolated from cell lysates or tumor pieces using TRIzol (Thermo Fisher Scientific) or the Maxwell® RSC simply RNA Tissue Kit (Promega), following the manufacturer's instructions. For each sample, 1 µg of RNA was reverse-transcribed into cDNA using 200 U Superscript II plus random hexamer oligos, following the manufacturer's protocol (Invitrogen). Then, 20 ng/well of cDNA for each PDX sample was analyzed for *RANK* and *RANKL* expression relative to *PPIA* with LightCycler® 480 Probes Master (UPL) (Roche). The rest of the gene expression analysis was performed with a LightCycler® 480 thermocycler (Roche) using SYBR Green Master I (Roche). LightCycler® 480 thermocycler (Roche) was used in any case. Analysis was performed in triplicate. *PPIA* and *Hprt1* were used as a reference for human and murine genes, respectively. Primer sequences used are shown in Table 2.

Human primers			
Gene name	Forward primer (5'>3')	Reverse primer (5'>3')	Method
<i>PPIA</i>	ATGCTGGACCCAACACAAT	TCTTTCACCTTGCCAAACACC	UPL
<i>RANK</i>	GCAGGTGGCTTTGCAGAT	GCATTTAGAAGACATGTACTTTCTG	UPL
<i>RANKL</i>	TGATTCATGTAGGAGAATTAACAGG	GATGTGCTGTGATCCAACGA	UPL
<i>PPIA</i>	ATGGTCAACCCACCGTT	TCTGCTGTCTTTGGGACCTTG	Syber Green
<i>RANK</i>	ATCTGGGACGGTGTGTAAC	GGCCTTGCCTGTATCACAAA	Syber Green
<i>RANKL</i>	TGATTCATGTAGGAGAATTAACAGG	GATGTGCTGTGATCCAACGA	Syber Green
<i>RANKL isof1</i>	GAAGGAGTTCGAACCATGCG	CCCATCTCCTCCGAGCCAC	Syber Green
<i>RANKL isof3</i>	TCGGTACCATGGATCCTAATAGA	GACTCTCCAGAGTTGTGTCTTG	Syber Green
<i>BIRC3</i>	GGTAACAGTGATGATGTCAAATG	TAACTGGCTTGAACCTTGACG	Syber Green
<i>ICAM1</i>	AACTGACACCTTTGTTAGCCACCTC	CCCAGTGAAATGCAAACAGGAC	Syber Green
<i>CCL2</i>	AGGTGACTGGGCATTGAT	GCCTCCAGCATGAAAGTCT	Syber Green
<i>CXCL8</i>	CTGCGCCAACACAGAAATTA	CATCTGGCAACCCTACAACA	Syber Green
<i>RELB</i>	CCCGACCTCTCCTCACTCTC	CAGGGTGACCGTGCTCAG	Syber Green
<i>NFkB2</i>	GGCGGGCGTCTAAAATTCTG	TCCAGACCTGGGTTGTAGCA	Syber Green
<i>OPG</i>	GAAGGGCGCTACCTTGAGAT	GCAAACCTGATTTTCGCTCTGG	Syber Green
<i>LGR4</i>	CCTTCACCCAAGCGCTACAA	CTCAGCCCTCGAATGGCTTC	Syber Green

Murine primers			
Gene name	Forward primer (5'>3')	Reverse primer (5'>3')	Method
<i>Hprt1</i>	TCAGTCAACGGGGGACATAAA	GGGGCTGTACTGCTTAACCAG	Syber Green
<i>Rank</i>	AGAGGCATTATGAGCATCTCG	CAGACTTTATGCAGCAAGCA	Syber Green
<i>Rankl</i>	CCCACAATGTGTTGCAGTTC	TCCTGAGACTCCATGAAAACG	Syber Green
<i>Birc3</i>	AGAGAGGAGCAGATGGAGCA	TTTGTTCCTCCGGATTAGTGC	Syber Green
<i>Icam1</i>	AAGATGACCTGCAGACGGAA	ATAAGAGGCTGCCATCACGA	Syber Green
<i>Relb</i>	CCGTTTCCAGGAGCACAGAT	CAGGGTGACCGTGCTCAG	Syber Green
<i>Nfkb2</i>	CGGAAAGAAGTCGGAACCAGA	TAGGATAGGTCTTCCGGCCC	Syber Green
<i>Opg</i>	GAGACACAGCTCACAAAGAGCAA	GCTTTCACAGAGGTCAATGTCTT	Syber Green
<i>Lgr4</i>	GGACTTGAATTATAATAACTTGATGA	TACAAATGGATAGTTCTTAGCAGTGG	Syber Green

Table 2: Human and mouse primers employed for Q-RT-PCR.

Western Blot

Five hundred thousand cells extracted from PDX tumors were cultured in growth medium DMEM/F-12 (Gibco) containing 5% FBS, EGF (10 ng/ml), hydrocortisone (0.5 µg/ml), insulin (5 µg/ml), cholera toxin (100 ng/ml), and 1% penicillin/streptomycin o/n and changed to starving medium DMEM/F-12 containing 0.5% FBS, EGF 10 ng/ml, hydrocortisone 0.5 µg/ml, insulin 5 µg/ml, cholera toxin 100 ng/ml, and 1% penicillin/streptomycin) for 24 h. Then, cells were stimulated with RANKL (500 ng/ml; Amgen Inc) for 24 h. Extracts for immunoblots from PDXs were prepared with modified RIPA buffer (50 mM Tris pH 7.4, 150 mM NaCl, 1% Triton X-100, and 0.25% sodium deoxycholate) containing PhosSTOP and Complete protease inhibitor cocktail (Roche). Protein concentrations were determined with DC protein assay reagents (BIO-RAD). Forty µg of total protein were mixed with loading buffer (final concentrations: 62 mM Tris pH 6.8, 12% glycerol, 2.5% SDS) and 5% β-mercaptoethanol, heated at 95 °C for 5 min and then resolved by SDS-PAGE and transferred to Immobilon-P 0.45-µm membranes (Millipore). Primary and secondary antibodies are indicated in Table 3. Blots were incubated with horseradish peroxidase-conjugated secondary antibodies (DAKO) and developed with the ECL detection kit (Amersham Biosciences).

Human markers						
Protein	Primary antibody			Secondary antibody		
	Clone	Brand	Concentration /Dilution	Clone	Brand	Dilution
Phospho-NFκB p65 (Ser536)	93H1 Rabbit mAb	Cell Signaling	1:1000	P0448 Goat-anti Rabbit HRP	DAKO	1:2000
NFκB p65	D14E12 Rabbit mAb	Cell Signaling	1:1000	P0448 Goat-anti Rabbit HRP	DAKO	1:2000
Phospho-κBα (Ser32/36)	5A5 Mouse mAb	Cell Signaling	1:1000	P0260 Goat-anti Mouse HRP	DAKO	1:2000
κBα	L35A5 Mouse mAb	Cell Signaling	1:1000	P0260 Goat-anti Mouse HRP	DAKO	1:2000
RANKL	M366 Mouse mAb	Amgen	4 ug/ml	P0260 Goat-anti Mouse HRP	DAKO	1:2000
β-tubulin	ab21058 Rabbit mAb	Abcam	1:10.000	-	-	-

Table 3: Primary and secondary antibodies employed for Western Blot.

RNA sequencing

RNA sequencing was performed independently in three experiments. For the HCI-001 *in vivo* experiment, 24 h after the last treatments with mock or human-RANK-Fc, the mice were sacrificed, and the RNA from the single tumor cells was extracted with Maxwell® RSC simplyRNA Tissue Kit (Promega), following the manufacturer's instructions. RNA samples were processed according to the following Affymetrix protocols: GeneChip 3' IVT Plus Reagent Kit (P/N 703210) and Expression Wash, Stain, and Scan User Manual (P/N 702731) (Affymetrix Inc., Santa Clara, CA, USA). For the B3277, AB521-X3, and STG139-M5 *in vivo* experiments, 24 h after the last treatments with mock, human-RANKL, human-RANK-Fc and DNS, the mice were sacrificed, and the RNA from the single tumor cells was extracted with Maxwell® RSC simplyRNA Tissue Kit (Promega), following the manufacturer's instructions. For the cell lines *in vitro* experiment, on day 0 DNS (XGEVA®), α -RL (clone IK22/5 from BioXCell) and their controls (isotype control human IgG2 kappa (P00698, MBLI) for DNS and rat IgG2a (clone 2A3 from BioXCell) for α -RL) were immobilized in 6-well plates (1 μ g/ml/well). Plates were incubated o/n at 4°C. On day 1, 300.000 cells/well were seeded after removing the immobilization solution. Immediately, DNS, α -RL, and their respective controls were added (1 μ g/ml/well). The cells were incubated in their usual growth medium for 24 h at 37°C in the presence of 5% CO₂ in humidified incubators o/n. On day 2, cell lines were collected for RNA extraction using Maxwell® RSC simplyRNA Tissue Kit (Promega) following the manufacturer's instructions. Total RNA samples were processed with the "QuantSeq 3' mRNA-Seq Library Prep Kit (FWD) for Illumina" (Lexogen, Cat. No. 015) with RNA Quality scores of 7.7 on average (range 4.2-9.2). Library generation was initiated by reverse transcription with oligodT priming, and a second strand synthesis was performed from random primers. Libraries were completed by PCR. cDNA libraries were purified, applied to an Illumina flow cell for cluster generation, and sequenced on an Illumina instrument. Read adapters and poly-A tails were removed with BBDuk v38.38. Then, human reads were separated from mice ones using Xenome v1.0.1 (37), and those classified as "human", "both" or "ambiguous" were selected. Sequencing quality was checked with FastQC v0.11.7 and FastQ Screen v0.13.0. Reads were aligned to the human reference genome (GRCh38) with TopHat v2.0.10 using Bowtie v1.0.0.0 and Samtools v0.1.19.0 (-library-type fr-secondstrand), allowing three mismatches and twenty multihits. Read counts were obtained with HTSeq-count v0.6.1 (--stranded=yes) using the human gene annotation from GENCODE (gencode.v34.GRCh38.Ensembl100).

Statistical analyses

TMA statistical analyses were performed with the support of the IDIBELL and Nottingham University Statistical Assessment Services. Associations between IHC scores and clinic-pathological parameters were evaluated using the Pearson chi-square test or Fisher's exact test. BCSS, DMFS, and DFS were analyzed using the Kaplan–Meier function, Cox regression analyses, and the log-rank test. IHC H-score values were log-transformed as follows: $\log_{10}(X+1)$.

All statistical tests comparing paired values were done using the sign test or Student's paired samples t-test. Data analysis experiments were performed using GraphPad Prism software version 8. Regression analysis of the growth curves for *in vivo* treatments was performed *** $p < 0.001$, ** $p < 0.01$, * $p < 0.05$, *n.s.* not significant.

For RNA sequencing, differential gene expression was executed with DESeq2, using a filter of 1.5-fold change (FC) and a p-value (p) < 0.05 . Genes were ranked according to the \log_2 FC. GSEA Preranked v2.2.2 was used to perform gene set enrichment analysis (GSEA) for Hallmark, Biocarta, Reactome, and KEGG v7.1 signatures setting 1000 gene set permutations and a classic enrichment statistic. Only signatures with significant enrichment levels (FDR q-value < 0.25) were considered. GSEA is represented by a bubble matrix that illustrates the Normalized Enrichment Score (NES) and False Discovery Rate (FDR) values adjusted for multiple tests. While the intensity of the red color represents the number of genes involved, the higher the intensity, the greater the number of genes involved. The $-\log_{10}$ (p-value) of FDR is represented by the size of the circumference, the larger the circumference, the greater the p-value. Gene sets were classified according to Pearson's R coefficient generated by public gene set databases.

RESULTS

CHAPTER 1

RANK is an independent biomarker of poor prognosis in estrogen receptor-negative breast cancer and a therapeutic target in patient-derived xenografts

Results from this chapter are deposited at: Biorxiv (Ciscar *et al.* 2021)

<https://doi.org/10.1101/2021.12.13.470911>

Abstract

Despite preclinical solid data, the therapeutic benefit of the RANKL inhibitor denosumab in BC patients beyond its bone-related effects is unclear. Here, we investigated the prognostic value of the RANK expression and its functionality in human BC. We analyzed RANK and RANKL expression in more than 2300 BC cases from four independent cohorts. We confirmed that RANK is more frequently expressed in ER⁻ tumors, but it is also found in a subset of ER⁺ tumors. In ER⁻ BC, RANK expression was independently associated with poor outcome, especially in postmenopausal patients and those who received adjuvant chemotherapy. Gene expression analyses unraveled distinct biology associated with RANK about ER expression and menopause and evidenced enhanced RANK activation in ER⁻ postmenopausal tumors, together with regulation of metabolic pathways. Functional studies and transcriptomic analyses in ER⁻ RANK⁺ patients-derived orthoxenografts demonstrated that activation of the RANK signaling pathway promotes tumor cell proliferation and stemness and regulates multiple biological processes, including tumor immune surveillance and metabolism. Our results indicate that RANK expression is an independent poor prognosis biomarker in postmenopausal ER⁻ BC patients and supports using RANK pathway inhibitors in combination with chemotherapy in ER⁻ BC.

Contributions

The contribution of the PhD candidate Marina Císcar to this work has been as follows:

- H-Score analysis of IHC (RANK and RANKL) in clinical samples (n=2377 samples), interpretation of the results, data assembly for presentation in main Figures 1.1, 1.2, 1.3., and Supplementary Figures 1.1, 1.2, 1.3, 1.4.
- Analysis of RNA-seq data (*METABRIC* dataset and *in vivo* experiment of PDXs implanted in NSG mice), interpretation of gene expression results, and data assembly for presentation in main Figure 1.6 and Supplementary Figure 1.7.
- Results interpretation, figure drafting, editing, and manuscript writing.

1.1. RANK expression in tumor cells associates with ER⁻ tumors and predicts poor survival in postmenopausal patients

To evaluate the potential of RANK and RANKL as prognosis biomarkers in BC, we analyzed the expression of both proteins in two independent TMA collections containing all BC subtypes: the *IDIBELL (IDB)* collection (n=404) (Martínez-Aranda *et al.*, 2015) and the *Nottingham Primary Series (NPS)* (n=1895 samples) (Green *et al.*, 2013); a subset of *NPS* samples (n=298) were included in the Molecular Taxonomy of Breast Cancer International Consortium (*METABRIC*) (Curtis *et al.*, 2012). RANK protein expression was observed in the tumor compartment in 18.3% of the samples in the *IDB* collection and 5.7% of the *NPS* (excluding *METABRIC* samples) (Fig. 1.1a-b). RANK expression was also detected in the stroma of approximately half of the cases, 55% and 46.3% from *IDB* and *NPS* cohorts, respectively (Fig. 1.1a-b). Tumor expression of tmRANKL was found in only 4.6% (*IDB*) and 3.5% (*NPS*) of adenocarcinomas, in agreement with previous observations (Gonzalez-Suarez *et al.*, 2010; Pfitzner *et al.*, 2014) and was rarely detected in the stroma (< 3%) (Figure 1.1a-b). Fig. S1.1a shows the H-Score (H) for samples expressing RANK or tmRANKL in the tumor compartment. RANK expression was significantly associated with ER/PR negativity and TNBC subtype, but not HER2, age, tumor size, or stage in both cohorts. Furthermore, in the *NPS* collection, RANK expression was also associated with a higher mitosis rate and grade (Fig. 1.1c; Table S1.1). The low frequency of tmRANKL hindered associations with clinic-pathologic parameters (RANKL expression associated with younger patients and low histological grade only in *NPS* collection) (Fig. S1.1b; Table S1.1). Similar expression patterns for RANK and RANKL were found in the *METABRIC* collection (Fig. S1.1c-e). Patients with RANK⁺ tumors (H > 0) from *IDB* and *NPS* tended to have a poorer distant metastasis-free survival (DMFS) compared to those with RANK⁻ tumors (H = 0) (Fig. 1.1d, Table S1.1) and worse 5-year BCSS (Fig. 1.1d). Interestingly, RANK positivity was associated with poor survival (DMFS and BCSS) in postmenopausal, but not in premenopausal patients from both collections (Fig. 1.1d, Table S1.1). In univariate survival analysis, patients in the *NPS* with RANK expression had a shorter 5-year BCSS compared to patients with no RANK expression, and this association was maintained in multivariate Cox regression analyses when ER, tumor grade, stage, and size were considered (Table S1.1). In postmenopausal, but not premenopausal women, RANK expression was associated with worse BCSS in univariate analyses, and worse BCSS and DMFS in multivariate analyses (Table S1.1). Tumor grade and stage, but not ER or tumor size, reached significance for all survival outcomes (Table S1.1). Altogether, our results confirm that RANK expression associates with ER⁻/PR⁻ tumors and TNBC subtype and

demonstrate that RANK expression is an independent biomarker of poor prognosis in postmenopausal BC patients.

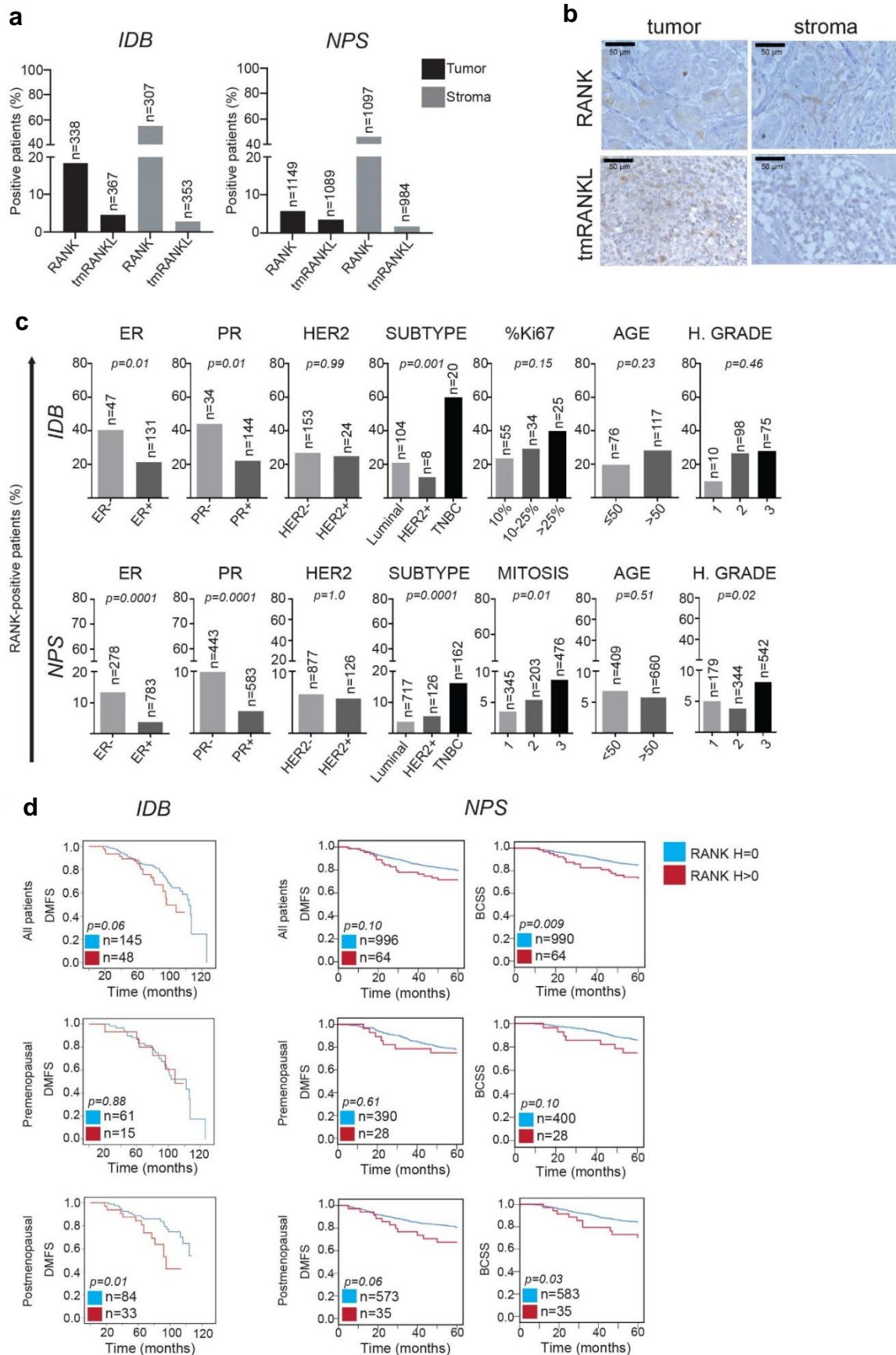


Figure 1. 1. RANK is expressed in tumor and stromal cells of human BC, and its expression in tumor cells associates with poor survival in postmenopausal patients. (a) Percentage of patients expressing tumor and stromal RANK or tmRANKL ($H > 0$) in BC samples from *IDB* and *NPS* collections. The total number of patients scored for RANK, and tmRANKL expression is indicated. **(b)** Representative images showing RANK and tmRANKL protein expression in tumor and stromal cells in human BC determined by IHC. **(c)** Percentage of BC patients with RANK⁺ tumor according to the indicated clinic-pathologic parameters in the *IDB* and *NPS* cohorts. The total number of patients analyzed per parameter, and p-values (calculated using the Pearson's chi-square test (Exact Sig. 2-Side)) are indicated. **(d)** DMFS and BCSS according to RANK expression (RANK⁻ ($H = 0$) or RANK⁺ ($H > 0$)) in all patients of the *IDB* and *NPS* collections and classified by menopause. The total number of patients analyzed per parameter and p-values (calculated using the Log-rank test (Mantel-Cox)) are indicated.

1.2. In ER⁺ BC, RANK expression does not associate with survival, and tmRANKL expression associates with younger patients

Given the different biology of ER⁺ and ER⁻ BC, next, we aimed to address the clinic-pathologic significance of RANK in each subgroup. In the ER⁺ subsets, RANK in tumor cells was detected in 21.3% (*IDB*) and 3.7% (*NPS*) of samples, whereas tmRANKL only in 5.5% (*IDB*) and 3.9% (*NPS*) (Fig. 1.2a). RANK (73.2% in *IDB* and 51.1% in *NPS*), but not tmRANKL (2% in *IDB* and *NPS*), was frequently found in the stroma (Fig. 1.2a). Tumor RANK expression in the ER⁺ subset of the *NPS* did not associate with any of the clinic-pathologic factors or survival parameters analyzed in neither premenopausal nor postmenopausal patients (Fig. 1.2b; Table S1.1). Tumor tmRANKL expression was associated with young women in the ER⁺ subset of *NPS* (Fig. S1.2a), and its expression correlated with better DFS (Fig. S1.2b).

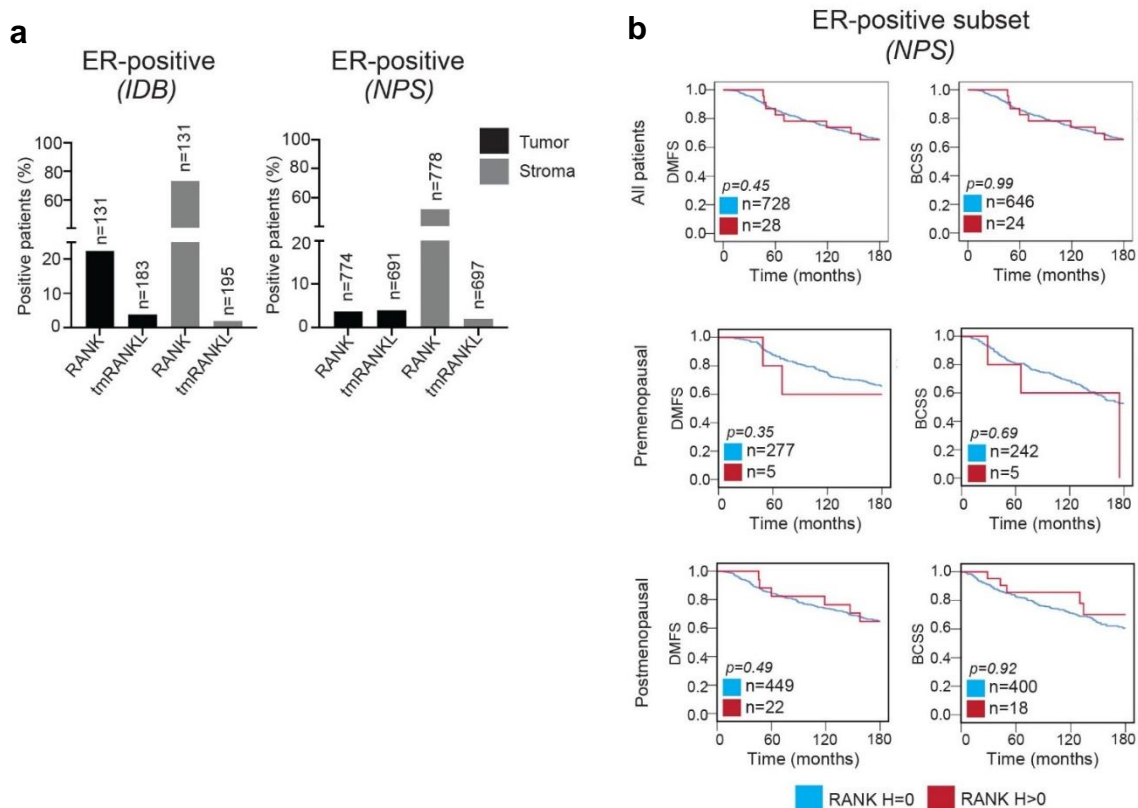


Fig. 1.2. RANK tumor expression is not associated with survival in ER⁺ BC. (a) Percentage of tumor and stromal RANK or tmRANKL ($H > 0$) in the BC ER⁺ subset from the *IDB* and *NPS* collections. The total number of patients who scored for RANK and tmRANKL proteins is indicated. **(b)** BCSS and DMFS in the ER⁺ subset from the *NPS* according to RANK expression in all patients, premenopausal and postmenopausal (15 years of follow-up). The total number of patients analyzed per parameter and p-values (calculated using the Log-rank test (Mantel-Cox)) are indicated.

1.3. RANK expression in ER⁻ tumors associates with poor response to chemotherapy and poor survival in postmenopausal patients

In the ER⁻ subsets, RANK was expressed in the tumor compartment in 40.4% and 13% of the samples from *IDB* and *NPS* collections, respectively, and frequently found in the stroma (69.2% (*IDB*) and 43.7% (*NPS*)) (Fig. 1.3a). Again, tmRANKL was rarely seen in the tumor or stroma of ER⁻ tumor samples (Fig. 1.3a). These RANK and RANKL expression patterns were confirmed in two additional and more recent collections of ER⁻ tumors: In the *ER-NEGATIVE ONLY* collection (396 ER⁻ tumors), tumor RANK and tmRANKL expression were found in 34% and 0.33% of samples, respectively (Fig. 1.3a). In the *TNBC* collection (n=66), 30.3% of tumor samples were positive for RANK and 3.38% for tmRANKL; in the stroma, RANK (65.2%), but not tmRANKL (6.7%) was commonly expressed (Fig. 1.3a). Tumor RANK expression in ER⁻ tumors was not associated with any clinic-pathologic factors analyzed (Fig. S1.3a, Table S1.1) but tended to associate with worse DMFS and BCSS in the *NPS* ER⁻ subset (Fig. 1.3b). However, when menopausal status was considered, RANK expression was associated with poorer survival at 5 years in the ER⁻ subset from postmenopausal, but not premenopausal, patients; the association of RANK with poor prognosis in this cohort was observed up to 15/20 years (Fig. 1.3b, Table S1.1). As the frequency of RANK positivity in the *NPS* collection was low (13%), we confirmed this finding in the *ER-NEGATIVE ONLY* collection, where RANK was detected in 34% of the samples (Fig. 1.3a). Importantly, in the *ER-NEGATIVE ONLY* collection, patients with RANK⁺ tumors showed a significantly poorer 10-year survival compared to those with RANK⁻ tumors. RANK association with worse survival was observed only in postmenopausal women (Fig. 1.3c, Table S1.1). Cox regression analyses demonstrated that RANK expression was an independent factor of worse 10-years DMFS and DFS in all ER⁻ patients and in postmenopausal patients, but not in premenopausal women from the *ER-NEGATIVE ONLY* collection. The tumor stage was independently associated with the three survival parameters analyzed (Table S1.1). Moreover, patients with ER⁻ RANK-expressing tumors showed poorer survival after adjuvant chemotherapy than those lacking RANK. In contrast, no survival differences associated with RANK were found in the absence of chemotherapy (Fig. 1.3d, Table S1.1). Similarly, in the *CNIO TNBC* collection (Fig.

S1.3b), tumors expressing RANK tended to have worse survival in patients receiving chemotherapy, particularly in the regimens containing taxanes (Fig. S1.3b, Table S1.1). The low frequency of tumor tmRANKL positivity in the ER⁻ subsets prevented reliable associations with any parameter (Fig. S1.3c-d). These results point out the importance of RANK expression in ER⁻ tumors as a biomarker of poor prognosis, mainly in postmenopausal ER⁻ BC.

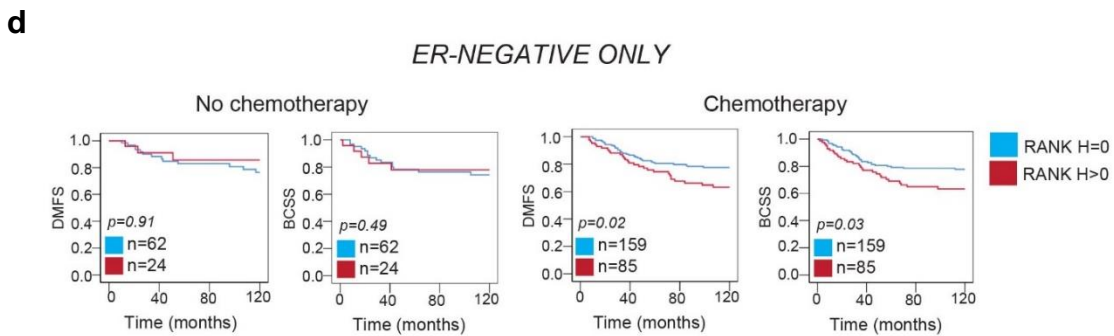
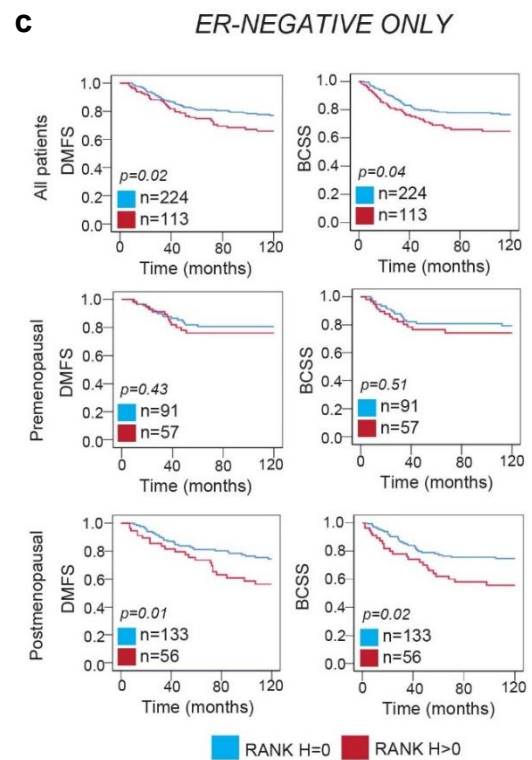
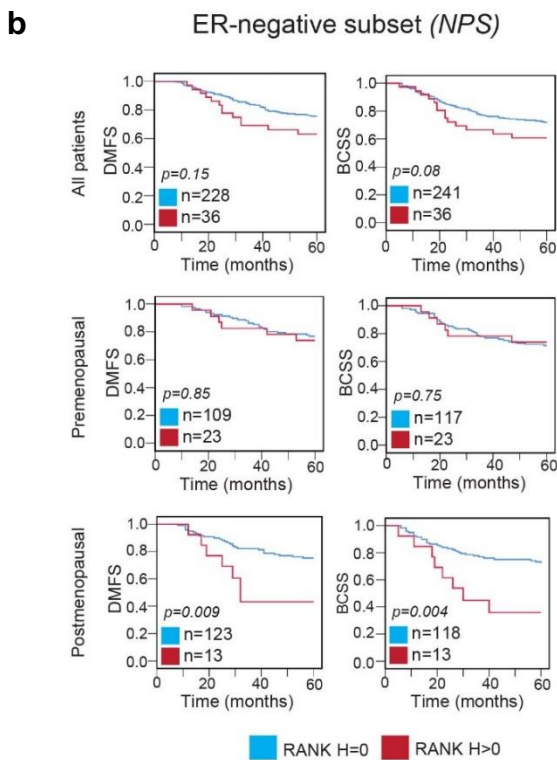
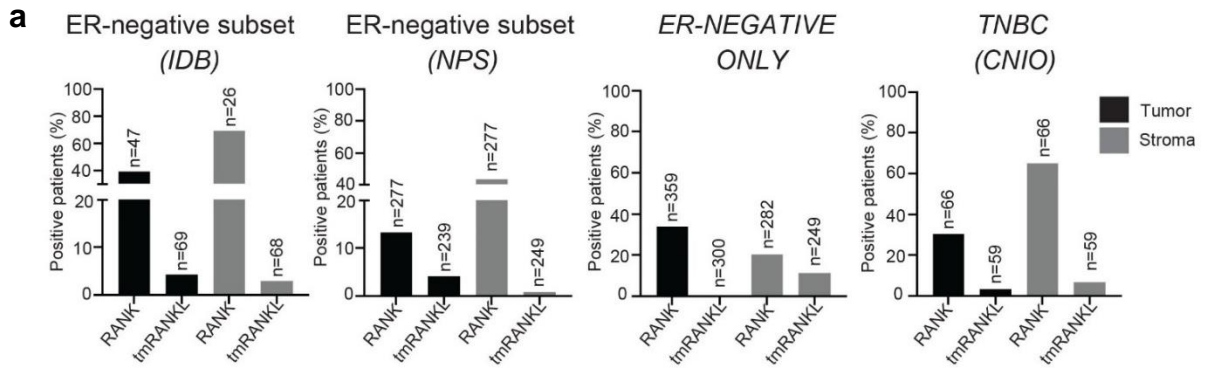


Fig. 1.3. RANK tumor expression is associated with reduced survival in postmenopausal patients with ER⁻ tumors and poor response to chemotherapy. (a) Percentage of patients expressing tumor and stromal RANK or tmRANKL ($H > 0$) in the ER⁻ subset from the *IDB* and *NPS* collections and in two additional cohorts containing ER⁻ samples exclusively: *ER-NEGATIVE ONLY* (Nottingham) and *TNBC* (CNIO). The total number of patients scored for RANK and tmRANKL protein expression is indicated. (b) DMFS and BCSS according to RANK expression in the ER⁻ subset from NPS (5 years of follow-up) in all patients and premenopausal and postmenopausal patients. (c) DMFS and BCSS according to RANK expression in all patients, premenopausal and postmenopausal patients with ER⁻ tumors in *ER-NEGATIVE ONLY* collection (10 years of follow-up). (d) DMFS and BCSS in the *ER-NEGATIVE ONLY* collection after chemotherapy or not, according to RANK expression (10 years of follow-up). (b, c, d) The total number of patients analyzed per parameter and *p-values* (calculated using the Log-rank test (Mantel-Cox)) are indicated.

1.4. Distinct RANK biology according to ER expression and menopause

Our previous results demonstrate that RANK expression in tumor cells is a biomarker of poor prognosis in ER⁻ but not in ER⁺ tumors, and postmenopausal, but not in premenopausal patients, suggesting putative differences in RANK tumor biology in both tumor subtypes. Thanks to the availability of gene expression data from the *METABRIC* dataset, we analyzed pathways differentially regulated between RANK⁺ and RANK⁻ tumors in ER⁺ and ER⁻ BC and in pre- and postmenopausal patients. Results from GSEA revealed 67 pathways associated with RANK protein expression in ER⁺ tumors and 17 in ER⁻ tumors ($FDR < 0.25$), with no overlap between them. Several pathways related to metabolism ($NES < 0$) and immunity ($NES > 0$) are associated with RANK in ER⁻ tumors (Fig. S1.4 and Table S1.2). In ER⁺ tumors, several pathways related to DNA replication and gene transcription were negatively associated with RANK expression ($NES < 0$) (Fig. S1.4a and Table S1.2). No common pathways related to RANK expression ($FDR < 0.25$) were observed between tumors from premenopausal and postmenopausal patients. Importantly, RANK expression in postmenopausal tumors positively associated ($NES > 0$) with multiple pathways related to TNF/NF- κ B signaling, including the RANKL pathway itself (Fig. S1.4 and Table S1.2), suggesting that RANK signaling is more active in BC after menopause, as happens in the bone (Streicher *et al.*, 2017). In ER⁻ premenopausal tumors, RANK only associated with two pathways, FGFR2, and hedgehog signaling; meanwhile, in ER⁻ postmenopausal RANK expression positively associated with 21 pathways, including TNF/NF- κ B signaling pathways and immune pathways, and negative associations with multiple metabolic pathways, insulin/IGF1 signaling, fatty acid metabolism, and mTOR were found (Fig. S1.4 and Table S1.2). Together, these results highlight the different biology of RANK signaling according to ER status and menopause and suggest that enhanced RANK signaling in postmenopausal tumors and regulation of tumor cell metabolism may contribute to the association of RANK expression with poor prognosis in ER⁻ postmenopausal tumors.

1.5. RANK is expressed and functional in ER⁻ BC PDXs

Our results support the relevance of RANK expression as a poor prognosis factor in human BC, particularly in ER⁻ disease, and response to chemotherapy. Despite encouraging results in mouse models (Yoldi *et al.*, 2016), direct demonstration of the functionality of RANK signaling in human BC is lacking. To this end, we analyzed human *RANK* and *RANKL* gene expression in several collections of BC PDXs (Derose *et al.*, 2011; Zhang and Lewis, 2013; Bruna *et al.*, 2016; Eyre *et al.*, 2016; Gómez-Miragaya *et al.*, 2017; Gris-Oliver *et al.*, 2020) derived from human BC (Fig. 1.4a). *RANK* mRNA was detected in all models tested, with expression levels varying 10-fold between different models. Tumors with the highest levels of *RANK* mRNA expression were found in the ER⁻ tumors, in accordance with clinical findings (Santini, Schiavon, *et al.*, 2011). Meanwhile, *RANKL* gene expression was low or undetectable in most PDX models, with some exceptions (Fig. 1.4a). RANK protein expression was found in 40% of ER⁻ and 14.3% of ER⁺ from the 76 PDX analyzed, recapitulating the clinical patterns (Fig. 1.4b, Table S1.3). We detected RANK protein expression in some of the selected PDXs (#) with high or intermediate *RANK* mRNA levels, whereas tmRANKL protein was only detected in HCI-001 and STG139-M (Fig. 1.4c). Next, we analyzed NF- κ B activation upon RANKL stimulation *in vitro*, as it is the main pathway regulated by RANK in BC, and we found it associated with RANK⁺ tumors (Fig. S1.4). Evident enhanced phosphorylation of I κ B α and/or p65 after RANKL treatment was observed only in the models AB521-X, BCM-3277, and STG139-M (Fig. 1.4d, Fig. S1.5a). Gene expression analyses of several RANK/NF- κ B targets confirmed RANK pathway activation in BCM-3277, AB521-X, and STG139-M (Fig. S1.5b). Although BCM-3277 was derived from a human luminal tumor, ER expression was not detected in the PDX, and PAM50 analyses classified it as “basal-like”. Analyses of the surface markers CD44, CD24, EpCAM, CD133, and CD10 confirmed similar expression patterns to those reported in BC PDXs (Fig. S1.5c) (Gómez-Miragaya *et al.*, 2017).

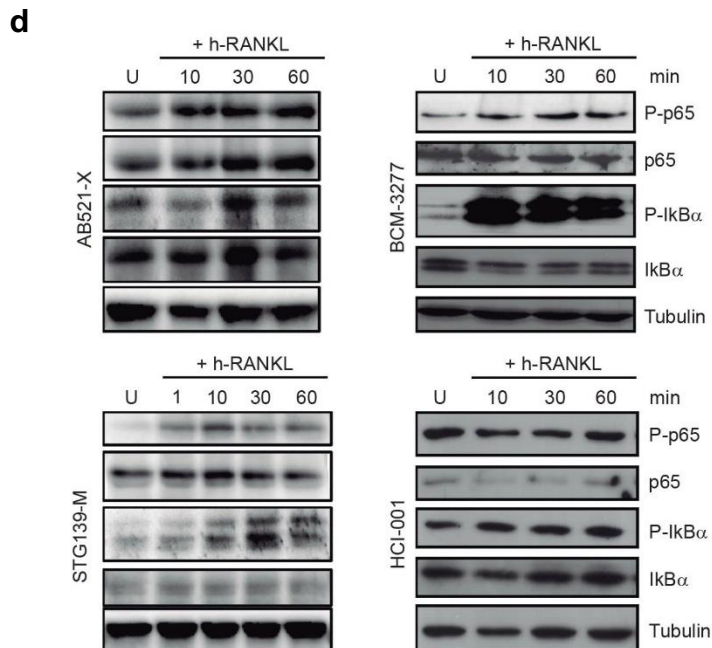
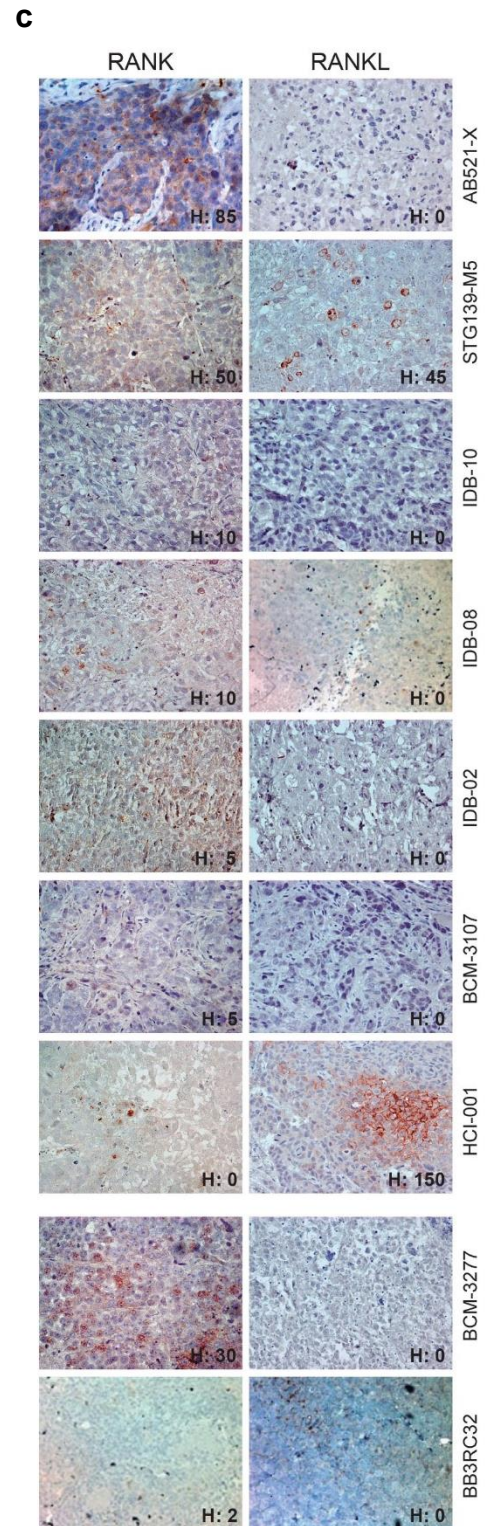
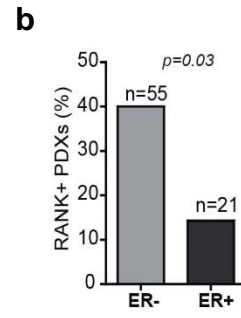
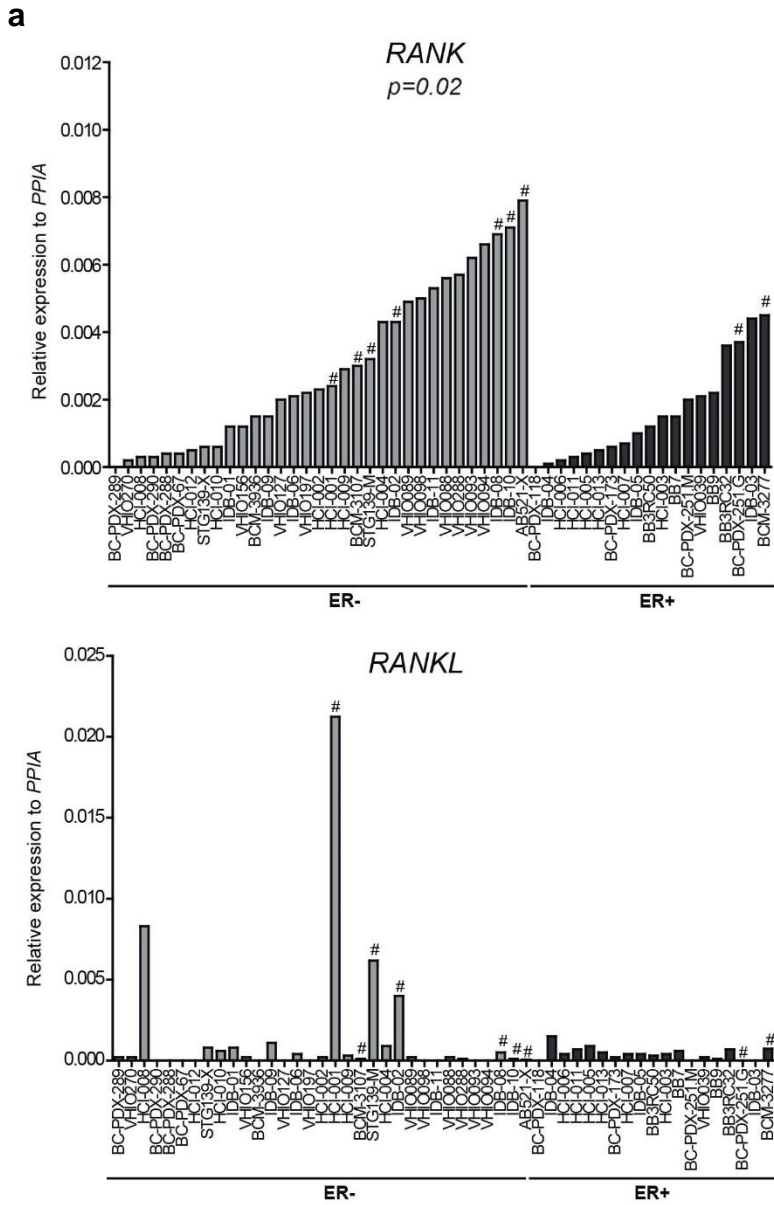


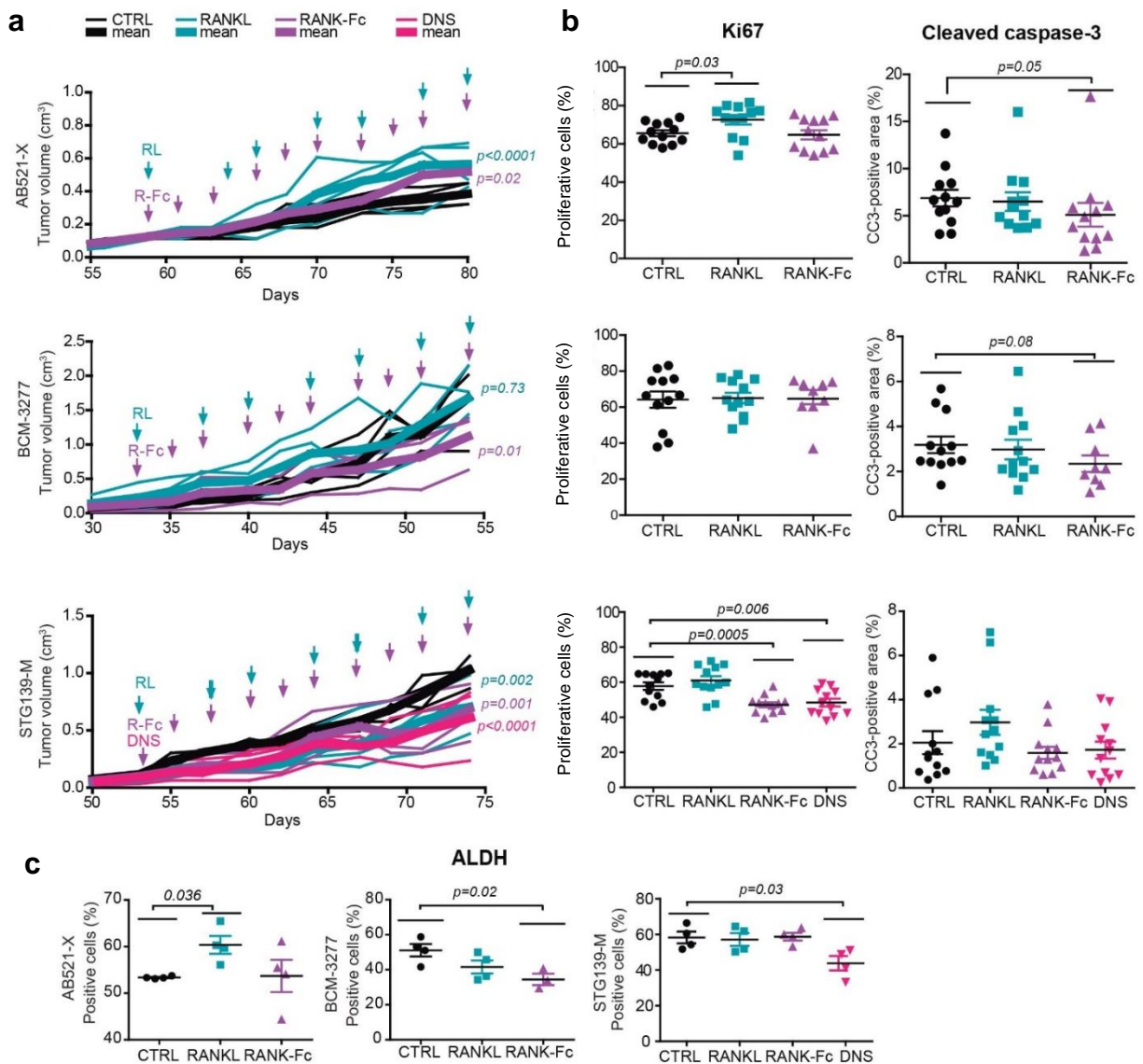
Fig. 1.4. RANK is expressed and functional in BC PDXs. (a) *RANK* and *RANKL* mRNA expression levels relative to *PPIA* in the indicated BC PDXs organized according to ER status in the human tumor of origin and *RANK* mRNA expression. The two-tailed t-student test evaluated the *RANK/RANKL* differential expression between ER⁻ and ER⁺ BC PDXs. # indicates models where *RANK* and *RANKL* expression were analyzed by IHC. (b) Percentage of PDXs-expressing *RANK* protein according to ER expression. A total number of independent PDXs analyzed is shown. P-value was calculated using a two-tailed t-student test. (c) Representative images of *RANK* and *RANKL* protein expression in BC PDXs detected by IHC. H-Score (H) of the models (and not the picture) is shown. A total of 3-5 independent tumors per PDX were scored for *RANK*. Photos are ordered according to *RANK* mRNA expression levels and subtype in the human samples of origin. (d) Western blot analyses of P-p65, P-IK β , and the corresponding total proteins after (1), 10, 30, and 60 minutes (min) upon *RANKL* stimulation in the indicated PDXs. Tubulin was used as a loading control.

1.6. RANK pathway promotes tumor cell proliferation and stemness in ER⁻ BC PDXs

Next, we evaluated the functional consequences of *RANK* pathway modulation *in vivo* in three independent BC PDX models responsive to *RANKL*. NSG mice were randomized for treatment with human *RANKL*, the inhibitor *RANK-Fc*, DNS (in the STG139-M model as it expresses human *RANKL*), or mock treatment (controls) for 4 weeks (Fig. S1.6a). Mice treated with *RANKL* showed increased levels of the bone remodeling marker, TRAP 5b, while those treated with *RANK-Fc*, which binds mouse and human *RANKL*, had lower TRAP 5b (Fig. S1.6b). *RANKL* inhibition slightly attenuated tumor growth, while *RANKL* stimulation modestly increased tumor growth in AB521-X (Fig. 1.5a). *RANKL* treatment increased tumor cell proliferation (ki-67) in the model AB521-X, which had the highest *RANK* protein expression. Conversely, inhibition of *RANKL* by *RANK-Fc* or denosumab decreased tumor cell proliferation in the STG139-M model and not in the BCM-3277 model (Fig. 1.5b, Fig. S1.6c). A slight decrease in tumor cell apoptosis (cleaved caspase 3) after *RANKL* inhibition was observed in AB521-X (Fig. 1.5b, Fig. S1.6c). An increase in ALDH activity after *RANKL* treatment was observed in the AB521-X model, and *RANKL* inhibition reduced ALDH activity in the other two models (Fig. 1.5c), in accordance with *RANK* signaling enhancing BC stemness (Yoldi *et al.*, 2016). *RANKL* treatment led to an increase in tumorsphere size in the AB521-X model. In contrast, its inhibition reduced the number of secondary tumorspheres in the AB521-X and the BCM-3277 models (Fig. 1.5d, Fig. S1.6d), supporting a decrease in BC stemness. STG139-M tumor cells did not grow as tumorspheres when plated in suspension. Together, these results demonstrate the functionality of *RANK* signaling in human BC and suggest that inhibition of *RANK* signaling in human BC can reduce tumor cell proliferation and stemness.

1.7. RANKL inhibitors improve the response to docetaxel in ER⁻ BC PDXs

Clinical analyses (Fig. 3d and Fig. S3b) evidenced that RANK expression in ER⁻ tumors were associated with poor survival after chemotherapy. To directly test whether RANK pathway inhibitors could improve response to chemotherapy, tumor-bearing NSG mice were randomized for treatment with docetaxel alone or combined with RANK-Fc or denosumab (for STG139-M) (Gomez-Miragaya and González-Suárez, 2017): docetaxel treatment was interrupted when tumor diameter decreased below 3 mm. The three PDX models were sensitive to docetaxel, but the increased benefit was observed when adding RANKL inhibitors (Fig. 5e and Fig. S6e). In the STG139-M model, docetaxel treatment could not be interrupted in some tumors, and they rapidly regrew even in the presence of docetaxel. In contrast, when denosumab or RANK-Fc were added to docetaxel, all tumors disappeared, and no tumor relapses were observed even 60 days after interruption of docetaxel treatment (Fig. 5e). Together, these results demonstrate that inhibition of RANK signaling can reduce tumor cell proliferation and stemness and improve response to chemotherapy in ER⁻ BC patients.



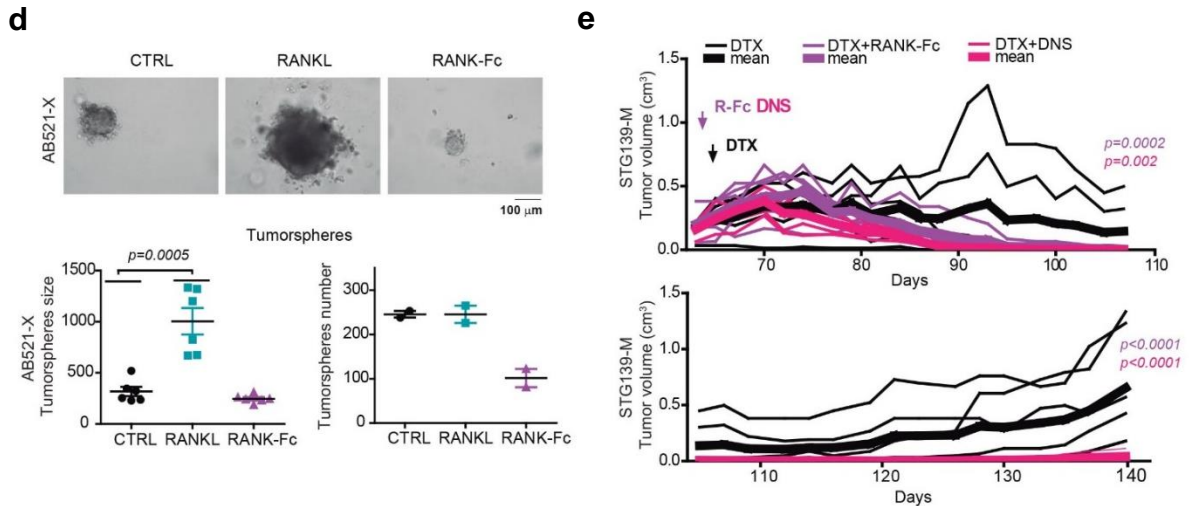
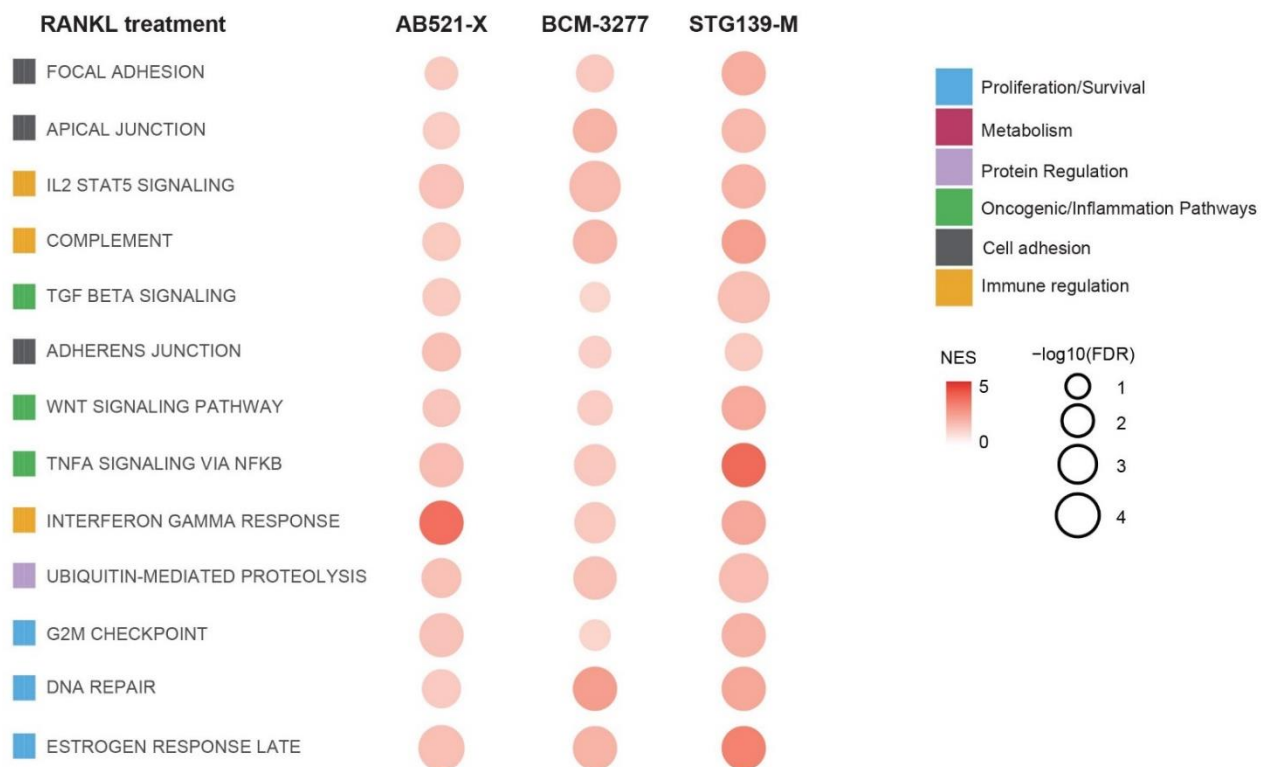


Fig. 1.5. RANK signaling regulates tumor cell proliferation, stemness, and chemotherapy response in BC PDXs.(a) Tumor growth curves ($(\pi \times \text{length} \times \text{width}^2)/6$) of the indicated PDXs after treatment with RANKL, RANK-Fc, DNS, or CTRL treatments. Treatment started as indicated by the arrows following the scheme in Fig. S1.6a. Each thin curve represents one single tumor, and each thick curve represents the mean of all tumors implanted. Linear regression analysis was performed, and a two-tailed p-value is shown. (b) Percentage of cells positive for Ki-67 and the cleaved caspase-3 positive area in tumors of the indicated PDXs collected 24 hours after the last treatment (Fig. S1.6a). Each dot represents one picture. Three representative pictures per tumor were quantified, and at least 3-to 4 tumors per condition were analyzed. Two-tailed t-test p-values are shown. (c) Percentage of cells with ALDH+ activity in tumors isolated from the indicated PDXs, collected 24 hours after last treatment (Fig. S1.5a). Each dot represents one tumor. The treated tumors were compared with controls using a two-tailed t-student test. (d) Representative images of secondary tumorspheres derived from tumor cells from *in vivo* treatments. A total number of secondary tumorspheres (each dot represents a tumor) and tumorsphere size (each dot represents an average by the tumor) are shown. P-value was calculated using a two-tailed t-student test. (e) Tumor growth curves ($(\pi \times \text{length} \times \text{width}^2)/6$) of indicated PDXs after treatment with docetaxel (DTX, 20 mg/kg, once per week) in combination with RANK-Fc or denosumab. Treatment started when indicated by the arrows. Each thin curve represents one single tumor, and each thick curve represents the mean of all tumors implanted. Linear regression analysis was performed and two-tailed p-value is shown.

1.8. RANK signaling in BC PDXs regulates pathways involved in cell proliferation, metabolism, stemness, and immunity

Considering BC heterogeneity, it is essential to identify the molecular mechanisms underlying the response to denosumab in human BC cells. To this aim, RNAseq analysis was performed after modulation of RANK signaling in the three PDX models (Table S1.4). GSEA results demonstrated the strong impact that modulation of RANK signaling caused in these BC PDX with approximately 200 pathways differentially regulated (FDR < 0.25) in each PDX after RANKL, RANK-Fc, or denosumab treatment (Table S1.4). Despite the significant heterogeneity in BC and between the PDX models, most pathways modulated by RANKL and RANK-Fc were shared between the three different PDX models (FDR < 0.25) (Table S1.4). The top-ranked RANKL-driven pathways shared by the three models (NES > 0) were related to TNF/NF- κ B signaling, immunity

(IL2/STAT5, complement, interferon gamma response), proliferation (G2M checkpoint, DNA repair), cell adhesion and stemness (WNT signaling). Metabolic pathways (*i.g.* insulin signaling, reactive oxygen species, glycolysis, adipogenesis) were positively associated (NES > 0) with RANK-Fc treatments (Fig. 1.6 and Table S1.4). Pathways related to adhesion, immunity, and estrogen response were found in both RANKL- and RANK-Fc-treated tumors. RANK-Fc and denosumab modulated the same pathways in STG139-M (Fig. 1.7a and Table S1.4). Next, we compared pathways regulated in PDX after pharmacological treatments with RANKL/RANK-Fc, with those associated with RANK in BC clinical samples (Fig. S1.4 and Table S1.2). Notably, there was more substantial overlap with ER⁻ BC and even more with ER⁻ postmenopausal, reinforcing that RANK signaling is more active in ER⁻ postmenopausal patients, which is a crucial regulator of tumor cell immunity and metabolism. To confirm the relevance of gene expression changes observed in PDXs and those identified in BC patients, GSEA was performed with the genes modulated by denosumab in early BC from the D-BEYOND clinical trial (NCT01864798) (Gómez-Aleza *et al.*, 2020). Importantly, the genes up-regulated by denosumab were significantly associated with RANK signaling inhibition in the three PDX models (Fig. S1.7b, Table S1.4). Together, these results evidence the pleiotropic effects of RANK signaling in human BC tumor cells and suggest that denosumab will impact not only on tumor cell proliferation and stemness but also in immunity, cell adhesion, and metabolism.



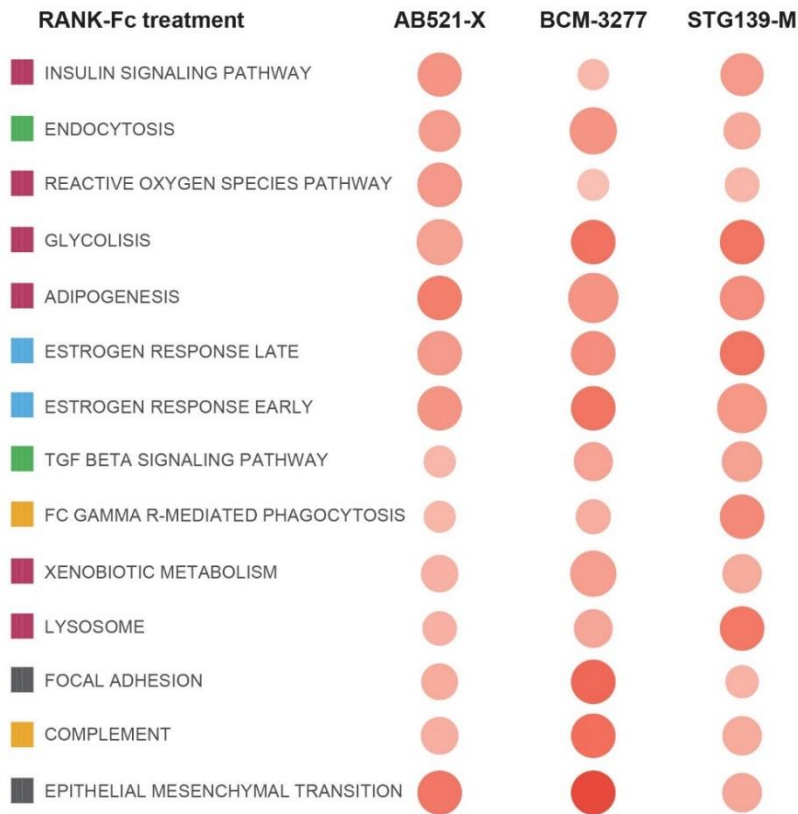
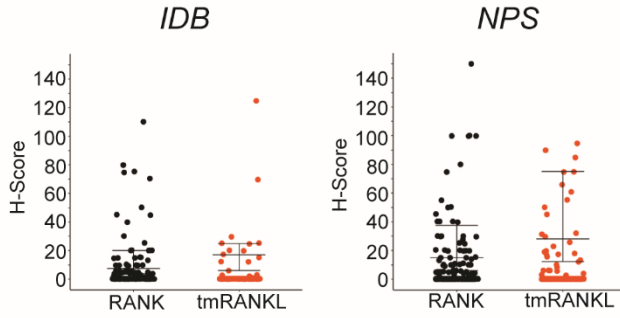
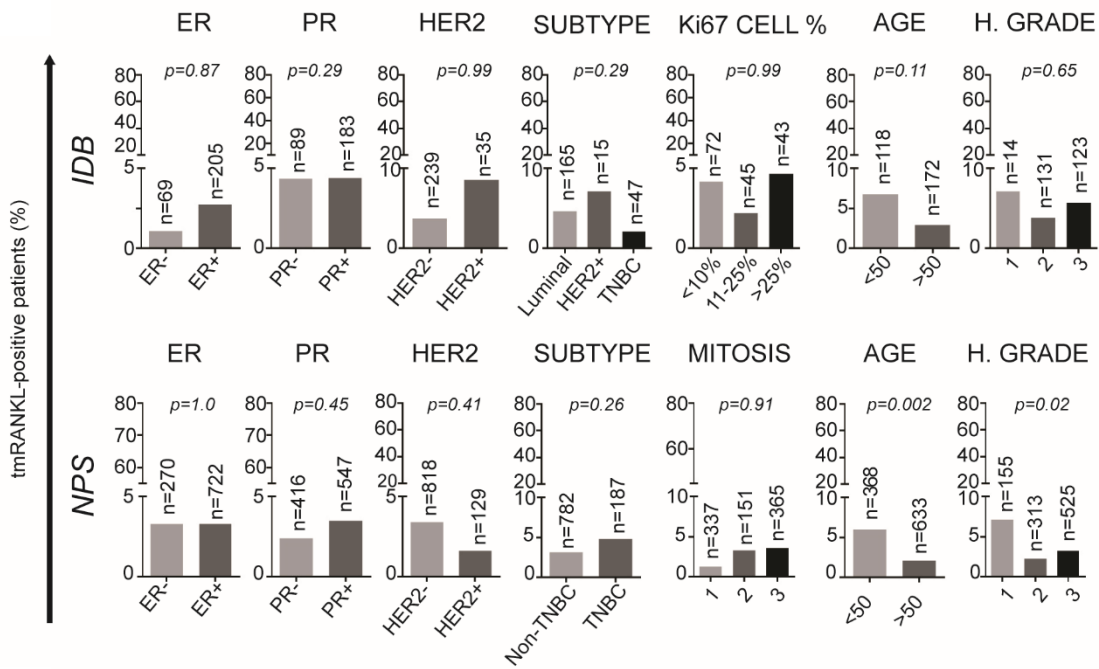
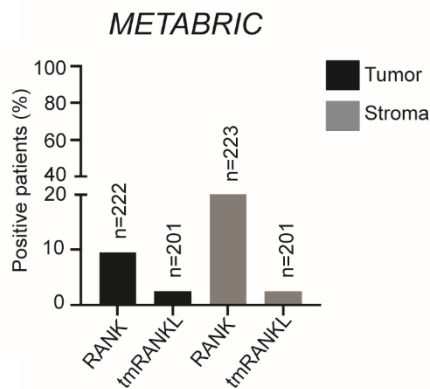
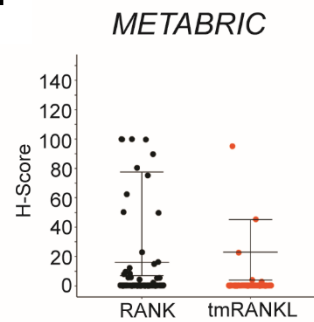
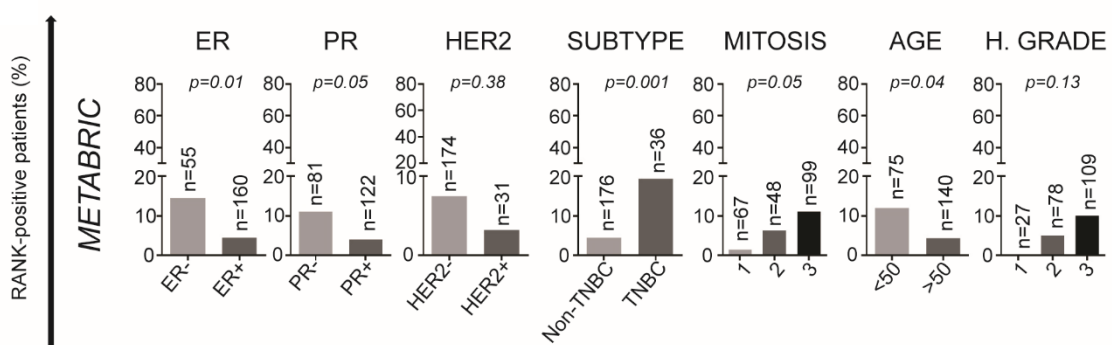
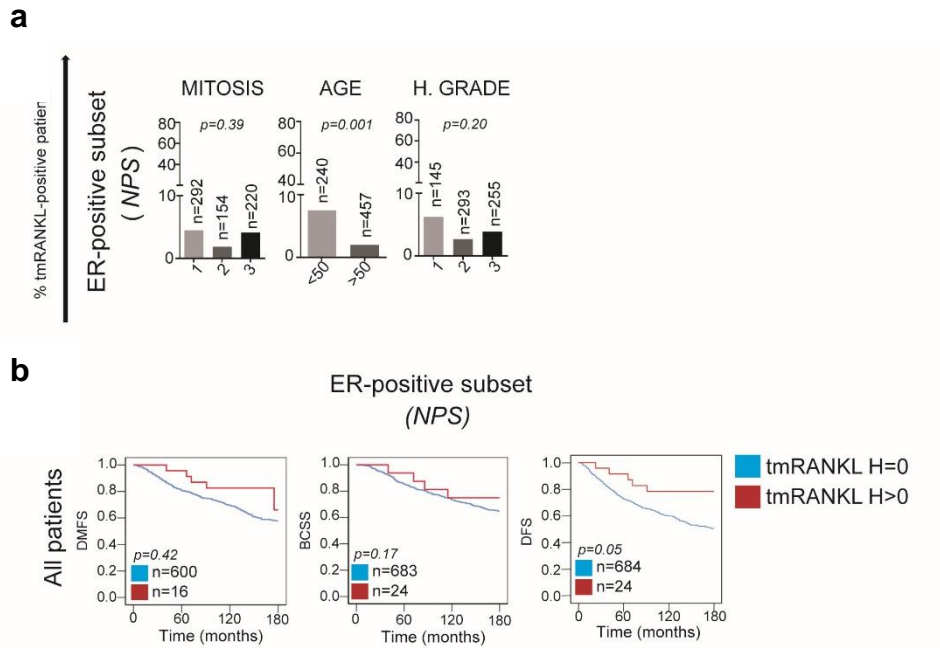


Figure 1.6. RANK signaling regulates proliferation, stemness, adhesion, metabolism and immunity in BC PDXs. The bubble matrix represents GSEA results of associated genes after *in vivo* treatments with RANKL and RANK-Fc in NSG mice, which are common for the studied 3 PDX models. The matrix illustrates NES and FDR values. The color scale represents the NES (the more intense the color, the more positive it is). The size of the bubbles is proportional to the $-\log_{10}$ of the FDR (the bigger the dot, the smaller the FDR). For those signatures with an FDR = 0 after 1000 permutations, we assigned an FDR = 10^{-3} for visualization purposes. The signatures selected for this plot belong to Hallmark, Biocarta, Reactome, and KEGG collections and have a reported FDR < 0.05 and a NES > 0 for all PDX models. The color legend indicates the main biological process associated with each signature.

Supplementary figures

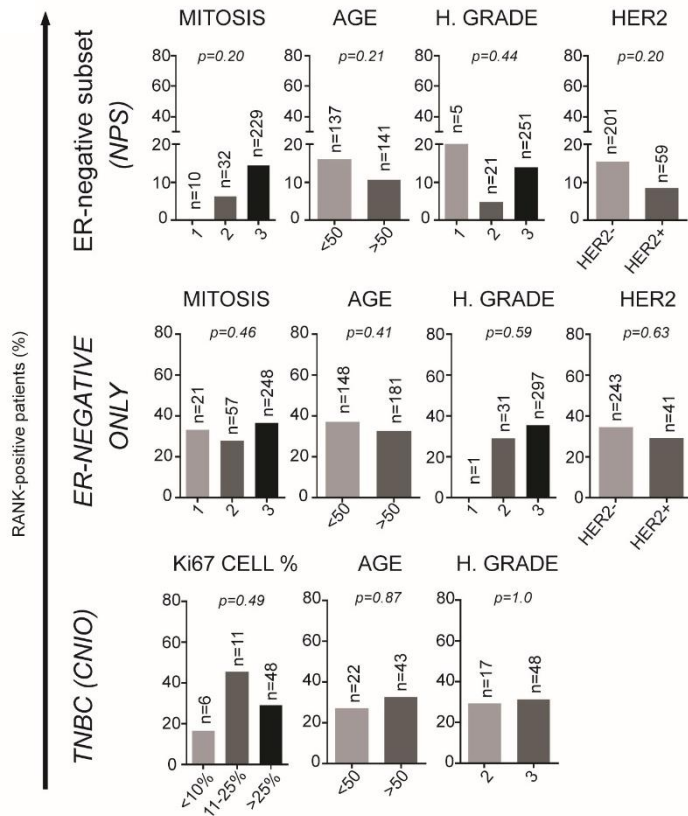
a**b****c****d****e**

Supplementary Figure 1.1. Tumor tmRANKL expression is not associated with clinic-pathologic factors in human breast adenocarcinomas. (a) H-Score values of tumor RANK and tmRANKL from *IDB* and *NPS* collections. **(b)** Percentage of BC patients with tumor tmRANKL⁺ tumors according to the indicated clinic-pathologic parameters in the *IDB* and *NPS* cohorts. The total number of patients analyzed per parameter and p-values (calculated using the Pearson's Chi-Square test (Exact Sig. 2- Side)) are indicated. **(c)** Percentage of patients expressing RANK or tmRANKL ($H > 0$) in tumor and stromal cells in BC samples from the *METABRIC* collection. The total number of patients scored for RANK and tmRANKL protein expression is indicated. **(d)** H-Score values of tumor RANK and tmRANKL from the *METABRIC* dataset. **(e)** Percentage of tumor RANK⁺ BC patients according to the indicated clinic-pathologic parameters in the *METABRIC* cohort. The total number of patients analyzed per parameter and p-values (calculated using the Pearson's chi-square test (Exact Sig. 2-Side)) are indicated.

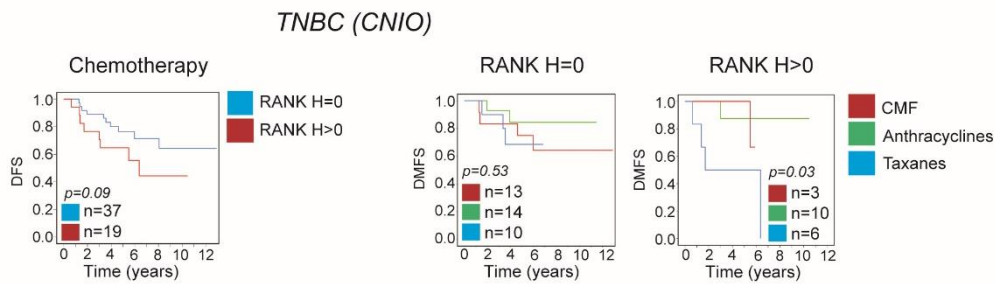


Supplementary Figure 1.2. RANK tumor expression is not related to any clinic-pathologic factor, and RANKL associates with younger patients in ER⁺ BC. (a) Percentage of tumor RANK⁺ BC patients according to the indicated clinic-pathologic parameters in the ER⁺ subset from the NPS. The total number of patients analyzed per parameter and p-values (calculated using the Pearson's ChiSquare tests (Exact Sig. 2-Side)) are indicated. **(b)** DMFS, BCSS, and DFS (15 years of follow-up) in the ER⁺ subset from the NPS collection according to tmRANKL expression. **(a)** The total number of patients analyzed per parameter and p-values (calculated using the Pearson's Chi-Square test (Exact Sig. 2-Side)) **(b)** and the Log-rank test (Mantel-Cox) are indicated.

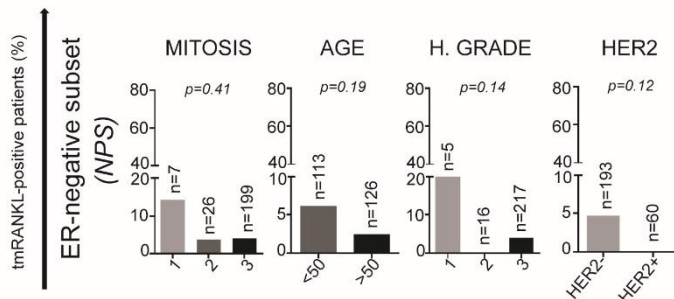
a



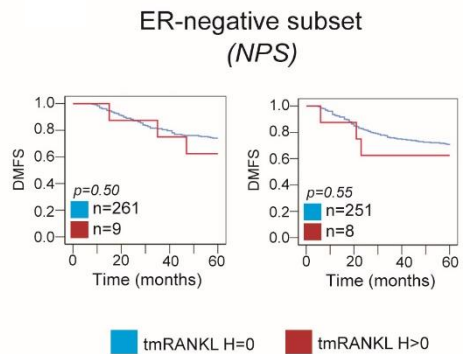
b



c

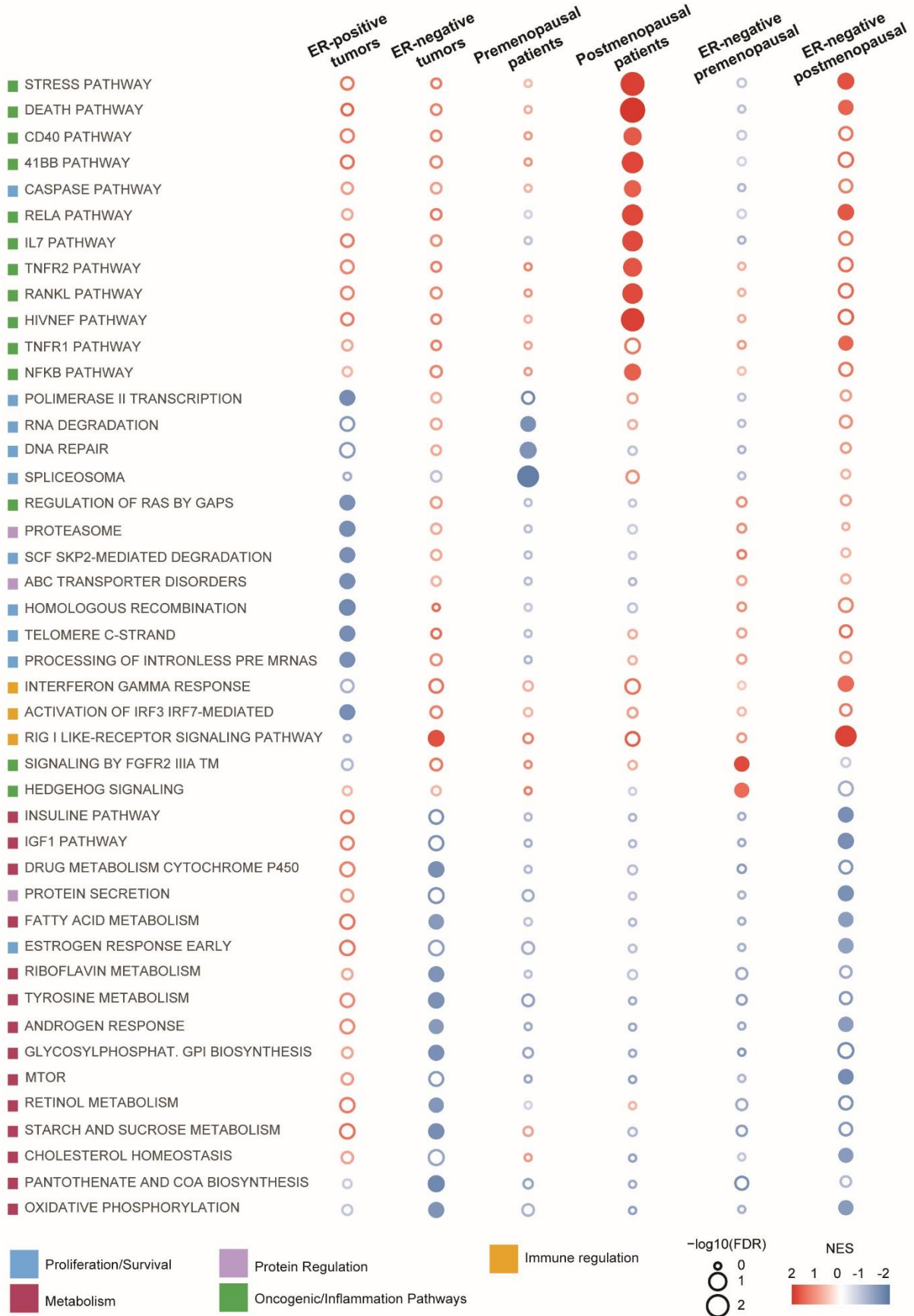


d

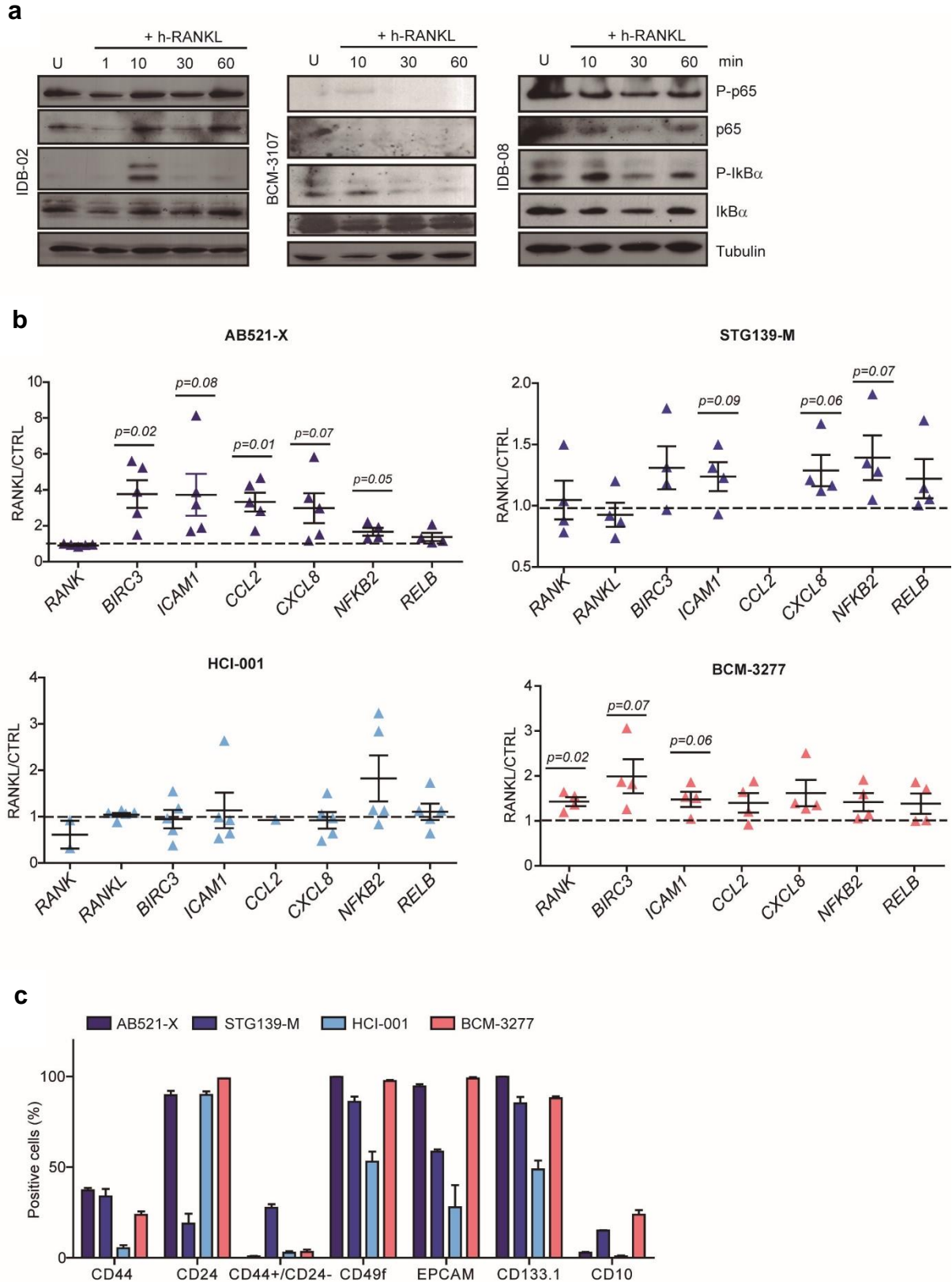


Supplementary Figure 1.3. RANK or RANKL tumor expression is not related to any clinic-pathologic factor in ER⁻ BC but RANK associates with poor response to chemotherapy, including taxanes (a) Percentage of tumor RANK⁺ BC patients according to the indicated clinic-pathologic parameters in the ER⁻ subset from NPS, in the ER-NEGATIVE ONLY and TNBC CNIO collections. **(b)** DFS in the TNBC CNIO collection (12 years of follow-up) after chemotherapy

according to RANK expression and DMFS in RANK⁻ (H = 0) and RANK⁺ (H > 0) tumor samples from *TNBC CNIO* collection according to the chemotherapy regimen (12 years of follow-up): CMF treatment (cyclophosphamide, methotrexate, 5-fluorouracil), anthracycline treatment (FAC/FEC: 5-fluorouracil, adriamycin, cyclophosphamide or 5-fluorouracil, epirubicin, and cyclophosphamide) and taxane group (CMF/FAC/FEC plus taxanes). **(c)** Percentage of tumor tmRANKL⁺ BC patients according to the indicated clinic-pathologic parameters in the ER⁻ subset from *NPS*. **(d)** DFS and DMFS in the ER⁻ subset from *NPS* (5 years of follow-up) according to the tmRANKL expression (tmRANKL⁻ (H-Score=0) or tmRANKL⁺ (HScore>0)). **(a, c)** The total number of patients analyzed per parameter and p-values (calculated using the Pearson's Chi-Square test (Exact Sig. 2-side)) are indicated. **(b, d)** The total number of patients analyzed per parameter and p-values (calculated using the Log-rank test (Mantel-Cox)) are shown.

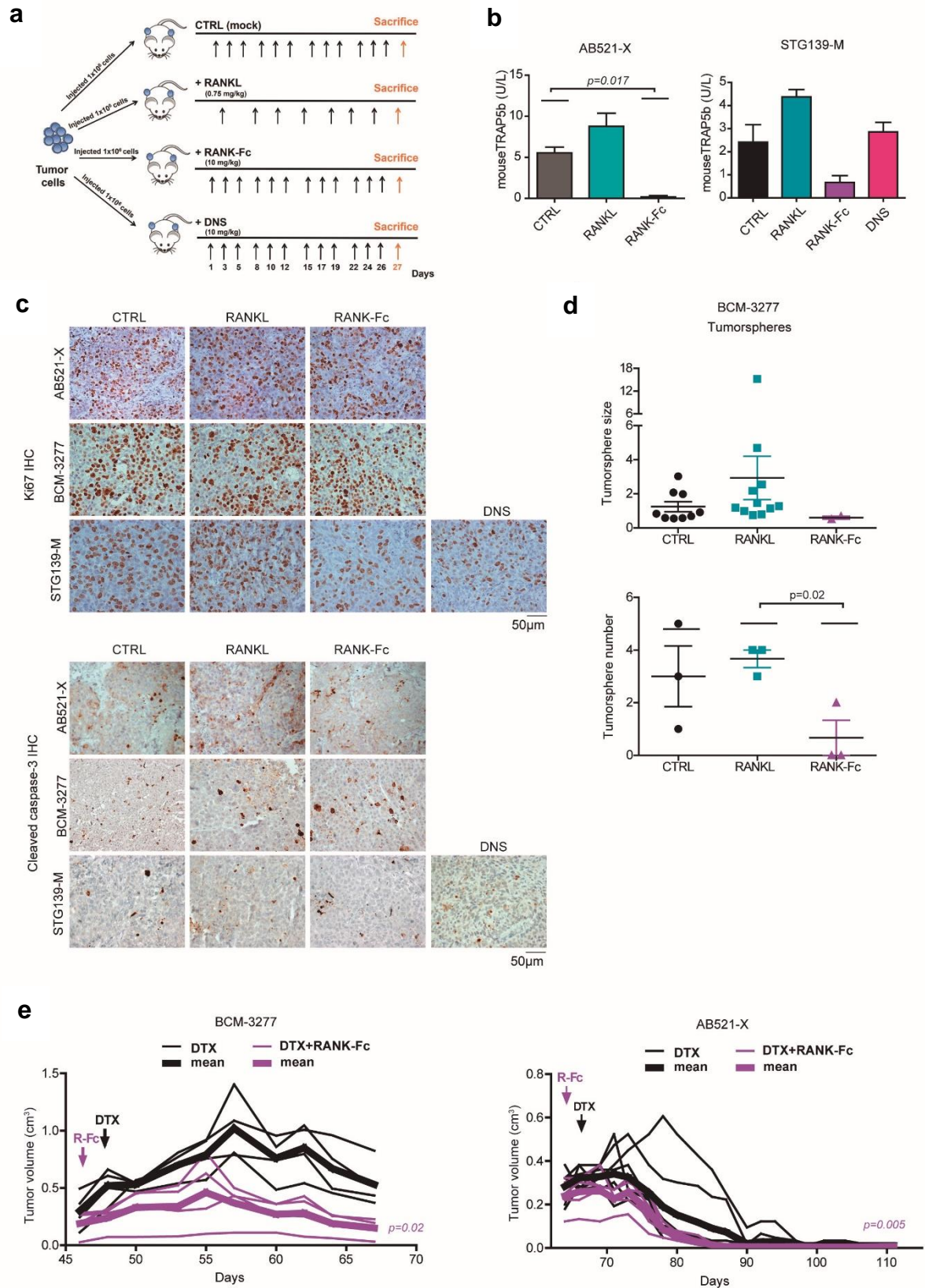


Supplementary Figure 1.4. Distinct biology of RANK signaling according to ER expression and menopausal status. The bubble matrix represents GSEA results of associated genes with RANK protein expression in the METABRIC collection classified by ER expression and menopausal status. Empty bubbles represent $FDR < 0.25$. The matrix illustrates the NES and FDR values. Color legend indicates the main biological process associated.



Supplementary Figure 1.5. RANK signaling is active in a subset of BC PDXs. (a) Western blot analyses of P-p65, P-IkB α and corresponding total proteins after RANKL stimulation in the indicated PDXs. Tubulin was used as a loading control. **(b)** Gene expression analyses of the indicated *NF- κ B* target genes in PDX tumor organoids, 24 hours after RANKL stimulation. Expression levels relative to the untreated controls are shown. Each dot represents organoids

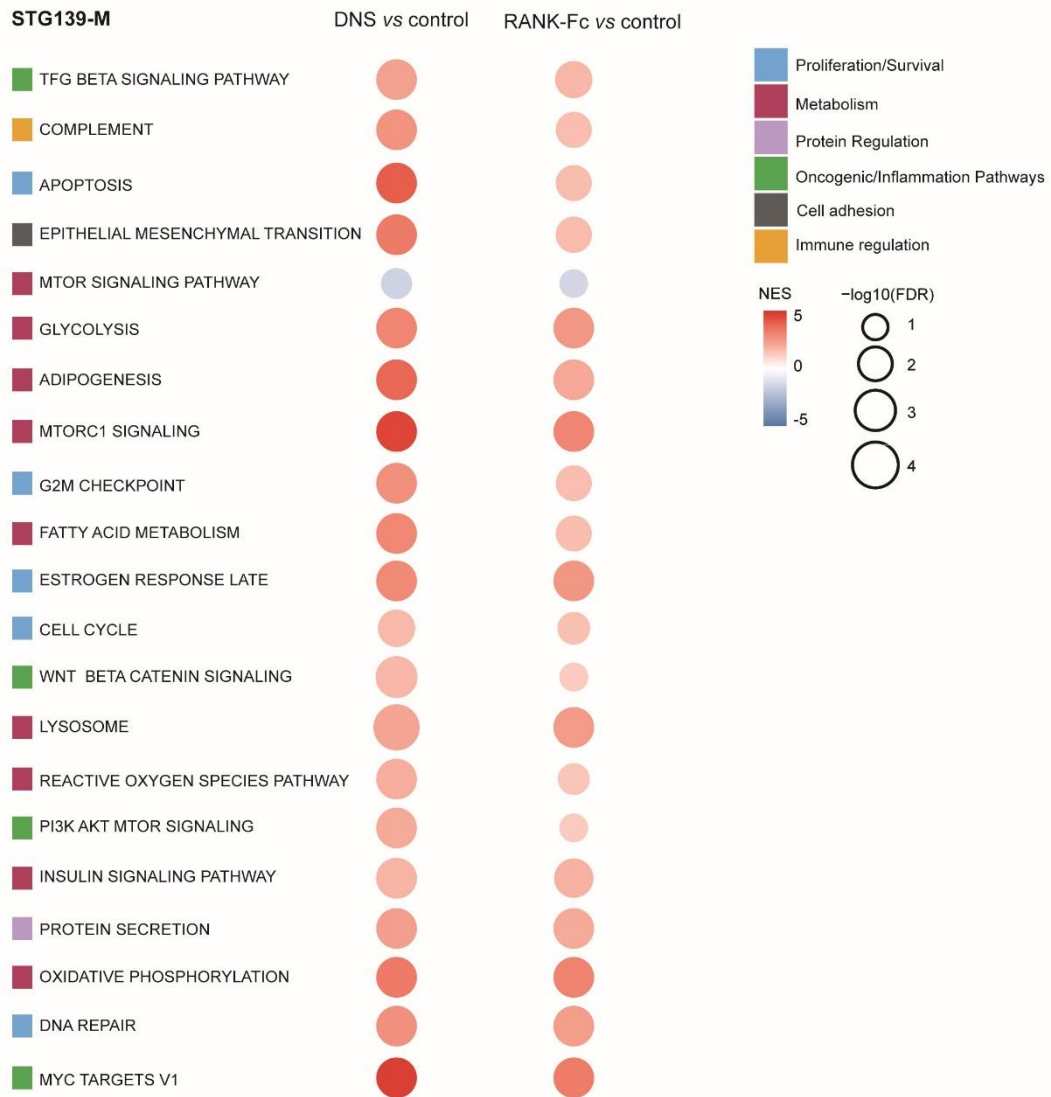
from an independent BC PDX tumor. **(c)** Percentage of cells expressing the indicated surface markers for the four PDXs analyzed.



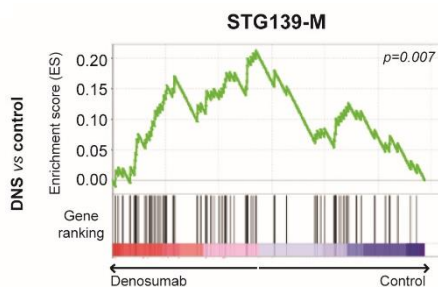
Supplementary Figure 1.6. Modulation of RANK signaling in BC PDXs. (a) Schematic representation of *in vivo* treatments. Dissociated tumor cells mixed 1:1 with Matrigel basement were transplanted orthotopically in NSG mice. When tumors reached 5 x 5 mm in diameter, mice were randomized for mock (CTRL), h-RANKL (0.75 mg/kg, 4-6 doses, twice times per week), h-RANK-Fc treatment (10 mg/kg, three times per week), denosumab (10 mg/kg, three times per

week). Tumor development was monitored once per week. Tumor volume was calculated by multiplying $\pi \times \text{length} \times \text{width}^2/6$ in cm. After 24 hours of the last treatment, mice were sacrificed, tumor cell proliferation and survival were measured, and RNAseq was performed. TRAP 5b levels were analyzed in serum. Tumor cells were isolated and tested for ALDH activity and tumorsphere forming ability. **(b)** TRAP 5b levels as determined by ELISA in mouse serum at the end of treatment. **(c)** Representative images of Ki-67 and cleaved caspase-3 staining measured by IHC; see quantifications in Fig. 1.5b. **(d)** Size and a total number of secondary tumorspheres stimulated in vitro with RANKL or RANK-Fc as indicated, stimulations were performed in triplicates, and each dot represents a replicate. Three independent pictures per replicate were quantified for tumorsphere size. P-value was calculated using a two-tailed t-student test **(e)** Tumor growth curves ($\pi \times \text{length} \times \text{width}^2/6$) of indicated PDXs after treatment with docetaxel (DTX, 20 mg/kg, once per week) in combination with RANK-Fc. Treatment started as indicated by the arrows. Each thin curve represents one single tumor and each thick curve represents the mean of all tumors implanted. Linear regression analysis was performed and two-tailed p-value is shown.

a



b



Supplementary Figure 1.7. RANK inhibition regulates proliferation and oncogenic pathways, mainly in BC PDXs. (a) The bubble matrix represents gene set enrichment analysis (GSEA) results of associated genes after in vivo treatment with denosumab and RANK-Fc in the STG139-M model. The matrix illustrates the NES and FDR values. The color scale represents the NES: red denotes a NES > 0 and blue a NES < 0. The size of the bubble is proportional to the $-\log_{10}$ of the FDR. Signatures belong to Hallmark, Biocarta, Reactome, and KEGG

collections. **(b)** GSEA and genes up-regulated by DNS treatment in the D-BEYOND clinical trial (Gómez-Aleza et al. 2020) in STG139M treated with denosumab.

Supplementary tables

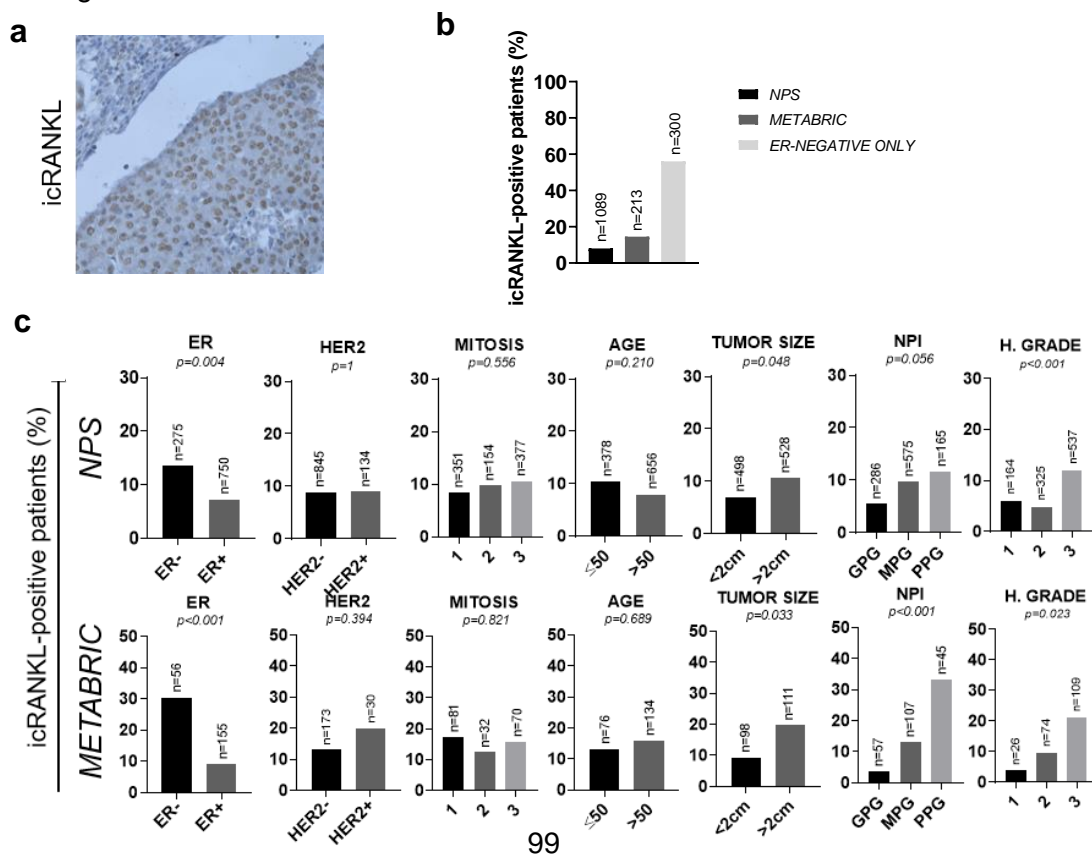
<https://www.biorxiv.org/content/10.1101/2021.12.13.470911v1.supplementary-material>

CHAPTER 2

The role of RANKL in Breast Cancer

2.1. An intracellular form of RANKL is associated with ER⁻ BC

In the analyses of RANKL expression in the BC TMA clinical datasets, besides the tmRANKL, we detected RANKL intracellular staining (icRANKL) in the cytoplasm and nuclei from tumor cells, which has not been described in clinical samples before (Fig. 2.1a). An 8% and 15% of the samples were positive for tumor icRANKL staining in *NPS* and *METABRIC* collections, respectively (Fig. 2.1b). The study of the association of icRANKL expression in the tumor cells with several clinic-pathological parameters revealed strong associations with the lack of ER expression in both collections ($p = 0.004$; $p < 0.001$), bigger tumor size ($p = 0.048$; $p = 0.033$), worse Nottingham Primary Index (NPI) ($p = 0.056$; $p < 0.001$) and histological grade ($p < 0.001$, $p = 0.023$) (Fig. 2.1c). However, the worse survival observed in patients with icRANKL in tumors in the *METABRIC* dataset was not further validated in the *NPS* collection (Table 2.1-2.2). Since icRANKL staining was detected in 56% (168/300) of the samples from the *ER-NEGATIVE ONLY* collection (Fig. 2.1b), we then considered ER⁻ and ER⁺ subsets independently. The expression of icRANKL within the tumor did not correlate with any clinic-pathological or survival parameters neither in ER⁺ subsets from *NPS* and *METABRIC* cohorts (Fig. 2.1d, Table 2.3-2.4) nor in ER⁻ samples from the three independent datasets: *NPS*, *METABRIC* and *ER-NEGATIVE ONLY* (Fig. 2.1e, Table 2.5, 2.6, 2.7). Our results indicate that the expression of a novel intracellular isoform of RANKL in breast cancer cells is associated with ER⁻ breast tumors and, therefore, with bad prognosis markers.



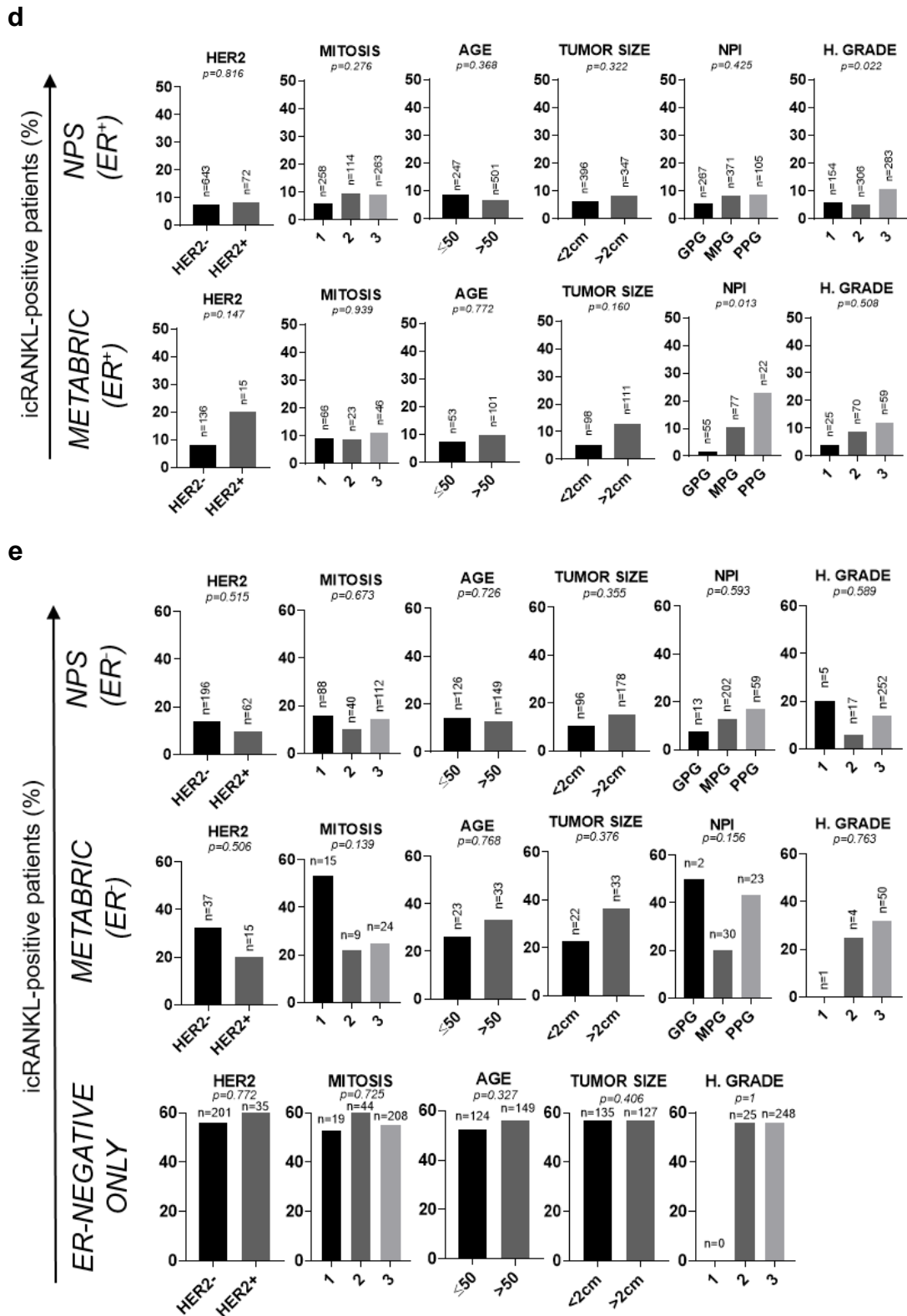


Figure 2.1. icRANKL is expressed in human BC and its expression in tumor cells associates with the ER⁻ subtype. (a) Representative images are showing intracellular staining of RANKL protein in human tumor cells, determined by IHC. **(b)** Percentage of patients expressing tumor RANKL (H > 0) in BC samples from NPS, METABRIC, and ER-NEGATIVE ONLY collections. **(c)** Percentage of BC patients with icRANKL tumor according to the indicated clinicopathologic parameters in the whole NPS and METABRIC cohorts **(d)** in the subset of ER⁺ samples from NPS and METABRIC and **(e)** in the subset of ER⁻ samples from NPS, METABRIC, and ER-

NEGATIVE ONLY datasets. The total number of patients analyzed per parameter and p-values (calculated using the Pearson's Chi-square test (Exact Sig. 2-Side)) are indicated.

2.2. RANKL3, unlike RANKL2, is evolutionary conserved, indicating functionality

Three RANKL isoforms have been reported up to now in the literature: RANKL1 (317 aa), RANKL2 (270 aa) and RANKL3 (244 aa) (Suzuki *et al.*, no date; Ikeda *et al.*, 2001). While RANKL1 has been described as a functional and canonical protein, little is known about non-canonical RANKL2 and RANKL3 isoforms (Ikeda *et al.*, 2003; Suzuki *et al.*, 2004, no date). To understand whether these non-canonical isoforms are biologically relevant, we used the APPRIS bioinformatic tool which selects principal isoforms based on protein structure and function features and cross-species conservation (Rodriguez *et al.*, 2013, 2022). First, the amino-terminal sequence based on the predicted ATGs of the *TNFSF11* (*RANKL*) gene was identified as MRRASR for RANKL1, MFVALL for RANKL2, and MDPNRI for RANKL3 (Fig. 2.2a). Interestingly, within the non-canonical isoforms, the amino-terminal sequence of RANKL2 was poorly conserved, whereas RANKL3 was maintained across mammals, being the only isoform present in some species (Fig. 2.2b). Furthermore, the analysis of the amino terminal sequence of RANKL3 protein in mammals, birds, and reptiles revealed the conservation of the Kozak sequence, corresponding to the seven first amino acids, across evolution (Fig. 2.2c). The evolutionary conservation of RANKL3 isoforms points to its plausible functional relevance.



c

Dog	<u>CAG*ATG*GAT*CCT*AAT*AGA*ATA</u>	Synonymous change
Panda	<u>CAG*ATG*GAT*CCT*AAT*AGA*ATA</u>	Conservative amino acid change
Hedgehog	<u>CAG*ATG*GAT*CCT*AAT*AGA*ATA</u>	Kozak sequence
Turkey	<u>CAG*ATG*GAC*CCT*AGT*AGA*ATT</u>	
Duck	<u>CAG*ATG*GAC*CCC*AGT*AGA*ATT</u>	
Sea turtle	<u>CAG*ATG*GAC*CCT*AAC*AGA*ATT</u>	
Lizard	<u>CAG*ATG*GAC*CCT*AAC*AGA*ATA</u>	
Alligator	<u>CAG*ATG*GAC*CCT*AAC*AGA*ATA</u>	

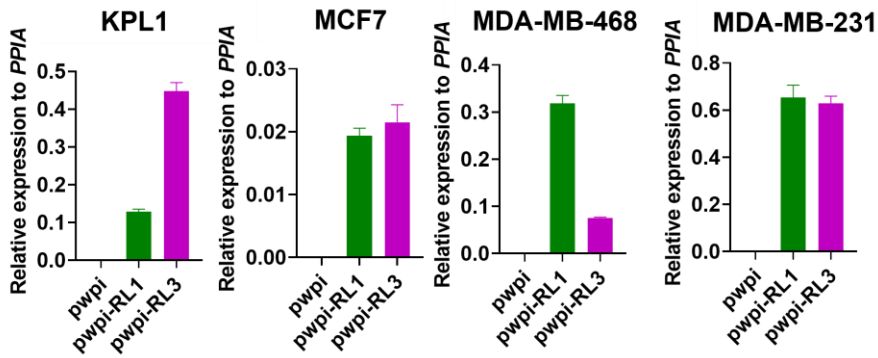
Figure 2.2. From non-canonical RANKL isoforms, only RANKL3 is conserved in mammals, birds, and reptiles. Through the APPRIS tool, different sequences have been obtained. **(a)** The human sequence of the first 140 amino acids of the RANKL1 and their respective amino acid in RANKL2 and RANKL3 isoforms. The absence of amino acid is written with “-”. In bold and green (RANKL1), blue (RANKL2), or purple (RANKL3) are highlighted the first six amino acids required to start the translation. **(b)** The sequence of the first amino acids of the RANKL2 and RANKL3 isoforms in different mammals. In bold and blue (RANKL2) or purple (RANKL3) are highlighted the first six amino acids of each protein. In red, the amino acid in that animal differs from the human sequence. **(c)** Nucleotide sequence corresponding to the first six amino acids of RANKL3 protein in different animals. In blue the synonymous change; in brown, the conservative amino acid change and underlined the Kozak sequence is indicated.

2.3. RANKL3 is confined to the cytoplasm of BC cells

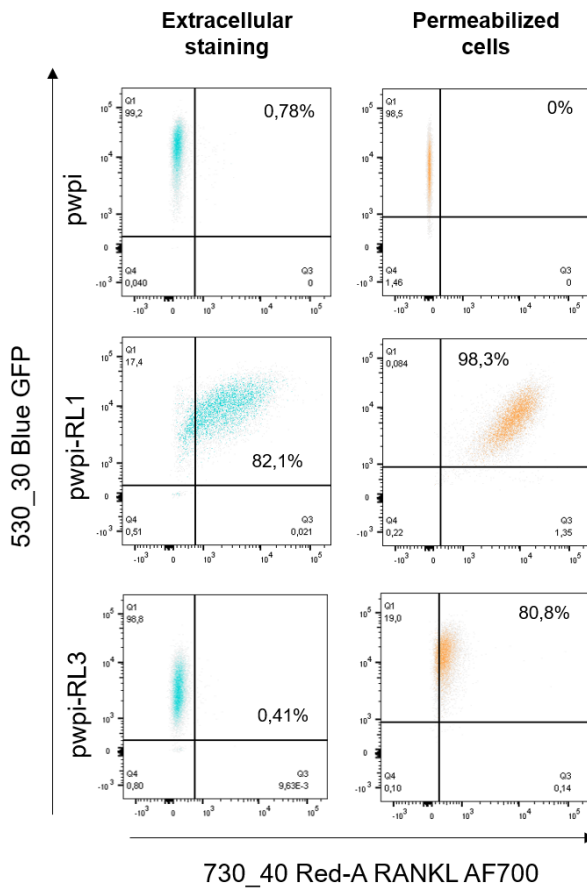
In mouse and human mammary glands, RANKL1, which corresponds to the tmRANKL isoform that results in sRANKL upon cleavage, is the main mediator of the proliferative effect of progesterone (Beleut *et al.*, 2010; Wang *et al.*, 2013), being responsible for the expansion of MaSCs and progenitor cells (Asselin-Labat *et al.*, 2010; Gonzalez-Suarez *et al.*, 2010; Joshi *et al.*, 2010; Schramek *et al.*, 2010a). However, in invasive BC tumors, RANKL1 expression is no longer associated with PR, and its functional relevance beyond the progesterone-driven effects is unknown. We hypothesized that the intracellular staining detected in the BC TMAs might correspond to the evolutionary conserved RANKL3 isoform. Our studies indicate that RANKL2 is not conserved and unlikely to be physiologically relevant. To study the specific functionality of RANKL1 and RANKL3 proteins, several BC cell lines (human luminal KPL1 and MCF7 and triple negative MDA-MB-468 and MDA-MB-231) were infected with lentiviruses harboring the expression vectors pwpi-control (pwpi), pwpi-RANKL1 (RL1) and pwpi-RANKL3 (RL3) to generate control-, RANKL1- and RANKL3-overexpressing stable cell lines. The overexpression (OE) of the corresponding RANKL isoforms was verified by qPCR (Fig. 2.3a). Extracellular RANKL1 (tmRANKL1) was detected in RL1-OE cells but not in RL3-OE cells by flow cytometry (Fig. 2.3b). Cell permeabilization allowed the detection of RANKL isoforms in RL1- and RL3-OE cells (Fig. 2.3b). Further analysis of RANKL detection by WB in cell lysates from RL1- and RL3-OE cells confirmed RANKL1 and RANKL3 expression in corresponding cells from all infected lines (Fig. 2.3c). When supernatants

from RL1- and RL3-OE cells were analyzed by ELISA, sRANKL was only observed in RL1-OE cells as expected (Fig. 2.3d). Altogether, these results indicate that the canonical RANKL1 isoform is a transmembrane protein that can be shed by proteases to release the soluble isoform sRANKL, while the non-canonical RANKL3 is not secreted and remains trapped in the intracellular compartment.

a



b



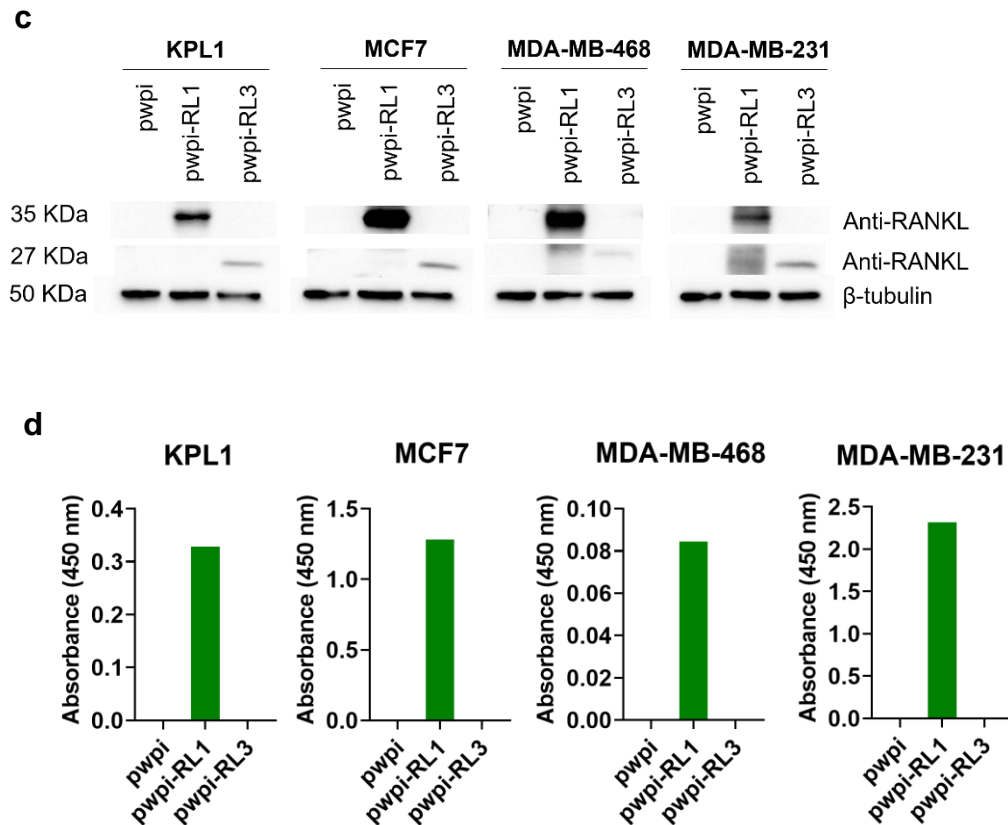


Figure 2.3. RANKL3 is trapped in the intracellular compartment. (a) *RANKL1* and *RANKL3* mRNA expression levels relative to *PPIA* in the indicated BC cell lines. (b) Representative dot blots of RANKL⁺ GFP⁺ cells gated within live cells performing the extracellular (left panel) and intracellular staining after the permeabilization of the cells (right panel). (c) RANKL1 and RANKL3 protein expression in the lysates from the corresponding cell lines. β -tubulin was used as a loading control. (d) Absorbance was obtained by measuring the sRANKL levels in the supernatant of the corresponding cells seeded for 24 h.

2.4. RANKL1 and RANKL3 overexpression in BC do not influence proliferation *in vitro*

We then analyzed the expression levels of the three receptors described to bind RANKL: RANK, OPG, and LGR4 (Renema *et al.*, 2016). All the cell lines expressed low levels of *RANK* and *LGR4* (Fig. 2.4a). *OPG* was expressed in MCF7 and MDA-MB-231, but very low levels were found in KPL1 and MDA-MB-468 cells (Fig. 2.4a). RANKL1 and RANKL3 overexpression did not change the expression levels of these receptors. To decipher whether deficient levels of *RANK* could be enough to trigger RANK signaling after RANKL1 and RANKL3 overexpression, we measured the main downstream effectors of RANK pathway activation: *NFKB2*, *RELB*, *BIRC3*, and *ICAM1*. As shown in Fig. 2.4b, we only observed upregulation of the downstream effector genes upon RANKL1 and RANKL3 overexpression in MDA-MB-231 cells, which showed the highest levels of *RANK* expression. In KPL1 and MCF7 cells, undetectable expression of the downstream

effectors was observed, while in MDA-MB-468 cells, very low *BIRC3* and *ICAM1* were detected. Upon RANKL1 and RANKL3 overexpression, no differences in the RANK pathway downstream targets were observed in KPL1, MCF7, and MDA-MB-468 cells (Fig. 2.4b). Analysis of cell proliferation by doubling time estimation and CCK8 assays revealed no differences in growth of RL1- and RL3-OE cells compared to their controls, not even in the MDA-MB-231 cell line (Fig. 2.5a, 2.5b). These results indicate that neither RANKL1 nor RANKL3 overexpression affects human BC cells' growth *in vitro*.

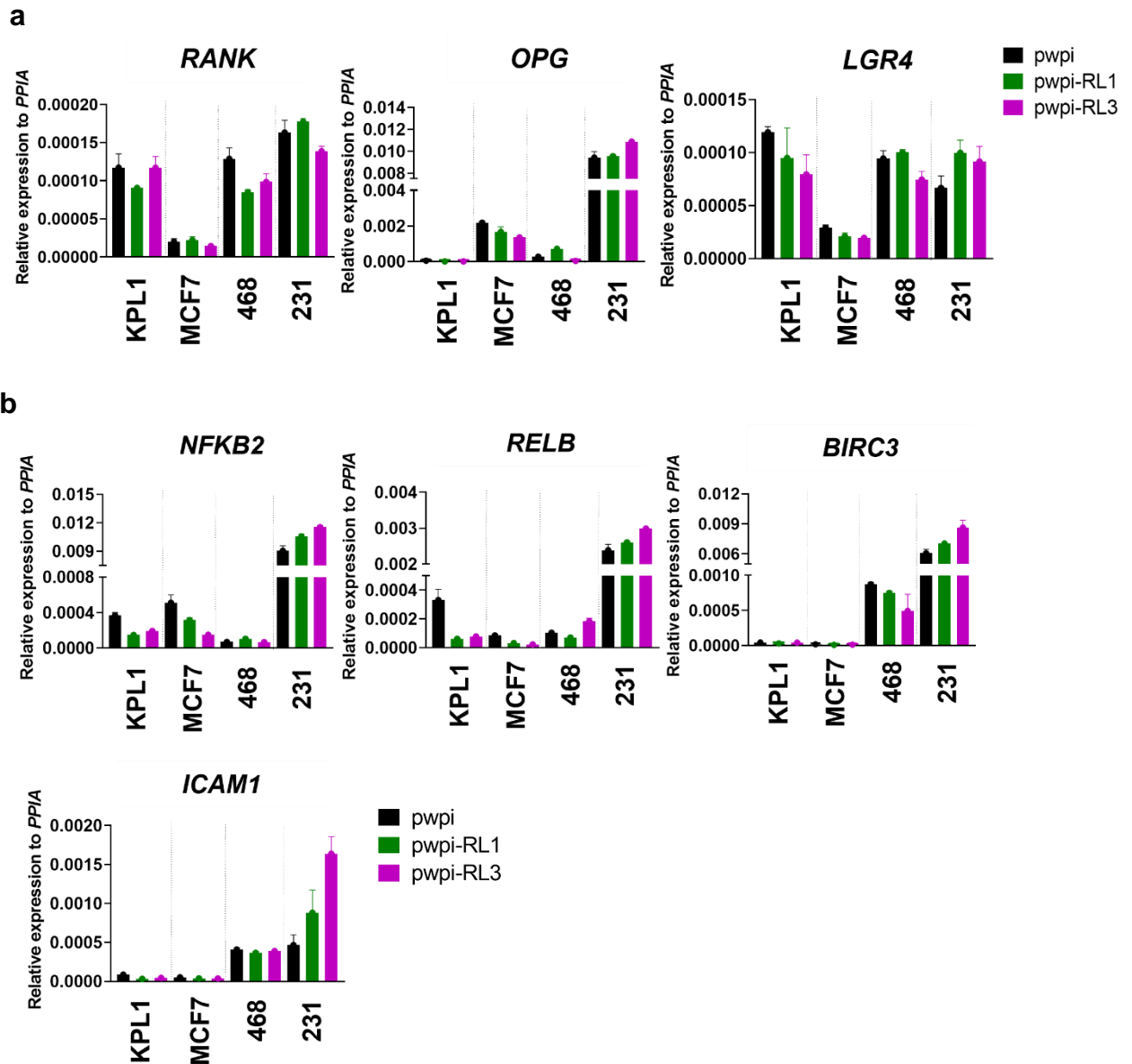


Figure 2.4. Characterization of RANKL-OE human cell lines. (a) *RANK*, *OPG*, *LGR4*, and (b) *NFKB2*, *RELB*, *BIRC3*, and *ICAM1* mRNA expression levels relative to *PPIA* in the indicated BC cells cultured *in vitro*. Error bars correspond to technical triplicates (n=1; biological replicate).

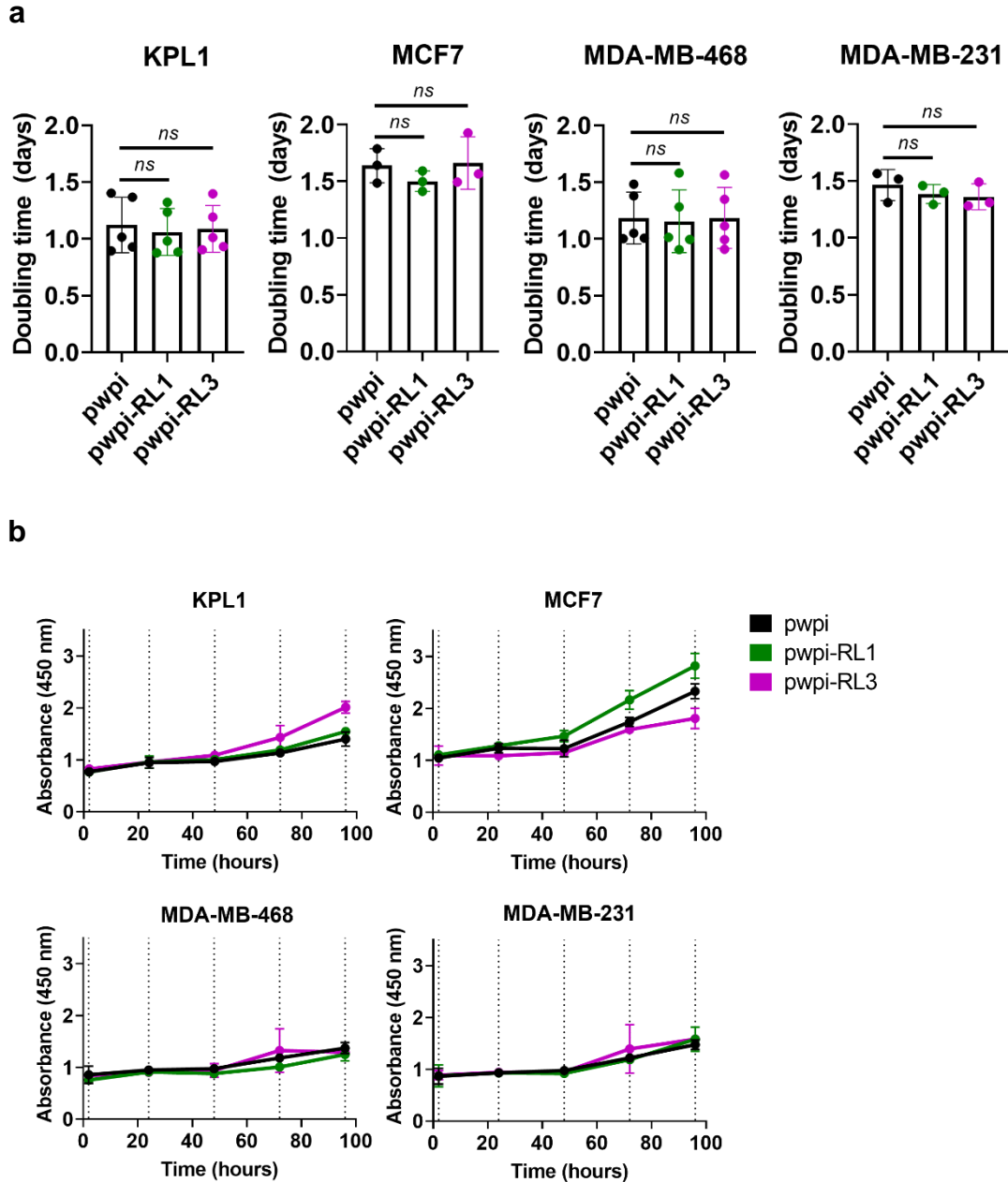


Figure 2.5. RANKL overexpression in BC cells does not regulate proliferation *in vitro*. (a) The proliferation rate of the corresponding cells *in vitro* following the formula = $\text{duration (days)} \cdot \log(2) / \log(\text{counted cells}) - \log(\text{seeded cells})$. Each point means a single passage. (b) Relative (to the first point of measurement, 2 h after cell seeding) number of indicated living cells incubated for different time points (2, 24, 48, 72, and 96 h). Cells were analyzed with CCK8 as detailed in the *Methods* section. T-test and p-values were calculated. **** $p < 0.0001$, *** $p < 0.001$, ** $p < 0.01$, * $p < 0.05$, ns not significant.

2.5 RANKL1 and RANKL3 overexpression promote tumor aggressiveness in immune-deficient mice

To study the consequences of RANKL overexpression for tumor development, 300.000 pwpi-, RL1- and RL3-OE MDA-MB-468 cells were injected into the two inguinal fat pads of T-cell-deficient nude mice (Szadvari, Krizanova and Babula, 2016). As shown in Fig.

2.6, both RL1- and RL3-OE MDA-MB-468 cells gave rise to tumors 60 days after injection, in contrast to the control pwpi-MDA-MB-468 cells, which did not form tumors after 150 days. Interestingly, faster tumor growth was observed in mice injected with RL3-OE cells compared to those overexpressing RANKL1 protein (Fig. 2.6).

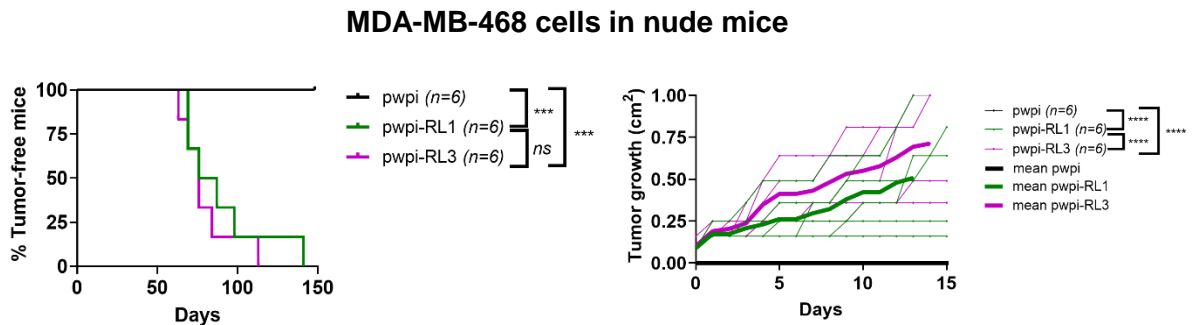


Figure 2.6. Human RL1- and RL3-OE MDA-MB-468 tumors led to tumor development in nude mice. $3 \cdot 10^5$ pwpi-, RL1-, and RL3-OE MDA-MB-468 cells were injected into the fat pad of nude mice. Kinetics of palpable tumor onset (left) and growth (right) after transplantation are shown. Each thin line represents one single tumor. Each thick line represents the mean of all the tumors. Log-rank test for latency and linear regression analysis was performed to compare the tumor growth slopes. N is indicated in each case. **** $p < 0.0001$, *** $p < 0.001$, ** $p < 0.01$, * $p < 0.05$, ns not significant.

Similar results were obtained when KPL1 cells were injected in nude mice; RL1-OE KPL1 cells but not control cells gave rise to tumors (Fig. 2.7a). In NSG mice, an immune-compromised murine strain lacking T, B, and NK cells (*NSGTM Variants Portfolio*), the tumors derived from RL1- and RL3-OE KPL1 cells showed an earlier onset and faster growth compared to the control ones (Fig. 2.7b).

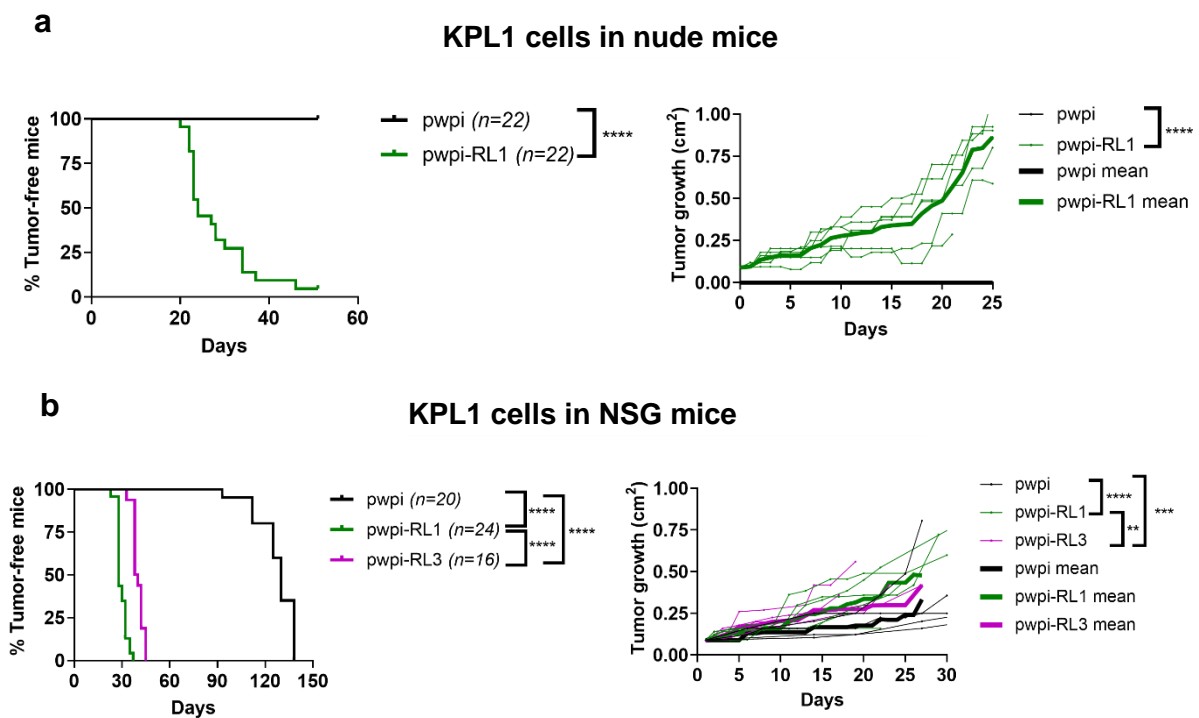


Figure 2.7. RANKL1 and RANKL3 overexpression in KPL1 cells triggered earlier tumor onset. (a) $3 \cdot 10^5$ pwpi- and RL1-OE KPL1 cells were injected into the fat pad of nude mice. (b) $3 \cdot 10^5$ pwpi-, RL1- and RL3-OE KPL1 cells were injected into the fat pad of NSG mice. (a, b) Kinetics of palpable tumor onset (left) and growth (right) after transplantation are shown. Each thin line represents one single tumor. Each thick line represents the mean of all the tumors. Log-rank test for latency and linear regression analysis was performed to compare the tumor growth slopes. N is indicated in each case. **** $p < 0.0001$, *** $p < 0.001$, ** $p < 0.01$, * $p < 0.05$, ns not significant.

In the aKPL1, a higher proliferative clone of KPL1 cells, tumors derived from RL1-OE aKPL1 cells, unlike RL3-OE aKPL1, showed shorter latency than control tumors when injected in nude mice. Still, no differences in growth were observed between cells (Fig. 2.8a). Importantly, increased bone resorption marker TRAP 5b (Yao *et al.*, 2017) levels were observed in the serum of nude mice injected with RL1-OE aKPL1 compared to control and RL3-OE aKPL1 cells (Fig. 2.8b), indicating that only RANKL1 overexpression leads to systemic changes in bone metabolism. These analyses revealed similar levels of GFP⁺ cells in tumors originated from pwpi-, RL1-, and RL3-OE aKPL1 cells (Fig. 2.8c), confirming that RANKL1 and RANKL3 expression was maintained throughout tumor development.

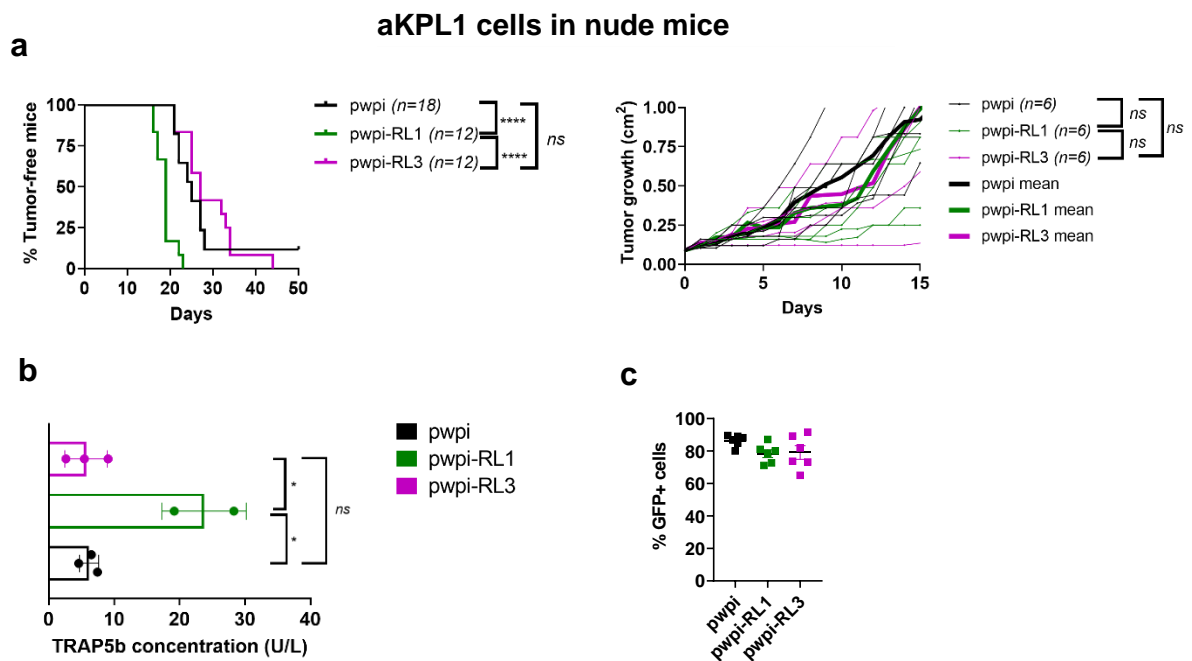
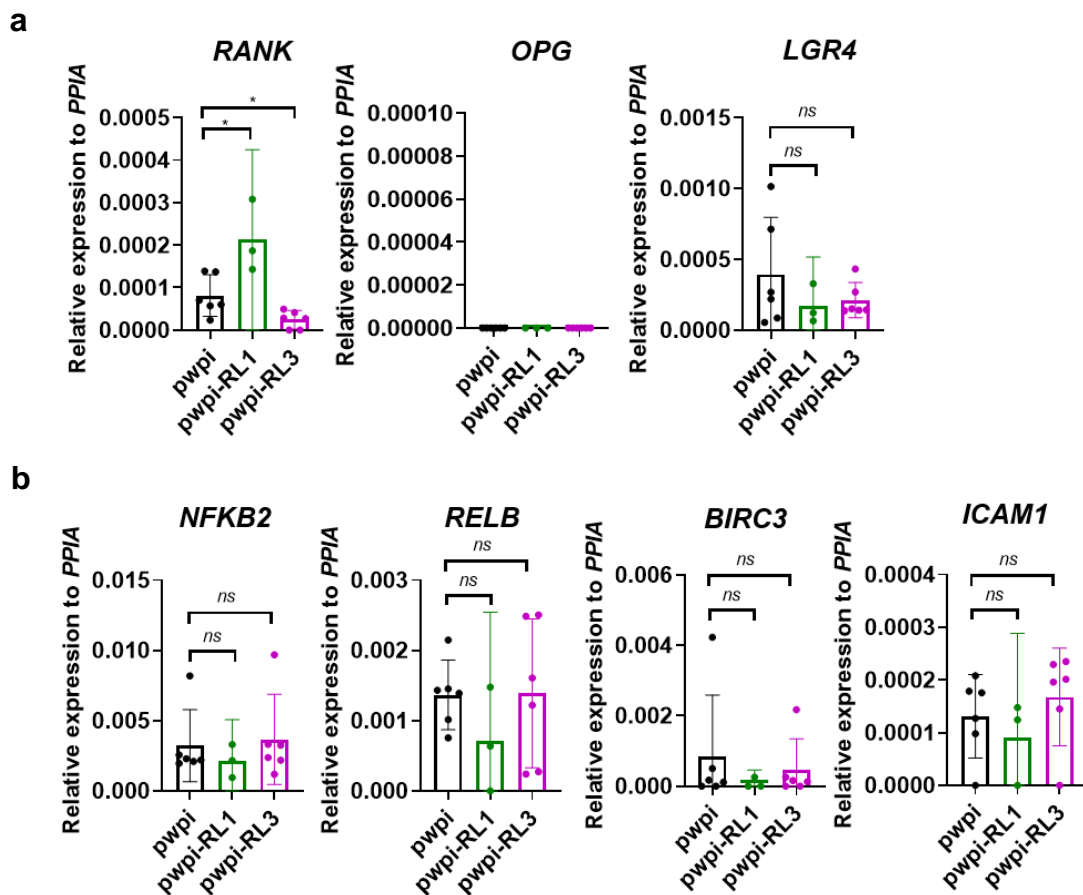


Figure 2.8. Human RL1-OE aKPL1 tumors showed a shorter tumor onset. (a) $3 \cdot 10^5$ pwpi-, RL1- and RL3-OE aKPL1 cells were injected into the fat pad of nude mice. Kinetics of palpable tumor onset (left) and growth (right) after transplantation are shown. Each thin line represents one single tumor. Each thick line represents the mean of all the tumors. Log-rank test for latency and linear regression analysis was performed to compare the tumor growth slopes. N is indicated in each case. (b) TRAP 5b concentration in the serum of nude mice injected with pwpi-, RL1- and RL3-OE aKPL1 cells. Each point indicates a single mouse. An unpaired t-test was performed. (c) Graph showing the percentage of GFP⁺ within alive cells obtained after tumor processing from nude mice injected with pwpi-, RL1-, and RL3-OE aKPL1 cells. Each point means a single tumor. Mean, SEM shown. T-test and p-values were calculated. **** $p < 0.0001$, *** $p < 0.001$, ** $p < 0.01$, * $p < 0.05$, ns not significant.

As shown in Fig. 2.9a, *RANK* mRNA expression was higher in RL1-OE tumors and lower in RL3-OE tumors implanted in nude mice compared to controls. There were no differences in *OPG* and *LGR4* expression among conditions (Fig. 2.9a). Despite the modulation of *RANK* expression in tumors, no changes in the *RANK* downstream genes (*NFKB2*, *RELB*, *BIRC3*, *ICAM1*) were found (Fig. 2.9b), suggesting that *RANKL* overexpression does not activate the canonical NF- κ B signaling pathway *in vivo*. As *RANKL* is a proinflammatory cytokine, we then analyzed putative changes in tumor immune infiltration by flow cytometry. An increase in infiltrating leucocytes (CD45⁺) and TAMs (F4/80⁺CD11b⁺CD45⁺) was found in RL1-OE aKPL1 tumors, while no changes in the myeloid cell (CD11b⁺CD45⁺) or NKs (NK11.1⁺CD3⁺CD45⁺) cell infiltration were observed (Fig. 2.9c). The increased frequency of leucocytes and TAMs, observed in RL1-OE aKPL1 tumors growing in nude mice, indicates that *RANKL1* expression in tumor cells changes the tumor immune microenvironment, which may also contribute to the observed differences in tumor growth. Our findings demonstrate that *RANKL1* and *RANKL3* promote tumor growth through immune-dependent and independent mechanisms.



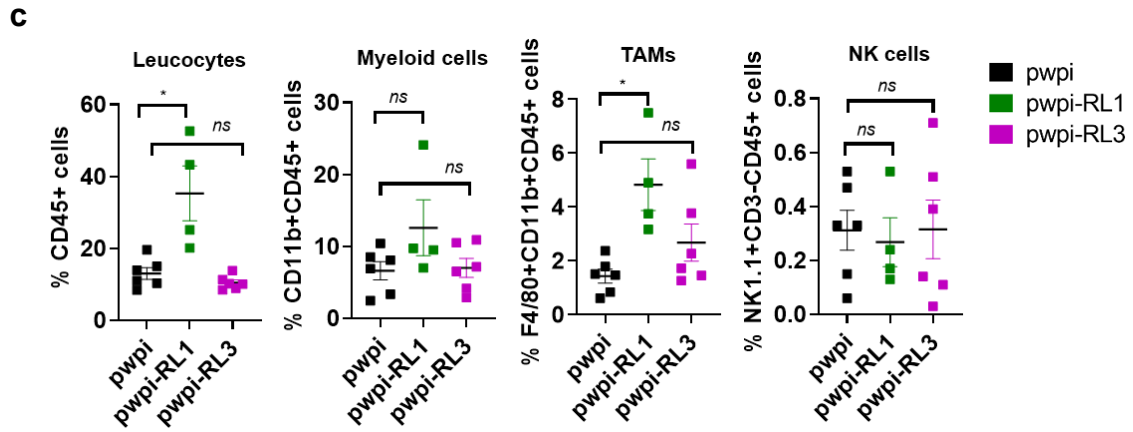
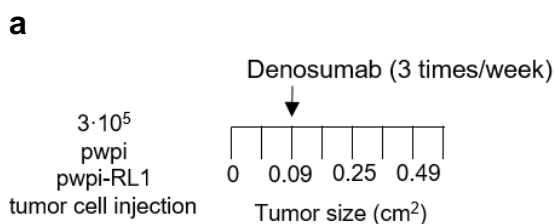


Figure 2.9. RL1-OE aKPL1 tumors show higher TAMs infiltration. (a) *RANK*, *OPG*, *LGR4* and **(b)** *NFKB2*, *RELB*, *BIRC3* and *ICAM1* mRNA expression levels relative to *PPIA* in the pwpi-, RL1- and RL3-OE aKPL1 tumors injected in nude mice. **(c)** Graphs showing the percentage of tumor-infiltrating leucocytes (CD45⁺), myeloid (CD11b⁺CD45⁺), TAMs (F4/80⁺CD11b⁺CD45⁺) and NKs (NK1.1⁺CD3⁻CD45⁺) in pwpi-, RL1- and RL3-OE aKPL1 cells derived from the tumors implanted previously in nude mice. Each point means a single tumor. Mean, SEM shown. T-test and p-values were calculated. **** $p < 0.0001$, *** $p < 0.001$, ** $p < 0.01$, * $p < 0.05$, ns not significant.

2.6. Denosumab attenuates the growth of RL1-OE tumors in nude but not in NSG mice

After demonstrating that RANKL1 overexpression induces faster tumor development in several BC cell lines, we analyzed the therapeutic potential of DNS in RL1-OE tumors. Because DNS cannot cross the cell membrane, mice implanted with RL3-OE cells were not treated. To study the effect of DNS in two different immune environments, NSG and nude mice with established pwpi- and RL1-OE KPL1 tumors were randomized into mock or DNS treatments once tumors reached 3 x 3 mm size (Fig. 2.10a). DNS did not attenuate the growth of tumors derived from RL1-OE KPL1 cells or controls growing in NSG mice (Fig. 2.10b). However, DNS treatment attenuated the growth of RL1-OE KPL1 tumors implanted in nude mice (Fig. 2.10c). Reduced tumor growth was also observed in DNS-treated RL1-OE aKPL1 tumors but not in control cells implanted in nude mice compared to their untreated counterparts (Fig. 2.10d). Analysis at the endpoint revealed a decrease of TRAP 5b serum levels in nude mice bearing RL1-OE aKPL1 tumors upon DNS treatment in contrast to mock treatment (Fig. 2.10e), confirming the efficiency of DNS in the inhibition of RANKL-induced bone resorption.



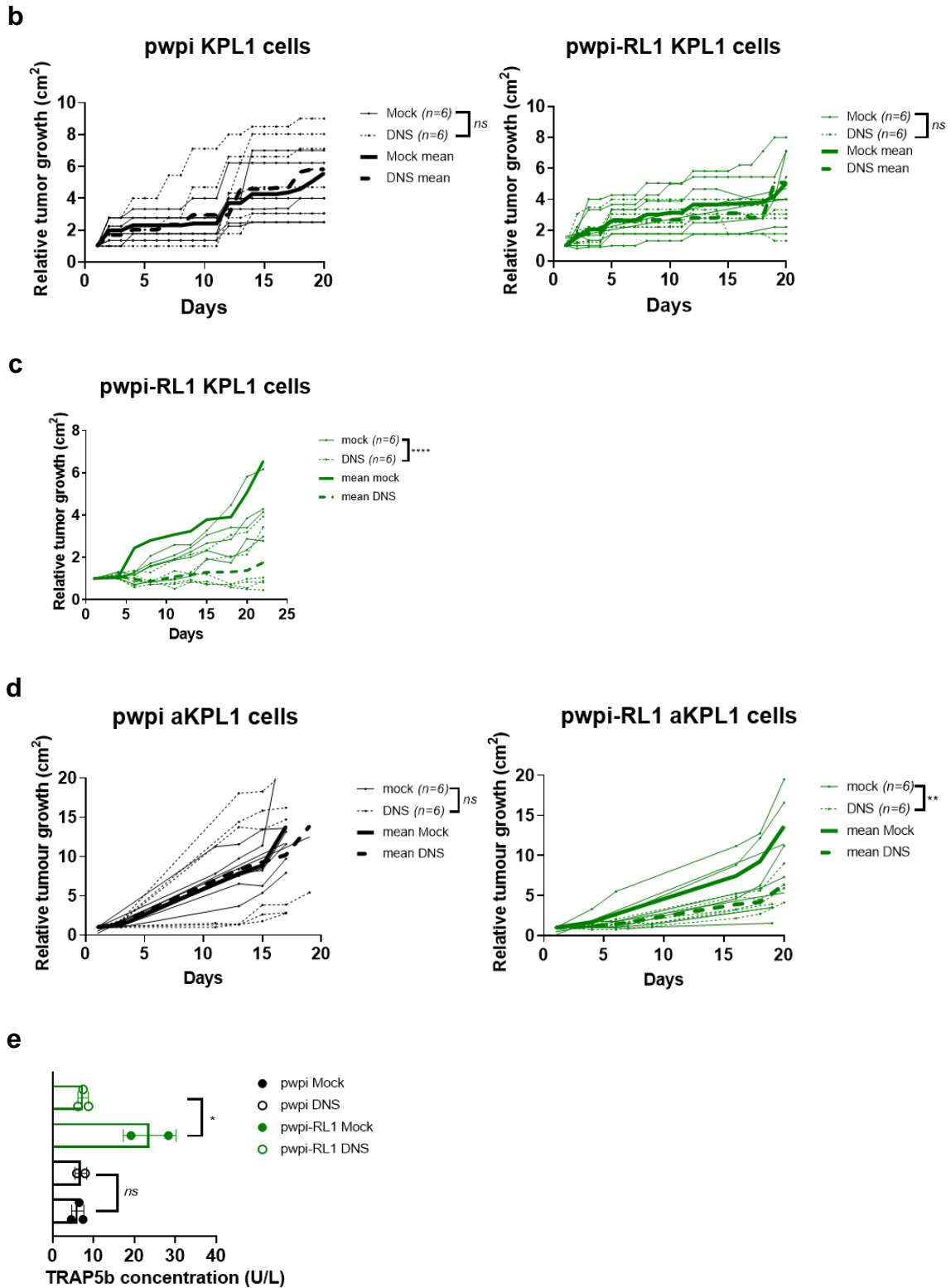
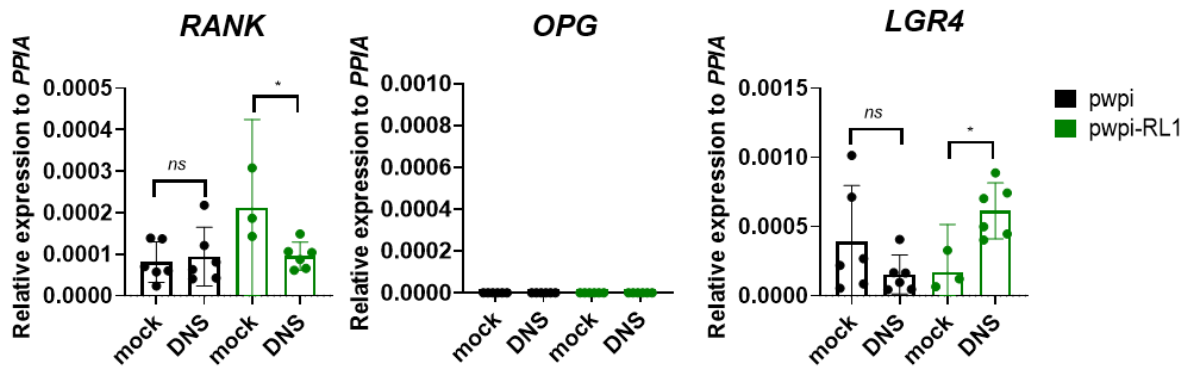


Figure 2.10. DNS treatment attenuated the growth of RL1-OE tumors implanted in nude mice. (a) Schematic overview of DNS treatment in orthotopic tumors. $5 \cdot 10^5$ cells were orthotopically injected into the fat pad of NSG or nude mice, which were randomized 1:1 for DNS or mock treatment when tumors reached 3 x 3 mm in diameter. Kinetics of relativized tumor growth upon DNS and mock treatments to the first day of treatment of (b) pwpi- and RL1-OE KPL1 tumors implanted in NSG, (c) RL1-OE KPL1 tumors implanted in nude mice, (d) pwpi- and RL1-OE aKPL1 tumors implanted in nude mice. Each thin line represents one single tumor. Each thick line represents the mean of all the tumors. Linear regression analysis was performed to

compare the tumor growth slopes. **(e)** TRAP 5b concentration in the serum of nude mice injected with pwpi- and RL1-OE aKPL1 cells and treated with mock or DNS. Each point means a single mouse. An unpaired test was performed. N is indicated in each case. . **** $p < 0.0001$, *** $p < 0.001$, ** $p < 0.01$, * $p < 0.05$, *ns* not significant.

Gene expression analysis revealed a significant reduction of *RANK* and an increase of *LGR4* expression in RL1- compared to pwpi-OE aKPL1 tumors upon DNS treatment implanted in nude mice (Fig. 2.11a). Analysis of the tumor immune infiltration after mock or DNS treatment revealed no differences in leucocyte populations, total myeloid cells, or NK cells. However, a significant decrease in the percentage of TAMs was found in RL1- compared to pwpi-OE aKPL1 tumors (Fig. 2.11b). The fact that DNS attenuated RL1-driven tumor growth in nude but not in NSG mice suggests that immune-dependent mechanisms contribute to the therapeutic potential of DNS in RANKL1⁺ BC.

a



b

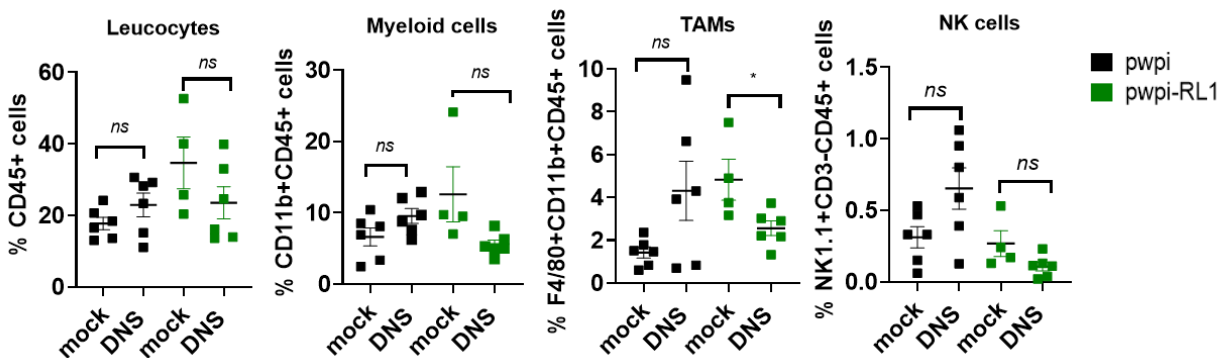
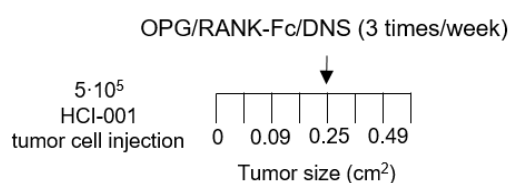


Figure 2.11. DNS treatment decreased the infiltration of TAMs in RL1-OE aKPL1 tumors. **(a)** *RANK*, *OPG*, and *LGR4* mRNA expression levels relative to *PPIA* in the pwpi- and RL1-OE aKPL1 tumors injected in nude mice and treated with mock or DNS. **(b)** Graphs showing the percentage of tumor-infiltrating leucocytes (CD45⁺), myeloid (CD11b⁺CD45⁺), TAMs (F4/80⁺CD11b⁺CD45⁺), and NKs (NK1.1⁺CD3⁻CD45⁺) in pwpi- and RL1-OE aKPL1 cells derived from the tumors implanted previously in nude mice and treated with mock or DNS. Each point means a single tumor. Mean, SEM shown. T-test and p-values were calculated. **** $p < 0.0001$, *** $p < 0.001$, ** $p < 0.01$, * $p < 0.05$, *ns* not significant.

2.7. Therapeutic benefit of RANKL inhibition is observed in RANKL1-expressing BC PDX

Our results in human cancer cell lines support the relevance of RANKL in the initiation and progression of breast tumorigenesis. The inhibition of human tumoral RANKL1 attenuated the growth of RL1-OE breast cancer cells growing in immune-compromised mice. The analysis of RANKL protein by IHC in an extensive collection of BC PDXs revealed high mRNA expression of the canonical *RANKL* in a small subset of breast adenocarcinomas luminal-like (5,5%) and TNBC (15,9%) (shown in chapter 1). Next, we evaluated the therapeutic effect of the pharmacologic RANKL inhibition in the HCI-001 PDX model, a RANKL1-expressing TNBC, as breast PDX has been shown to recapitulate clinical behavior. Tumor cells from HCI-001 were orthotopically injected into the inguinal fat pads of NSG mice due to this tumor does not grow in nude mice. Once tumors reached 5 x 5 mm in diameter, mice were randomized and treated with mock, DNS, RANK-Fc, and OPG (Fig. 2.12a). While DNS inhibits human RANKL, RANK-Fc and OPG inhibit both mouse and human RANKL, and OPG inhibits TRAIL. Attenuation of tumor growth upon DNS, RANK-Fc, and OPG treatments was observed in Fig. 2.12b. Results from three independent experiments corroborated the attenuation of tumor growth upon RANKL inhibition. A decrease in TRAP 5b serum levels was observed after RANK-Fc and OPG but not after DNS treatment (Fig. 2.12c). As the tumor growth attenuation was comparable in the three treatment arms, we concluded that the tumor attenuation was due to inhibition of tumoral RANKL, rather than systemic RANKL. Twenty-four hours after the last treatment, mice were sacrificed, the tumors were extracted, and the proliferation (Ki-67) and apoptosis (cleaved caspase-3) rates were evaluated in mock, DNS, and RANK-Fc-treated tumors. Despite the attenuation in tumor growth, no differences in cell proliferation nor apoptosis were detected in RL1-expressing HCI-001 tumors upon any of the treatments (Fig. 2.12d). Transcriptomic analyses of RANK-Fc treated mice with established HCI-001 tumors revealed up-regulation of processes related to cell cycle arrest and down-regulation of metabolic pathways, hypoxia, and epithelial-mesenchymal and angiogenesis processes (Table 2.8). These promising results indicate that RANKL1-expressing tumors would benefit from anti-RANKL therapies, turning the tumors into a less aggressive tumor type.

a



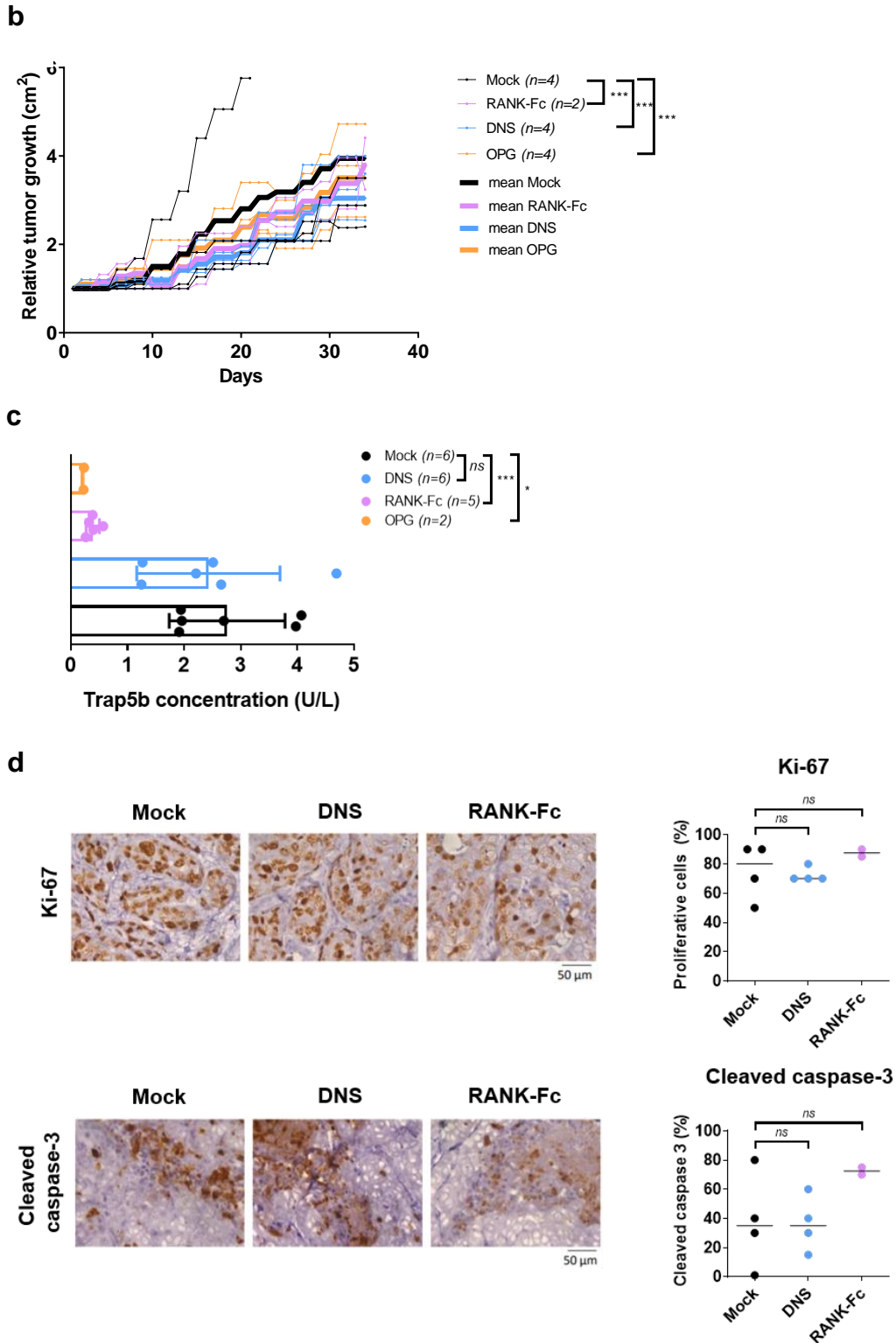
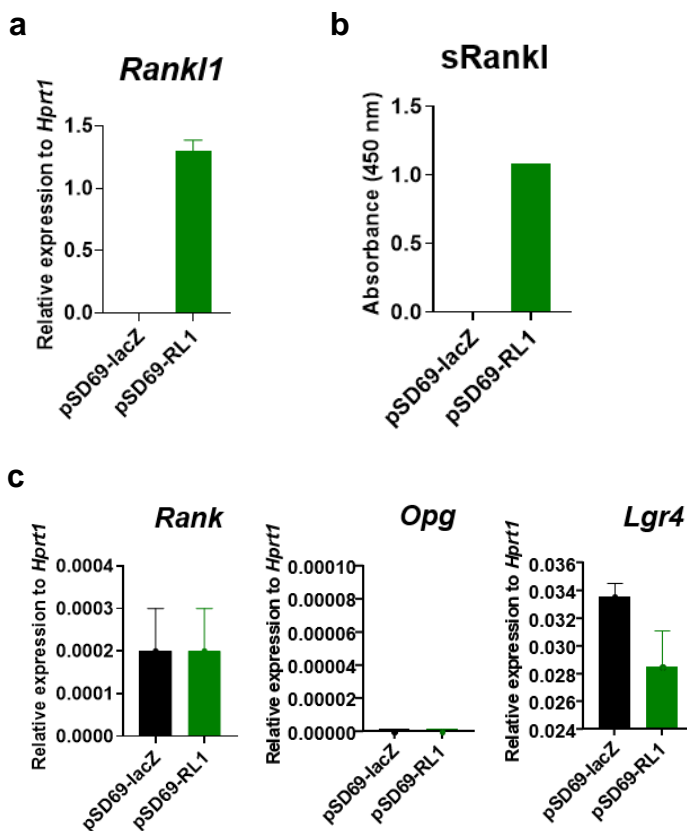


Figure 2.12. RANKL inhibitors attenuated the growth of HCI-001 tumors. (a) Schematic overview of RL inhibitors treatment in orthotopic HCI-001 tumors. $5 \cdot 10^5$ cells isolated from one HCI-001 TNBC PDX was orthotopically injected into the fat pad of NSG mice, which were randomized 1:1 for DNS, RANK-Fc, OPG, or mock treatment when tumors reached 5×5 mm of diameter. (b) Relativized tumor growth to the first day of treatment. Each thin line represents one single tumor, and each thick line represents the mean of all tumors receiving the indicated treatment. Linear regression analysis was performed and a two-tailed p-value was calculated to compare the tumor growth slopes. (c) TRAP 5b concentration in the serum of the NSG mice injected with HCI-001 tumor cells and lately treated with the different treatments. Each point

means a single mouse. Unpaired test was performed. **(d)** Representative images and quantification of the positive cleaved caspase-3 and Ki-67 tumor cells for DNS, RANK-Fc, and mock treatments. Each point means a single tumor. Unpaired test was performed. N is indicated in each case. **** $p < 0.0001$, *** $p < 0.001$, ** $p < 0.01$, * $p < 0.05$, *ns* not significant.

2.8. RL1-OE E0771 cells give rise to tumors with shorter latency and faster tumor growth regardless of the immune system

A limitation of the experiments using human BC cell lines is that the contribution of the immune system to tumor progression cannot be adequately addressed. For this reason, we overexpressed mouse Rank1 protein using lentiviral vectors (pSD69-lacZ (control, lacZ) or pSD69-RL1 (RL1)) in the E0771 cells, a C57BL/6 murine BC cell line (Fig. 2.13a). As previously observed for human RANKL, murine sRank1 was detected by ELISA in the supernatants of RL1-OE E0771 cells, indicating that tmRank1 was shredded as a soluble protein (Fig. 2.13b). E0771 cells expressed endogenous *Lgr4* and low levels of *Rank*, being *Opg* undetectable. No significant differences in *Rank*, *Opg*, and *Lgr4* gene expression (Fig. 2.13c) or the downstream NF- κ B genes were observed upon Rank1 overexpression (Fig. 2.13d). Besides, Rank1 did not influence E0771 cell proliferation *in vitro* (Fig. 2.13e, 2.13f) as observed in human cells.



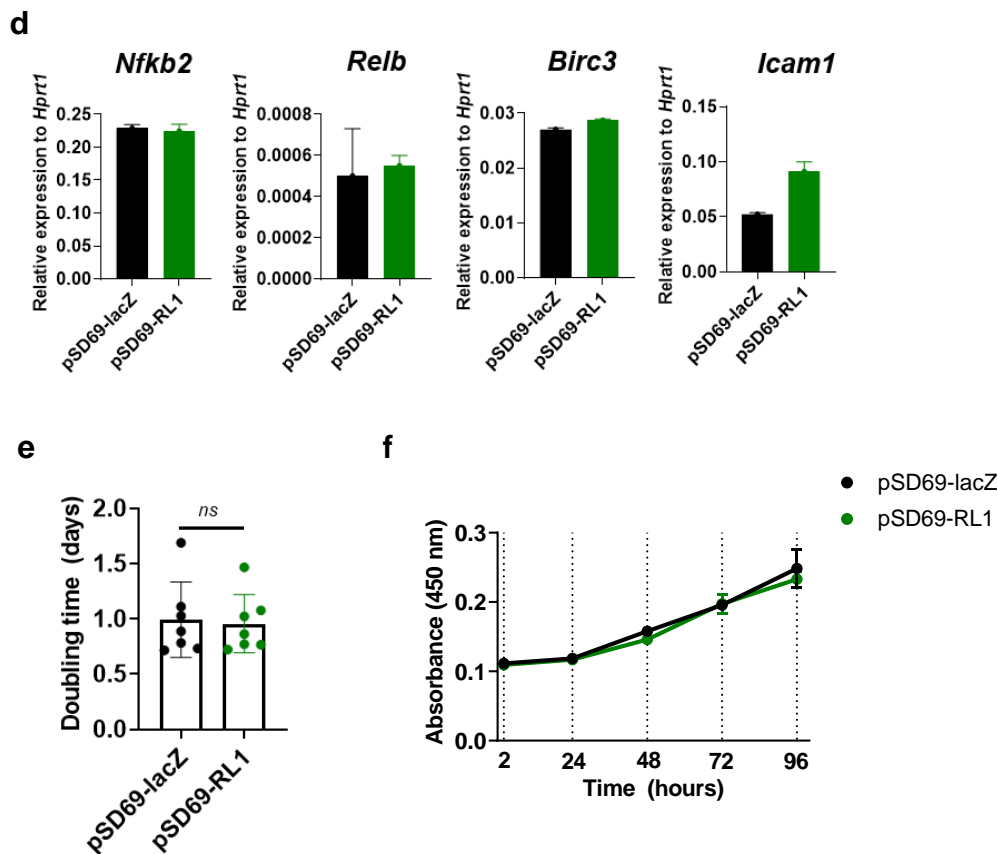


Figure 2.13. The overexpression of Rank1 did not increase the growth of E0771 cells *in vitro*. (a) *Rank1* mRNA expression level relative to *Hprt1* in E0771 overexpressed with pSD69-lacZ and pSD69-RL1 plasmids. (b) Absorbance was obtained through the measurement of the murine sRank1 level in the supernatant of the lacZ- and RL1-OE E0771 cells seeded for 24 h. (c) *Rank*, *Opg*, *Lgr4*, and (d) *Nfkb2*, *Relb*, *Birc3*, and *Icam1* mRNA expression levels relative to *Hprt1* in the lacZ- and RL1-OE E0771 cells cultured *in vitro*. (e) The proliferation rate of the corresponding cells *in vitro* following the formula = $duration\ (days) \cdot \log(2) / \log(\text{counted cells}) - \log(\text{seeded cells})$. Each point means a single passage. (f) Relative (to the first point of measurement, 2h after cell seeding) number of living cells (cell lines are indicated) incubated for different time points (2, 24, 48, 72, and 96 h). Cells were analyzed with CCK8 as detailed in the *Methods* section. T-test and p-values were calculated. **** $p < 0.0001$, *** $p < 0.001$, ** $p < 0.01$, * $p < 0.05$, ns not significant.

To study the contribution of the immune system to the development of Rank1 overexpressing tumors, lacZ- and RL1-OE E0771 cells were injected into the inguinal fat pads of NSG and C57BL/6 mice. Our data revealed a shorter latency and faster growth for RL1-OE E0771 tumors compared to controls in NSG mice (Fig. 2.14a). Importantly, these differences in tumor latency and growth were enhanced when the cells were injected in syngeneic C57BL/6 mice (Fig. 2.14b), indicating that Rank1 accelerates tumor onset and fosters BC growth by immune-dependent and independent mechanisms. Gene expression analysis revealed a significant decrease in *Opg* levels in RL1- compared to lacZ-OE E0771 tumors implanted in NSG mice, but no differences in *Rank* nor *Lgr4* expression were observed (Fig. 2.14c). Finally, the study of immune populations infiltrating the tumors implanted in immune-competent mice indicated a

decrease of NK cells in those tumors that overexpressed Rank1 compared to their controls. Still, no differences in total leucocytes, myeloid cells, or TAMs were detected (Fig. 2.14d). In summary, we demonstrate that Rank1 overexpression in murine E0771 cells promotes faster tumor progression in an immune-competent and immune-compromised setting.

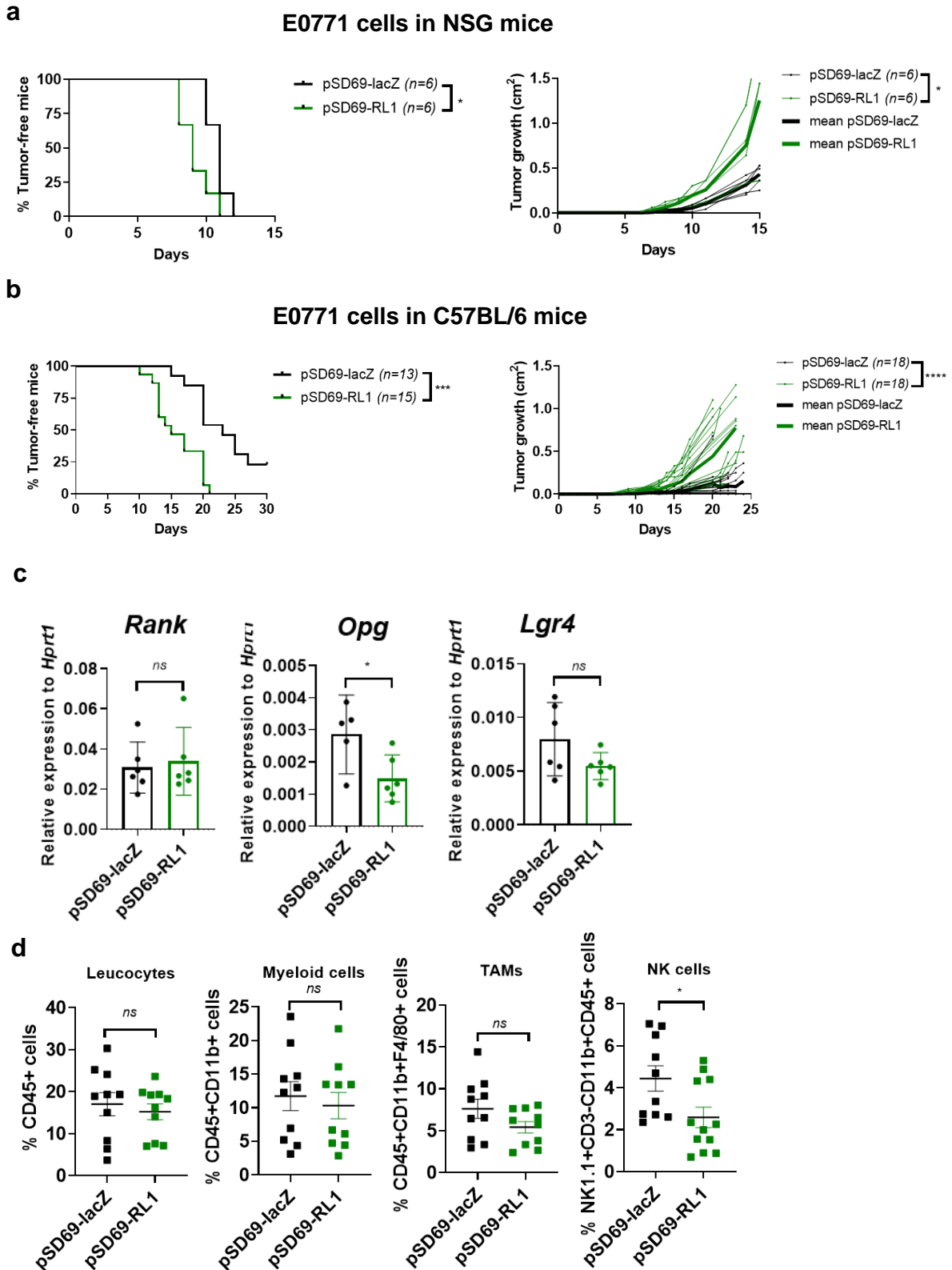


Figure 2.14. RL1-OE E0771 tumors showed a shorter latency and faster tumor growth in immune-deficient and immune-competent mice. $3 \cdot 10^5$ lacZ- and RL1- OE E0771 cells were injected into the fat pad of (a) NSG and (b) C57BL/6 mice. (a, b) Kinetics of palpable tumor onset (left) and growth (right) after transplantation are shown. Each thin line represents one single tumor. Each thick line represents the mean of all the tumors. Log-rank test for latency and linear regression analysis was performed to compare the tumor growth slopes. N is indicated in each case. (c) *Rank*, *Opg*, and *Lgr4* mRNA expression levels relative to *Hprt1* in the indicated lacZ- and RL1-OE E0771 tumors implanted in NSG mice. (d) Graphs showing the percentage of tumor infiltrating leucocytes (CD45⁺), myeloid (CD11b⁺CD45⁺), TAMs (F4/80⁺CD11b⁺CD45⁺) and NKs (NK1.1⁺CD3⁺CD45⁺) in lacZ- and RL1-OE E0771 cells implanted in C57BL/6 mice. (c,d,e) Each point means a single tumor. Mean, SEM shown. T-test and p-values were calculated. **** $p < 0.0001$, *** $p < 0.001$, ** $p < 0.01$, * $p < 0.05$, ns not significant.

2.9. Non-tumoral RANK promotes the initiation and contributes to the progression of RL1-OE E0771 tumors

Since E0771 BC cells expressed low levels of *Rank*, we hypothesized that Rank expressing stromal cells might foster RL1-E0771 tumor growth. We injected lacZ- and RL1-OE E0771 cells into the inguinal fat pad of constitutive *Rank* KO mice. As shown in Fig. 2.15, no differences in latency were observed between lacZ- and RL1-OE E0771 tumors, and despite RL1-OE E0771 tumors growing slightly faster than controls, differences were smaller than in C57BL/6 WT mice. These results suggest that Rank1 enhances tumor growth mainly through the crosstalk with non-tumoral *Rank*-expressing cells.

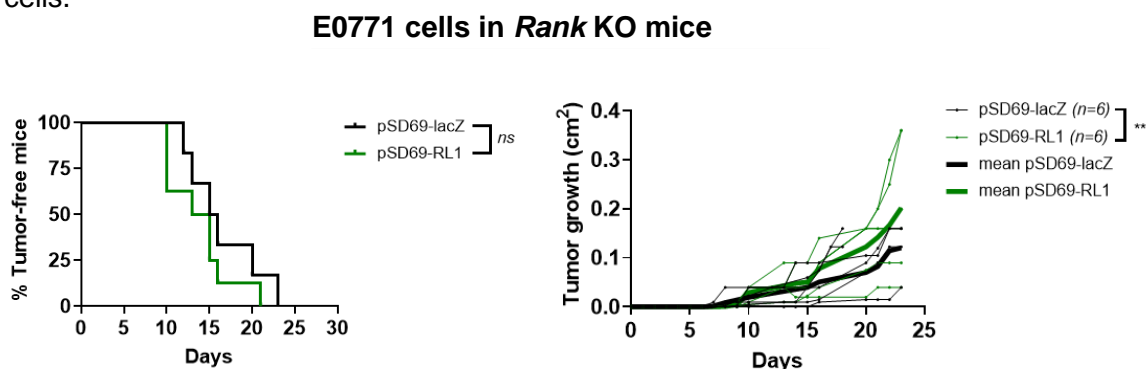
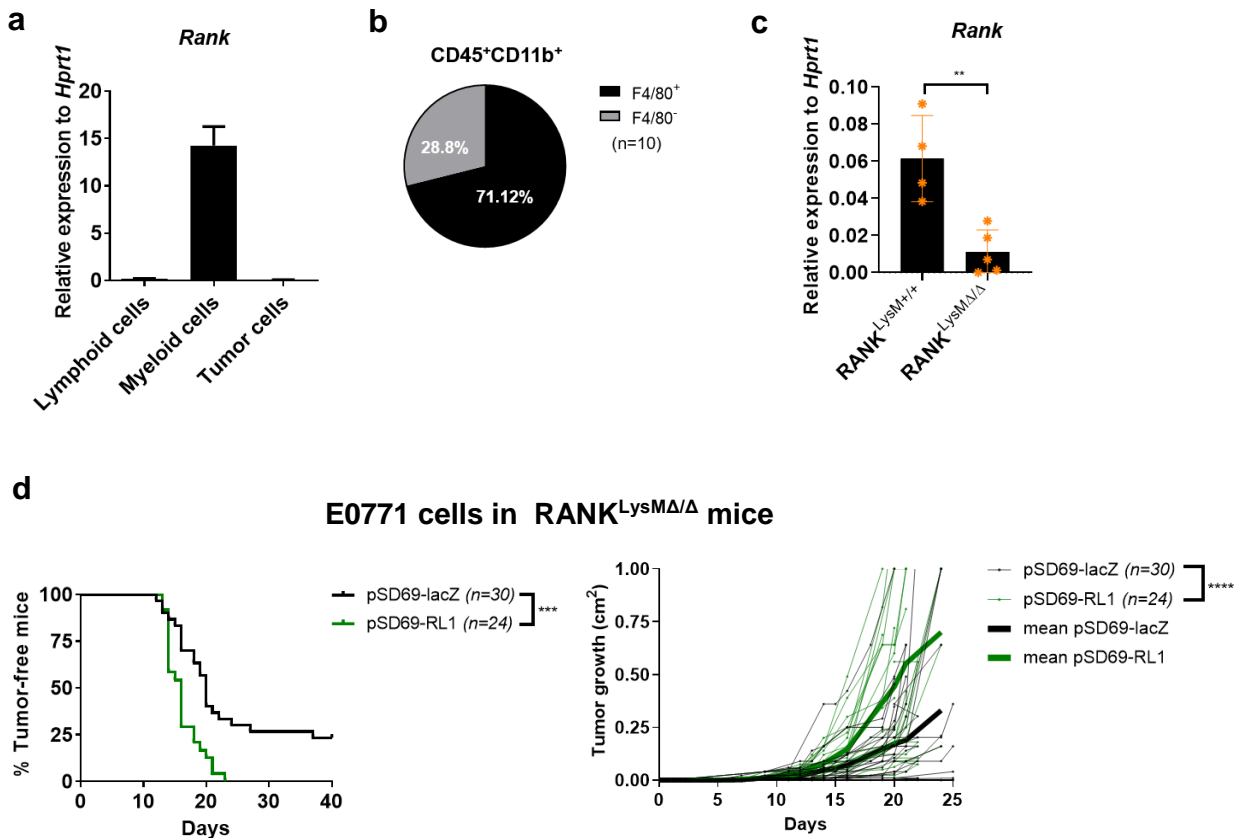


Figure 2.15. Constitutive genetic RANK deletion contributed to the initiation of RL1-OE E0771 tumors. $3 \cdot 10^5$ pSD69-lacZ and -RL1 cells were injected into the fat pad of *Rank* KO mice. Kinetics of palpable tumor onset (left) and growth (right) are shown. Each thin line represents one single tumor. Each thick line represents the mean of all the tumors. Log-rank test for latency and linear regression analysis was performed to compare the tumor growth slopes. N is indicated in each case. **** $p < 0.0001$, *** $p < 0.001$, ** $p < 0.01$, * $p < 0.05$, ns not significant.

2.10. The earlier onset and faster growth of RL1-OE E0771 tumors are not affected by RANK-expressing TAMs

Given the relevance of Rank expressing stromal cells in the growth of RL1-OE E0771 tumors, we analyzed *Rank* gene expression in the main cell populations present in the tumor microenvironment: total leucocytes (CD45⁺), myeloid cells (CD45⁺CD11b⁺) and the population enriched in tumor cells (CD45⁻CD31⁻). Interestingly, we found the highest source of *Rank* expression in the myeloid compartment (Fig. 2.16a), encompassing TAMs (F4/80⁺) and representing around 70% of the myeloid cell infiltrated in lacZ-OE E0771 tumors (Fig. 2.16b). To decipher whether Rank-expressing TAMs foster RL1 tumor growth, we used the LysM-Cre-RANK^{flox/flox} (RANK^{LysMΔ/Δ}) mouse model, which lacks Rank expression specifically in macrophages (Clausen *et al.*, 1999). *Rank* expression decreased in peritoneal macrophages (pMØs) from RANK^{LysMΔ/Δ} and control RANK^{LysM+/+} mice confirming the efficiency of recombination by LysM-Cre (Fig. 2.16c). Upon cell injection in the fat pads of RANK^{LysMΔ/Δ} mice, RL1-OE E0771 tumors showed earlier onset and faster growth than lacZ-OE E0771 tumors (Fig. 2.16d) comparable to the one observed in WT mice. Further analysis of the immune populations did not reveal differences between both groups (Fig. 2.16e). Since TAMs-lacking Rank did not influence the onset nor the growth of RL1-OE E0771 tumors, we conclude that the expression of Rank in TAMs is not contributing to the RL1-OE E0771 tumor phenotype.



e

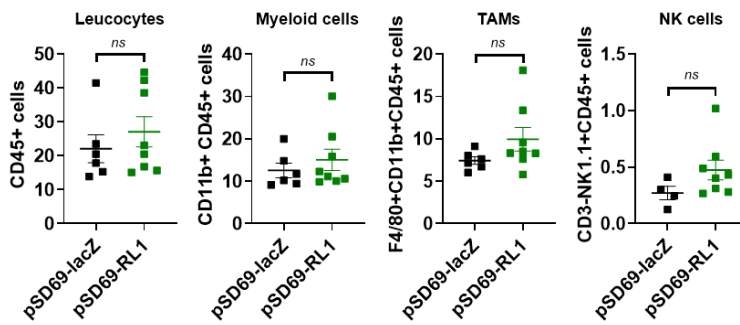


Figure 2.16. RL1-OE E0771 tumors promoted shorter tumor onset and faster growth than control tumors in $RANK^{LysM\Delta/\Delta}$ mice. (a) *Rank* mRNA expression level relative to *Hprt1* in lymphoid cells ($CD45^+CD11b^-$), myeloid cells ($CD45^+CD11b^+$), and population enriched in tumor cells ($CD45^+CD31^-$) sorted from E0771 tumors implanted into the fat pad of C57BL/6 mice. (b) Mean of the percentage of $F4/80^+$ and $F4/80^-$ cells within myeloid cells infiltrated into E0771 tumors implanted into C57BL/6 mice. (c) *Rank* mRNA expression level relative to *Hprt1* of pMØs of $RANK^{LysM+/+}$ and $RANK^{LysM\Delta/\Delta}$ mice. (d) $3 \cdot 10^5$ pSD69-lacZ and -RL1 cells were injected into the fat pad of $RANK^{LysM\Delta/\Delta}$ mice. Kinetics of palpable tumor onset (left) and growth (right) are shown. Each thin line represents one single tumor. Each thick line represents the mean of all the tumors. Log-rank test for latency and linear regression analysis was performed to compare the tumor growth slopes. N is indicated in each case. (e) Graphs showing the percentage of tumor infiltrating leukocytes ($CD45^+$), myeloid, TAMs ($F4/80^+CD11b^+CD45^+$), NKs ($NK1.1^+CD3^+CD45^+$) in lacZ- and RL1-OE E0771 tumors in $RANK^{LysM\Delta/\Delta}$ mice. Each point means a single tumor. Mean, SEM shown. T-test and p-values were calculated. **** $p < 0.0001$, *** $p < 0.001$, ** $p < 0.01$, * $p < 0.05$, ns not significant.

2.11. RANKL blockade delays the tumor onset of RL1-OE tumors in immune-competent mice

Next, we studied the therapeutic potential of anti-Rankl in a fully competent environment. E0771 mouse breast cancer cells were orthotopically implanted in the inguinal fat pad of syngeneic C57BL/6 mice, randomized for IgG or α -RL (3 times per week) at the time of implantation and the treatments were maintained until endpoint. The systemic blockade of RL attenuated tumor growth in RL1-OE tumors but not in controls (Fig. 2.17), reinforcing the therapeutic potential of RANKL inhibitors for BC patients with tumors-expressing RANKL1. However, α -RL-treated RL1-E0771 tumors grew faster than controls, suggesting an intrinsic mechanism, such as the reverse signaling triggered by RANKL, which DNS cannot inhibit.

E0771 cells in C57BL/6 mice

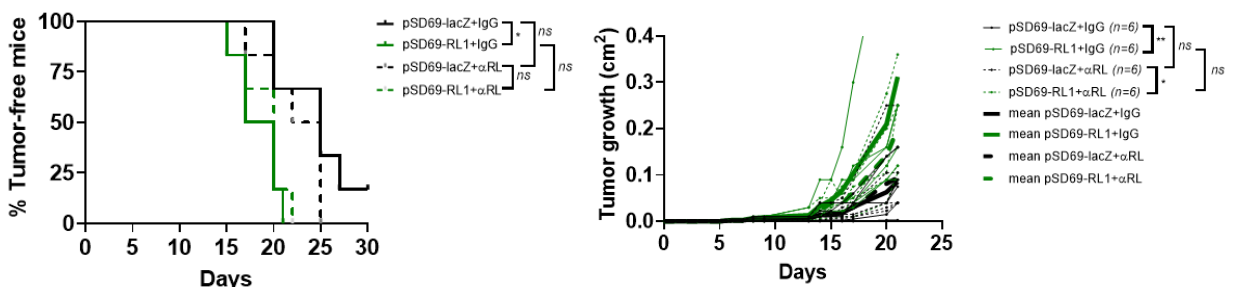


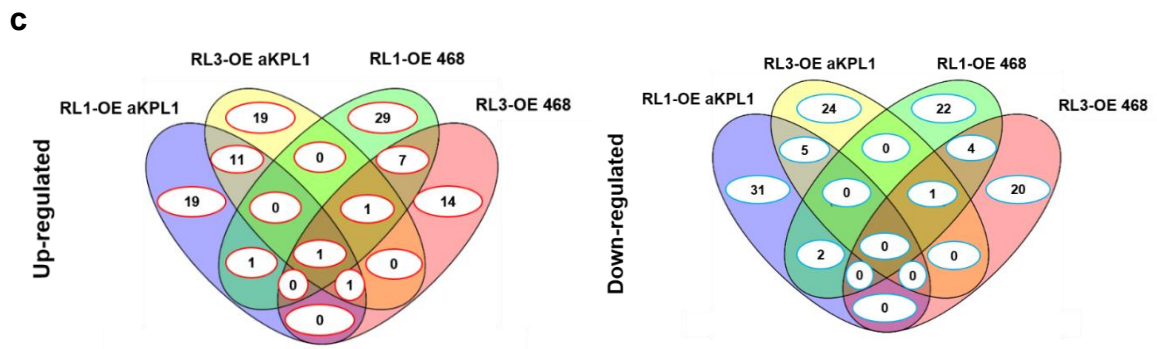
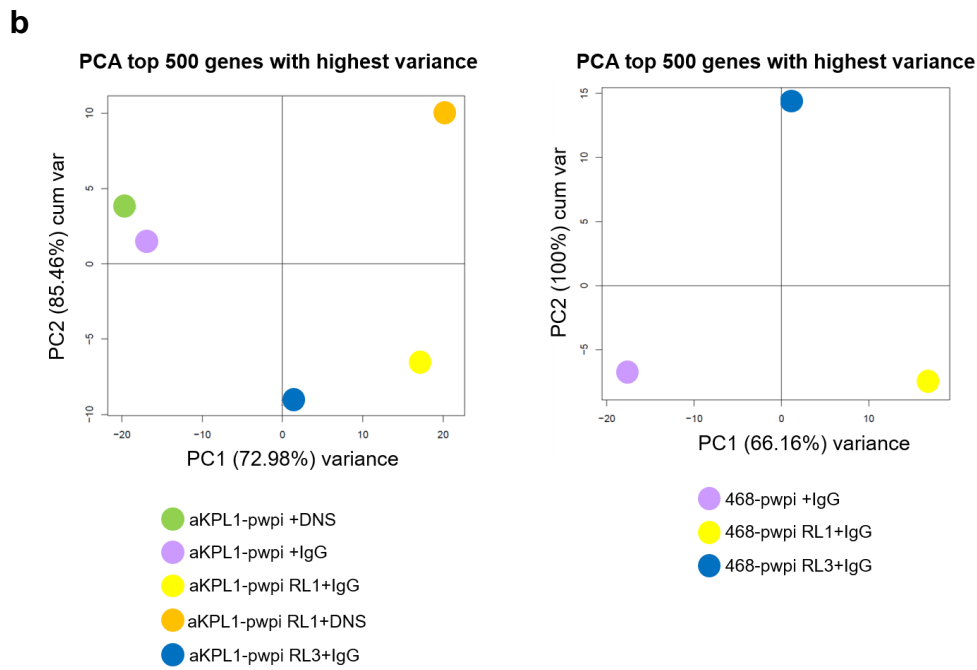
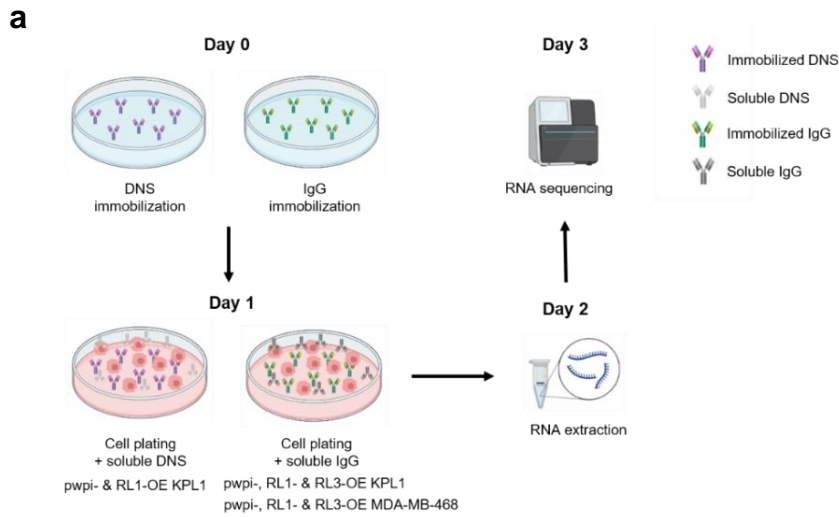
Figure 2.17. Pharmacological and systemic inhibition of RANKL reduced the aggressiveness of RL1-OE E0771 tumors. $3 \cdot 10^5$ pSD69-lacZ and -RL1 cells were injected into the fat pad of C57BL/6 mice, which were randomized 1:1 for α -RL or mock treatment at day 0 of transplantation. Kinetics of palpable tumor onset (left) and growth (right) for all the conditions are shown. Each thin line represents one single tumor. Each thick line represents the mean of all the tumors. Log-rank test for latency and linear regression analysis was performed to compare the tumor growth slopes. N is indicated in each case. **** $p < 0.0001$, *** $p < 0.001$, ** $p < 0.01$, * $p < 0.05$, ns not significant.

2.12. The overexpression of RANKL1 and RANKL3 triggers a similar gene expression profile

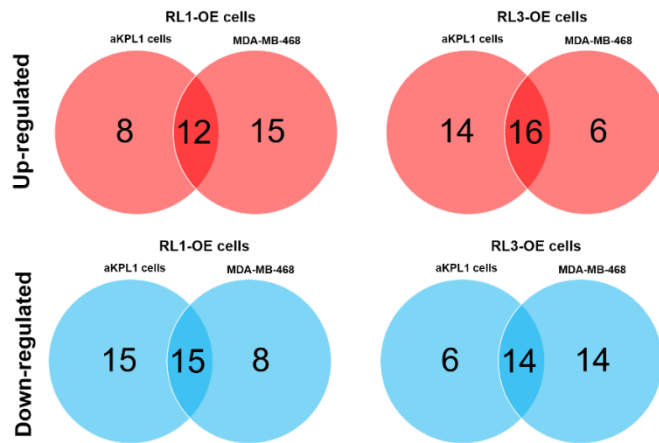
Aiming to understand the tumor cell-intrinsic mechanisms underlying RANKL1 and RANKL3 functionality, we performed RNA-seq analysis of pwpi-, RL1- and RL3-OE MDA-MB-468 and aKPL1 cells growing *in vitro*. To study the effect of RANKL1 inhibition, RL1-OE cells and the corresponding controls were seeded on a plate pre-covered with immobilized DNS (only in aKPL1 cells) or IgG and incubated with soluble DNS or IgG. For RL3-OE cells only IgG was used. After 24 h, cells were collected, and their RNA purified for RNA-seq analyses (Fig. 2.18a). Principal component analysis (PCA) based on the 500 genes with the highest variance allowed us to discern an immediate visualization of the genetic differences in the aKPL1 cells after overexpressing RANKL1 or RANKL3, compared to controls in the two cell lines, MDA-MB-468, and aKPL1 cells, indicating different transcriptomic profiles (Fig. 2.18b). Moreover, while pwpi-OE aKPL1 cells upon IgG and DNS treatments grouped in PCA, RL1-OE aKPL1 cells upon DNS were separated from the IgG-treated cells and the controls cells, indicating that DNS could not revert all changes driven by RANKL1 overexpression (Fig. 2.18b). Differential expression analysis selecting a FC > 2.5 (up-regulation) and FC < -2.5 (down-regulation) revealed 68 genes regulated by RANKL1 and 49 genes by RANKL3 in MDA-MB-468 and 71 genes regulated by RANKL1 and 63 by RANKL3 in aKPL1 (Fig. 2.18c; Table 2.9). RL1- and RL3-OE MDA-MB-468 cells shared 9 up- and 5 down-regulated genes, while RL1- and RL3-OE aKPL1 cells shared 12 up- and 5 down-regulated genes (Fig. 2.18c; Table 2.9). When both cell lines were compared, 8 genes were similarly regulated by RANKL1 and 4 by RANKL3 between aKPL1 and MDA-MB-468 cells (Fig. 2.18c; Table 2.9). Next, SingScore (Foroutan *et al.*, 2018) was used to perform functional analysis on the Hallmark gene set collection (Liberzon *et al.*, 2015) at a single sample level. SingScore returned a table with the calculated scores for each signature in each sample. Angiogenesis, oxidative phosphorylation, unfolded protein response, and MYC targets were included in the top ten pathways up-regulated by RANKL1 in MDA-MB-468 cells. In contrast, signaling pathways such as Notch, KRAS, and apical junction, among others, were downregulated (Table 2.10). In the same cell line, RANKL3 overexpression up-

regulated fatty acid and glucose metabolism while down-regulated signaling pathways such as Hedgehog, Notch, and WNT- β Catenin (Table 2.11). In aKPL1 cells, the most positively regulated processes upon RANKL1 overexpression were the epithelial-mesenchymal transition, TNF- α signaling, and inflammation pathways such as IFN- α and IFN- γ (Table 2.12). Opposite, RANKL1 down-regulated signaling such as PI3K AKT MTOR signaling (Table 2.12). Finally, RANKL3 overexpression up-regulated inflammation-related pathways such as IFN- α , IFN- γ , and complement while down-regulated IL6 JAK STAT3 signaling pathway, among other processes (Table 2.13). Despite the low number of genes in common, the overlap of the up-and down-regulated pathways upon the same protein (RANKL1 or RANKL3) in the basal MDA-MB-468 and luminal aKPL1 cells revealed a very close pattern of expression showing a high number of processes in common: RANKL1 controlled 27 pathways, 12 up-regulated (such as IFN- γ response, TNF- α signaling via NF- κ B, reactive oxygen species pathway and MYC targets) and 15 down-regulated (such as apical junction and surface). In comparison, RANKL3 managed 30 pathways, 16 up-regulated (such as immune-related pathways, epithelial-mesenchymal transition, and oncogenic signaling E2F and MYC targets) and 14 down-regulated (such as apical surface, PI3K AKT MTOR signaling) (Fig. 2.18d; Table 2.14). Our results highlight some commonalities between RANKL1 and RANKL3 suggesting an intracellular role of RANKL1 previously unrecognized, and distinct biological functions between RANKL1 and RANKL3, but a pro-tumorigenic genetic profile after overexpressing either of the two RANKL isoforms.

Next, we aimed to decipher whether DNS could reverse the RANKL1-driven effects. In aKPL1 cells, there were more down-regulated than up-regulated pathways in RL1-OE aKPL1 cells upon DNS treatment compared to IgG treatment (Table 2.15). DNS up-regulated pathways related to cell cycle arrest and immune system regulation, such as IFN- α response, while down-regulated oncogenic processes such as epithelial-mesenchymal transition, angiogenesis, IFN- γ response, peroxisome regulation, and glycolysis (Table 2.15). Of note, relevant pathways involved in oncogenic processes were modulated after RANKL1 overexpression and subsequently reversed by the addition of DNS. Pathways such as MYC, unfolded protein response, WNT- β catenin signaling, and epithelial mesenchymal-transition were up-regulated in RL1-OE aKPL1 cells and down-regulated after DNS addition (Fig. 2.18e). Protein secretion, complement, hypoxia, or IL2 STAT5 pathways were down-regulated in RL1-OE aKPL1 cells and upregulated upon DNS treatment (Fig. 2.18e). These results indicate that DNS was able to block only some of the pro-tumorigenic pathways driven by RANKL1.



d



e

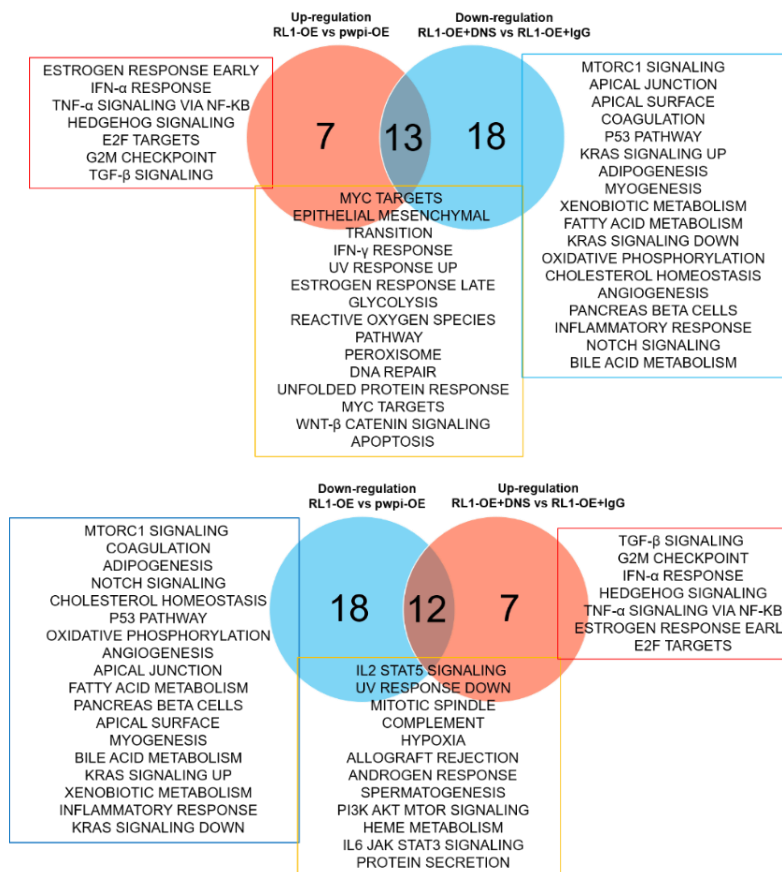
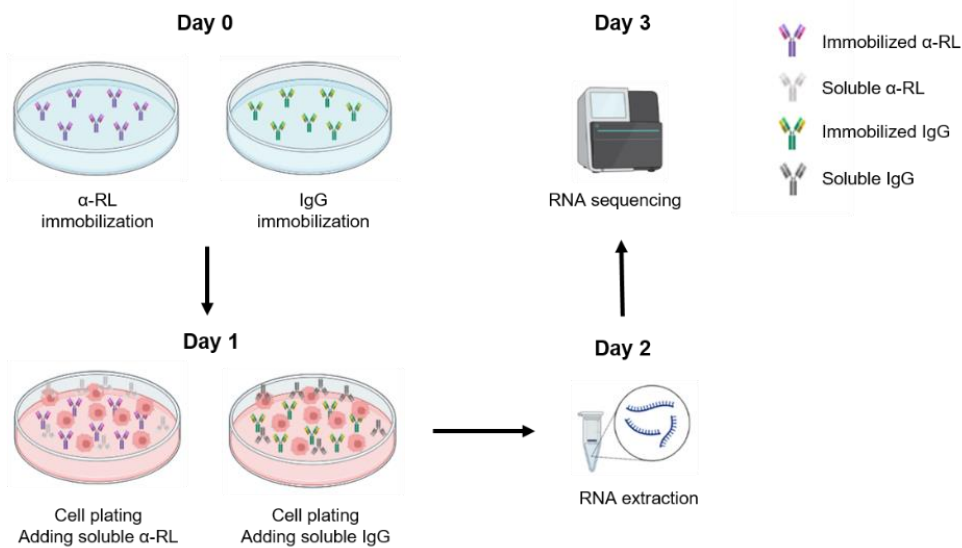


Figure 2.18. Expression profile in RL1- and RL3-OE human cell lines. (a) Schematic overview of the experimental design. On day 0, the protein (IgG or DNS) was immobilized in the plate as detailed in the *Methods* section. On day 1, cells were seeded, and the soluble stimuli were added at the same time. On day 2, cells were collected, and RNA isolation and subsequent sequencing were performed. (b) PCA top 500 genes with the highest variance for (left) pwpi-, RL1- and RL3-OE aKPL1 cells treated with IgG and pwpi- and RL1-OE aKPL1 cells treated with DNS and (right) pwpi-, RL1- and RL3-OE MDA-MB-468 cells treated with IgG. (c) Compared with their controls, venn diagrams of the shared up-regulated and down-regulated genes between RL1- and RL3-OE MDA-MB-468 and aKPL1 cell lines. (d) Venn diagrams of shared up-regulated and down-regulated pathways between RL1-OE cells (left) or RL3-OE cells (right) compared with their controls. (e) Venn diagrams showing the shared up-regulated pathways in RL1-OE aKPL1 cells

(vs. pwpi-OE aKPL1 cells) which are down-regulated in RL1-OE aKPL1 cells treated with DNS (vs. RL1-OE aKPL1 cells treated with IgG). Venn diagrams showing the shared down-regulated pathways in RL1-OE aKPL1 cells (vs pwpi-OE aKPL1 cells) which are up-regulated in RL1-OE aKPL1 cells treated with DNS (vs RL1-OE KPL1 cells treated with IgG). Pathways exclusively regulated in a single condition are also indicated.

Next, transcriptomic changes were analyzed in psd69-lacZ and RL1-OE E0771 cells following the same protocol detailed above using α -RL (Fig. 2.19a). RNA-seq analyses unveiled that RL1-OE E0771 shared with human RL1-OE BC cells the up-regulation of the apoptosis pathway. In contrast, processes such as hypoxia, apical junction, and mitotic spindle were down-regulated (Table 2.16). As in humans, to clarify which pathways were triggered by RANKL1 and reversed by anti-RANKL, we treated the RL1-OE E0771 cells and their control with α -RL. As shown in Figure 2.19b, epithelial mesenchymal transition and apical surface processes up-regulated in RL-OE E0771 cells compared to with its control were down-regulated after α -RL treatment. On the opposite hand, immune-related pathways and metabolism processes, down-regulated in RL-OE E0771 cells, were up-regulated upon α -RL treatment (Fig. 2.19b). Our results confirm that the overexpression of two different RANKL isoforms that localize in separate cell compartments modulate a very similar expression profile of pathways. Moreover, the inhibition of human or murine RANKL1 triggers the inhibition of epithelial mesenchymal transition, which is directly involved in tumor progression and the generation of tumor cells with stem cell properties, indicating a possible role of RANKL1 in that process.

a



b

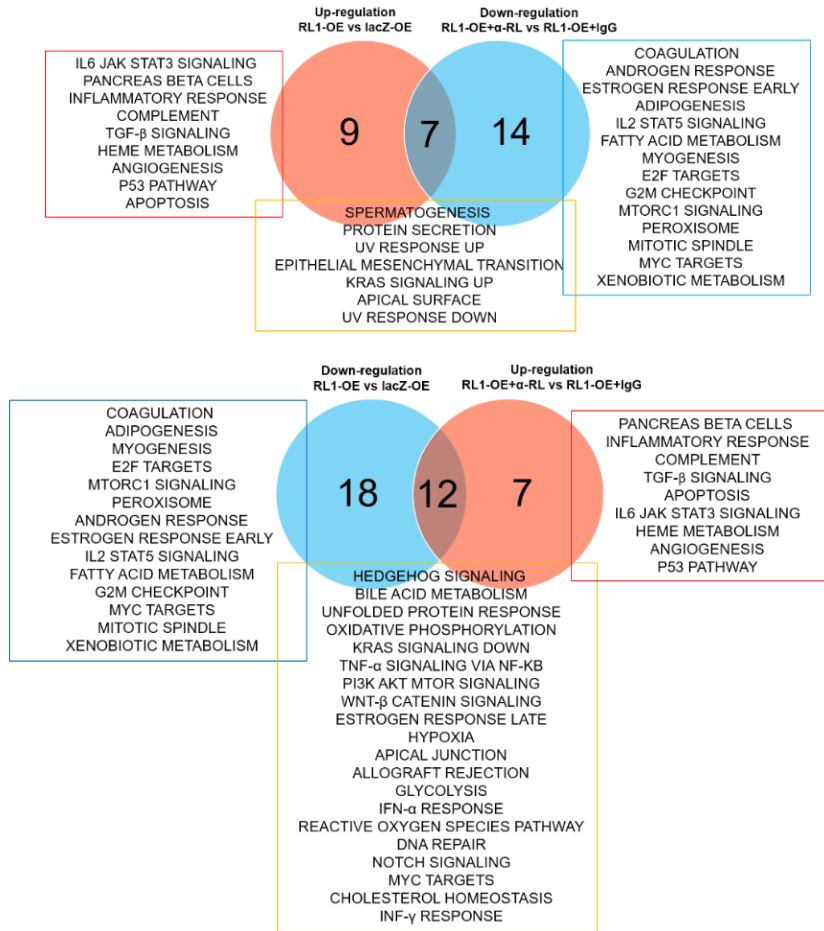


Figure 2.19. Expression profile in RL1-OE murine E0771 cell line. (a) Schematic overview of the experimental design. At day 0, the protein (IgG or α-RL) was immobilized in the plate as detailed in *Methods section*. On day 1 cells were seeded, and the soluble stimuli was added at the same time. On day 2 cells were collected and RNA isolation and subsequent sequencing was performed. **(b)** Venn diagrams showing the shared up-regulated pathways in RL1-OE E0771 cells (vs. lacZ-OE E0771 cells) which are down-regulated in RL1-OE E0771 cells treated with α-RL (vs. RL1-OE E0771 cells treated with IgG). Venn diagrams showing the shared down-regulated pathways in RL1-OE E0771 cells (vs lacZ-OE E0771 cells) which are up-regulated in RL1-OE E0771 cells treated with α-RL (vs RL1-OE E0771 cells treated with IgG). Pathways exclusively regulated in a single condition are also indicated.

Tables

**NPS COLLECTION
WHOLE PATIENTS**

Disease Free-Survival (5y)				Distant Metastasis Free-Survival (5y)				Breast Cancer Specific Survival (5y)						
icRANKL	Total N	N of events	Censored		icRANKL	Total N	N of events	Censored		icRANKL	Total N	N of events	Censored	
			N	Percent				N	Percent				N	Percent
Negative expression	921	270	651	70.7%	Negative expression	920	197	723	78.6%	Negative expression	935	149	786	84.1%
Positive expression	89	23	66	74.2%	Positive expression	89	19	70	78.7%	Positive expression	91	13	78	85.7%
Overall	1010	293	717	71.00%	Overall	1009	216	793	78.6%	Overall	1026	162	864	84.2%
Chi-Square		df		Sig.	Chi-Square		df		Sig.	Chi-Square		df		Sig.
Log Rank (Mantel-Cox)	0.389	1	0.533		Log Rank (Mantel-Cox)	0.001	1	0.974		Log Rank (Mantel-Cox)	0.175	1	0.676	
Disease Free-Survival (10y)				Distant Metastasis Free-Survival (10y)				Breast Cancer Specific Survival (10y)						
icRANKL	Total N	N of events	Censored		icRANKL	Total N	N of events	Censored		icRANKL	Total N	N of events	Censored	
			N	Percent				N	Percent				N	Percent
Negative expression	921	362	559	60.7%	Negative expression	920	280	640	69.6%	Negative expression	935	234	701	75.00%
Positive expression	89	31	58	65.2%	Positive expression	89	28	61	68.5%	Positive expression	91	21	70	76.9%
Overall	1010	393	617	61.1%	Overall	1009	308	701	69.5%	Overall	1026	255	771	75.1%
Chi-Square		df		Sig.	Chi-Square		df		Sig.	Chi-Square		df		Sig.
Log Rank (Mantel-Cox)	0.488	1	0.485		Log Rank (Mantel-Cox)	0.056	1	0.813		Log Rank (Mantel-Cox)	0.184	1	0.668	
Disease Free-Survival (15y)				Distant Metastasis Free-Survival (15y)				Breast Cancer Specific Survival (15y)						
icRANKL	Total N	N of events	Censored		icRANKL	Total N	N of events	Censored		icRANKL	Total N	N of events	Censored	
			N	Percent				N	Percent				N	Percent
Negative expression	921	391	530	57.5%	Negative expression	920	326	594	64.6%	Negative expression	819	284	535	65.3%
Positive expression	89	34	55	61.8%	Positive expression	89	33	56	62.9%	Positive expression	75	29	46	61.3%
Overall	1010	425	585	57.9%	Overall	1009	359	650	64.4%	Overall	894	313	581	65.00%
Chi-Square		df		Sig.	Chi-Square		df		Sig.	Chi-Square		df		Sig.
Log Rank (Mantel-Cox)	0.215	1	0.643		Log Rank (Mantel-Cox)	0.425	1	0.515		Log Rank (Mantel-Cox)	0.275	1	0.60	
Disease Free-Survival (20y)				Breast Cancer Specific Survival (25y)										
icRANKL	Total N	N of events	Censored		icRANKL	Total N	N of events	Censored						
			N	Percent				N	Percent					
Negative expression	921	398	523	56.8%	Negative expression	935	312	623	66.6%					
Positive expression	89	34	55	61.8%	Positive expression	91	34	57	62.6%					
Overall	1010	432	578	57.2%	Overall	1026	346	680	66.3%					
Chi-Square		df		Sig.	Chi-Square		df		Sig.					
Log Rank (Mantel-Cox)	0.231	1	0.631		Log Rank (Mantel-Cox)	0.55	1	0.458						

Table 2.1. Survival data of patients (whole cohort) from NPS dataset.

**METABRIC COLLECTION
WHOLE PATIENTS**

Disease Free-Survival (5y)				Distant Metastasis Free-Survival (5y)				Breast Cancer Specific Survival (5y)			
icRANKL		Censored		icRANKL		Censored		icRANKL		Censored	
N	Percent	N	Percent	N	Percent	N	Percent	N	Percent	N	Percent
46	74%	131	74%	36	79.7%	141	79.7%	27	59.1%	152	84.9%
10	66.7%	20	66.7%	10	20	20	66.7%	9	18.4%	22	71.00%
56	72.9%	151	72.9%	46	77.8%	161	77.8%	36	77.8%	174	92.9%
df	Sig.	df	Sig.	df	Sig.	df	Sig.	df	Sig.	df	Sig.
1,002	0.317	1	0.317	3,030	0.082	1	0.082	4,341	0.037	1	0.037
Disease Free-Survival (10y)				Distant Metastasis Free-Survival (10y)				Breast Cancer Specific Survival (10y)			
c/rRANKL		Censored		icRANKL		Censored		icRANKL		Censored	
N	Percent	N	Percent	N	Percent	N	Percent	N	Percent	N	Percent
64	63.8%	113	63.8%	54	69.5%	123	69.5%	44	56.4%	135	75.4%
15	50.00%	15	50.00%	14	16	16	53.3%	12	19	19	61.3%
79	61.8%	128	61.8%	68	67.1%	139	67.1%	56	56	154	73.3%
df	Sig.	df	Sig.	df	Sig.	df	Sig.	df	Sig.	df	Sig.
2,603	0.107	1	0.107	3,651	0.056	1	0.056	3,543	0.060	1	0.060
Disease Free-Survival (15y)				Distant Metastasis Free-Survival (15y)				Breast Cancer Specific Survival (15y)			
icRANKL		Censored		icRANKL		Censored		icRANKL		Censored	
N	Percent	N	Percent	N	Percent	N	Percent	N	Percent	N	Percent
71	59.9%	106	59.9%	64	63.8%	113	63.8%	53	98	98	64.9%
15	50.00%	15	50.00%	16	14	14	46.7%	15	14	14	48.3%
86	58.5%	121	58.5%	80	61.4%	127	61.4%	68	112	112	62.2%
df	Sig.	df	Sig.	df	Sig.	df	Sig.	df	Sig.	df	Sig.
2,112	0.146	1	0.146	4,898	0.027	1	0.027	3,684	0.055	1	0.055
Disease Free-Survival (20y)				Breast Cancer Specific Survival (25y)				Breast Cancer Specific Survival (25y)			
icRANKL		Censored		icRANKL		Censored		icRANKL		Censored	
N	Percent	N	Percent	N	Percent	N	Percent	N	Percent	N	Percent
71	59.9%	106	59.9%	59	67.00%	120	67.00%	59	120	120	67.00%
15	50.00%	15	50.00%	15	16	16	51.6%	15	16	16	51.6%
86	58.5%	121	58.5%	74	64.8%	136	64.8%	74	136	136	64.8%
df	Sig.	df	Sig.	df	Sig.	df	Sig.	df	Sig.	df	Sig.
2,112	0.146	1	0.146	4,096	0.043	1	0.043	4,096	0.043	1	0.043

Table 2.2. Survival data of patients (whole cohort) from METABRIC dataset.

NPS COLLECTION

ER+ PATIENTS

Disease Free-Survival (5y)				Distant Metastasis Free-Survival (5y)				Breast Cancer Specific Survival (5y)			
Censored				Censored				Censored			
icRANKL	Total N	N of events	Percent	icRANKL	Total N	N of events	Percent	icRANKL	Total N	N of events	Percent
Negative expression	683	181	73.5%	Negative expression	682	125	81.7%	Negative expression	688	86	87.5%
Positive expression	53	13	75.5%	Positive expression	53	11	79.2%	Positive expression	54	6	88.9%
Overall	736	194	73.6%	Overall	735	136	81.5%	Overall	742	92	87.6%
Chi-Square		df	Sig.	Chi-Square		df	Sig.	Chi-Square		df	Sig.
Log Rank (Mantel-Cox)	0.028	1	0.867	Log Rank (Mantel-Cox)	0.294	1	0.588	Log Rank (Mantel-Cox)	0.070	1	0.791
Disease Free-Survival (10y)				Distant Metastasis Free-Survival (10y)				Breast Cancer Specific Survival (10y)			
Censored				Censored				Censored			
icRANKL	Total N	N of events	Percent	icRANKL	Total N	N of events	Percent	icRANKL	Total N	N of events	Percent
Negative expression	683	261	61.8%	Negative expression	682	195	71.4%	Negative expression	688	155	77.5%
Positive expression	53	18	66.00%	Positive expression	53	16	69.8%	Positive expression	54	9	83.3%
Overall	736	279	62.1%	Overall	735	211	71.3%	Overall	742	164	77.9%
Chi-Square		df	Sig.	Chi-Square		df	Sig.	Chi-Square		df	Sig.
Log Rank (Mantel-Cox)	0.178	1	0.673	Log Rank (Mantel-Cox)	0.126	1	0.723	Log Rank (Mantel-Cox)	0.848	1	0.357
Disease Free-Survival (15y)				Distant Metastasis Free-Survival (15y)				Breast Cancer Specific Survival (15y)			
Censored				Censored				Censored			
icRANKL	Total N	N of events	Percent	icRANKL	Total N	N of events	Percent	icRANKL	Total N	N of events	Percent
Negative expression	683	290	57.5%	Negative expression	682	238	65.1%	Negative expression	595	197	66.9%
Positive expression	53	20	62.3%	Positive expression	53	20	62.3%	Positive expression	46	15	67.4%
Overall	736	310	57.9%	Overall	735	258	64.9%	Overall	641	212	66.9%
Chi-Square		df	Sig.	Chi-Square		df	Sig.	Chi-Square		df	Sig.
Log Rank (Mantel-Cox)	0.074	1	0.785	Log Rank (Mantel-Cox)	0.554	1	0.457	Log Rank (Mantel-Cox)	0.013	1	0.908
Disease Free-Survival (20y)				Distant Metastasis Free-Survival (20y)				Breast Cancer Specific Survival (20y)			
Censored				Censored				Censored			
icRANKL	Total N	N of events	Percent	icRANKL	Total N	N of events	Percent	icRANKL	Total N	N of events	Percent
Negative expression	683	296	56.7%	Negative expression	688	222	67.7%	Negative expression	688	222	67.7%
Positive expression	53	20	62.3%	Positive expression	54	19	64.8%	Positive expression	54	19	64.8%
Overall	736	316	57.1%	Overall	742	241	67.5%	Overall	742	241	67.5%
Chi-Square		df	Sig.	Chi-Square		df	Sig.	Chi-Square		df	Sig.
Log Rank (Mantel-Cox)	0.090	1	0.764	Log Rank (Mantel-Cox)	0.126	1	0.723	Log Rank (Mantel-Cox)	0.126	1	0.723

Table 2.3. Survival data of patients (ER+ cohort) from NPS dataset.

METABRIC COLLECTION

ER+ PATIENTS

Disease Free-Survival (10y)			Distant Metastasis Free-Survival (5y)			Breast Cancer Specific Survival (5y)		
icRANKL	Total N	N of events	icRANKL	Total N	N of events	icRANKL	Total N	N of events
Positive expression	13	3	Negative expression	140	26	Negative expression	141	16
Overall	153	38	Positive expression	13	3	Positive expression	14	3
Chi-Square		df	Overall	153	29	Overall	155	19
Log Rank (Mantel-Cox)	0.0001	1	Log Rank (Mantel-Cox)	0.293	1	Log Rank (Mantel-Cox)	1.360	1
Disease Free-Survival (10y)			Distant Metastasis Free-Survival (10y)			Breast Cancer Specific Survival (10y)		
icRANKL	Total N	N of events	icRANKL	Total N	N of events	icRANKL	Total N	N of events
Negative expression	140	51	Negative expression	140	39	Negative expression	141	30
Positive expression	13	6	Positive expression	13	6	Positive expression	14	4
Overall	153	57	Overall	153	45	Overall	155	34
Chi-Square		df	Chi-Square		df	Chi-Square		df
Log Rank (Mantel-Cox)	0.542	1	Log Rank (Mantel-Cox)	2.245	1	Log Rank (Mantel-Cox)	0.585	1
Disease Free-Survival (15y)			Distant Metastasis Free-Survival (15y)			Breast Cancer Specific Survival (15y)		
icRANKL	Total N	N of events	icRANKL	Total N	N of events	icRANKL	Total N	N of events
Negative expression	140	57	Negative expression	140	48	Negative expression	119	38
Positive expression	13	6	Positive expression	13	7	Positive expression	14	6
Overall	153	63	Overall	153	55	Overall	133	44
Chi-Square		df	Chi-Square		df	Chi-Square		df
Log Rank (Mantel-Cox)	0.340	1	Log Rank (Mantel-Cox)	2.831	1	Log Rank (Mantel-Cox)	0.920	1
Disease Free-Survival (20y)			Distant Metastasis Free-Survival (20y)			Breast Cancer Specific Survival (20y)		
icRANKL	Total N	N of events	icRANKL	Total N	N of events	icRANKL	Total N	N of events
Negative expression	140	57	Negative expression	141	43	Negative expression	141	43
Positive expression	13	6	Positive expression	14	6	Positive expression	14	6
Overall	153	63	Overall	155	49	Overall	155	49
Chi-Square		df	Chi-Square		df	Chi-Square		df
Log Rank (Mantel-Cox)	0.340	1	Log Rank (Mantel-Cox)	1.436	1	Log Rank (Mantel-Cox)	1.436	1
Censored			Censored			Censored		
N	Percent		N	Percent		N	Percent	
83	59.3%		92	65.7%		81	68.1%	
7	53.8%		6	46.2%		8	67.1%	
90	58.8%		98	64.1%		89	66.9%	
	Sig.			Sig.			Sig.	
	0.560			0.092			0.338	

Table 2.4. Survival data of patients (ER+ cohort) from METABRIC dataset.

NPS COLLECTION

ER' PATIENTS

Disease Free-Survival (5y)				Distant Metastasis Free-Survival (5y)				Distant Metastasis Free-Survival (10y)							
icRANKL	Total N	N of events	Censored N Percent	icRANKL	Total N	N of events	Censored N Percent	icRANKL	Total N	N of events	Censored N Percent	icRANKL	Total N	N of events	Censored N Percent
Negative expression	228	85	143 62.7%	Negative expression	228	69	159 69.7%	Negative expression	238	62	176 73.9%	Negative expression	238	62	176 73.9%
Positive expression	36	10	26 72.2%	Positive expression	36	8	28 77.8%	Positive expression	37	7	30 81.1%	Positive expression	37	7	30 81.1%
Overall	264	95	169 64.00%	Overall	264	77	187 70.8%	Overall	275	69	206 74.9%	Overall	275	69	206 74.9%
Chi-Square		df	Sig.	Chi-Square		df	Sig.	Chi-Square		df	Sig.	Chi-Square		df	Sig.
Log Rank (Mantel-Cox)	1.611	1	0.204	Log Rank (Mantel-Cox)	1.138	1	0.286	Log Rank (Mantel-Cox)	1.041	1	0.308	Log Rank (Mantel-Cox)	1.041	1	0.308
Disease Free-Survival (10y)				Distant Metastasis Free-Survival (10y)				Distant Metastasis Free-Survival (10y)							
icRANKL	Total N	N of events	Censored N Percent	icRANKL	Total N	N of events	Censored N Percent	icRANKL	Total N	N of events	Censored N Percent	icRANKL	Total N	N of events	Censored N Percent
Negative expression	228	97	131 57.5%	Negative expression	228	82	146 64%	Negative expression	238	77	161 67.6%	Negative expression	238	77	161 67.6%
Positive expression	36	13	23 63.9%	Positive expression	36	12	24 66.7%	Positive expression	37	12	25 67.6%	Positive expression	37	12	25 67.6%
Overall	264	110	154 58.3%	Overall	264	94	170 64.4%	Overall	275	89	186 67.6%	Overall	275	89	186 67.6%
Chi-Square		df	Sig.	Chi-Square		df	Sig.	Chi-Square		df	Sig.	Chi-Square		df	Sig.
Log Rank (Mantel-Cox)	0.888	1	0.346	Log Rank (Mantel-Cox)	0.249	1	0.618	Log Rank (Mantel-Cox)	0.074	1	0.785	Log Rank (Mantel-Cox)	0.074	1	0.785
Disease Free-Survival (15y)				Distant Metastasis Free-Survival (15y)				Distant Metastasis Free-Survival (15y)							
icRANKL	Total N	N of events	Censored N Percent	icRANKL	Total N	N of events	Censored N Percent	icRANKL	Total N	N of events	Censored N Percent	icRANKL	Total N	N of events	Censored N Percent
Negative expression	228	97	131 57.5%	Negative expression	228	85	143 62.7%	Negative expression	215	84	131 60.9%	Negative expression	215	84	131 60.9%
Positive expression	36	14	22 61.1%	Positive expression	36	13	23 63.9%	Positive expression	29	14	15 51.7%	Positive expression	29	14	15 51.7%
Overall	264	111	153 58.00%	Overall	264	98	166 62.9%	Overall	244	98	146 59.8%	Overall	244	98	146 59.8%
Chi-Square		df	Sig.	Chi-Square		df	Sig.	Chi-Square		df	Sig.	Chi-Square		df	Sig.
Log Rank (Mantel-Cox)	0.478	1	0.489	Log Rank (Mantel-Cox)	0.077	1	0.781	Log Rank (Mantel-Cox)	0.259	1	0.611	Log Rank (Mantel-Cox)	0.259	1	0.611
Disease Free-Survival (20y)				Distant Metastasis Free-Survival (20y)				Distant Metastasis Free-Survival (20y)							
icRANKL	Total N	N of events	Censored N Percent	icRANKL	Total N	N of events	Censored N Percent	icRANKL	Total N	N of events	Censored N Percent	icRANKL	Total N	N of events	Censored N Percent
Negative expression	228	98	130 57%	Negative expression	238	86	152 63.9%	Negative expression	238	86	152 63.9%	Negative expression	238	86	152 63.9%
Positive expression	36	14	22 61.1%	Positive expression	37	15	22 59.5%	Positive expression	37	15	22 59.5%	Positive expression	37	15	22 59.5%
Overall	264	112	152 57.6%	Overall	275	101	174 63.3%	Overall	275	101	174 63.3%	Overall	275	101	174 63.3%
Chi-Square		df	Sig.	Chi-Square		df	Sig.	Chi-Square		df	Sig.	Chi-Square		df	Sig.
Log Rank (Mantel-Cox)	0.496	1	0.481	Log Rank (Mantel-Cox)	0.034	1	0.853	Log Rank (Mantel-Cox)	0.034	1	0.853	Log Rank (Mantel-Cox)	0.034	1	0.853

Table 2.5. Survival data of patients (ER' cohort) from NPS dataset.

METABRIC COLLECTION

ER+ PATIENTS

Disease Free-Survival (5y)				Distant Metastasis Free-Survival (5y)				Distant Metastasis Free-Survival (5y)							
		Censored				Censored				Censored					
icRANKL	Total N	N of events	N	Percent	icRANKL	Total N	N of events	N	Percent	icRANKL	Total N	N of events	N	Percent	
Negative expression	37	11	26	70.3%	Negative expression	37	10	27	73%	Negative expression	38	11	27	71.1%	
Positive expression	17	7	10	58.8%	Positive expression	17	7	10	58.8%	Positive expression	17	6	11	64.7%	
Overall	54	18	36	66.7%	Overall	54	17	37	68.5%	Overall	55	17	38	69.1%	
Chi-Square		df		Sig.	Chi-Square		df		Sig.	Chi-Square		df		Sig.	
Log Rank (Mantel-Cox)	1,551	1	0.372	0.213	Log Rank (Mantel-Cox)	1,077	1	0.239	0.517	Log Rank (Mantel-Cox)	0.421	1	0.517	0.517	
Disease Free-Survival (10y)				Distant Metastasis Free-Survival (10y)				Distant Metastasis Free-Survival (10y)							
		Censored				Censored				Censored				Censored	
icRANKL	Total N	N of events	N	Percent	icRANKL	Total N	N of events	N	Percent	icRANKL	Total N	N of events	N	Percent	
Negative expression	37	13	24	64.9%	Negative expression	37	15	22	59.5%	Negative expression	38	14	24	63.2%	
Positive expression	17	9	8	47.1%	Positive expression	17	8	9	52.9%	Positive expression	17	8	9	52.9%	
Overall	54	22	32	59.3%	Overall	54	23	31	57.4%	Overall	55	22	33	60.00%	
Chi-Square		df		Sig.	Chi-Square		df		Sig.	Chi-Square		df		Sig.	
Log Rank (Mantel-Cox)	1,551	1	0.213	0.213	Log Rank (Mantel-Cox)	0.316	1	0.574	0.574	Log Rank (Mantel-Cox)	0.658	1	0.417	0.417	
Disease Free-Survival (15y)				Distant Metastasis Free-Survival (15y)				Distant Metastasis Free-Survival (15y)							
		Censored				Censored				Censored				Censored	
icRANKL	Total N	N of events	N	Percent	icRANKL	Total N	N of events	N	Percent	icRANKL	Total N	N of events	N	Percent	
Negative expression	37	14	23	62.2%	Negative expression	37	16	21	56.8%	Negative expression	32	15	17	53.1%	
Positive expression	17	9	8	47.1%	Positive expression	17	9	8	47.1%	Positive expression	15	9	6	40.00%	
Overall	54	23	31	57.4%	Overall	54	25	29	53.7%	Overall	47	24	23	48.9%	
Chi-Square		df		Sig.	Chi-Square		df		Sig.	Chi-Square		df		Sig.	
Log Rank (Mantel-Cox)	1,551	1	0.213	0.213	Log Rank (Mantel-Cox)	0.767	1	0.381	0.381	Log Rank (Mantel-Cox)	0.710	1	0.399	0.399	
Disease Free-Survival (20y)				Distant Metastasis Free-Survival (20y)				Distant Metastasis Free-Survival (20y)							
		Censored				Censored				Censored				Censored	
icRANKL	Total N	N of events	N	Percent	icRANKL	Total N	N of events	N	Percent	icRANKL	Total N	N of events	N	Percent	
Negative expression	37	14	23	62.2%	Negative expression	38	16	22	57.9%	Negative expression	38	16	22	57.9%	
Positive expression	17	9	8	47.1%	Positive expression	17	9	8	47.1%	Positive expression	17	9	8	47.1%	
Overall	54	23	31	57.4%	Overall	55	25	30	54.5%	Overall	55	25	30	54.5%	
Chi-Square		df		Sig.	Chi-Square		df		Sig.	Chi-Square		df		Sig.	
Log Rank (Mantel-Cox)	1,551	1	0.213	0.213	Log Rank (Mantel-Cox)	0.730	1	0.393	0.393	Log Rank (Mantel-Cox)	0.730	1	0.393	0.393	

Table 2.6. Survival data of patients (ER+ cohort) from METABRIC dataset.

ER-NEGATIVE ONLY COLLECTION

ER⁺ PATIENTS

Disease Free-Survival (5y)			Distant Metastasis Free-Survival (5y)			Breast Cancer Specific Survival (5y)		
Censored			Censored			Censored		
icRANKL	Total N	N of events	icRANKL	Total N	N of events	icRANKL	Total N	N of events
Negative expression	141	37	Negative expression	141	30	Negative expression	141	27
Positive expression	139	37	Positive expression	139	31	Positive expression	139	27
Overall	280	74	Overall	280	61	Overall	280	54
Chi-Square		df	Chi-Square		df	Chi-Square		df
Log Rank (Mantel-Cox)	0.019	1	Log Rank (Mantel-Cox)	0.026	1	Log Rank (Mantel-Cox)	0.013	1
Disease Free-Survival (10y)			Distant Metastasis Free-Survival (10y)			Breast Cancer Specific Survival (10y)		
Censored			Censored			Censored		
icRANKL	Total N	N of events	icRANKL	Total N	N of events	icRANKL	Total N	N of events
Negative expression	141	42	Negative expression	141	34	Negative expression	141	28
Positive expression	139	40	Positive expression	139	33	Positive expression	139	35
Overall	280	82	Overall	280	67	Overall	280	63
Chi-Square		df	Chi-Square		df	Chi-Square		df
Log Rank (Mantel-Cox)	0.005	1	Log Rank (Mantel-Cox)	0.006	1	Log Rank (Mantel-Cox)	1.036	1
Disease Free-Survival (15y)			Distant Metastasis Free-Survival (15y)			Breast Cancer Specific Survival (15y)		
Censored			Censored			Censored		
icRANKL	Total N	N of events	icRANKL	Total N	N of events	icRANKL	Total N	N of events
Negative expression	141	45	Negative expression	141	36	Negative expression	141	30
Positive expression	139	41	Positive expression	139	33	Positive expression	139	35
Overall	280	86	Overall	280	69	Overall	280	65
Chi-Square		df	Chi-Square		df	Chi-Square		df
Log Rank (Mantel-Cox)	0.098	1	Log Rank (Mantel-Cox)	0.114	1	Log Rank (Mantel-Cox)	0.573	1
Disease Free-Survival (20y)			Distant Metastasis Free-Survival (20y)			Breast Cancer Specific Survival (25y)		
Censored			Censored			Censored		
icRANKL	Total N	N of events	icRANKL	Total N	N of events	icRANKL	Total N	N of events
Negative expression	141	47	Negative expression	141	36	Negative expression	141	31
Positive expression	139	41	Positive expression	139	33	Positive expression	139	35
Overall	280	88	Overall	280	69	Overall	280	66
Chi-Square		df	Chi-Square		df	Chi-Square		df
Log Rank (Mantel-Cox)	0.397	1	Log Rank (Mantel-Cox)	0.114	1	Log Rank (Mantel-Cox)	0.384	1

Table 2.7. Survival data of patients from ER-NEGATIVE ONLY dataset.

UP-REGULATED SIGNATURES						
NAME	SIZE	ES	NES	NOM p-val	FDR q-val	FWER p-val
SOTIRIOU_BREAST_CANCER_GRADE_1_VS_3_UP	146	0.61038	2.58353	0	0	0
REACTOME_MITOTIC_PROMETAPHASE	83	0.56036	2.16426	0	0.002062224	0.015
WHITFIELD_CELL_CYCLE_LITERATURE	44	0.62482	2.1398	0	0.001799795	0.02
GO_SISTER_CHROMATID_COHESION	106	0.52024	2.09079	0	0.021183854	0.053
MOLENAAR_TARGETS_OF_CCND1_AND_CDK4_DN	53	0.57704	2.08478	0	0.003507723	0.047
GO_CHROMOSOME_SEGREGATION	260	0.45096	2.06262	0	0.016912105	0.084
REACTOME_G1_S_SPECIFIC_TRANSCRIPTION	17	0.74835	2.06145	0	0.004202748	0.071
GO_MITOTIC_SISTER_CHROMATID_SEGREGATION	88	0.52033	2.02884	0	0.025356049	0.153
FARMER_BREAST_CANCER_CLUSTER_2	32	0.63054	2.02548	0	0.006111844	0.122
GO_NUCLEAR_CHROMOSOME_SEGREGATION	217	0.45703	2.02378	0	0.022924535	0.163
TOYOTA_TARGETS_OF_MIR34B_AND_MIR34C	424	0.42061	2.01683	0	0.006710952	0.141
REACTOME_MITOTIC_M_M_G1_PHASES	165	0.47146	2.01453	0	0.00664101	0.146
ELVIDGE_HIF1A_TARGETS_UP	64	0.54362	1.99536	0	0.008443013	0.201
REACTOME_DNA_REPLICATION	185	0.45502	1.9855	0	0.009430789	0.227
REICHERT_MITOSIS_LIN9_TARGETS	28	0.63238	1.97781	0	0.010201583	0.256
REACTOME_CELL_CYCLE_MITOTIC	304	0.42174	1.95211	0	0.01451381	0.363
KONG_E2F3_TARGETS	95	0.48869	1.93767	0	0.017060405	0.435
KEGG_CITRATE_CYCLE_TCA_CYCLE	30	0.60897	1.93713	0	0.016457314	0.436
REACTOME_G2_M_CHECKPOINTS	41	0.57278	1.93304	0.002380953	0.016621092	0.453
PID_PLK1_PATHWAY	44	0.55639	1.91366	0	0.01955365	0.557
PUJANA_BREAST_CANCER_LIT_INT_NETWORK	99	0.47717	1.90211	0	0.022413436	0.626
REACTOME_E2F_MEDIATED_REGULATION_OF_DNA_REPLICATION	33	0.60539	1.89774	0	0.021931516	0.638
SMD_BREAST_CANCER_LUMINAL_A_DN	18	0.68874	1.88896	0	0.022521978	0.671
SCIAN_CELL_CYCLE_TARGETS_OF_TP53_AND_TP73_DN	22	0.63899	1.87909	0.008810572	0.02486301	0.708
PID_ATM_PATHWAY	34	0.57888	1.87466	0	0.02491748	0.73
PID_ATR_PATHWAY	39	0.56577	1.87144	0	0.024929456	0.748
SHEN_SMARCA2_TARGETS_UP	414	0.38828	1.84927	0	0.03019789	0.835
CHANG_CYCLING_GENES	141	0.43689	1.84841	0	0.029820371	0.836
ISHIDA_E2F_TARGETS	51	0.52709	1.84447	0	0.030259905	0.845
GINESTIER_BREAST_CANCER_20Q13_AMPLIFICATION_DN	159	0.43974	1.84396	0	0.029846959	0.847
ODONNELL_TFRC_TARGETS_DN	129	0.43686	1.83126	0	0.03311033	0.891
NADERI_BREAST_CANCER_PROGNOSIS_UP	47	0.52634	1.82906	0.0025	0.03196037	0.898
PUJANA_BREAST_CANCER_WITH_BRCA1_MUTATED_UP	56	0.49884	1.81677	0	0.034065474	0.921
BENPORATH_PROLIFERATION	138	0.4365	1.81494	0	0.034238875	0.924
REACTOME_G0_AND_EARLY_G1	23	0.62143	1.81138	0	0.03507761	0.929
EGUCHI_CELL_CYCLE_RB1_TARGETS	23	0.61528	1.80787	0.004192872	0.035069752	0.934
REACTOME_CITRIC_ACID_CYCLE_TCA_CYCLE	19	0.64134	1.79576	0	0.038577978	0.951
REACTOME_CELL_CYCLE_CHECKPOINTS	111	0.43293	1.77009	0	0.048404295	0.985

DOWN-REGULATED SIGNATURES						
NAME	SIZE	ES	NES	NOM p-val	FDR q-val	FWER p-val
ELVIDGE_HYPOXIA_UP	165	-0.6719	-2.6815	0	0	0
ELVIDGE_HYPOXIA_BY_DMOG_UP	127	-0.6929	-2.6483	0	0	0
HARRIS_HYPOXIA	79	-0.6376	-2.2908	0	0	0
FARDIN_HYPOXIA_11	32	-0.7618	-2.2776	0	0	0
MENSE_HYPOXIA_UP	95	-0.6129	-2.2626	0	5.74E-05	0.001
MANALO_HYPOXIA_UP	203	-0.5509	-2.254	0	5.22E-05	0.001
NAKAMURA_ADIPOGENESIS_LATE_DN	37	-0.7195	-2.2271	0	8.91E-05	0.002
SERVITJA_ISLET_HNF1A_TARGETS_UP	163	-0.5728	-2.2224	0	1.29E-04	0.003
KIM_GLS2_TARGETS_UP	84	-0.6155	-2.2024	0	1.09E-04	0.003
SENESE_HDAC1_AND_HDAC2_TARGETS_DN	212	-0.5296	-2.1741	0	1.97E-04	0.007
HAN_JNK_SIGNALING_UP	35	-0.7108	-2.1666	0	1.88E-04	0.007
KANG_GIST_WITH_PDGFR_A_UP	48	-0.6584	-2.1552	0	2.16E-04	0.009
HELLEBREKERS_SILENCED_DURING_TUMOR_ANGIOGENESIS	78	-0.5959	-2.1364	0	2.22E-04	0.011
REACTOME_EXTRACELLULAR_MATRIX_ORGANIZATION	83	-0.5898	-2.1353	0	2.18E-04	0.011
PID_INTEGRIN_A9B1_PATHWAY	25	-0.7403	-2.1255	0	3.39E-04	0.018
PID_HIF1_TF_PATHWAY	65	-0.6123	-2.1234	0	3.33E-04	0.018
OXFORD_RALA_OR_RALB_TARGETS_DN	23	-0.748	-2.1139	0	4.01E-04	0.023
PID_SYNDECAN_1_PATHWAY	46	-0.6597	-2.1103	0	4.72E-04	0.028
GO_FATTY_ACID_DERIVATIVE_BIOSYNTHETIC_PROCESS	45	-0.6525	-2.1047	0	0.017355205	0.029
GO_UNSATURATED_FATTY_ACID_BIOSYNTHETIC_PROCESS	56	-0.623	-2.0924	0	0.016957263	0.043
GO_EXTRACELLULAR_STRUCTURE_ORGANIZATION	298	-0.491	-2.0895	0	0.013587282	0.046
PETROVA_ENDOTHELIUM_LYMPHATIC_VS_BLOOD_DN	157	-0.5346	-2.0891	0	7.14E-04	0.046
KIM_HYPOXIA	25	-0.7239	-2.0858	0	7.41E-04	0.049
PID_INTEGRIN1_PATHWAY	66	-0.5932	-2.0484	0.001633987	0.001276835	0.094
GROSS_ELK3_TARGETS_UP	27	-0.7011	-2.0475	0	0.001300185	0.097
DASU_IL6_SIGNALING_SCAR_DN	16	-0.7963	-2.04	0	0.001430928	0.106
GO_EPITHELIAL_TO_MESENCHYMAL_TRANSITION	56	-0.6172	-2.0399	0	0.018036643	0.101
ANASTASSIOU_CANCER_MESENCHYMAL_TRANSITION_SIGNATURE	63	-0.604	-2.0226	0	0.001853968	0.142
TIAN_TNF_SIGNALING_NOT_VIA_NFKB	21	-0.761	-2.0218	0	0.001846982	0.143
GO_REGULATION_OF_CARDIAC_MUSCLE_CELL_CONTRACTION	27	-0.6942	-2.0214	0	0.024036404	0.153
BURTON_ADIPOGENESIS_9	91	-0.5457	-2.0171	0	0.001913131	0.15
PACHER_TARGETS_OF_IGF1_AND_IGF2_UP	35	-0.6547	-2.0079	0	0.002099659	0.175
WINTER_HYPOXIA_METAGENE	233	-0.477	-1.983	0	0.002964661	0.266
LEONARD_HYPOXIA	47	-0.6081	-1.9697	0	0.003513027	0.318
FRIDMAN_SENESCENCE_UP	77	-0.5442	-1.968	0	0.003556694	0.325
KEGG_FOCAL_ADHESION	199	-0.4863	-1.9675	0	0.003529335	0.325
GO_CARDIAC_EPITHELIAL_TO_MESENCHYMAL_TRANSITION	24	-0.6903	-1.955	0	0.038109254	0.396
GO_UNSATURATED_FATTY_ACID_METABOLIC_PROCESS	107	-0.5133	-1.9493	0	0.032881804	0.423
NAGASHIMA_EGF_SIGNALING_UP	57	-0.5771	-1.9491	0	0.004275969	0.409

GO_ANGIOGENESIS	287	-0.4594	-1.9365	0	0.032915365	0.483
BIOCARTA_CCR5_PATHWAY	17	-0.7195	-1.9342	0.001865672	0.004961154	0.48
PID_AP1_PATHWAY	69	-0.5575	-1.9328	0	0.005011837	0.484
QI_HYPOXIA	136	-0.4957	-1.9284	0	0.005208736	0.512
PID_AVB3_INTEGRIN_PATHWAY	74	-0.5438	-1.9277	0	0.005226776	0.516
GO_REGULATION_OF_CALCIUM_ION_TRANSPORT	201	-0.4725	-1.9252	0	0.034063492	0.543
NAKAMURA_ADIPOGENESIS_EARLY_DN	38	-0.6232	-1.9204	0	0.005602687	0.552
GO_MULTICELLULAR_ORGANISM_METABOLIC_PROCESS	87	-0.5281	-1.9188	0	0.034857392	0.573
GO_FATTY_ACID_DERIVATIVE_METABOLIC_PROCESS	95	-0.526	-1.9087	0	0.031919792	0.621
PID_INTEGRIN5_PATHWAY	17	-0.7157	-1.9071	0.001879699	0.006563465	0.626
PID_INTEGRIN3_PATHWAY	43	-0.5946	-1.8954	0	0.007485681	0.69
GROSS_HYPOXIA_VIA_ELK3_AND_HIF1A_UP	139	-0.4872	-1.8935	0	0.007631316	0.703
GO_FATTY_ACID_BIOSYNTHETIC_PROCESS	106	-0.4982	-1.8867	0	0.039255396	0.742
GO_LEUKOTRIENE_BIOSYNTHETIC_PROCESS	23	-0.6628	-1.88	0	0.041099787	0.764
QI_HYPOXIA_TARGETS_OF_HIF1A_AND_FOXA2	37	-0.6027	-1.8734	0	0.009613405	0.791
JECHLINGER_EPITHELIAL_TO_MESENCHYMAL_TRANSITION_UP	70	-0.5372	-1.8725	0	0.009609127	0.797
GO_MESENCHYME_MORPHOGENESIS	38	-0.5787	-1.8551	0.001805054	0.04696393	0.854
GO_GLIOGENESIS	169	-0.4688	-1.8529	0	0.0475219	0.865
CROMER_TUMORIGENESIS_UP	61	-0.5489	-1.8473	0	0.012645554	0.895
IGLESIAS_E2F_TARGETS_UP	151	-0.4698	-1.8281	0	0.01487248	0.954
PID_PDGFRA_PATHWAY	22	-0.6735	-1.8206	0.003546099	0.015212109	0.963
PLASARI_TGFB1_TARGETS_10HR_UP	197	-0.446	-1.817	0	0.015905537	0.966
TONKS_TARGETS_OF_RUNX1_RUNX1T1_FUSION_HSC_UP	179	-0.4573	-1.8167	0	0.01590662	0.966
SCHOEN_NFKB_SIGNALING	33	-0.5971	-1.816	0.001763668	0.015952881	0.968
GRAHAM_NORMAL QUIESCENT VS NORMAL DIVIDING UP	65	-0.5312	-1.8157	0	0.01592396	0.968
TAKEDA_TARGETS_OF_NUP98_HOXA9_FUSION_10D_UP	180	-0.4586	-1.8153	0	0.015904738	0.969
GO_MEMBRANE_BIOGENESIS	30	-0.6041	-1.8022	0	0.04993218	0.976
LU_TUMOR_ANGIOGENESIS_UP	25	-0.6319	-1.8015	0.001801802	0.017602805	0.985
BURTON_ADIPOGENESIS_8	85	-0.5019	-1.7934	0	0.018931577	0.991
SANA_TNF_SIGNALING_UP	81	-0.4976	-1.786	0	0.02035556	0.994
BURTON_ADIPOGENESIS_PEAK_AT_0HR	61	-0.5265	-1.7792	0.001686341	0.021303194	0.997
WU_CELL_MIGRATION	181	-0.4386	-1.7732	0	0.022184059	0.997

Table 2.8. GSEA between RANK-Fc vs. mock treatments in the HCI-001 PDX implanted in NSG hosts.

IgG TREATMENT		
Cells	Overlapped genes (up-regulated)	Overlapped genes (down-regulated)
RL1-OE MDA-MB-468	CAVIN2, FOXP2, KCNH2, KCNT1, LRRC55, MADCAM1, RAB39B, ROBO4, SAMD14, SLC12A7, SERF1B, STK31, HMX1, IL13RA2, PCDHA6, TBX3, FLG, LDB3, ADRA1B, CFAP54, NPIPA2, SMCO2, COL27A1, ITGAM, PNLIPRP3, NPIPB8, MYO16, DOCK2, APOBEC3D	SLX1B, HSPB8, CLDN11, KCNC1, VWA5A, MESP2, DSC1, RBP5, RBMS3, PTPRO, RNF112, UMODL1, B3GALT5, SEMA5B, TGM5, SERF1A, RAMP2, ANKRD31, NOXRED1, NPIPB9, NTF4, HOGA1
RL3-OE MDA-MB-468	FGF18, PPIAL4A, EEF1A2, CGA, FGFBP2, GLIPR1L2, TBC1D3G, PDX1, MAFA, BEST1, GOLGA6L4, RADX, SLFN12L, MECOM	NOTCH2NLA, GAL3ST2, PRDM6, EFNA2, PCDHB7, SLC7A10, SYN2, PI16, WAS, CUZD1, PDLIM3, HHIPL1, TMEM191C, RASA4, DDR2, A2M, GGN, SEPTIN5, COL28A1, SCNN1B
RL1 -OE aKPL1	ARMC12, ATP10D, CCDC160, CR2, DIPK1C, EFCAB10, GPR139, GRIN1, IGFL1, IGHG3, KCNMB1, KLK12, LDHB, MKRN3, NOTCH2NLA, S100A3, TNNC2, TNP1, TRPV6	ZSCAN18, SEMA6D, OAS2, PTGER3, NAIP, TDRD1, PRLH, BIN2, EYA4, OSR1, LRRC4C, MX2, DNAAF4, CD36, SLITRK1, CPS1, SPRR3, TM4SF1, ARMH1, CD200R1, CBY3, NDUFA4L2, COL4A3, NHLRC4, DNAI3, CFAP54, HAPLN1, GBP3, BOLA2B, CD99, SLC25A6
RL3 -OE aKPL1	AMHR2, CBY2, FXD2, KLRG1, MAT1A, MATN4, PACRG, PTGER1, ABCC9, MYRIP, TMEM31, NPIPB2, NPIPA8, ADAMTS6, VSIR, NPIPA5, RBM44, GNAT3, FSTL5	SMIM11B, SRGAP2D, INHBE, B3GNT7, OLIG2, ZNF221, CILP, CTSS, CARD6, CLTRN, PDE10A, CD79A, ZACN, RIMBP3, PAH, APLN, AGBL1, CYP4F8, DNAH2, SPIB, ADAMTS1, NME5, CFAP61, NPIPA2
RL1-OE MDA-MB-468	KISS1, SLC38A4, TMEM191B, NT5DC4, FBP1, OTUD7A, CDH26	CUBN, MAGEA2B, FILIP1, HTR2C
RL3-OE MDA-MB-468		
RL1 -OE aKPL1	BAALC, GJA3, IL1RL1, KDR, LRGUK, MAGEC3, MAP3K15, P3H2, PDLIM3, SOX5, SSC5D	CFAP58, VWA2, ARL10, A1BG, TBC1D3E
RL3 -OE aKPL1		
RL1-OE MDA-MB-468	TUBB2B	USP6, NPIPA7
RL1 -OE aKPL1		
RL3-OE MDA-MB-468	-	WASH6P
RL3 -OE aKPL1		
RL3-OE MDA-MB-468	NPIPA9	-
RL1 -OE aKPL1		
RL3 -OE aKPL1	DDTL	NPIPA3
RL1-OE MDA-MB-468		
RL3-OE MDA-MB-468		
RL3 -OE aKPL1	TNFSF11	-
RL1-OE MDA-MB-468		
RL3-OE MDA-MB-468		
RL1 -OE aKPL1		
RL3 -OE aKPL1		

Table 2.9. Up-regulated and down-regulated genes in a single or shared between different human cell lines.

Signature	log2FC(pwpi-RL1+IgG/pwpi+IgG)
ANGIOGENESIS	0.086070575
COAGULATION	0.034762854
PANCREAS BETA CELLS	0.027824732
OXIDATIVE PHOSPHORYLATION	0.020431524
ESTROGEN RESPONSE LATE	0.018355344
BILE ACID METABOLISM	0.017226246
UNFOLDED PROTEIN RESPONSE	0.015798897
FATTY ACID METABOLISM	0.01305679
DNA REPAIR	0.012428197
MYC TARGETS V1	0.01193465
E2F TARGETS	0.011786948
APOPTOSIS	0.010158276
PEROXISOME	0.008876916
CHOLESTEROL HOMEOSTASIS	0.008603981
P53 PATHWAY	0.008340787
MTORC1 SIGNALING	0.007880641
REACTIVE OXYGEN SPECIES PATHWAY	0.007342831
ALLOGRAFT REJECTION	0.006809844
SPERMATOGENESIS	0.006343513
GLYCOLYSIS	0.004800348
TNF- α SIGNALING VIA NF-KB	0.004148019
UV RESPONSE UP	0.003419524
ADIPOGENESIS	0.003334596
ANDROGEN RESPONSE	0.001789161
IFN- γ RESPONSE	0.001694193
IL2 STAT5 SIGNALING	0.001536563
COMPLEMENT	0.000144814
G2M CHECKPOINT	-0.000718149
PROTEIN SECRETION	-0.002244514
IFN- α RESPONSE	-0.0033812
XENOBIOTIC METABOLISM	-0.003759198
APICAL SURFACE	-0.006036545
MYC TARGETS V2	-0.006147973
HYPOXIA	-0.006466626
WNT- β CATENIN SIGNALING	-0.008507711
HEME METABOLISM	-0.009371766
TGF- β SIGNALING	-0.011152534
ESTROGEN RESPONSE EARLY	-0.016746316
PI3K AKT MTOR SIGNALING	-0.018382143
EPITHELIAL MESENCHYMAL TRANSITION	-0.020549287
NOTCH SIGNALING	-0.021346406
KRAS SIGNALING DOWN	-0.024383337
APICAL JUNCTION	-0.025984751
KRAS SIGNALING UP	-0.027188726
MITOTIC SPINDLE	-0.028527151
MYOGENESIS	-0.046409947
UV RESPONSE DOWN	-0.048272948
INFLAMMATORY RESPONSE	-0.051988041
IL6 JAK STAT3 SIGNALING	-0.054076831
HEDGEHOG SIGNALING	-0.071283152

Table 2.10. Up-regulated and down-regulated pathways in RL1-OE MDA-MB-468 cells (vs pwpi-OE MDA-MB-468 cells).

Signature	log2FC(pwpi-RL3+IgG/pwpi+IgG)
FATTY ACID METABOLISM	0.025169996
COAGULATION	0.018579842
OXIDATIVE PHOSPHORYLATION	0.01816018
MTORC1 SIGNALING	0.016451086
ALLOGRAFT REJECTION	0.014625756
GLYCOLYSIS	0.013817653
E2F TARGETS	0.013661279
COMPLEMENT	0.012159857
MYC TARGETS V1	0.011958598
EPITHELIAL MESENCHYMAL TRANSITION	0.008601767
IFN- α RESPONSE	0.008137772
PEROXISOME	0.007970903
UNFOLDED PROTEIN RESPONSE	0.007686976
ANDROGEN RESPONSE	0.007009547
ADIPOGENESIS	0.006512854
IL2 STAT5 SIGNALING	0.005798462
DNA REPAIR	0.005392262
CHOLESTEROL HOMEOSTASIS	0.004373694
IFN- γ RESPONSE	0.003833947
MYC TARGETS V2	0.003346013
HEME METABOLISM	0.003121816
PANCREAS BETA CELLS	0.000743662
UV RESPONSE UP	-0.000485555
APOPTOSIS	-0.000594698
G2M CHECKPOINT	-0.001079003
XENOBIOTIC METABOLISM	-0.001332083
INFLAMMATORY RESPONSE	-0.002289541
ANGIOGENESIS	-0.002543647
APICAL SURFACE	-0.003594776
P53 PATHWAY	-0.003663505
PI3K AKT MTOR SIGNALING	-0.005734212
REACTIVE OXYGEN SPECIES PATHWAY	-0.006576457
SPERMATOGENESIS	-0.006639269
ESTROGEN RESPONSE LATE	-0.007310557
HYPOXIA	-0.009220568
MYOGENESIS	-0.011176724
ESTROGEN RESPONSE EARLY	-0.01212993
TNF- α SIGNALING VIA NF-KB	-0.012773652
KRAS SIGNALING DOWN	-0.01369522
IL6 JAK STAT3 SIGNALING	-0.01503395
APICAL JUNCTION	-0.015807385
MITOTIC SPINDLE	-0.016406264
PROTEIN SECRETION	-0.020393647
BILE ACID METABOLISM	-0.020421632
KRAS SIGNALING UP	-0.025231164
UV RESPONSE DOWN	-0.029716845
WNT- β CATENIN SIGNALING	-0.030148442
TGF- β SIGNALING	-0.030401082
NOTCH SIGNALING	-0.036747598
HEDGEHOG SIGNALING	-0.040044876

Table 2.11. Up-regulated and down-regulated pathways in RL3-OE MDA-MB-468 cells (vs pwpi-OE MDA-MB-468 cells).

Signature	log2FC(pwpi-RL1+IgG/pwpi+IgG)
MYC TARGETS V2	0.064821465
EPITHELIAL MESENCHYMAL TRANSITION	0.041280575
ESTROGEN RESPONSE EARLY	0.035714305
IFN- γ RESPONSE	0.032867271
IFN- α RESPONSE	0.027301667
TNF- α SIGNALING VIA NF-KB	0.023639544
UV RESPONSE UP	0.022601386
ESTROGEN RESPONSE LATE	0.01794832
HEDGEHOG SIGNALING	0.015195582
E2F TARGETS	0.014487146
G2M CHECKPOINT	0.013314744
GLYCOLYSIS	0.012479055
TGF- β SIGNALING	0.012285738
REACTIVE OXYGEN SPECIES PATHWAY	0.01215039
PEROXISOME	0.007896687
DNA REPAIR	0.007475201
UNFOLDED PROTEIN RESPONSE	0.006316119
MYC TARGETS V1	0.006182819
WNT- β CATENIN SIGNALING	0.005681065
APOPTOSIS	0.003538015
MTORC1 SIGNALING	-0.000949829
COAGULATION	-0.001994123
ADIPOGENESIS	-0.004133895
IL2 STAT5 SIGNALING	-0.005013832
NOTCH SIGNALING	-0.00544749
UV RESPONSE DN	-0.005615955
CHOLESTEROL HOMEOSTASIS	-0.00621525
MITOTIC SPINDLE	-0.006216742
P53 PATHWAY	-0.008250466
OXIDATIVE PHOSPHORYLATION	-0.010622739
ANGIOGENESIS	-0.011134158
COMPLEMENT	-0.011883587
HYPOXIA	-0.012497219
APICAL JUNCTION	-0.012838896
FATTY ACID METABOLISM	-0.013390981
PANCREAS BETA CELLS	-0.014769045
ALLOGRAFT REJECTION	-0.017600278
APICAL SURFACE	-0.018568123
ANDROGEN RESPONSE	-0.019150684
MYOGENESIS	-0.023035685
SPERMATOGENESIS	-0.023427378
BILE ACID METABOLISM	-0.026083881
PI3K AKT MTOR SIGNALING	-0.027037293
HEME METABOLISM	-0.03210899
IL6 JAK STAT3 SIGNALING	-0.033185825
KRAS SIGNALING UP	-0.039369694
XENOBIOTIC METABOLISM	-0.04106309
PROTEIN SECRETION	-0.04557961
INFLAMMATORY RESPONSE	-0.046893273
KRAS SIGNALING DOWN	-0.049272412

Table 2.12. Up-regulated and down-regulated pathways in RL1-OE aKPL1 cells (vs pwpi-OE aKPL1 cells).

Signature	log2FC(pwpi-RL3+IgG/pwpi+IgG)
IFN- α RESPONSE	0.059746587
IFN- γ RESPONSE	0.058225995
APOPTOSIS	0.033946281
ESTROGEN RESPONSE LATE	0.033531002
TGF- β SIGNALING	0.032743911
ESTROGEN RESPONSE EARLY	0.031639267
COMPLEMENT	0.0295769
MYC TARGETS V2	0.028838085
E2F TARGETS	0.028102006
ALLOGRAFT REJECTION	0.026098676
SPERMATOGENESIS	0.024979106
UV RESPONSE UP	0.023146487
G2M CHECKPOINT	0.022460029
COAGULATION	0.022412983
TNF- α SIGNALING VIA NF-KB	0.021521669
EPITHELIAL MESENCHYMAL TRANSITION	0.018928969
HYPOXIA	0.017097042
WNT BETA CATENIN SIGNALING	0.01535744
UV RESPONSE DN	0.011338902
IL2 STAT5 SIGNALING	0.011020306
NOTCH SIGNALING	0.010599007
MYC TARGETS V1	0.00716734
KRAS SIGNALING UP	0.006854778
DNA REPAIR	0.006593809
UNFOLDED PROTEIN RESPONSE	0.005403245
ANGIOGENESIS	0.005042554
PEROXISOME	0.004435105
GLYCOLYSIS	0.004416058
MTORC1 SIGNALING	0.004382631
ANDROGEN RESPONSE	0.003611202
CHOLESTEROL HOMEOSTASIS	-0.001108238
FATTY ACID METABOLISM	-0.002722674
MITOTIC SPINDLE	-0.003780854
APICAL SURFACE	-0.007556426
PI3K AKT MTOR SIGNALING	-0.009607384
ADIPOGENESIS	-0.011274208
P53 PATHWAY	-0.011800513
APICAL JUNCTION	-0.013627499
HEDGEHOG SIGNALING	-0.013848229
PANCREAS BETA CELLS	-0.013886646
REACTIVE OXYGEN SPECIES PATHWAY	-0.013948532
INFLAMMATORY RESPONSE	-0.014001905
OXIDATIVE PHOSPHORYLATION	-0.016390573
PROTEIN SECRETION	-0.018974048
MYOGENESIS	-0.020580854
IL6 JAK STAT3 SIGNALING	-0.02115098
HEME METABOLISM	-0.024323135
BILE ACID METABOLISM	-0.025905242
KRAS SIGNALING DOWN	-0.027498346
XENOBIOTIC METABOLISM	-0.032459701

Table 2.13. Up-regulated and down-regulated pathways in RL3-OE aKPL1 cells (vs pwpi-OE aKPL1 cells).

IgG TREATMENT		
Cells	Overlapped pathways (up-regulated)	Overlapped pathways (down-regulated)
RL1-OE MDA-MB-468	ANGIOGENESIS, COAGULATION, PANCREAS BETA CELLS, OXIDATIVE PHOSPHORYLATION, BILE ACID METABOLISM, FATTY ACID METABOLISM, CHOLESTEROL HOMEOSTASIS, P53 PATHWAY, MTORC1 SIGNALING, ALLOGRAFT REJECTION, SPERMATOGENESIS, ADIPOGENESIS, ANDROGEN RESPONSE, IL2 STAT5 SIGNALING, COMPLEMENT	G2M CHECKPOINT, IFN- α RESPONSE, MYC TARGETS V2, WNT- β CATENIN SIGNALING, TGF- β SIGNALING, ESTROGEN RESPONSE EARLY, EPITHELIAL MESENCHYMAL TRANSITION, HEDGEHOG SIGNALING
RL3-OE MDA-MB-468	FATTY ACID METABOLISM, OXIDATIVE PHOSPHORYLATION, ADIPOGENESIS, CHOLESTEROL HOMEOSTASIS, HEME METABOLISM, PANCREAS BETA CELLS	UV RESPONSE UP, APOPTOSIS, G2M CHECKPOINT, ANGIOGENESIS, SPERMATOGENESIS, ESTROGEN RESPONSE LATE, HYPOXIA, ESTROGEN RESPONSE EARLY, TNF- α SIGNALING VIA NF-KB, KRAS SIGNALING UP, UV RESPONSE DOWN, WNT- β CATENIN SIGNALING, TGF- β SIGNALING, NOTCH SIGNALING
RL1 -OE aKPL1	MYC TARGETS V2, EPITHELIAL MESENCHYMAL TRANSITION, ESTROGEN RESPONSE EARLY, IFN α RESPONSE, HEDGEHOG SIGNALING, G2M CHECKPOINT, TGF BETA SIGNALING, WNT BETA CATENIN SIGNALING	MTORC1 SIGNALING, COAGULATION, ADIPOGENESIS, IL2 STAT5 SIGNALING, CHOLESTEROL HOMEOSTASIS, P53 PATHWAY, OXIDATIVE PHOSPHORYLATION, ANGIOGENESIS, COMPLEMENT, FATTY ACID METABOLISM, PANCREAS BETA CELLS, ALLOGRAFT REJECTION, ANDROGEN RESPONSE, SPERMATOGENESIS, BILE ACID METABOLISM
RL3 -OE aKPL1	ANGIOGENESIS, KRAS SIGNALING UP, NOTCH SIGNALING, UV RESPONSE DOWN, WNT- β CATENIN SIGNALING, HYPOXIA, TNF- α SIGNALING VIA NF-KB, G2M CHECKPOINT, UV RESPONSE UP, SPERMATOGENESIS, ESTROGEN RESPONSE EARLY, TGF- β SIGNALING, ESTROGEN RESPONSE LATE, APOPTOSIS	HEME METABOLISM, OXIDATIVE PHOSPHORYLATION, PANCREAS BETA CELLS, ADIPOGENESIS, FATTY ACID METABOLISM, CHOLESTEROL HOMEOSTASIS
RL1-OE MDA-MB-468	COAGULATION, PANCREAS BETA CELLS, OXIDATIVE PHOSPHORYLATION, UNFOLDED PROTEIN RESPONSE, FATTY ACID METABOLISM, DNA REPAIR, MYC TARGETS V1, E2F TARGETS, PEROXISOME, CHOLESTEROL HOMEOSTASIS, MTORC1 SIGNALING, ALLOGRAFT REJECTION, GLYCOLYSIS, ADIPOGENESIS, ANDROGEN RESPONSE, IFN γ RESPONSE, IL2 STAT5 SIGNALING, COMPLEMENT	HEDGEHOG SIGNALING, IL6 JAK STAT3 SIGNALING, INFLAMMATORY RESPONSE, UV RESPONSE DN, MYOGENESIS, MITOTIC SPINDLE, KRAS SIGNALING UP, APICAL JUNCTION, KRAS SIGNALING DN, NOTCH SIGNALING, PI3K AKT MTOR SIGNALING, ESTROGEN RESPONSE EARLY, TGF BETA SIGNALING, WNT BETA CATENIN SIGNALING, HYPOXIA, APICAL SURFACE, XENOBIOTIC METABOLISM, PROTEIN SECRETION, G2M CHECKPOINT
RL3-OE MDA-MB-468		
RL1-OE aKPL1	MYC TARGETS V2, EPITHELIAL MESENCHYMAL TRANSITION, ESTROGEN RESPONSE EARLY, IFN- γ RESPONSE, IFN- α RESPONSE, TNF- α SIGNALING VIA NF-KB, UV RESPONSE UP, ESTROGEN RESPONSE LATE, E2F TARGETS, G2M CHECKPOINT, GLYCOLYSIS, TGF- β SIGNALING, PEROXISOME, DNA REPAIR, UNFOLDED PROTEIN RESPONSE, MYC TARGETS V1, WNT- β CATENIN SIGNALING, APOPTOSIS	KRAS SIGNALING DOWN, INFLAMMATORY RESPONSE, PROTEIN SECRETION, XENOBIOTIC METABOLISM, IL6 JAK STAT3 SIGNALING, HEME METABOLISM, PI3K AKT MTOR SIGNALING, BILE ACID METABOLISM, MYOGENESIS, APICAL SURFACE, PANCREAS BETA CELLS, FATTY ACID METABOLISM, APICAL JUNCTION, OXIDATIVE PHOSPHORYLATION, P53 PATHWAY, MITOTIC SPINDLE, CHOLESTEROL HOMEOSTASIS, ADIPOGENESIS
RL3-OE aKPL1		
RL1-OE MDA-MB-468	IFN γ RESPONSE, TNF α SIGNALING VIA NF-KB, UV RESPONSE UP, ESTROGEN RESPONSE LATE, E2F TARGETS, GLYCOLYSIS, REACTIVE OXYGEN SPECIES PATHWAY, PEROXISOME, DNA REPAIR, UNFOLDED PROTEIN RESPONSE, MYC TARGETS V1, APOPTOSIS	NOTCH SIGNALING, UV RESPONSE DN, MITOTIC SPINDLE, HYPOXIA, APICAL JUNCTION, APICAL SURFACE, MYOGENESIS, PI3K AKT MTOR SIGNALING, HEME METABOLISM, IL6 JAK STAT3 SIGNALING, KRAS SIGNALING UP, XENOBIOTIC METABOLISM, PROTEIN SECRETION, INFLAMMATORY RESPONSE, KRAS SIGNALING DN
RL1 -OE aKPL1		
RL3-OE MDA-MB-468	ANDROGEN RESPONSE, MTORC1 SIGNALING, GLYCOLYSIS, PEROXISOME, UNFOLDED PROTEIN RESPONSE, DNA REPAIR, MYC TARGETS V1, IL2 STAT5 SIGNALING, EPITHELIAL MESENCHYMAL TRANSITION, COAGULATION, ALLOGRAFT REJECTION, E2F TARGETS, MYC TARGETS V2, COMPLEMENT, IFN- γ RESPONSE, IFN- α RESPONSE	XENOBIOTIC METABOLISM, KRAS SIGNALING DOWN, BILE ACID METABOLISM, IL6 JAK STAT3 SIGNALING, MYOGENESIS, PROTEIN SECRETION, INFLAMMATORY RESPONSE, REACTIVE OXYGEN SPECIES PATHWAY, HEDGEHOG SIGNALING, APICAL JUNCTION, P53 PATHWAY, PI3K AKT MTOR SIGNALING, APICAL SURFACE, MITOTIC SPINDLE
RL3 -OE aKPL1		
RL1-OE MDA-MB-468		
RL3-OE MDA-MB-468	UNFOLDED PROTEIN RESPONSE, DNA REPAIR, MYC TARGETS V1, E2F TARGETS, PEROXISOME, GLYCOLYSIS, IFN- γ RESPONSE	IL6 JAK STAT3 SIGNALING, INFLAMMATORY RESPONSE, MYOGENESIS, MITOTIC SPINDLE, APICAL JUNCTION, KRAS SIGNALING DOWN, PI3K AKT MTOR SIGNALING, APICAL SURFACE, XENOBIOTIC METABOLISM, PROTEIN SECRETION
RL1 -OE aKPL1		
RL3 -OE aKPL1		

Table 2.14. Up-regulated and down-regulated pathways in a single or shared between different human cell lines.

Signature	log2FC(pwpi-RL1+DNS/pwpi-RL1+IgG)
IL6 JAK STAT3 SIGNALING	0.0460
TGF- β SIGNALING	0.0445
UV RESPONSE DOWN	0.0216
MITOTIC SPINDLE	0.0199
PROTEIN SECRETION	0.0175
G2M CHECKPOINT	0.0166
IFN- α RESPONSE	0.0165
HEDGEHOG SIGNALING	0.0136
PI3K AKT MTOR SIGNALING	0.0136
SPERMATOGENESIS	0.0103
TNF- α SIGNALING VIA NF-KB	0.0099
HEME METABOLISM	0.0093
ALLOGRAFT REJECTION	0.0089
ESTROGEN RESPONSE EARLY	0.0074
ANDROGEN RESPONSE	0.0062
IL2 STAT5 SIGNALING	0.0058
COMPLEMENT	0.0053
E2F TARGETS	0.0038
HYPOXIA	0.0014
APOPTOSIS	-0.0003
MYC TARGETS V1	-0.0015
GLYCOLYSIS	-0.0038
MTORC1 SIGNALING	-0.0073
APICAL JUNCTION	-0.0076
MYC TARGETS V2	-0.0089
ESTROGEN RESPONSE LATE	-0.0094
IFN- γ RESPONSE	-0.0095
APICAL SURFACE	-0.0101
REACTIVE OXYGEN SPECIES PATHWAY	-0.0114
UNFOLDED PROTEIN RESPONSE	-0.0115
COAGULATION	-0.0124
UV RESPONSE UP	-0.0134
EPITHELIAL MESENCHYMAL TRANSITION	-0.0135
DNA REPAIR	-0.0150
P53 PATHWAY	-0.0161
KRAS SIGNALING UP	-0.0166
ADIPOGENESIS	-0.0174
MYOGENESIS	-0.0174
XENOBIOTIC METABOLISM	-0.0179
FATTY ACID METABOLISM	-0.0235
KRAS SIGNALING DOWN	-0.0239
OXIDATIVE PHOSPHORYLATION	-0.0246
CHOLESTEROL HOMEOSTASIS	-0.0255
ANGIOGENESIS	-0.0270
PANCREAS BETA CELLS	-0.0288
INFLAMMATORY RESPONSE	-0.0300
PEROXISOME	-0.0318
WNT- β CATENIN SIGNALING	-0.0347
NOTCH SIGNALING	-0.0406
BILE ACID METABOLISM	-0.0571

Table 2.15. Up-regulated and down-regulated pathways in RL1-OE aKPL1 cells treated with DNS (vs RL1-OE aKPL1 cells treated with IgG).

IgG TREATMENT		
Cells	Overlapped pathways (up-regulated)	Overlapped pathways (down-regulated)
RL1-OE MDA-MB-468	UV RESPONSE UP, APOPTOSIS	UV RESPONSE DN, APICAL SURFACE, HEME METABOLISM, IL6 JAK STAT3 SIGNALING, KRAS SIGNALING UP, PROTEIN SECRETION, INFLAMMATORY RESPONSE
RL1-OE aKPL1		
RL1 -OE E0771		
RL1-OE aKPL1	EPITHELIAL MESENCHYMAL TRANSITION, TGF- β SIGNALING	MTORC1 SIGNALING, COAGULATION, ADIPOGENESIS, IL2 STAT5 SIGNALING, CHOLESTEROL HOMEOSTASIS, OXIDATIVE PHOSPHORYLATION, FATTY ACID METABOLISM, ALLOGRAFT REJECTION, ANDROGEN RESPONSE, BILE ACID METABOLISM
RL1 -OE E0771		
RL1-OE MDA-MB-468	ANGIOGENESIS, PANCREAS BETA CELLS, P53 PATHWAY, SPERMATOGENESIS, COMPLEMENT	G2M CHECKPOINT, IFN- α RESPONSE, MYC TARGETS V2, WNT- β CATENIN SIGNALING, ESTROGEN RESPONSE EARLY, HEDGEHOG SIGNALING
RL1 -OE E0771		

Table 2.16. Up-regulated and down-regulated pathways in a single or shared between different cell lines.

DISCUSSION

BC is a complex disease with high intra- and inter-tumor heterogeneity that varies from good to poor prognosis (Skol, Sasaki and Onel, 2016; Turashvili and Brogi, 2017). Originally, BC was segregated by hierarchical clustering into two different groups depending on the *ER* gene expression, which correlated with basal (ER⁻ tumors), and luminal (ER⁺ tumors) characteristics (Perou *et al.*, 2000). During the last two decades, as genomic studies evolve, additional insights into this complex scenario and further sub-classification of BC into new molecular entities have been coming out. The intrinsic classification based on global gene expression has defined differences in incidence (Carey *et al.*, 2006), survival (Perou *et al.*, 2000; Sørlie *et al.*, 2001; Cheang *et al.*, 2009), and response to the treatment (Bernard *et al.*, 2009b; Prat *et al.*, 2010; Voduc *et al.*, 2010; Yersal and Barutca, 2014) for each BC subtype. As a result, it has complemented and expanded the information provided by the classical clinic-pathological biomarkers associated with IHC expression of ER, PR, and HER2 (Geyer *et al.*, 2009) that nowadays still dictate BC prognosis and treatment (Effi *et al.*, 2016). Although the development of new therapies has improved the prognosis and survival rates of BC patients (Lin *et al.*, 2010; Schütz *et al.*, 2019), many tumors remain therapy-resistant or acquire resistance with time (Gonzalez-Angulo, Morales-Vasquez and Hortobagyi, 2007). Current studies aim to develop and search for new prognostic and predictive factors to provide an efficient and personalized therapy for BC patients (Weigel and Dowsett, 2010).

In the first chapter of the present work, we aimed to evaluate the potential value of RANK and RANKL as clinical predictors of BC prognosis. Furthermore, we assessed the response to chemotherapy treatment in ER⁻ tumors according to RANK expression. We also studied the role of RANK in BC initiation, progression, and recurrence using preclinical PDX models. In addition, we defined the transcriptomic profile behind RANK⁺ BC. In the second chapter, we focused our work on understanding the role of RANKL in BC, evaluating direct effects on the tumor cells as well as the changes in the microenvironment, and investigating the contribution of certain immune populations in humans, and murine cell lines implanted in different transgenic murine models. We further investigated the therapeutic effect of RANKL inhibition and the transcriptomic portrait that underlies the mechanism of action of RANKL isoforms in BC tumors.

RANK is an independent biomarker of poor prognosis in HR negative BC and a therapeutic target in patient-derived xenografts

It has been widely described that RANK is expressed in BC, however, this is the first study in which, through the analysis of more than 2300 BC clinical samples from four

independent cohorts of patients, we define RANK as an independent poor prognosis biomarker for postmenopausal patients with ER⁻ BC disease.

Initially, our results determined that RANK was more frequently found in ER⁻ BC samples and correlated with bad prognosis markers such as higher mitosis rate, worse histological grade, and the lack of estrogen and progesterone receptors. In this vein, our results agree with several studies which have reported that RANK is expressed in healthy breast gland tissue but also in primary tumors and metastatic tumor cells. In 2011, Santini *et al.* observed a correlation between higher *RANK* gene expression and poorer prognosis in primary BC (Santini, Perrone, *et al.*, 2011). Although it was not possible to discern whether the source of RANK was from the tumor or stromal cells, a posterior immunohistochemical analysis revealed an incidence of RANK protein expression in 41% of the primary tumors that correlated with shorter skeletal disease-free survival (SDFS) and higher risk of developing bone metastasis (Santini, Perrone, *et al.*, 2011). Similar incidence was found in metastatic BC which was significantly associated with poorer progression-free survival (PFS) and DFS and classified as an independent predictor of BMFS and DFS in patients with bone metastasis (Zhang *et al.*, 2012). Our laboratory also found that the expression of RANK was also significantly associated with ER⁻PR⁻ human BC samples and progressively increased with pathological grade and higher proliferation index (Palafox *et al.*, 2012). Pfitzner and collaborators validated our previous results in a larger collection of clinical samples belonging to the GeparTrio study (Pfitzner *et al.*, 2014). They showed a correlation between higher RANK expression with bad prognosis markers and interestingly, those patients showed higher pathological pCR rate, shorter DFS, and OS (Pfitzner *et al.*, 2014). In a posterior study using microarray gene expression, *RANK* also correlated with worse RFS (Vidula *et al.*, 2017). These findings were driven by the fact that RANK is more frequently expressed in tumors that lack HR, which, by their intrinsic characteristics and the lack of efficient treatments, present worse outcomes. In our TMA datasets, the frequency of RANK expression was variable, being lower in the *NPS/METABRIC* series than in the *IDB* dataset. These discrepancies are most probably due to the preservation of the samples as RANK, is a delicate epitope to be detected by IHC, then, the age and the maintenance of the sample are essential. We cannot rule out that differences in the tumor aggressiveness could also contribute to the distinct frequency. *NPS/METABRIC* contain non-metastatic BC samples collected from 1990 to 1997, while *IDB* includes tissues from metastatic breasts gathered from 1989 to 2009. Despite these differences comparing the collections, RANK expression was more frequently found in ER⁻ tumors, and therefore, with poorer outcome (DMFS and BCSS).

Considering the high heterogeneity of BC, and the important differences in prognosis between ER⁺ and ER⁻ tumors, the two subtypes were analyzed independently. Then, we found that RANK expression was associated with a poorer prognosis in ER⁻ but not in ER⁺ BC. Given the heterogeneity of TNBC, RANK could be used as a biomarker to discriminate ER⁻ tumors with the worst outcome. The distinct biology associated with RANK signaling according to ER status may explain why RANK, while expressed also in ER⁺ samples, only predicts poor response in ER⁻ BC. In the GeparTrio trial also was reported the existence of RANK in 14% of the ER⁺ BC samples (Pfitzner *et al.*, 2014). We found that RANK protein expression in the tumor cells of ER⁺ tumors was negatively associated with proliferation while in ER⁻ tumors it was associated with metabolism pathways. The counterintuitive finding of a negative association with proliferation in ER⁺ tumors was in line with our recent results showing that RANK overexpression induces senescence in the luminal mammary epithelial cells and associates with senescence in luminal BC from the TCGA, but not in basal-like tumors (Sandra Benítez *et al.*, 2021).

In contrast, other researchers have described that RANK overexpression in ER⁺ BC cell lines induced the acquisitions of mesenchymal traits suggesting a more invasive behavior (Gomes *et al.*, 2020) as in ER⁻ BC tumors (Palafox *et al.*, 2012). Moreover, it has been reported that fulvestrant, one of the current standard treatments for patients with ER⁺ tumors, was less effective in RANK⁺ cells, accumulating therapy-resistant clones and contributing to cancer progression (Gomes *et al.*, 2020). As explained, we are probably underestimating the frequency of RANK expression in the NPS collection, due to technical limitations in RANK detection. Therefore, additional, more recent collections, containing more aggressive luminal tumors should be analyzed to rule out whether RANK expression in tumor cells could act as a prognosis factor of ER⁺ BC.

GSEA results in the ER⁻ tumors and RANKL/RANK-Fc treated-ER⁻ BC PDXs evidence a pleiotropic role of RANK signaling in BC, regulating multiple biological processes and oncogenic/inflammatory pathways together with tumor cell proliferation/differentiation, metabolism, immunity, and adhesion, in line with previous findings (Gonzalez-Suarez *et al.*, 2010; Yoldi *et al.*, 2016; Rao *et al.*, 2017; Gómez-Aleza *et al.*, 2020). It is striking that even in a severe immune-deficient condition such as the NSG mice, several immune-related pathways are regulated. This agrees with our recent findings, demonstrating that RANK expression in tumor cells is a key regulator of the tumor immune response in preclinical models, but also in the BC patients (Gómez-Aleza *et al.*, 2020). RANK loss in tumor cells led to greater anti-tumor effects in immune-competent compared to immune-

deficient models. Thus, we are underestimating the therapeutic benefit of RANKL inhibitors when using PDX models. The functional studies in ER⁻ BC PDX support that RANK-RANKL signaling promotes tumor progression and recurrence of ER⁻ tumors, increasing tumor cell proliferation and stemness. However, given the immunomodulatory role of RANK signaling, it is likely that these effects will be greater when adding the denosumab-driven anti-tumor immune response. Despite BC heterogeneity and the diversity of the PDX models used, the transcriptomic analyses revealed a wide range of overlap in RANK-driven mechanisms, and, even more important, overlap with associations found in clinical samples and genes regulated by denosumab in BC patients. The main advantage of using PDX models is that they allow us to identify “biomarkers of response to denosumab in human BC”, without the confounding effects of infiltrating immune cells. These findings could prove useful in understanding RANK biology in tumor cells and for the selection of BC patients who may benefit from denosumab and the evaluation of drug responsiveness during treatment.

It is already known that while ER⁺ tumors are considered eligible for endocrine therapy, patients with ER⁻ tumors are more likely to benefit from chemotherapy (Goldhirsch *et al.*, 2003). Indeed, it has been demonstrated that RANK⁺ BC showed a higher response to chemotherapy (Pfitzner *et al.*, 2014), but again, this result is biased by the higher expression of RANK in the most chemotherapy-responsive tumors, which are the ER⁻ tumors (Yersal and Barutca, 2014). Our results indicate that RANK expression in ER⁻ and TNBC is associated with a worse response to chemotherapy, particularly, to the chemotherapy regimens that include taxanes. We speculate that the worse response to chemotherapy associated with RANK could be related to the fact that RANK identifies patients with the worst outcome, which are the ones that undergo chemotherapy treatment (Yin *et al.*, 2020). However, functional results in the preclinical RANK-expressing PDX models combining taxanes with RANK pathway inhibitors demonstrated the enhanced benefit (faster attenuation of tumor growth and lower recurrence rates) of the combination compared to chemotherapy alone. Then, it seems that not only RANK is identifying the BC tumors with the worse prognosis, but also RANK signaling is contributing to the aggressiveness of the tumors. Our latter publication revealed that RANK expression increased lapatinib resistance of different HER2⁺ BC cell lines while RANK depletion sensitized lapatinib-resistant cells to the drug (Sanz-Moreno *et al.*, 2021). These results highlight the role of the RANK signaling pathway in resistance. However, results from the GeparX clinical trial demonstrated that neoadjuvant denosumab in combination with Nab-Paclitaxel did not increase the pathological pCR in patients with early BC, not even in patients with RANK⁺ early tumors (GeparX:

Denosumab (Dmab) as add-on to different regimen of nab-paclitaxel (nP)-anthracycline based neoadjuvant chemotherapy (NACT) in early breast... | OncologyPRO, no date); however, putative effects on survival remain to be evaluated.

Paradoxically to the well-characterized role of RANK signaling as a mediator of progesterone in the healthy breast or preneoplastic lesions (Gonzalez-Suarez *et al.*, 2010; Schramek *et al.*, 2010b), our results demonstrated that RANK is a factor of poor prognosis in postmenopausal patients but not in premenopausal, even in ER⁻ postmenopausal patients. Menopause does not cause a higher risk of developing cancer, it is known that menopause has a protective effect against BC due to the substantial reduction of ovarian hormones (Surakasula, Nagarjunapu and Raghavaiah, 2014). Indeed, it has been reported that the risk of developing cancer increases in both pre-and post-menopausal patients who had early onset of menarche and late menopause due to the increase in the duration of hormonal exposure (Surakasula, Nagarjunapu and Raghavaiah, 2014). After menopause, the drop in estrogen levels leads to a reduction in OPG enhancing activation of RANK signaling in the bone, triggering osteoporosis (Streicher *et al.*, 2017). Santini *et al.* described that high RANK and low OPG levels in primary tumors are predictive of the worst prognosis and the other way around, higher OPG expression was found in the good prognosis signature population as previously reported by Poznak *et al.* (Van Poznak *et al.*, 2006a; Santini, Perrone, *et al.*, 2011). Although the role of OPG in the breast remains poorly explored, following the same rationale, one might expect enhanced activation of RANK signaling also in the breast tumors after menopause, particularly in ER⁻ tumors, which have the highest levels of RANK. Indeed, GSEA analyses revealed that multiple pathways related to TNF/NF- κ B, including the RANKL pathway, were positively associated with RANK protein expression in postmenopausal, but not in premenopausal patients, and these pathways overlapped with those regulated in PDX after RANK modulation.

Metastasis is responsible for most cancer deaths and, 20-30% of BC patients will develop distant metastases (Eckhardt *et al.*, 2012). Different studies suggest that the expression of RANK in BC determines whether tumors predominantly migrate into bone or other tissues (Jones *et al.*, 2006a; Kennecke *et al.*, 2010; Santini, Schiavon, *et al.*, 2011; Gerratana *et al.*, 2015; Wu *et al.*, 2016, 2017). Despite we have not analyzed the expression of RANK in metastatic samples, it has been already described that RANK is expressed in primary and metastatic samples (Bhatia, Sanders and Hansen, 2005). Specifically in bone, the levels of the RANK show, on average, a complete concordance with the related primary tumors (Santini, Perrone, *et al.*, 2011). We find clear evidence

of the association between RANK and a higher rate of DMFS, but no significant results were observed when bone metastases were studied. However, based on the published results, we propose the use of RANK-RANKL pathway inhibitors such as denosumab as an adjuvant treatment not only for patients with primary RANK-expressing BC but also for RANK-expressing metastatic disease. The meta-analysis by the Early Breast Cancer Clinical Trialists' Collaborative Group supports the idea that adjuvant treatment of early BC might be more efficacious with the addition of a bone-modifying agent, particularly in postmenopausal women or in combination with ovarian function suppression (T, Y and A, 2019; Perrone and Gravina, 2020). Previous results from ABCSG18 revealed that adjuvant denosumab reduced the risk of clinical fractures and improved DFS of HR⁺ postmenopausal BC patients receiving aromatase inhibitors (Gnant *et al.*, 2018), but this was not validated in the D-CARE trial (Coleman *et al.*, 2020). However, in these trials RANK expression or RANK pathway activation was not considered. We propose that retrospective analyses categorizing the groups according to RANK expression and/or RANK pathway activation based on gene expression signatures such as the RANK metagene (Gómez-Aleza *et al.*, 2020) or the pathways identified in this study would be required to fully comprehend the therapeutic potential of RANK pathway inhibitors in BC. So far, denosumab has been included in more than 270 clinical trials, though, 35% were carried out for patients with cancer and only 10% of them aimed to analyze the potential value of denosumab for BC patients, but in none of them, RANK expression was considered. Although the mechanism behind the behavior of RANK⁺ tumors seems to be highly complex this is the first study defining RANK as an independent poor prognosis factor in the ER⁻ BC disease and postmenopausal patients, and able to predict worse BCSS in the whole BC population.

[RANKL in breast cancer](#)

Unlike RANK, tmRANKL was rarely expressed in primary breast cancer, which contrasts with RANKL expression being expressed in ER⁺ cells in the healthy breast. We found less than 5% of tmRANKL⁺ samples in both heterogeneous *IDB* and *NPS* datasets, in line with previous studies in which tmRANKL, was found only in 6% of the cases (Pfitzner *et al.*, 2014). Other studies, however, demonstrated the expression of RANKL in around 60% and 31% of non-metastatic and metastatic BC samples respectively, but the localization of the RANKL staining was not revealed (Bhatia, Sanders and Hansen, 2005; Van Poznak *et al.*, 2006b). Despite the low frequency, tmRANKL protein tended to be more frequently detected in ER⁺ compared to ER⁻ BC samples following previous findings by Azim *et al.* who demonstrated high tmRANKL expression in luminal A-like tumors (Azim *et al.*, 2015) and a positive correlation between RANKL and PR (Gonzalez-Suarez

et al., 2010). On the contrary, we did not observe associations with PgR, but we noticed that ER⁺ tmRANKL⁺ tumors were significantly associated with younger women, as already reported (Azim *et al.*, 2012). Interestingly, our results showed that patients with ER⁺ tmRANKL⁺ had better DFS after 15 years of follow-up. We previously mentioned that OPG is the decoy receptor for RANKL, however, it is also described as the inhibitor for TRAIL, another TNF member that binds to death receptors inducing apoptosis in cancer cells (MacFarlane, 2003). As RANKL is a high affinity-binding molecule for OPG, the expression of RANKL could decrease the binding OPG-TRAIL, allowing TRAIL-induced tumor cell apoptosis to occur. TRAIL expression has been detected in 30% of good prognosis BC cases (Simon S. Cross *et al.*, 2006). This hypothesis could explain the mechanism that underlies our findings in survival. Despite the low frequency of tmRANKL in clinical samples, high tmRANKL expression was observed in some ER⁻ adenocarcinomas and a subset of TNBC PDX samples. In line with our findings, it was reported a significant association of RANKL with the lack of ER and worse tumor grade (S S Cross *et al.*, 2006). Considering the well-established regulation of RANKL by progesterone (Schramek, Sigl and Penninger, 2011), this result was unexpected. Based on these data, elucidating the functionality of RANKL in TNBC as well as in luminal cancer could have an impact in the clinics given the availability of RANKL-targeted therapies. So far, RANKL has been described as a marker to predict the clinical outcome but only when co-expressed with RANK (Reyes *et al.*, 2017). In our TMA collections, we rarely observed the simultaneous presence of both proteins in the tumor compartment.

Besides the tmRANKL staining, our results from patient tumor samples revealed icRANKL staining in all the TMA collections being more frequent in ER⁻ samples. Looking at the compartments where the RANKL isoforms could be located, it has been shown by immunoelectron microscopy that RANKL1, but not RANKL2 and RANKL3, bound with the cell membrane efficiently. This data suggests that transmembrane staining found in patient samples corresponds with the canonical RANKL1 isoform. In contrast, the RANKL3 transcript lacks the signal peptide present in the transmembrane sequence, losing the capacity to be transported to the membrane and secreted outside the cell. Other researchers reported that even if RANKL3 was located in the cytoplasmic region because of issues in the transport to the membrane and posterior secretion, there is a possibility that RANKL3 could be secreted as a soluble form protein (Ikeda *et al.*, 2003). Our data demonstrated for the first time, that the human RANKL3 isoform was not detected in the supernatant, remaining trapped inside the BC cells, suggesting that it may correspond to the intracellular staining identified in patient samples.

The information about the role of non-canonical RANKL isoforms is limited. Studies in bone revealed that the RANKL2 isoform is inactive (Suzuki *et al.*, 2004). Indeed, analysis of conserved sequences in the three described isoforms revealed a lack of evolutionary preservation for RANKL2, categorizing it as a non-functional RANKL. Based on our observations in patient samples and the detection of membrane and intracellular RANKL in other types of cancers (Grimaud *et al.*, 2003; Chuang *et al.*, 2009; Azim *et al.*, 2015), we focused the study on RANKL1 and RANKL3 role in BC. Unlike RANKL2, both RANKL1 and RANKL3 have been described as functional proteins; while RANKL1 induces osteoclastogenesis *in vitro*, RANKL3 inhibits osteoclastogenesis when co-expressed with RANKL1 (Suzuki *et al.*, 2004). Up to now, the RANK expression has been shown to promote BC initiation and progression (Palafox *et al.*, 2012; González-Suárez and Sanz-Moreno, 2016; Yoldi *et al.*, 2016). However, this is the first study demonstrating that RANKL1, but also RANKL3, accelerates tumor onset and increases tumor growth in RANK-deficient BC.

Given the low, almost undetectable expression of RANK in the tumor cell lines, we hypothesize that tumoral RANKL1 may accelerate tumor growth by interacting with RANK expressed by the stroma. This hypothesis is also supported by the fact that we did not find differences in growth when the cells were cultured *in vitro*. RANKL1 and RANKL3 overexpression led to faster tumor growth in immune-deficient, immune-compromised and immune-competent mice. The increased tumor growth driven by murine RANKL was greater in syngeneic mice than NSGs, suggesting that RANKL acts through immune-dependent and independent mechanisms. To decipher whether the RANK-expressing non-tumoral cells were contributing to the faster tumor development, we used the constitutive *Rank*^{-/-} mice model. Although we still observed faster growth in RL1-OE tumors growing in full knockout *Rank* mice, the differences were much lower compared to the *Rank* WT mice. On the one hand, our data suggest that RANK-expressing non-tumoral cells are essential for the earlier tumor onset and progression of RL1-OE tumors. However, we may consider that the mouse model of full-body constitutive *Rank* deletion has many other phenotypes (Dougall *et al.*, 1999) that may impair the development of RANKL1 tumors. Different cell populations, such as TAMs, which are massively infiltrating E0771 tumors, express RANK. Clinical and preclinical evidence suggests that TAMs are involved in both tumor initiation and progression (Sica and Bronte, 2007; Qian and Pollard, 2010). Our results indicate that the pro-tumoral effect observed after overexpressing RANKL1 is independent of RANK-expressing TAMs. However, this finding does not exclude the involvement of TAMs as a population, since the tumoral infiltration of RANK-deficient TAMs is still high.

In addition, in our clinical samples, RANK in the stroma compartment was also found in the endothelial cells. It has already been described that human RANKL binds to RANK-expressing endothelial cells stimulating the angiogenesis process (Kim *et al.*, 2002) and in a tumor context, RANKL-expressing tumors harbor more tumor vessels than control tumors, demonstrating that RANKL promotes angiogenesis in a manner independent of VEGF (Yamada *et al.*, 2011). Given that the early tumor onset and faster growth were observed in RL1-OE tumors independently of the presence of immune cells, we propose that RANK-expressing endothelial blood vessels may underlie the mechanism of action of RANKL1 tumors. Intriguingly, our results after using Singscore to perform functional analysis on the Hallmark gene set collection revealed that RL1-OE MDA-MB-468 cells show angiogenesis as the highest process up-regulated compared to control cells. Interestingly, the overexpression of RANKL1 also showed up-regulation of TNF- α signaling via NF- κ B in two independent human cell lines. TNF- α is a pro-inflammatory cytokine, highly increased in BC, linked to angiogenesis, among other steps of tumorigenesis, and associated with poor prognosis (Wu and Zhou, 2010; Mercogliano *et al.*, 2020). Of the two different receptors described for TNF- α , type II receptors are expressed only on endothelial and immune cells, mediating angiogenesis among other processes (Wu and Zhou, 2010). In advance, different studies have demonstrated the joint role of TNF- α , RANKL, and RANK to increase the osteoclastogenesis process (Weitzmann, 2013; Córdova *et al.*, 2015; Luo *et al.*, 2018), however, the underlying mechanism remains unclear. Given the high number of pathways regulated upon RANKL1 overexpression compared with control cells in *in vitro* conditions, we cannot exclude the involvement of tumoral RANK, despite its low expression, or more interestingly, the participation of a novel receptor. Pathways such as epithelial-mesenchymal transition up-regulated upon human and mouse RANKL1 overexpression and more intriguing, the use of different RANKL-inhibitors down-regulated the process. Many studies demonstrated that RANKL induces EMT, cell migration, and invasion through the binding to RANK-expressing cells, activation of NF- κ B, and upregulation of Snail and Twist (Jones *et al.*, 2006b; Santini, Perrone, *et al.*, 2011; Tan *et al.*, 2011; Tsubaki *et al.*, 2013). However, further experiments are necessary to identify the key mechanism underlying the aggressiveness of RANKL1-overexpressing BC tumors.

Considering our results, the therapeutic impact of RANKL1 inhibition could be potentially useful for patients with RANKL1-expressing BC. DNS binds human RANKL1 with high affinity while RANK-Fc and OPG bind to both human and murine RANKL1. The treatment of DNS only attenuated the growth of RL1-OE tumors implanted into immune-

compromised nude mice, but not in the immune-deficient NSG, emphasizing the therapeutic potential of DNS in the presence of active immune cells (innate). However, when we used a RANKL1-expressing PDX implanted into immune-deficient mice, DNS was also beneficial, demonstrating immune cell-dependent and independent effects of denosumab. In addition to the inhibition of tumoral RANKL1, we have demonstrated that also systemic blockage of RANKL1 using OPG, RANK-Fc, or α -RANKL *in vivo* attenuated the growth of expressing- and overexpressing-RANKL1 human or mouse BC cells in immuno-deficient and immune-competent mice. Currently, DNS has been involved in 95 clinical trials aimed at cancer patients, of which 40% are in BC patients (*Search of denosumab | Breast Cancer - List Results - ClinicalTrials.gov*, no date). Despite the high number of women with BC, RANK or RANKL expression has rarely been checked.

Additionally, to the canonical form of RANKL, our work also demonstrates the pro-tumorigenic role of the non-canonical form of RANKL, RANKL3, in BC. The mechanism behind is more intriguing since the protein is trapped inside cells. Multiple studies have reported the existence of intracellular oncogenic proteins, for example, cytoplasmic PAR-3, highly expressed in renal cell carcinomas and significantly associated with worse histopathological factors (Dagher *et al.*, 2014). Published data suggest that the proteins localized in the cytoplasm may control the expression levels of second molecules and the proteins that are present in the nucleus may modulate the transcriptional machinery of the cell (Weinberg, 1985). Further experiments are needed to decipher the localization within the intracellular compartment and analyze potential interacting binding partners. In *in vitro* conditions, the overexpression of RANKL3 in two different cell lines up-regulated MYC targets. Members of the MYC family have been associated with proliferation and apoptosis and identified in the cytoplasm and nuclei of other types of cancer cells (Ruzinova, Caron and Rodig, 2010). But only MYC proteins, also components of the Ras family can signal from different locations, such as the cytoplasm, regulating cell growth, proliferation, and differentiation (Hancock, 2003). However, no data about how RANKL3 can signal has been already reported. Other immune-related pathways such as IFN- α , IFN- γ , complement response, and epithelial-mesenchymal transition were up-regulated upon RANKL3 overexpression. Previous reports showed that IFN- γ promotes EMT in pancreatic and papillary thyroid cancer (Lv *et al.*, 2015; Imai *et al.*, 2019), but, the link between RANKL3 and oncogenic processes has not been described.

It's really interesting the fact that RANKL1 and RANKL3 proteins, located in different cell compartments such as intracellular and membrane places, show similar phenotypes, and share the regulation of a high number of pathways. Despite RANKL3 is not secreted outside the cell and no increase of TRAP 5b protein being detected in mice implanted with these tumors, the tumors were equally aggressive to those overexpressing RANKL1. This begs the question as to whether the "outside-to-inside" signaling, also named reverse signaling, is promoted by RANKL1. Reverse signaling has been mainly described within the TNF superfamily (Eissner, Kolch and Scheurich, 2004b). Different studies showed evidence that reverse RANK-RANKL signaling regulates bone formation (Cao, no date; Ma *et al.*, 2019a). Interestingly, the addition of soluble RANK to RANKL-expressing CD4⁺ Th1 cells suppresses the IFN- γ secretion through p38 activation (Chen, Huang and Hsieh, 2001). In this vein, one of the shared up-regulated pathways between RL1- and RL3-OE MDA-MB-468 and aKPL1 cells compared to their control in basal conditions is IFN- γ response. In our study, the activation of the IFN- γ pathway happens without external stimulus. However, as described for RANK (Anderson *et al.*, 1997c), we speculate that tmRANKL1 overexpression may be enough to trigger intracellular signaling without the need for the RANK receptor to act as a stimulus. Then, intrinsic signaling promoted by RANKL1 may activate similar pathways triggered by RANKL3 within the cells. This fact can be mirrored in our *in vivo* experiment where we observed that although the growth of RL1-OE tumors was decreased in full knockout *Rank* mice, was faster than in control tumors suggesting a RANK-independent mechanism. Moreover, data from RNAseq indicated some pathways in common between RL1- and RL3-overexpressing cells that were not reversed by anti-RANKL inhibitors. If constitutive intrinsic signaling is demonstrated in both RL1- and RL3-overexpressing cell lines, further research will be needed to decipher other options to block the signaling. Due to DNS cannot cross the membrane, patients with RANKL3-expressing BC could not benefit from its use. Proteins such as the small molecules, which, owing to their small size and amphiphilic properties pass through cell membranes (Miersch and Sidhu, 2016) could be the solution for those patients. As it happens with RANKL3, DNS could not inhibit the intrinsic signaling triggered by RANKL1, and the combinations with small molecules could improve the prognosis of patients with RANKL1-expressing BC. Although important findings have been found for two proteins that are products from the same gene by alternative splicing, future efforts are needed to determine the mechanism by which, a transmembrane protein that is cleaved and released as a soluble form and, an intracellular protein that cannot escape from the cell promotes the aggressiveness of BC.

CONCLUSIONS

1. RANK protein is more frequently expressed in ER-negative breast adenocarcinomas, but it is also expressed in a subset of ER-positive BC. Similar expression patterns are found in PDXs.
2. RANK protein expression in BC cells is an independent marker of poor survival in postmenopausal BC patients (independent of ER expression, BC tumor grade, stage, and size).
3. RANK protein expression in BC cells is an independent marker of poor survival in ER-negative BC and postmenopausal ER-negative BC patients.
4. RANK expression predicts poor response to chemotherapy in ER-negative BC.
5. The inhibition of RANK signaling in RANK-expressing PDXs reduces tumor cell proliferation and stemness, and improves response to chemotherapy.
6. There are two functional and conserved RANKL isoforms: RANKL1, transmembrane protein (tmRANKL1) that can be shredded as a soluble protein (sRANKL1), and RANKL3, an intracellular protein.
7. The canonical tmRANKL1 is rarely expressed in BC cells from clinical adenocarcinomas and PDX models from ER-positive and ER-negative subtypes.
8. RANKL1 isoform has a protumoral role in ER-positive and ER-negative BC, promoting tumor initiation and progression through tumor intrinsic and extrinsic mechanisms that involve RANK-expressing cells.
9. RANKL inhibitors, such as denosumab, attenuate the growth of RANKL1-OE BC through immune-dependent and independent mechanisms but do not fully reverse the RANKL1 protumorigenic effects.
10. The intracellular RANKL3 is frequently expressed in patients' BC cells, mainly in ER- BC disease.
11. RANKL3 promotes earlier tumor onset and faster growth of human ER-positive and ER-negative BC cell lines.
12. RANKL1 and RANKL3 share some molecular mechanisms, suggesting an intracellular role for RANKL1 that cannot be therapeutically inhibited by denosumab. Anti-RANKL treatment cannot reverse all molecular mechanisms driven by RANKL1.

REFERENCES

Abaan, O. D. *et al.* (2013) 'The exomes of the NCI-60 panel: A genomic resource for cancer biology and systems pharmacology', *Cancer Research*. *Cancer Res*, 73(14), pp. 4372–4382. doi: 10.1158/0008-5472.CAN-12-3342.

Abd El-Rehim, D. M. *et al.* (2005) 'High-throughput protein expression analysis using tissue microarray technology of a large well-characterised series identifies biologically distinct classes of breast cancer confirming recent cDNA expression analyses', *International Journal of Cancer*. *Int J Cancer*, 116(3), pp. 340–350. doi: 10.1002/ijc.21004.

Al-Hajj, M. *et al.* (2003) 'Prospective identification of tumorigenic breast cancer cells', *Proceedings of the National Academy of Sciences of the United States of America*, 100(7), pp. 3983–3988. doi: 10.1073/pnas.0530291100.

Amgen Europe BV. *Prolia™ (denosumab) European Union summary of product characteristics.*

Anderson, D. M. *et al.* (1997a) 'A homologue of the TNF receptor and its ligand enhance T-cell growth and dendritic-cell function', *Nature*. Nature Publishing Group, 390(6656), pp. 175–179. doi: 10.1038/36593.

Anderson, D. M. *et al.* (1997b) 'A homologue of the TNF receptor and its ligand enhance T-cell growth and dendritic-cell function', *Nature*. *Nature*, 390(6656), pp. 175–179. doi: 10.1038/36593.

Anderson, D. M. *et al.* (1997c) 'A homologue of the TNF receptor and its ligand enhance T-cell growth and dendritic-cell function', *Nature*, 390(6656), pp. 175–179. doi: 10.1038/36593.

Armstrong, A. P. *et al.* (2002) 'A RANK/TRAF6-dependent signal transduction pathway is essential for osteoclast cytoskeletal organization and resorptive function', *The Journal of biological chemistry*. *J Biol Chem*, 277(46), pp. 44347–44356. doi: 10.1074/JBC.M202009200.

Asselin-Labat, M.-L. *et al.* (2010) 'Control of mammary stem cell function by steroid hormone signalling.', *Nature*, 465(7299), pp. 798–802. doi: 10.1038/nature09027.

Atkins, G. J. *et al.* (2006) 'RANK expression as a cell surface marker of human osteoclast precursors in peripheral blood, bone marrow, and giant cell tumors of bone', *Journal of Bone and Mineral Research*, 21(9), pp. 1339–1349. doi: 10.1359/jbmr.060604.

Azim, H. A. *et al.* (2012) 'Elucidating Prognosis and Biology of Breast Cancer Arising in Young Women Using Gene Expression Profiling', *Clinical Cancer Research*. American Association for Cancer Research, 18(5), pp. 1341–1351. doi: 10.1158/1078-0432.CCR-11-2599.

Azim, H. A. *et al.* (2015) 'RANK-ligand (RANKL) expression in young breast cancer patients and during pregnancy', *Breast Cancer Research*. BioMed Central Ltd., 17(1), p. 24. doi: 10.1186/s13058-015-0538-7.

Azim, J. A. *et al.* (2013) 'Utility of prognostic genomic tests in breast cancer practice: The impact 2012 working group consensus statement', *Annals of Oncology*. Oxford University Press, 24(3), pp. 647–654. doi: 10.1093/annonc/mds645.

Bai, S. *et al.* (2005) 'FHL2 inhibits the activated osteoclast in a TRAF6-dependent manner', *Journal of Clinical Investigation*. J Clin Invest, 115(10), pp. 2742–2751. doi: 10.1172/JCI24921.

Banks, E. *et al.* (2003) 'Breast cancer and hormone-replacement therapy in the Million Women Study', *Lancet*. Lancet Publishing Group, 362(9382), pp. 419–427. doi: 10.1016/S0140-6736(03)14065-2.

Baud'huin, M. *et al.* (2013) 'Osteoprotegerin: Multiple partners for multiple functions', *Cytokine and Growth Factor Reviews*. Cytokine Growth Factor Rev, pp. 401–409. doi: 10.1016/j.cytogfr.2013.06.001.

Bekker, P. J. *et al.* (2001) 'The effect of a single dose of osteoprotegerin in postmenopausal women', *Journal of Bone and Mineral Research*. J Bone Miner Res, 16(2), pp. 348–360. doi: 10.1359/jbmr.2001.16.2.348.

Beleut, M. *et al.* (2010) 'Two distinct mechanisms underlie progesterone-induced proliferation in the mammary gland.', *Proceedings of the National Academy of Sciences of the United States of America*, 107(7), pp. 2989–94. doi: 10.1073/pnas.0915148107.

Bell, A. D. and Bell, B. R. (2011) 'The FREEDOM trial: Is family medicine ready for biologic therapies?', *Canadian Family Physician*. College of Family Physicians of Canada, pp. 438–441. Available at: /pmc/articles/PMC3076475/ (Accessed: 23 May 2021).

Bergstrom, C. *et al.* (2020) 'Clinicopathological Features and Outcomes in Individuals with Breast Cancer and ATM, CHEK2, or PALB2 Mutations', *Annals of Surgical Oncology*. Springer Science and Business Media Deutschland GmbH. doi:

10.1245/s10434-020-09158-2.

Bernard, P. S. *et al.* (2009a) 'Supervised risk predictor of breast cancer based on intrinsic subtypes', *Journal of Clinical Oncology*. American Society of Clinical Oncology, 27(8), pp. 1160–1167. doi: 10.1200/JCO.2008.18.1370.

Bernard, P. S. *et al.* (2009b) 'Supervised risk predictor of breast cancer based on intrinsic subtypes', *Journal of Clinical Oncology*. J Clin Oncol, 27(8), pp. 1160–1167. doi: 10.1200/JCO.2008.18.1370.

Bhatia, P., Sanders, M. M. and Hansen, M. F. (2005) 'Expression of Receptor Activator of Nuclear Factor- κ B Ligand Is Inversely Correlated with Metastatic Phenotype in Breast Carcinoma', *Clinical Cancer Research*, 11(1).

Body, J. J. *et al.* (2003) 'A phase I study of AMGN-0007, a recombinant osteoprotegerin construct, in patients with multiple myeloma or breast carcinoma related bone metastases', in *Cancer*. John Wiley and Sons Inc., pp. 887–892. doi: 10.1002/cncr.11138.

Bone, H. G. *et al.* (2017) '10 years of denosumab treatment in postmenopausal women with osteoporosis: results from the phase 3 randomised FREEDOM trial and open-label extension', *The Lancet Diabetes and Endocrinology*. Lancet Publishing Group, 5(7), pp. 513–523. doi: 10.1016/S2213-8587(17)30138-9.

Bord, S. *et al.* (2004) 'Synthesis of osteoprotegerin and RANKL by megakaryocytes is modulated by oestrogen', *British Journal of Haematology*, 126(2), pp. 244–251. doi: 10.1111/j.1365-2141.2004.05024.x.

Bray, F. *et al.* (2018) 'Global cancer statistics 2018: GLOBOCAN estimates of incidence and mortality worldwide for 36 cancers in 185 countries', *CA: A Cancer Journal for Clinicians*. Wiley, 68(6), pp. 394–424. doi: 10.3322/caac.21492.

Breast Cancer Facts and Statistics (no date). Available at: <https://www.breastcancer.org/facts-statistics> (Accessed: 28 March 2022).

Breast Disease: Diagnosis and Pathology.

Brisken, C. and Ataca, D. (2015) 'Endocrine hormones and local signals during the development of the mouse mammary gland', *Wiley interdisciplinary reviews. Developmental biology*. Wiley Interdiscip Rev Dev Biol, 4(3), pp. 181–195. doi: 10.1002/WDEV.172.

- Brown, K. A. and Simpson, E. R. (2010) 'Obesity and breast cancer: Progress to understanding the relationship', *Cancer Research*. American Association for Cancer Research, pp. 4–7. doi: 10.1158/0008-5472.CAN-09-2257.
- Bruna, A. *et al.* (2016) 'A Biobank of Breast Cancer Explants with Preserved Intra-tumor Heterogeneity to Screen Anticancer Compounds', *Cell*. Elsevier, 167(1), pp. 260–274.e22. doi: 10.1016/J.CELL.2016.08.041.
- Bulun, S. E. *et al.* (2012) 'Aromatase, breast cancer and obesity: A complex interaction', *Trends in Endocrinology and Metabolism*. Elsevier Current Trends, pp. 83–89. doi: 10.1016/j.tem.2011.10.003.
- Burstein, H. J. *et al.* (2019) 'Adjuvant endocrine therapy for women with hormone receptor-positive breast cancer: ASCO clinical practice guideline focused update', *Journal of Clinical Oncology*. American Society of Clinical Oncology, 37(5), pp. 423–438. doi: 10.1200/JCO.18.01160.
- Byrne, A. T. *et al.* (2017) 'Interrogating open issues in cancer precision medicine with patient-derived xenografts', *Nature Reviews Cancer*. Nature Publishing Group, pp. 254–268. doi: 10.1038/nrc.2016.140.
- Calles, A., Rubio-Viqueira, B. and Hidalgo, M. (2013) 'Primary human non-small cell lung unit and pancreatic tumorgraft models-utility and applications in drug discovery and tumor biology', *Current Protocols in Pharmacology*. Blackwell Publishing Inc., Chapter 14(SUPPL.61). doi: 10.1002/0471141755.ph1426s61.
- Cao, X. 'RANKL-RANK signaling regulates osteoblast differentiation and bone formation'. doi: 10.1038/s41413-018-0040-9.
- Carbognin, L. *et al.* (2019) 'Prognostic and predictive implications of PTEN in breast cancer: Unfulfilled promises but intriguing perspectives', *Cancers*. MDPI AG. doi: 10.3390/cancers11091401.
- Carey, L. A. *et al.* (2006) 'Race, breast cancer subtypes, and survival in the Carolina Breast Cancer Study', *Journal of the American Medical Association*. JAMA, 295(21), pp. 2492–2502. doi: 10.1001/jama.295.21.2492.
- Cassidy, J. W., Caldas, C. and Bruna, A. (2015) 'Maintaining tumor heterogeneity in patient-derived tumor xenografts', *Cancer Research*. American Association for Cancer Research Inc., pp. 2963–2968. doi: 10.1158/0008-5472.CAN-15-0727.

Charles A Janeway, J. *et al.* (2001) 'The components of the immune system'. Garland Science. Available at: <https://www.ncbi.nlm.nih.gov/books/NBK27092/> (Accessed: 30 March 2022).

Cheang, M. C. U. *et al.* (2009) 'Ki67 index, HER2 status, and prognosis of patients with luminal B breast cancer.', *Journal of the National Cancer Institute*, 101(10), pp. 736–50. doi: 10.1093/jnci/djp082.

Chen, G. *et al.* (2006) 'Expression of RANKL/RANK/OPG in primary and metastatic human prostate cancer as markers of disease stage and functional regulation', *Cancer*. John Wiley and Sons Inc., 107(2), pp. 289–298. doi: 10.1002/cncr.21978.

Chen, N.-J., Huang, M.-W. and Hsieh, S.-L. (2001) 'Enhanced Secretion of IFN- γ by Activated Th1 Cells Occurs Via Reverse Signaling Through TNF-Related Activation-Induced Cytokine', *The Journal of Immunology*. The American Association of Immunologists, 166(1), pp. 270–276. doi: 10.4049/jimmunol.166.1.270.

Cheng, T. *et al.* (2009) 'Mutations within the TNF-Like Core Domain of RANKL Impair Osteoclast Differentiation and Activation', *Molecular Endocrinology*. The Endocrine Society, 23(1), p. 35. doi: 10.1210/ME.2007-0465.

Chuang, F. H. *et al.* (2009) 'Immunohistochemical expression of RANKL, RANK, and OPG in human oral squamous cell carcinoma', *Journal of Oral Pathology and Medicine*, 38(10), pp. 753–758. doi: 10.1111/j.1600-0714.2009.00793.x.

Claus, E. B., Risch, N. J. and Thompson, W. D. (1990) 'Age at onset as an indicator of familial risk of breast cancer', *American Journal of Epidemiology*. Oxford University Press, 131(6), pp. 961–972. doi: 10.1093/oxfordjournals.aje.a115616.

Clausen, B. E. *et al.* (1999) 'Conditional gene targeting in macrophages and granulocytes using LysMcre mice', *Transgenic Research*, 8(4), pp. 265–277. doi: 10.1023/A:1008942828960.

Cleary, M. P. and Grossmann, M. E. (2009) 'Obesity and Breast Cancer: The Estrogen Connection', *Endocrinology*. Oxford Academic, 150(6), pp. 2537–2542. doi: 10.1210/en.2009-0070.

Coleman, R. *et al.* (2020) 'Adjuvant denosumab in early breast cancer (D-CARE): an international, multicentre, randomised, controlled, phase 3 trial', *The Lancet Oncology*. Lancet Publishing Group, 21(1), pp. 60–72. doi: 10.1016/S1470-2045(19)30687-4.

Conte, N. *et al.* (2019) 'PDX Finder: A portal for patient-derived tumor xenograft model discovery', *Nucleic Acids Research*. Oxford University Press, 47(D1), pp. D1073–D1079. doi: 10.1093/nar/gky984.

Córdova, L. A. *et al.* (2015) 'Inhibition of osteolysis and increase of bone formation after local administration of siRNA-targeting RANK in a polyethylene particle-induced osteolysis model', *Acta Biomaterialia*. Elsevier, 13, pp. 150–158. doi: 10.1016/j.actbio.2014.10.042.

Cortés, J. *et al.* (2022) 'Trastuzumab Deruxtecan versus Trastuzumab Emtansine for Breast Cancer', *New England Journal of Medicine*, 386(12), pp. 1143–1154. doi: 10.1056/NEJMoa2115022.

Cottu, P. *et al.* (2012) 'Modeling of response to endocrine therapy in a panel of human luminal breast cancer xenografts', *Breast Cancer Research and Treatment*, 133(2), pp. 595–606. doi: 10.1007/s10549-011-1815-5.

Cristea, S. and Polyak, K. (no date) 'Dissecting the mammary gland one cell at a time'. doi: 10.1038/s41467-018-04905-2.

Cross, Simon S. *et al.* (2006) 'Expression of receptor activator of nuclear factor κ B ligand (RANKL) and tumour necrosis factor related, apoptosis inducing ligand (TRAIL) in breast cancer, and their relations with osteoprotegerin, oestrogen receptor, and clinicopathological variables', *Journal of Clinical Pathology*. BMJ Publishing Group, 59(7), pp. 716–720. doi: 10.1136/jcp.2005.030031.

Cross, S S *et al.* (2006) 'Expression of receptor activator of nuclear factor kb ligand (RANKL) and tumour necrosis factor related, apoptosis inducing ligand (TRAIL) in breast cancer, and their relations with osteoprotegerin, oestrogen receptor, and clinicopathological variables', *J Clin Pathol*, 59, pp. 716–720. doi: 10.1136/jcp.2005.030031.

Croucher, P. I., McDonald, M. M. and Martin, T. J. (2016) 'Bone metastasis: The importance of the neighbourhood', *Nature Reviews Cancer*. Nature Publishing Group, pp. 373–386. doi: 10.1038/nrc.2016.44.

Cupedo, T. and Mebius, R. E. (2005) 'Cellular Interactions in Lymph Node Development', *The Journal of Immunology*. The American Association of Immunologists, 174(1), pp. 21–25. doi: 10.4049/jimmunol.174.1.21.

Curtis, C. *et al.* (2012) 'The genomic and transcriptomic architecture of 2,000 breast

tumours reveals novel subgroups', *Nature*, 486(7403), pp. 346–352. doi: 10.1038/nature10983.

Dagher, J. *et al.* (2014) 'Cytoplasmic PAR-3 protein expression is associated with adverse prognostic factors in clear cell renal cell carcinoma and independently impacts survival', *Human pathology*. *Hum Pathol*, 45(8), pp. 1639–1646. doi: 10.1016/J.HUMPATH.2014.03.018.

Darnay, B. G. *et al.* (1998) 'Characterization of the intracellular domain of receptor activator of NF- κ B (RANK): Interaction with tumor necrosis factor receptor-associated factors and activation of NF- κ B and c-JUN N-terminal kinase', *Journal of Biological Chemistry*. *J Biol Chem*, 273(32), pp. 20551–20555. doi: 10.1074/jbc.273.32.20551.

Darnay, B. G. *et al.* (1999) 'Activation of NF- κ B by RANK Requires Tumor Necrosis Factor Receptor-associated Factor (TRAF) 6 and NF- κ B-inducing Kinase', *Journal of Biological Chemistry*, 274(12), pp. 7724–7731. doi: 10.1074/jbc.274.12.7724.

Davies, A. H., Wang, Y. and Zoubeidi, A. (2018) 'Patient-derived xenografts: A platform for accelerating translational research in prostate cancer', *Molecular and Cellular Endocrinology*. Elsevier Ireland Ltd, 462, pp. 17–24. doi: 10.1016/j.mce.2017.03.013.

Derose, Y. S. *et al.* (2011) 'Tumor grafts derived from women with breast cancer authentically reflect tumor pathology, growth, metastasis and disease outcomes', *Nature Medicine*. Nature Publishing Group, 17(11), pp. 1514–1520. doi: 10.1038/nm.2454.

DeSantis, C. E. *et al.* (2019) 'Breast cancer statistics, 2019', *CA: A Cancer Journal for Clinicians*. Wiley, 69(6), pp. 438–451. doi: 10.3322/caac.21583.

Dias, K. *et al.* (2017) 'Claudin-low breast cancer; clinical & pathological characteristics', *PLoS ONE*. Edited by P.-Y. Chu. Public Library of Science, 12(1), p. e0168669. doi: 10.1371/journal.pone.0168669.

Ding, L. *et al.* (2010) 'Genome remodelling in a basal-like breast cancer metastasis and xenograft', *Nature*. *Nature*, 464(7291), pp. 999–1005. doi: 10.1038/nature08989.

Dobrolecki, L. E. *et al.* (2016) 'Patient-derived xenograft (PDX) models in basic and translational breast cancer research', *Cancer and Metastasis Reviews*. Springer New York LLC, 35(4), pp. 547–573. doi: 10.1007/s10555-016-9653-x.

van Dooijeweert, C., van Diest, P. J. and Ellis, I. O. (2021) 'Grading of invasive breast carcinoma: the way forward', *Virchows Archiv*. Springer Science and Business Media

LLC, 1, p. 3. doi: 10.1007/s00428-021-03141-2.

Dougall, W. C. *et al.* (1999) 'RANK is essential for osteoclast and lymph node development', *Genes and Development*, 13(18), pp. 2412–2424. doi: 10.1101/gad.13.18.2412.

Drugarin D, Drugarin M, Negru S, Cioaca R. RANKL-RANK/ OPG molecular complex-control factors in bone remodeling. Timisora Med J. 2003;53:297–302.

Eckhardt, B. L. *et al.* (2012) 'Strategies for the discovery and development of therapies for metastatic breast cancer', *Nature reviews. Drug discovery*. Nat Rev Drug Discov, 11(6), pp. 479–497. doi: 10.1038/NRD2372.

Effi, A. B. *et al.* (2016) 'Breast cancer molecular subtypes defined by ER/PR and HER2 Status: Association with clinicopathologic parameters in Ivorian patients', *Asian Pacific Journal of Cancer Prevention*. Asian Pacific Organization for Cancer Prevention, 17(4), pp. 1973–1978. doi: 10.7314/APJCP.2016.17.4.1973.

Eghbali-Fatourehchi, G. *et al.* (2003) 'Role of RANK ligand in mediating increased bone resorption in early postmenopausal women', *Journal of Clinical Investigation*. American Society for Clinical Investigation, 111(8), pp. 1221–1230. doi: 10.1172/jci17215.

Eirew, P. *et al.* (2015) 'Dynamics of genomic clones in breast cancer patient xenografts at single-cell resolution', *Nature*. Nature Publishing Group, 518(7539), pp. 422–426. doi: 10.1038/nature13952.

Eissner, G., Kolch, W. and Scheurich, P. (2004a) 'Ligands working as receptors: Reverse signaling by members of the TNF superfamily enhance the plasticity of the immune system', *Cytokine and Growth Factor Reviews*. Cytokine Growth Factor Rev, pp. 353–366. doi: 10.1016/j.cytogfr.2004.03.011.

Eissner, G., Kolch, W. and Scheurich, P. (2004b) 'Ligands working as receptors: Reverse signaling by members of the TNF superfamily enhance the plasticity of the immune system', *Cytokine and Growth Factor Reviews*, pp. 353–366. doi: 10.1016/j.cytogfr.2004.03.011.

Eliyatkina, N. *et al.* (2015) 'Molecular Classification of Breast Carcinoma: From Traditional, Old-Fashioned Way to A New Age, and A New Way', *Journal of Breast Health*. AVES Publishing Co., 11(2), pp. 59–66. doi: 10.5152/tjbh.2015.1669.

ELSTON, C. W. and ELLIS, I. O. (1991) 'pathological prognostic factors in breast cancer.

I. The value of histological grade in breast cancer: experience from a large study with long-term follow-up', *Histopathology*, 19(5), pp. 403–410. doi: 10.1111/j.1365-2559.1991.tb00229.x.

Emery, J. G. *et al.* (1998) 'Osteoprotegerin is a receptor for the cytotoxic ligand TRAIL', *Journal of Biological Chemistry*. *J Biol Chem*, 273(23), pp. 14363–14367. doi: 10.1074/jbc.273.23.14363.

Engel, C. and Fischer, C. (2015) 'Breast cancer risks and risk prediction models', *Breast Care*. S. Karger AG, pp. 7–12. doi: 10.1159/000376600.

Eyre, R. *et al.* (2016) 'Patient-derived mammosphere and xenograft tumour initiation correlates with progression to metastasis', *Journal of Mammary Gland Biology and Neoplasia*. Springer Science and Business Media, LLC, 21(3–4), pp. 99–109. doi: 10.1007/s10911-016-9361-8.

Fang, P. *et al.* (2018) 'Immune cell subset differentiation and tissue inflammation', *Journal of Hematology and Oncology*. BioMed Central Ltd. doi: 10.1186/s13045-018-0637-x.

Fata, J. E. *et al.* (2000) 'The osteoclast differentiation factor osteoprotegerin-ligand is essential for mammary gland development', *Cell*. Cell Press, 103(1), pp. 41–50. doi: 10.1016/S0092-8674(00)00103-3.

Fiebig, H. H. *et al.* (1985) 'Development of three human small cell lung cancer models in nude mice.', *Recent results in cancer research. Fortschritte der Krebsforschung. Progrès dans les recherches sur le cancer*. Springer, Berlin, Heidelberg, 97, pp. 77–86. doi: 10.1007/978-3-642-82372-5_8.

Finkel, E. (2002) 'Consortium Piecing Together Role of ATM Gene in Breast Cancer', *CancerSpectrum Knowledge Environment*. Oxford University Press, 94(3), pp. 158–159. doi: 10.1093/jnci/94.3.158.

Foroutan, M. *et al.* (2018) 'Single sample scoring of molecular phenotypes', *BMC Bioinformatics*. BioMed Central Ltd., 19(1), pp. 1–10. doi: 10.1186/S12859-018-2435-4/FIGURES/2.

Fougner, C. *et al.* (2019) 'Claudin-low-like mouse mammary tumors show distinct transcriptomic patterns uncoupled from genomic drivers', *Breast Cancer Research*. BioMed Central Ltd., 21(1), p. 85. doi: 10.1186/s13058-019-1170-8.

Fu, N. Y. *et al.* (2020) 'Stem cells and the differentiation hierarchy in mammary gland development', *Physiological Reviews*. American Physiological Society, 100(2), pp. 489–523. doi:

10.1152/PHYSREV.00040.2018/ASSET/IMAGES/LARGE/Z9J0012029270010.JPEG.

Fujimura, T. *et al.* (2015) 'Receptor Activator of NF- κ B Ligand Promotes the Production of CCL17 from RANK+ M2 Macrophages', *Journal of Investigative Dermatology*. Nature Publishing Group, pp. 2884–2887. doi: 10.1038/jid.2015.209.

Fujimura, T. *et al.* (2016) 'Receptor activator of nuclear factor kappa-B ligand (RANKL)/RANK signaling promotes cancer-related inflammation through M2 macrophages', *Experimental Dermatology*. Blackwell Publishing Ltd, pp. 397–399. doi: 10.1111/exd.12949.

Fulford, L. G. *et al.* (2007) 'Basal-like grade III invasive ductal carcinoma of the breast: Patterns of metastasis and long-term survival', *Breast Cancer Research*, 9(1), p. R4. doi: 10.1186/bcr1636.

Galea, M. H. *et al.* (1992) 'The Nottingham prognostic index in primary breast cancer', *Breast Cancer Research and Treatment*. Kluwer Academic Publishers, 22(3), pp. 207–219. doi: 10.1007/BF01840834.

Galibert, L. *et al.* (1998) 'The involvement of multiple tumor necrosis factor receptor (TNFR)- associated factors in the signaling mechanisms of receptor activator of NF- κ B, a member of the TNFR superfamily', *Journal of Biological Chemistry*. J Biol Chem, 273(51), pp. 34120–34127. doi: 10.1074/jbc.273.51.34120.

Gao, Y. H. *et al.* (1998) 'Potential role of Cbfa1, an essential transcriptional factor for osteoblast differentiation, in osteoclastogenesis: Regulation of mRNA expression of osteoclast differentiation factor (ODF)', *Biochemical and Biophysical Research Communications*. Academic Press Inc., 252(3), pp. 697–702. doi: 10.1006/bbrc.1998.9643.

GeparX: Denosumab (Dmab) as add-on to different regimen of nab-paclitaxel (nP)-anthracycline based neoadjuvant chemotherapy (NACT) in early breast cancer.

GeparX (GBG 88) - GBG. Available at: <https://www.gbg.de/en/trials/geparx.php>

Gerratana, L. *et al.* (2015) 'Pattern of metastasis and outcome in patients with breast cancer', *Clinical & experimental metastasis*. Clin Exp Metastasis, 32(2), pp. 125–133. doi: 10.1007/S10585-015-9697-2.

Geyer, F. C. *et al.* (2009) 'Genetic characterization of breast cancer and implications for clinical management', *Journal of Cellular and Molecular Medicine*. Wiley-Blackwell, pp. 4090–4103. doi: 10.1111/j.1582-4934.2009.00906.x.

Gillet, J. P. *et al.* (2011) 'Redefining the relevance of established cancer cell lines to the study of mechanisms of clinical anti-cancer drug resistance', *Proceedings of the National Academy of Sciences of the United States of America*. Proc Natl Acad Sci U S A, 108(46), pp. 18708–18713. doi: 10.1073/pnas.1111840108.

Gnant, M. *et al.* (2018) 'Adjuvant denosumab in early breast cancer: Disease-free survival analysis of 3,425 postmenopausal patients in the ABCSG-18 trial.', *Journal of Clinical Oncology*. American Society of Clinical Oncology (ASCO), 36(15_suppl), pp. 500–500. doi: 10.1200/jco.2018.36.15_suppl.500.

Goldhirsch, A. *et al.* (2003) 'Meeting highlights: updated international expert consensus on the primary therapy of early breast cancer', *Journal of clinical oncology : official journal of the American Society of Clinical Oncology*. J Clin Oncol, 21(17), pp. 3357–3365. doi: 10.1200/JCO.2003.04.576.

Gomes Do Nascimento, R. and Otoni, K. M. (2020) 'Histological and molecular classification of breast cancer: what do we know?', *Mastology*, 30, p. 20200024. doi: 10.29289/25945394202020200024.

Gomes, I. *et al.* (2020) 'Expression of receptor activator of NFkB (RANK) drives stemness and resistance to therapy in ER+HER2- breast cancer', *Oncotarget*. Impact Journals, LLC, 11(19), p. 1714. doi: 10.18632/ONCOTARGET.27576.

Gómez-Acebo, I. *et al.* (2021) 'Adequacy of early-stage breast cancer systemic adjuvant treatment to Saint Gallen-2013 statement: the MCC-Spain study', *Scientific reports*. NLM (Medline), 11(1), p. 5375. doi: 10.1038/s41598-021-84825-2.

Gómez-Aleza, C. *et al.* (2020) 'Inhibition of RANK signaling in breast cancer induces an anti-tumor immune response orchestrated by CD8+ T cells', *Nature Communications*. Nature Research, 11(1), pp. 1–18. doi: 10.1038/s41467-020-20138-8.

Gómez-Miragaya, J. *et al.* (2017) 'Resistance to Taxanes in Triple-Negative Breast Cancer Associates with the Dynamics of a CD49f+ Tumor-Initiating Population', *Stem Cell Reports*. Cell Press, 8(5), pp. 1392–1407. doi: 10.1016/j.stemcr.2017.03.026.

Gomez-Miragaya, J. and González-Suárez, E. (2017) 'Tumor-initiating CD49f cells are a hallmark of chemoresistant triple negative breast cancer', *Molecular and Cellular*

Oncology. Taylor and Francis Ltd., 4(4), pp. e1338208–e1338208. doi: 10.1080/23723556.2017.1338208.

Gonzalez-Angulo, A. M., Morales-Vasquez, F. and Hortobagyi, G. N. (2007) 'Overview of resistance to systemic therapy in patients with breast cancer', *Advances in Experimental Medicine and Biology*. Springer, New York, NY, pp. 1–22. doi: 10.1007/978-0-387-74039-3_1.

Gonzalez-Suarez, E. *et al.* (2007) 'RANK overexpression in transgenic mice with mouse mammary tumor virus promoter-controlled RANK increases proliferation and impairs alveolar differentiation in the mammary epithelia and disrupts lumen formation in cultured epithelial acini.', *Molecular and cellular biology*, 27(4), pp. 1442–54. doi: 10.1128/MCB.01298-06.

Gonzalez-Suarez, E. *et al.* (2010) 'RANK ligand mediates progesterin-induced mammary epithelial proliferation and carcinogenesis.', *Nature*, 468(7320), pp. 103–7. doi: 10.1038/nature09495.

González-Suárez, E. and Sanz-Moreno, A. (2016) 'RANK as a therapeutic target in cancer', *The FEBS journal*, pp. 2018–2033. doi: 10.1111/febs.13645.

Green, A. R. *et al.* (2013) 'Identification of key clinical phenotypes of breast cancer using a reduced panel of protein biomarkers', *British Journal of Cancer*. Nature Publishing Group, 109(7), pp. 1886–1894. doi: 10.1038/bjc.2013.528.

Grimaud, E. *et al.* (2003) 'Receptor Activator of Nuclear Factor κ B Ligand (RANKL)/Osteoprotegerin (OPG) Ratio Is Increased in Severe Osteolysis', *American Journal of Pathology*. American Society for Investigative Pathology Inc., 163(5), pp. 2021–2031. doi: 10.1016/S0002-9440(10)63560-2.

Gris-Oliver, A. *et al.* (2020) 'Genetic Alterations in the PI3K/AKT Pathway and Baseline AKT Activity Define AKT Inhibitor Sensitivity in Breast Cancer Patient-derived Xenografts', *Clinical Cancer Research*. American Association for Cancer Research Inc., 26(14), pp. 3720–3731. doi: 10.1158/1078-0432.CCR-19-3324.

de Groot, A. F. *et al.* (2018) 'The anti-tumor effect of RANKL inhibition in malignant solid tumors – A systematic review', *Cancer Treatment Reviews*. W.B. Saunders Ltd, pp. 18–28. doi: 10.1016/j.ctrv.2017.10.010.

Guidelines Detail. Available at: <https://www.nccn.org/guidelines/guidelines-detail?category=1&id=1419>.

Haffty, B. G., Euhus, D. M. and Pierce, L. J. (2020) 'Genetic factors in the locoregional management of breast cancer', *Journal of Clinical Oncology*. American Society of Clinical Oncology, pp. 2220–2229. doi: 10.1200/JCO.19.02859.

Hanada, R. *et al.* (2009) 'Central control of fever and female body temperature by RANKL/RANK', *Nature*, 462(7272), pp. 505–509. doi: 10.1038/nature08596.

Hancock, J. F. (2003) 'Ras proteins: Different signals from different locations', *Nature Reviews Molecular Cell Biology*, 4(5), pp. 373–384. doi: 10.1038/NRM1105.

'Health Effects of Overweight and Obesity in 195 Countries over 25 Years' (2017) *New England Journal of Medicine*. New England Journal of Medicine (NEJM/MMS), 377(1), pp. 13–27. doi: 10.1056/nejmoa1614362.

Hennighausen, L. and Robinson, G. W. (2001) 'Signaling Pathways in Mammary Gland Development', *Developmental Cell*, pp. 467–475. doi: 10.1016/S1534-5807(01)00064-8.

Hidalgo, M. *et al.* (2014) 'Patient Derived Xenograft Models: An Emerging Platform for Translational Cancer Research Europe PMC Funders Group', *Cancer Discov*, 4(9), pp. 998–1013. doi: 10.1158/2159-8290.CD-14-0001.

Hikosaka, Y. *et al.* (2008) 'The Cytokine RANKL Produced by Positively Selected Thymocytes Fosters Medullary Thymic Epithelial Cells that Express Autoimmune Regulator', *Immunity*, 29(3), pp. 438–450. doi: 10.1016/j.immuni.2008.06.018.

Hofbauer, L. C. *et al.* (1999) 'Interleukin-1 β and tumor necrosis factor- α , but not interleukin-6, stimulate osteoprotegerin ligand gene expression in human osteoblastic cells', *Bone*. Bone, 25(3), pp. 255–259. doi: 10.1016/S8756-3282(99)00162-3.

Hofbauer, L. C. *et al.* (2000) 'The roles of osteoprotegerin and osteoprotegerin ligand in the paracrine regulation of bone resorption', *Journal of Bone and Mineral Research*. American Society for Bone and Mineral Research, pp. 2–12. doi: 10.1359/jbmr.2000.15.1.2.

Hofbauer, L. C. and Heufelder, A. E. (2001) 'Role of receptor activator of nuclear factor- κ B ligand and osteoprotegerin in bone cell biology', *Journal of Molecular Medicine*. J Mol Med (Berl), pp. 243–253. doi: 10.1007/s001090100226.

Hofbauer, L. C. and Schoppet, M. (2004) 'Clinical implications of the osteoprotegerin/RANKL/RANK system for bone and vascular diseases', *Journal of the*

American Medical Association. JAMA, pp. 490–495. doi: 10.1001/jama.292.4.490.

Hsu, S. Y., Liang, S. G. and Hsueh, A. J. W. (1998) 'Characterization of two LGR genes homologous to gonadotropin and thyrotropin receptors with extracellular leucine-rich repeats and a G protein-coupled, seven-transmembrane region', *Molecular Endocrinology*. Endocrine Society, 12(12), pp. 1830–1845. doi: 10.1210/mend.12.12.0211.

<https://www.cancer.org/cancer/breast-cancer/treatment.html>

Huang, R. *et al.* (2017) 'RANKL-induced M1 macrophages are involved in bone formation', *Bone Research*. Sichuan University, 5(1), pp. 1–13. doi: 10.1038/boneres.2017.19.

Ikebuchi, Y. *et al.* (2018) 'Coupling of bone resorption and formation by RANKL reverse signalling', *Nature*. Nature Publishing Group, 561(7722), pp. 195–200. doi: 10.1038/s41586-018-0482-7.

Ikeda, T. *et al.* (2001) *Determination of Three Isoforms of the Receptor Activator of Nuclear Factor-Ligand and Their Differential Expression in Bone and Thymus**. Available at: <https://academic.oup.com/endo/article/142/4/1419/2988702> (Accessed: 23 May 2021).

Ikeda, T. *et al.* (2003) 'Multimerization of the Receptor Activator of Nuclear Factor- κ B Ligand (RANKL) Isoforms and Regulation of Osteoclastogenesis', *Journal of Biological Chemistry*, 278(47), pp. 47217–47222. doi: 10.1074/jbc.M304636200.

Imai, D. *et al.* (2019) 'IFN- γ Promotes Epithelial-Mesenchymal Transition and the Expression of PD-L1 in Pancreatic Cancer', *Journal of Surgical Research*. Academic Press Inc., 240, pp. 115–123. doi: 10.1016/J.JSS.2019.02.038.

Inman, J. L. *et al.* (2015) 'Mammary gland development: Cell fate specification, stem cells and the microenvironment', *Development (Cambridge)*. Company of Biologists Ltd, pp. 1028–1042. doi: 10.1242/dev.087643.

Italiani, P. and Boraschi, D. (2014) 'From monocytes to M1/M2 macrophages: Phenotypical vs. functional differentiation', *Frontiers in Immunology*. Frontiers Research Foundation, p. 514. doi: 10.3389/fimmu.2014.00514.

Ito, S. *et al.* (2002) 'Crystal structure of the extracellular domain of mouse RANK ligand at 2.2-Å resolution', *Journal of Biological Chemistry*. J Biol Chem, 277(8), pp. 6631–

6636. doi: 10.1074/jbc.M106525200.

Iwasaki, H. and Akashi, K. (2007) 'Hematopoietic developmental pathways: On cellular basis', *Oncogene*. Nature Publishing Group, pp. 6687–6696. doi: 10.1038/sj.onc.1210754.

J, S., L, L. and CP, B. (2001) 'Biochemical and pharmacological criteria define two shedding activities for TRANCE/OPGL that are distinct from the tumor necrosis factor alpha convertase', *The Journal of biological chemistry*. J Biol Chem, 276(18), pp. 14665–14674. doi: 10.1074/JBC.M010741200.

Jimi, E. *et al.* (2019) 'The role of NF- κ B in physiological bone development and inflammatory bone diseases: Is NF- κ B inhibition “killing two birds with one stone”?', *Cells*. MDPI, p. 1636. doi: 10.3390/cells8121636.

Jin, W. *et al.* (2008) 'Deubiquitinating enzyme CYLD negatively regulates RANK signaling and osteoclastogenesis in mice', *Journal of Clinical Investigation*, 118(5), pp. 1858–1866. doi: 10.1172/JCI34257.

Jones, D. H. *et al.* (2006a) 'Regulation of cancer cell migration and bone metastasis by RANKL', *Nature 2006 440:7084*. Nature Publishing Group, 440(7084), pp. 692–696. doi: 10.1038/nature04524.

Jones, D. H. *et al.* (2006b) 'Regulation of cancer cell migration and bone metastasis by RANKL', *Nature*. Nature, 440(7084), pp. 692–696. doi: 10.1038/NATURE04524.

Joshi, P. A. *et al.* (2010) 'Progesterone induces adult mammary stem cell expansion.', *Nature*, 465(7299), pp. 803–7. doi: 10.1038/nature09091.

Kamalakar, A. *et al.* (2017) 'PTHrP(12-48) Modulates the Bone Marrow Microenvironment and Suppresses Human Osteoclast Differentiation and Lifespan', *Journal of Bone and Mineral Research*. John Wiley and Sons Inc., 32(7), pp. 1421–1431. doi: 10.1002/jbmr.3142.

Katzen, F. (2007) 'Gateway® recombinational cloning: A biological operating system', *Expert Opinion on Drug Discovery*, pp. 571–589. doi: 10.1517/17460441.2.4.571.

Kearns, A. E., Khosla, S. and Kostenuik, P. J. (2008) 'Receptor activator of nuclear factor κ B ligand and osteoprotegerin regulation of bone remodeling in health and disease', *Endocrine Reviews*. Endocr Rev, pp. 155–192. doi: 10.1210/er.2007-0014.

Kelland, L. R. (2004) "Of mice and men": Values and liabilities of the athymic nude

mouse model in anticancer drug development', *European Journal of Cancer*. Elsevier Ltd, 40(6), pp. 827–836. doi: 10.1016/j.ejca.2003.11.028.

Kennecke, H. *et al.* (2010) 'Metastatic behavior of breast cancer subtypes', *Journal of Clinical Oncology*, 28(20), pp. 3271–3277. doi: 10.1200/JCO.2009.25.9820.

Kim, H. J. *et al.* (2009) 'The Src family kinase, Lyn, suppresses osteoclastogenesis in vitro and in vivo', *Proceedings of the National Academy of Sciences of the United States of America*. Proc Natl Acad Sci U S A, 106(7), pp. 2325–2330. doi: 10.1073/pnas.0806963106.

Kim, M. P. *et al.* (2009) 'Generation of orthotopic and heterotopic human pancreatic cancer xenografts in immunodeficient mice', *Nature Protocols*. Nat Protoc, 4(11), pp. 1670–1680. doi: 10.1038/nprot.2009.171.

Kim, N.-S. *et al.* (2006) 'Receptor Activator of NF- κ B Ligand Regulates the Proliferation of Mammary Epithelial Cells via Id2', *Molecular and Cellular Biology*. American Society for Microbiology, 26(3), pp. 1002–1013. doi: 10.1128/mcb.26.3.1002-1013.2006.

Kim, Young Mi *et al.* (2002) 'TNF-related activation-induced cytokine (TRANCE) induces angiogenesis through the activation of Src and phospholipase C (PLC) in human endothelial cells', *Journal of Biological Chemistry*. American Society for Biochemistry and Molecular Biology Inc., 277(9), pp. 6799–6805. doi: 10.1074/jbc.M109434200.

Kisiswa, L. *et al.* (2013) 'TNF α reverse signaling promotes sympathetic axon growth and target innervation', *Nature Neuroscience*, 16(7), pp. 865–873. doi: 10.1038/nn.3430.

Ko, S.-H. and Kim, H.-S. (2020) 'Menopause-Associated Lipid Metabolic Disorders and Foods Beneficial for Postmenopausal Women', *Nutrients*. MDPI AG, 12(1), p. 202. doi: 10.3390/nu12010202.

Kondo, T. *et al.* (2004) '1 α ,25 dihydroxyvitamin D3 rapidly regulates the mouse osteoprotegerin gene through dual pathways', *Journal of Bone and Mineral Research*. John Wiley & Sons, Ltd, 19(9), pp. 1411–1419. doi: 10.1359/JBMR.040604.

Kong, Y. Y. *et al.* (1999) 'OPGL is a key regulator of osteoclastogenesis, lymphocyte development and lymph-node organogenesis', *Nature*. Nature, 397(6717), pp. 315–323. doi: 10.1038/16852.

Kostenuik, P. J. *et al.* (2009) 'Denosumab, a fully human monoclonal antibody to RANKL, inhibits bone resorption and increases BMD in knock-in mice that express chimeric

(murine/human) RANKL', in *Journal of Bone and Mineral Research*. *J Bone Miner Res*, pp. 182–195. doi: 10.1359/jbmr.081112.

Kumar, S., Bajaj, S. and Bodla, R. (2016) 'Preclinical screening methods in cancer', *Indian Journal of Pharmacology*. Medknow Publications, pp. 481–486. doi: 10.4103/0253-7613.190716.

Kwon, B. S. *et al.* (1998) 'TR1, a new member of the tumor necrosis factor receptor superfamily, induces fibroblast proliferation and inhibits osteoclastogenesis and bone resorption', *The FASEB Journal*. Wiley, 12(10), pp. 845–854. doi: 10.1096/fasebj.12.10.845.

Lacey, D. L. *et al.* (1998) 'Osteoprotegerin ligand is a cytokine that regulates osteoclast differentiation and activation', *Cell*. Cell Press, 93(2), pp. 165–176. doi: 10.1016/S0092-8674(00)81569-X.

Lehmann, B. D. *et al.* (2011) 'Identification of human triple-negative breast cancer subtypes and preclinical models for selection of targeted therapies', *Journal of Clinical Investigation*. American Society for Clinical Investigation, 121(7), pp. 2750–2767. doi: 10.1172/JCI45014.

Liberzon, A. *et al.* (2015) 'The Molecular Signatures Database (MSigDB) hallmark gene set collection', *Cell systems*. Cell Syst, 1(6), pp. 417–425. doi: 10.1016/J.CELS.2015.12.004.

Lin, S. X. *et al.* (2010) 'Molecular therapy of breast cancer: Progress and future directions', *Nature Reviews Endocrinology*, pp. 485–493. doi: 10.1038/nrendo.2010.92.

Lipton, A. *et al.* (2012) 'Superiority of denosumab to zoledronic acid for prevention of skeletal-related events: A combined analysis of 3 pivotal, randomised, phase 3 trials', *European Journal of Cancer*. *Eur J Cancer*, 48(16), pp. 3082–3092. doi: 10.1016/j.ejca.2012.08.002.

Loh, E. D. *et al.* (2000) 'Chromosomal localization of GPR48, a novel glycoprotein hormone receptor like GPCR, in human and mouse with radiation hybrid and interspecific backcross mapping', *Cytogenetics and Cell Genetics*. *Cytogenet Cell Genet*, 89(1–2), pp. 2–5. doi: 10.1159/000015576.

Loh, E. D., Broussard, S. R. and Kolakowski, L. F. (2001) 'Molecular characterization of a novel glycoprotein hormone G-protein-coupled receptor', *Biochemical and Biophysical Research Communications*. Academic Press Inc., 282(3), pp. 757–764. doi:

10.1006/bbrc.2001.4625.

Loi, S. (2008) 'Molecular analysis of hormone receptor positive (luminal) breast cancers - What have we learnt?', *European Journal of Cancer*. Eur J Cancer, 44(18), pp. 2813–2818. doi: 10.1016/j.ejca.2008.09.012.

Loibl, S. *et al.* (2021) 'Breast cancer.', *Lancet (London, England)*. Elsevier, 0(0). doi: 10.1016/S0140-6736(20)32381-3.

Lundgren, C. *et al.* (2019) 'Agreement between molecular subtyping and surrogate subtype classification: a contemporary population-based study of ER-positive/ HER2-negative primary breast cancer', *Breast Cancer Research and Treatment*, 178, pp. 459–467. doi: 10.1007/s10549-019-05378-7.

Luo, G. *et al.* (2018) 'TNF- α and RANKL promote osteoclastogenesis by upregulating RANK via the NF- κ B pathway', *Molecular Medicine Reports*. Spandidos Publications, 17(5), pp. 6605–6611. doi: 10.3892/MMR.2018.8698/HTML.

Luo, J. *et al.* (2016) 'LGR4 is a receptor for RANKL and negatively regulates osteoclast differentiation and bone resorption', *Nature Medicine*. Nature Publishing Group, 22(5), pp. 539–546. doi: 10.1038/nm.4076.

Lv, N. *et al.* (2015) 'Inflammatory mediators, tumor necrosis factor- α and interferon- γ , induce EMT in human PTC cell lines', *Oncology Letters*. Spandidos Publications, 10(4), pp. 2591–2597. doi: 10.3892/OL.2015.3518/HTML.

Ma, Q. *et al.* (2019a) 'Mature osteoclast- derived apoptotic bodies promote osteogenic differentiation via RANKL-mediated reverse signaling', *Journal of Biological Chemistry*. American Society for Biochemistry and Molecular Biology Inc., 294(29), pp. 11240–11247. doi: 10.1074/jbc.RA119.007625.

Ma, Q. *et al.* (2019b) 'Mature osteoclast- derived apoptotic bodies promote osteogenic differentiation via RANKL-mediated reverse signaling', *Journal of Biological Chemistry*. American Society for Biochemistry and Molecular Biology Inc., 294(29), pp. 11240–11247. doi: 10.1074/jbc.RA119.007625.

Maani, N. *et al.* (2019) 'NF1 patients receiving breast cancer screening: Insights from the ontario high risk breast screening program', *Cancers*. MDPI AG, 11(5), p. 707. doi: 10.3390/cancers11050707.

MacCìò, A. and Madeddu, C. (2011) 'Obesity, inflammation, and postmenopausal breast

cancer: Therapeutic implications', *TheScientificWorldJournal*, 11, pp. 2020–2036. doi: 10.1100/2011/806787.

MacFarlane, M. (2003) 'TRAIL-induced signalling and apoptosis', *Toxicology letters*. *Toxicol Lett*, 139(2–3), pp. 89–97. doi: 10.1016/S0378-4274(02)00422-8.

Manson, J. A. E. *et al.* (2013) 'Menopausal hormone therapy and health outcomes during the intervention and extended poststopping phases of the women's health initiative randomized trials', *JAMA - Journal of the American Medical Association*. American Medical Association, 310(13), pp. 1353–1368. doi: 10.1001/jama.2013.278040.

Marangoni, E. *et al.* (2007) 'A new model of patient tumor-derived breast cancer xenografts for preclinical assays', *Clinical Cancer Research*. American Association for Cancer Research, 13(13), pp. 3989–3998. doi: 10.1158/1078-0432.CCR-07-0078.

Martínez-Aranda, A. *et al.* (2015) 'FN14 and GRP94 expression are prognostic/predictive biomarkers of brain metastasis outcome that open up new therapeutic strategies', *Oncotarget*. Impact Journals, LLC, 6(42), p. 44254. doi: 10.18632/ONCOTARGET.5471.

Maruyama, K. *et al.* (2012) 'TRAF family member-associated NF- κ B activator (TANK) is a negative regulator of osteoclastogenesis and bone formation', *Journal of Biological Chemistry*. *J Biol Chem*, 287(34), pp. 29114–29124. doi: 10.1074/jbc.M112.347799.

Masoud, V. and Pagès, G. (2017) 'Targeted therapies in breast cancer: New challenges to fight against resistance', *World Journal of Clinical Oncology*. Baishideng Publishing Group Co., Limited, pp. 120–134. doi: 10.5306/wjco.v8.i2.120.

McClung, M. R. *et al.* (2006) 'Denosumab in Postmenopausal Women with Low Bone Mineral Density', *New England Journal of Medicine*, 354(8), pp. 821–831. doi: 10.1056/NEJMoa044459.

Mcnally, S. and Stein, T. (no date) 'Overview of Mammary Gland Development: A Comparison of Mouse and Human', *Methods in Molecular Biology*, 1501. doi: 10.1007/978-1-4939-6475-8_1.

Meng, Y. H. *et al.* (2017) 'RANKL-mediated harmonious dialogue between fetus & mother guarantees smooth gestation by inducing decidual M2 macrophage polarization', *Cell Death and Disease*. Nature Publishing Group, 8(10), p. 3105. doi: 10.1038/cddis.2017.505.

Menopause.

Available

at:

<https://www.clevelandclinicmeded.com/medicalpubs/diseasemanagement/womens-health/menopause/>.

Mercogliano, M. F. *et al.* (2020) 'Tumor Necrosis Factor α Blockade: An Opportunity to Tackle Breast Cancer', *Frontiers in Oncology*. Frontiers Media S.A., p. 584. doi: 10.3389/fonc.2020.00584.

Miersch, S. and Sidhu, S. S. (2016) 'Intracellular targeting with engineered proteins', *F1000Research*. Faculty of 1000 Ltd, 5. doi: 10.12688/F1000RESEARCH.8915.1.

Miller, J. S. and Lanier, L. L. (2019) 'Natural Killer Cells in Cancer Immunotherapy', *Annual Review of Cancer Biology*. Annual Reviews Inc., 3(1), pp. 77–103. doi: 10.1146/annurev-cancerbio-030518-055653.

Ming, J., Cronin, S. J. F. and Penninger, J. M. (2020) 'Targeting the RANKL/RANK/OPG Axis for Cancer Therapy', *Frontiers in Oncology*. Frontiers Media S.A., p. 1283. doi: 10.3389/fonc.2020.01283.

Molecular Subtypes of Breast Cancer: A Review for Breast Radiologists Karen S. Johnson, MD,¹, * Emily F. Conant, MD,² Mary Scott Soo.

Moon, H. G. *et al.* (2015) 'Prognostic and functional importance of the engraftment-associated genes in the patient-derived xenograft models of triple-negative breast cancers', *Breast Cancer Research and Treatment*. Springer New York LLC, 154(1), pp. 13–22. doi: 10.1007/s10549-015-3585-y.

Mosheimer, B. A. *et al.* (2005) 'Syndecan-1 is involved in osteoprotegerin-induced chemotaxis in human peripheral blood monocytes', *Journal of Clinical Endocrinology and Metabolism*. J Clin Endocrinol Metab, 90(5), pp. 2964–2971. doi: 10.1210/jc.2004-1895.

Mueller, C. G. and Hess, E. (2012) 'Emerging functions of RANKL in lymphoid tissues', *Frontiers in Immunology*. Front Immunol. doi: 10.3389/fimmu.2012.00261.

Nakashima, T., Hayashi, M. and Takayanagi, H. (2012) 'New insights into osteoclastogenic signaling mechanisms', *Trends in Endocrinology and Metabolism*. Trends Endocrinol Metab, pp. 582–590. doi: 10.1016/j.tem.2012.05.005.

Naundorf, H. *et al.* (1992) 'Characterization of two human mammary carcinomas, MT-1 and MT-3, suitable for in vivo testing of ether lipids and their derivatives', *Breast Cancer Research and Treatment*. Kluwer Academic Publishers, 23(1–2), pp. 87–95. doi: 10.1007/BF01831480.

Neuhouser, M. L. *et al.* (2015) 'Overweight, obesity, and postmenopausal invasive breast cancer risk: A secondary analysis of the women's health initiative randomized clinical trials', *JAMA Oncology*. American Medical Association, 1(5), pp. 611–621. doi: 10.1001/jamaoncol.2015.1546.

Nolan, E. *et al.* (2016) 'RANK ligand as a potential target for breast cancer prevention in BRCA1-mutation carriers', *Nature Medicine*. Nature Publishing Group, 22(8), pp. 933–939. doi: 10.1038/nm.4118.

NSG™ Variants Portfolio. Available at: <https://www.jax.org/jax-mice-and-services/find-and-order-jax-mice/nsg-portfolio>.

Oberaigner, W. *et al.* (2010) 'Breast cancer incidence and mortality in Tyrol/Austria after fifteen years of opportunistic mammography screening', *BMC Public Health*. BMC Public Health, 10. doi: 10.1186/1471-2458-10-86.

Okamoto, K. *et al.* (2017) 'Osteoimmunology: The conceptual framework unifying the immune and skeletal systems', *Physiological Reviews*. American Physiological Society, 97(4), pp. 1295–1349. doi: 10.1152/physrev.00036.2016.

Ominsky, M. S. *et al.* (2007) 'The RANKL inhibitor OPG-Fc increases cortical and trabecular bone mass in young gonad-intact cynomolgus monkeys', *Osteoporosis International*. Osteoporos Int, 18(8), pp. 1073–1082. doi: 10.1007/s00198-007-0363-7.

Onitilo, A. A. *et al.* (no date) 'Breast Cancer Subtypes Based on ER/PR and Her2 Expression: Comparison of Clinicopathologic Features and Survival', *Original Research Clinical Medicine & Research*, 7(1), pp. 4–13. doi: 10.3121/cmr.2009.825.

Ono, T. *et al.* (2020) 'RANKL biology: Bone metabolism, the immune system, and beyond', *Inflammation and Regeneration*. BioMed Central Ltd. doi: 10.1186/s41232-019-0111-3.

Pagé, M. (1997) 'High-Volume Screening', in *Anticancer Drug Development Guide*. Humana Press, pp. 3–21. doi: 10.1007/978-1-4615-8152-9_1.

Paget Disease of the Breast - National Cancer Institute (no date). Available at: <https://www.cancer.gov/types/breast/paget-breast-fact-sheet> (Accessed: 16 May 2020).

Palafox, M. *et al.* (2012) 'RANK induces epithelial-mesenchymal transition and stemness in human mammary epithelial cells and promotes tumorigenesis and metastasis', *Cancer Research*, 72(11), pp. 2879–2888. doi: 10.1158/0008-5472.CAN-12-0044.

Papanastasiou, A. D., Sirinian, C. and Kalofonos, H. P. (2012) *Identification of novel human receptor activator of nuclear factor- κ B isoforms generated through alternative splicing: implications in breast cancer cell survival and migration*, *Breast Cancer Research*. doi: 10.1186/bcr3234.

Parise, C. A. and Caggiano, V. (2014) 'Breast cancer survival defined by the er/pr/her2 subtypes and a surrogate classification according to tumor grade and immunohistochemical biomarkers', *Journal of Cancer Epidemiology*. Hindawi Publishing Corporation, 2014. doi: 10.1155/2014/469251.

Park, H. S. *et al.* (2014) 'Expression of receptor activator of nuclear factor kappa-B as a poor prognostic marker in breast cancer', in *Journal of Surgical Oncology*. John Wiley and Sons Inc, pp. 807–812. doi: 10.1002/jso.23737.

Park, J. W. *et al.* (2021) 'Obesity and breast cancer risk for pre- and postmenopausal women among over 6 million Korean women', *Breast Cancer Research and Treatment*. Springer, 185(2), pp. 495–506. doi: 10.1007/s10549-020-05952-4.

Pasquale, P. *et al.* (2013) 'Constitutive activation of RANK disrupts mammary cell fate leading to tumorigenesis', *Stem cells (Dayton, Ohio)*. Stem Cells, 31(9), pp. 1954–1965. doi: 10.1002/STEM.1454.

'PDX-MI: Minimal Information for Patient-Derived Tumor Xenograft Models' (no date). doi: 10.1158/0008-5472.CAN-17-0582.

Pernas, S. and Tolaney, S. M. (2019) 'HER2-positive breast cancer: new therapeutic frontiers and overcoming resistance', *Therapeutic Advances in Medical Oncology*. SAGE Publications Inc. doi: 10.1177/1758835919833519.

Perou, C. M. *et al.* (2000) 'Molecular portraits of human breast tumours', *Nature*. Nature Publishing Group, 406(6797), pp. 747–752. doi: 10.1038/35021093.

Perrone, F. and Gravina, A. (2020) 'Denosumab in early breast cancer: negative data and a call to action', *The Lancet Oncology*. Lancet Publishing Group, pp. 5–6. doi: 10.1016/S1470-2045(19)30717-X.

Peters, S. *et al.* (2019) 'The RANK–RANKL axis: an opportunity for drug repurposing in cancer?', *Clinical and Translational Oncology*. Springer-Verlag Italia s.r.l., pp. 977–991. doi: 10.1007/s12094-018-02023-5.

Pfitzner, B. M. *et al.* (2014) 'RANK expression as a prognostic and predictive marker in

breast cancer', *Breast Cancer Research and Treatment*. Springer New York LLC, 145(2), pp. 307–315. doi: 10.1007/s10549-014-2955-1.

Pharoah, P. D. P., Guilford, P. and Caldas, C. (2001) 'Incidence of gastric cancer and breast cancer in CDH1 (E-cadherin) mutation carriers from hereditary diffuse gastric cancer families', *Gastroenterology*. Elsevier, 121(6), pp. 1348–1353. doi: 10.1053/gast.2001.29611.

Pourteimoor, V., Mohammadi-Yeganeh, S. and Paryan, M. (2016) 'Breast cancer classification and prognostication through diverse systems along with recent emerging findings in this respect; the dawn of new perspectives in the clinical applications', *Tumor Biology*. Springer Netherlands, pp. 14479–14499. doi: 10.1007/s13277-016-5349-7.

Van Poznak, C. *et al.* (2006a) 'Expression of osteoprotegerin (OPG), TNF related apoptosis inducing ligand (TRAIL), and receptor activator of nuclear factor κB ligand (RANKL) in human breast tumours', *Journal of Clinical Pathology*. BMJ Publishing Group, 59(1), pp. 56–63. doi: 10.1136/jcp.2005.026534.

Van Poznak, C. *et al.* (2006b) 'Expression of osteoprotegerin (OPG), TNF related apoptosis inducing ligand (TRAIL), and receptor activator of nuclear factor κB ligand (RANKL) in human breast tumours', *Journal of Clinical Pathology*. BMJ Publishing Group, 59(1), pp. 56–63. doi: 10.1136/jcp.2005.026534.

Prat, A. *et al.* (2010) 'Phenotypic and molecular characterization of the claudin-low intrinsic subtype of breast cancer', *Breast Cancer Research*. Breast Cancer Res, 12(5). doi: 10.1186/bcr2635.

Prat, A. *et al.* (2015) 'Clinical implications of the intrinsic molecular subtypes of breast cancer', *Breast*. Churchill Livingstone, 24, pp. S26–S35. doi: 10.1016/j.breast.2015.07.008.

Prat, A. and Perou, C. M. (2011) 'Deconstructing the molecular portraits of breast cancer', *Molecular Oncology*. John Wiley and Sons Ltd, pp. 5–23. doi: 10.1016/j.molonc.2010.11.003.

Prosigna Breast Cancer Prognostic Gene Signature Assay | Breastcancer.org (no date). Available at: <https://www.breastcancer.org/symptoms/testing/types/prosigna> (Accessed: 30 December 2021).

Qian, B. Z. and Pollard, J. W. (2010) 'Macrophage Diversity Enhances Tumor Progression and Metastasis', *Cell*. NIH Public Access, pp. 39–51. doi:

10.1016/j.cell.2010.03.014.

Rachner, T. D. *et al.* (2019) 'Prognostic value of RANKL/OPG serum levels and disseminated tumor cells in nonmetastatic breast cancer', *Clinical Cancer Research*. American Association for Cancer Research Inc., 25(4), pp. 1369–1378. doi: 10.1158/1078-0432.CCR-18-2482.

Radiation Therapy for Breast Cancer Treatment: Types, Side Effects and More (no date). Available at: <https://www.breastcancer.org/treatment/radiation> (Accessed: 3 May 2021).

Rakha, E. A. *et al.* (2008) 'Prognostic significance of nottingham histologic grade in invasive breast carcinoma', *Journal of Clinical Oncology*. J Clin Oncol, 26(19), pp. 3153–3158. doi: 10.1200/JCO.2007.15.5986.

Rao, S. *et al.* (2017) 'RANK rewires energy homeostasis in lung cancer cells and drives primary lung cancer', *Genes and Development*. Cold Spring Harbor Laboratory Press, 31(20), pp. 2099–2111. doi: 10.1101/GAD.304162.117.

Rao, S. *et al.* (2018) 'RANKL and RANK: From Mammalian Physiology to Cancer Treatment', *Trends in Cell Biology*. Elsevier Ltd, pp. 213–223. doi: 10.1016/j.tcb.2017.11.001.

Ravdin, P. M. *et al.* (2007) 'The Decrease in Breast-Cancer Incidence in 2003 in the United States', *New England Journal of Medicine*. New England Journal of Medicine (NEJM/MMS), 356(16), pp. 1670–1674. doi: 10.1056/NEJMs070105.

Renema, N. *et al.* (2016) 'RANK-RANKL signalling in cancer', *Bioscience Reports*. Portland Press Ltd. doi: 10.1042/BSR20160150.

Reyes, M. E. *et al.* (2017) 'Poor prognosis of patients with triple-negative breast cancer can be stratified by RANK and RANKL dual expression', *Breast Cancer Research and Treatment*. Springer New York LLC, 164(1), pp. 57–67. doi: 10.1007/s10549-017-4233-5.

Ricarte, F. R. *et al.* (2018) 'Parathyroid hormone(1–34) and its analogs differentially modulate osteoblastic Rankl expression via PKA/SIK2/SIK3 and PP1/PP2A–CRTC3 signaling', *Journal of Biological Chemistry*. American Society for Biochemistry and Molecular Biology Inc., 293(52), pp. 20200–20213. doi: 10.1074/jbc.RA118.004751.

Roberts, N. A. *et al.* (2012) 'Rank Signaling Links the Development of Invariant $\gamma\delta$ T Cell Progenitors and Aire + Medullary Epithelium', *Immunity*. Immunity, 36(3), pp. 427–437.

doi: 10.1016/j.immuni.2012.01.016.

Rodriguez, J. M. *et al.* (2013) 'APPRIS: Annotation of principal and alternative splice isoforms', *Nucleic Acids Research*. *Nucleic Acids Res*, 41(D1). doi: 10.1093/nar/gks1058.

Rodriguez, J. M. *et al.* (2022) 'APPRIS: Selecting functionally important isoforms', *Nucleic Acids Research*. Oxford University Press, 50(D1), pp. D54–D59. doi: 10.1093/nar/gkab1058.

Rosenberg, L. U. *et al.* (2006) 'Risk factors for hormone receptor-defined breast cancer in postmenopausal women', *Cancer Epidemiology Biomarkers and Prevention*. *Cancer Epidemiol Biomarkers Prev*, 15(12), pp. 2482–2488. doi: 10.1158/1055-9965.EPI-06-0489.

Rossi, S. W. *et al.* (2007) 'RANK signals from CD4+3- inducer cells regulate development of Aire-expressing epithelial cells in the thymic medulla', *Journal of Experimental Medicine*, 204(6), pp. 1267–1272. doi: 10.1084/jem.20062497.

Rossouw, J. E. *et al.* (2002a) 'Risks and benefits of estrogen plus progestin in healthy postmenopausal women: Principal results from the women's health initiative randomized controlled trial', *Journal of the American Medical Association*. *JAMA*, 288(3), pp. 321–333. doi: 10.1001/jama.288.3.321.

Rossouw, J. E. *et al.* (2002b) 'Risks and benefits of estrogen plus progestin in healthy postmenopausal women: Principal results from the women's health initiative randomized controlled trial', *Journal of the American Medical Association*. *JAMA*, 288(3), pp. 321–333. doi: 10.1001/jama.288.3.321.

Ruzinova, M. B., Caron, T. and Rodig, S. J. (2010) 'Altered subcellular localization of c-myc protein identifies aggressive B-cell lymphomas harboring a c-MYC translocation', *American Journal of Surgical Pathology*, 34(6), pp. 882–891. doi: 10.1097/PAS.0B013E3181DB83AF.

Sandra Benítez, A. *et al.* (2021) 'RANK links senescence to stemness in the mammary epithelia, delaying tumor onset but increasing tumor aggressiveness', *Developmental Cell*, 56, pp. 1727-1741.e7. doi: 10.1016/j.devcel.2021.04.022.

Santini, D., Perrone, G., *et al.* (2011) 'Expression pattern of receptor activator of NFκB (RANK) in a series of primary solid tumors and related bone metastases', *Journal of Cellular Physiology*. John Wiley & Sons, Ltd, 226(3), pp. 780–784. doi:

10.1002/JCP.22402.

Santini, D., Schiavon, G., *et al.* (2011) 'Receptor activator of NF- κ B (rank) expression in primary tumors associates with bone metastasis occurrence in breast cancer patients', *PLoS ONE*. PLoS One, 6(4). doi: 10.1371/journal.pone.0019234.

Sanz-Moreno, A. *et al.* (2021) 'RANK signaling increases after anti-HER2 therapy contributing to the emergence of resistance in HER2-positive breast cancer', *Breast Cancer Research*. BioMed Central Ltd, 23(1). doi: 10.1186/s13058-021-01390-2.

Schindelin, J. *et al.* (2012) 'Fiji: An open-source platform for biological-image analysis', *Nature Methods*. Nat Methods, pp. 676–682. doi: 10.1038/nmeth.2019.

Schramek, D. *et al.* (2010a) 'Osteoclast differentiation factor RANKL controls development of progestin-driven mammary cancer', *Nature*. Nature, 468(7320), pp. 98–102. doi: 10.1038/nature09387.

Schramek, D. *et al.* (2010b) 'Osteoclast differentiation factor RANKL controls development of progestin-driven mammary cancer', *Nature*, 468(7320), pp. 98–102. doi: 10.1038/nature09387.

Schramek, D., Sigl, V. and Penninger, J. M. (2011) 'RANKL and RANK in sex hormone-induced breast cancer and breast cancer metastasis', *Trends in Endocrinology and Metabolism*. Elsevier, pp. 188–194. doi: 10.1016/j.tem.2011.02.007.

Schütz, F. *et al.* (2019) 'Update Breast Cancer 2019 Part 4 - Diagnostic and Therapeutic Challenges of New, Personalised Therapies for Patients with Early Breast Cancer', *Geburtshilfe und Frauenheilkunde*. Georg Thieme Verlag, 79(10), pp. 1079–1089. doi: 10.1055/a-1001-9925.

Schwarz, E. M. and Ritchlin, C. T. (2007) 'Clinical development of anti-RANKL therapy', *Arthritis Research and Therapy*. BioMed Central, p. S7. doi: 10.1186/ar2171.

Search of: denosumab | Breast Cancer - List Results - ClinicalTrials.gov. Available at: <https://www.clinicaltrials.gov/ct2/results?cond=Breast+Cancer&term=denosumab&cntry=&state=&city=&dist=>.

Shen, B. *et al.* (2013) 'Generation of gene-modified mice via Cas9/RNA-mediated gene targeting', *Cell Research*. Nature Publishing Group, pp. 720–723. doi: 10.1038/cr.2013.46.

Shoemaker, R. H. (2006) 'The NCI60 human tumour cell line anticancer drug screen', in

Nature Reviews Cancer. Nat Rev Cancer, pp. 813–823. doi: 10.1038/nrc1951.

Shoemaker, R. H., Wolpert-DeFilippes, M. K. and Venditti, J. M. (1984) 'Potentials and drawbacks of the human tumor stem cell assay.', *Behring Institute Mitteilungen*, (74), pp. 262–272. Available at: <https://europepmc.org/article/med/6477356> (Accessed: 24 April 2021).

Shozu, M. *et al.* (2003) 'Estrogen Excess Associated with Novel Gain-of-Function Mutations Affecting the Aromatase Gene', *New England Journal of Medicine*. Massachusetts Medical Society, 348(19), pp. 1855–1865. doi: 10.1056/nejmoa021559.

Shultz, L. D., Ishikawa, F. and Greiner, D. L. (2007) 'Humanized mice in translational biomedical research', *Nature Reviews Immunology*. Nat Rev Immunol, pp. 118–130. doi: 10.1038/nri2017.

Sica, A. and Bronte, V. (2007) 'Altered macrophage differentiation and immune dysfunction in tumor development', *Journal of Clinical Investigation*. American Society for Clinical Investigation, pp. 1155–1166. doi: 10.1172/JCI31422.

Sigl, V. *et al.* (2016) 'RANKL/RANK control Brca1 mutation-driven mammary tumors', *Cell Research*. Nature Publishing Group, 26(7), pp. 761–774. doi: 10.1038/cr.2016.69.

Sigl, V., Jones, L. P. and Penninger, J. M. (2016) 'RANKL/Rank: From bone loss to the prevention of breast cancer', *Open Biology*. Royal Society Publishing. doi: 10.1098/rsob.160230.

Simonet, W. S. *et al.* (1997) 'Osteoprotegerin: A novel secreted protein involved in the regulation of bone density', *Cell*. Cell Press, 89(2), pp. 309–319. doi: 10.1016/S0092-8674(00)80209-3.

Skol, A. D., Sasaki, M. M. and Onel, K. (2016) 'The genetics of breast cancer risk in the post-genome era: Thoughts on study design to move past BRCA and towards clinical relevance', *Breast Cancer Research*. BioMed Central Ltd. doi: 10.1186/s13058-016-0759-4.

Smalley, M. J. (2010) 'Isolation, culture and analysis of mouse mammary epithelial cells.', *Methods in molecular biology (Clifton, N.J.)*. Methods Mol Biol, 633, pp. 139–170. doi: 10.1007/978-1-59745-019-5_11.

Smid, M. *et al.* (2008) 'Subtypes of breast cancer show preferential site of relapse', *Cancer Research*. American Association for Cancer Research, 68(9), pp. 3108–3114.

doi: 10.1158/0008-5472.CAN-07-5644.

Soleja, M., Raj, G. V. and Unni, N. (2019) 'An evaluation of fulvestrant for the treatment of metastatic breast cancer', *Expert opinion on pharmacotherapy*. *Expert Opin Pharmacother*, 20(15), pp. 1819–1829. doi: 10.1080/14656566.2019.1651293.

Sordillo, E. M. and Pearse, R. N. (2003) 'Rank-Fc: A therapeutic antagonist for RANK-L in myeloma', in *Cancer*. John Wiley and Sons Inc., pp. 802–812. doi: 10.1002/cncr.11134.

Sørli, T. *et al.* (2001) 'Gene expression patterns of breast carcinomas distinguish tumor subclasses with clinical implications', *Proceedings of the National Academy of Sciences of the United States of America*, 98(19), pp. 10869–10874. doi: 10.1073/pnas.191367098.

Sørli, T. *et al.* (2003) 'Repeated observation of breast tumor subtypes in independent gene expression data sets', *Proceedings of the National Academy of Sciences of the United States of America*. *Proc Natl Acad Sci U S A*, 100(14), pp. 8418–8423. doi: 10.1073/pnas.0932692100.

Sørli, T. (2004) 'Molecular portraits of breast cancer: Tumour subtypes as distinct disease entities', *European Journal of Cancer*. Elsevier Ltd, 40(18), pp. 2667–2675. doi: 10.1016/j.ejca.2004.08.021.

Streicher, C. *et al.* (2017) 'Estrogen Regulates Bone Turnover by Targeting RANKL Expression in Bone Lining Cells', *Scientific Reports*. Nature Publishing Group, 7(1). doi: 10.1038/s41598-017-06614-0.

Sugiyama, M. *et al.* (2012) 'Expression pattern changes and function of RANKL during mouse lymph node microarchitecture development', *International Immunology*. Oxford University Press, 24(6), pp. 369–378. doi: 10.1093/intimm/dxs002.

Sung, H. *et al.* (2021) 'Global Cancer Statistics 2020: GLOBOCAN Estimates of Incidence and Mortality Worldwide for 36 Cancers in 185 Countries', *CA: A Cancer Journal for Clinicians*. Wiley, 71(3), pp. 209–249. doi: 10.3322/caac.21660.

Surakasula, A., Nagarjunapu, G. C. and Raghavaiah, K. V. (2014) 'A comparative study of pre- and post-menopausal breast cancer: Risk factors, presentation, characteristics and management', *Journal of Research in Pharmacy Practice*. Wolters Kluwer -- Medknow Publications, 3(1), p. 12. doi: 10.4103/2279-042X.132704.

Suzuki, J. *et al.* (2004) 'Regulation of osteoclastogenesis by three human RANKL isoforms expressed in NIH3T3 cells', *Biochemical and Biophysical Research Communications*. Academic Press Inc., 314(4), pp. 1021–1027. doi: 10.1016/j.bbrc.2003.12.191.

Suzuki, J. *et al.* (no date) 'Regulation of osteoclastogenesis by three human RANKL isoforms expressed in NIH3T3 cells'. doi: 10.1016/j.bbrc.2003.12.191.

Szadvari, I., Krizanova, O. and Babula, P. (2016) 'Athymic nude mice as an experimental model for cancer treatment', *Physiological Research*. Czech Academy of Sciences, pp. S441–S453. doi: 10.33549/physiolres.933526.

T, C., Y, L. and A, F. (2019) 'Antiresorptive agents' bone-protective and adjuvant effects in postmenopausal women with early breast cancer', *British journal of clinical pharmacology*. *Br J Clin Pharmacol*, 85(6), pp. 1125–1135. doi: 10.1111/BCP.13834.

Tan, W. *et al.* (2011) 'Tumour-infiltrating regulatory T cells stimulate mammary cancer metastasis through RANKL-RANK signalling', *Nature*, 470(7335), pp. 548–553. doi: 10.1038/nature09707.

Tang, P. and Tse, G. M. (2016) 'Immunohistochemical surrogates for molecular classification of breast carcinoma: A 2015 update', in *Archives of Pathology and Laboratory Medicine*. College of American Pathologists, pp. 806–814. doi: 10.5858/arpa.2015-0133-RA.

Terpos, E. and Dimopoulos, M. A. (2011) 'Interaction between the skeletal and immune systems in cancer: Mechanisms and clinical implications', *Cancer Immunology, Immunotherapy*. *Cancer Immunol Immunother*, pp. 305–317. doi: 10.1007/s00262-011-0974-x.

Theoleyre, S. *et al.* (2004) 'The molecular triad OPG/RANK/RANKL: Involvement in the orchestration of pathophysiological bone remodeling', *Cytokine and Growth Factor Reviews*. *Cytokine Growth Factor Rev*, pp. 457–475. doi: 10.1016/j.cytogfr.2004.06.004.

TransBCR | Clinical Trial - BRCA. Available at: <https://www.transbcr.org.au/brca-d>.

Tsubaki, M. *et al.* (2013) 'Activation of NF- κ B by the RANKL/RANK system up-regulates snail and twist expressions and induces epithelial-to-mesenchymal transition in mammary tumor cell lines', *Journal of Experimental and Clinical Cancer Research*. *BioMed Central*, 32(1), pp. 1–9. doi: 10.1186/1756-9966-32-62/FIGURES/4.

Tsuda, E. *et al.* (1997) 'Isolation of a novel cytokine from human fibroblasts that specifically inhibits osteoclastogenesis', *Biochemical and Biophysical Research Communications*. Academic Press Inc., 234(1), pp. 137–142. doi: 10.1006/bbrc.1997.6603.

Turashvili, G. and Brogi, E. (2017) 'Tumor heterogeneity in breast cancer', *Frontiers in Medicine*. Frontiers Media S.A., p. 227. doi: 10.3389/fmed.2017.00227.

Types of Breast Cancer - National Breast Cancer Foundation. Available at: <https://www.nationalbreastcancer.org/types-of-breast-cancer/>.

V, C. *et al.* (2003) 'Catalytic properties of ADAM19', *The Journal of biological chemistry*. J Biol Chem, 278(25), pp. 22331–22340. doi: 10.1074/JBC.M302781200.

Vidula, N. *et al.* (2017) 'Receptor activator of nuclear factor kappa B (RANK) expression in primary breast cancer correlates with recurrence-free survival and development of bone metastases in I-SPY1 (CALGB 150007/150012; ACRIN 6657)', *Breast Cancer Research and Treatment*. Springer New York LLC, 165(1), pp. 129–138. doi: 10.1007/s10549-017-4318-1.

Visonneau, S. *et al.* (1998) 'Growth characteristics and metastatic properties of human breast cancer xenografts in immunodeficient mice', *American Journal of Pathology*. American Society for Investigative Pathology, 152(5), pp. 1299–1311. Available at: </pmc/articles/PMC1858587/?report=abstract> (Accessed: 24 April 2021).

Voduc, K. D. *et al.* (2010) 'Breast cancer subtypes and the risk of local and regional relapse', *Journal of Clinical Oncology*. J Clin Oncol, 28(10), pp. 1684–1691. doi: 10.1200/JCO.2009.24.9284.

Vuong, D. *et al.* (2014) 'Molecular classification of breast cancer', *Virchows Archiv*. Springer Verlag, pp. 1–14. doi: 10.1007/s00428-014-1593-7.

Wada, T. *et al.* (2005) 'The molecular scaffold Gab2 is a crucial component of RANK signaling and osteoclastogenesis', *Nature Medicine*. Nature Publishing Group, 11(4), pp. 394–399. doi: 10.1038/nm1203.

Wada, T. *et al.* (2006) 'RANKL-RANK signaling in osteoclastogenesis and bone disease.', *Trends in molecular medicine*, 12(1), pp. 17–25. doi: 10.1016/j.molmed.2005.11.007.

Waks, A. G. and Winer, E. P. (2019) 'Breast Cancer Treatment: A Review', *JAMA* -

Journal of the American Medical Association. American Medical Association, pp. 288–300. doi: 10.1001/jama.2018.19323.

Walsh, M. C. *et al.* (2006) 'Osteoimmunology: Interplay between the immune system and bone metabolism', *Annual Review of Immunology*. Annu Rev Immunol, pp. 33–63. doi: 10.1146/annurev.immunol.24.021605.090646.

Walsh, M. C. and Choi, Y. (2003) 'Biology of the TRANCE axis', *Cytokine & Growth Factor Reviews*. Elsevier BV, 14(3–4), pp. 251–263. doi: 10.1016/S1359-6101(03)00027-3.

Wang, D. Y. *et al.* (2019) 'Molecular stratification within triple-negative breast cancer subtypes', *Scientific Reports*. Nature Research, 9(1), pp. 1–10. doi: 10.1038/s41598-019-55710-w.

Wang, J. *et al.* (2013) 'Comment on "Progesterone/RANKL is a major regulatory axis in the human breast"', *Science Translational Medicine*, 5(215), p. 215le4. doi: 10.1126/scitranslmed.3006883.

Weigel, M. T. and Dowsett, M. (2010) 'Current and emerging biomarkers in breast cancer: Prognosis and prediction', *Endocrine-Related Cancer*. Society for Endocrinology, pp. R245–R262. doi: 10.1677/ERC-10-0136.

Weinberg, R. A. (1985) 'The action of oncogenes in the cytoplasm and nucleus', *Science*, 230(4727), pp. 770–776. doi: 10.1126/SCIENCE.2997917.

Weinstein, J. N. (2012) 'Drug discovery: Cell lines battle cancer', *Nature*. Nature Publishing Group, pp. 544–545. doi: 10.1038/483544a.

Weischer, M. *et al.* (2012) 'CHEK2*1100delC heterozygosity in women with breast cancer associated with early death, breast cancer-specific death, and increased risk of a second breast cancer', *Journal of Clinical Oncology*. J Clin Oncol, 30(35), pp. 4308–4316. doi: 10.1200/JCO.2012.42.7336.

Weitzmann, M. N. (2013) 'The Role of Inflammatory Cytokines, the RANKL/OPG Axis, and the Immunoskeletal Interface in Physiological Bone Turnover and Osteoporosis', *Scientifica*. Scientifica (Cairo), 2013, pp. 1–29. doi: 10.1155/2013/125705.

What is Immunotherapy - Cancer Research Institute (CRI). Available at: <https://www.cancerresearch.org/immunotherapy/what-is-immunotherapy>.

White, A. J. *et al.* (2014) 'An Essential Role for Medullary Thymic Epithelial Cells during

the Intrathymic Development of Invariant NKT Cells', *The Journal of Immunology*. The American Association of Immunologists, 192(6), pp. 2659–2666. doi: 10.4049/jimmunol.1303057.

Wiley, S. R. *et al.* (1995) 'Identification and characterization of a new member of the TNF family that induces apoptosis', *Immunity*. Immunity, 3(6), pp. 673–682. doi: 10.1016/1074-7613(95)90057-8.

Wong, B. R., Josien, R., *et al.* (1997) 'TRANCE (Tumor necrosis factor [TNF]-related Activation-induced Cytokine), a new TNF family member predominantly expressed in T cells, is a dendritic cell-specific survival factor', *Journal of Experimental Medicine*. J Exp Med, 186(12), pp. 2075–2080. doi: 10.1084/jem.186.12.2075.

Wong, B. R., Rho, J., *et al.* (1997) 'TRANCE is a novel ligand of the tumor necrosis factor receptor family that activates c-Jun N-terminal kinase in T cells', *Journal of Biological Chemistry*. American Society for Biochemistry and Molecular Biology, 272(40), pp. 25190–25194. doi: 10.1074/jbc.272.40.25190.

Wong, B. R. *et al.* (1998) 'The TRAF family of signal transducers mediates NF- κ B activation by the TRANCE receptor', *Journal of Biological Chemistry*. J Biol Chem, 273(43), pp. 28355–28359. doi: 10.1074/jbc.273.43.28355.

Wong, B. R. *et al.* (1999) 'TRANCE, a TNF family member, activates Akt/PKB through a signaling complex involving TRAF6 and c-Src', *Molecular Cell*. Cell Press, 4(6), pp. 1041–1049. doi: 10.1016/S1097-2765(00)80232-4.

Wright, H. L. *et al.* (2009) 'RANK, RANKL and osteoprotegerin in bone biology and disease'. doi: 10.1007/s12178-009-9046-7.

Wu, Q. *et al.* (2017) 'Breast cancer subtypes predict the preferential site of distant metastases: a SEER based study', *Oncotarget*, 8(17), pp. 27990–27996. Available at: www.impactjournals.com/oncotarget/.

Wu, S. G. *et al.* (2016) 'Patterns of distant metastasis in Chinese women according to breast cancer subtypes', *Oncotarget*. Oncotarget, 7(30), pp. 47975–47984. doi: 10.18632/ONCOTARGET.10099.

Wu, Y. and Zhou, B. P. (2010) 'TNF- α /NF- κ B/Snail pathway in cancer cell migration and invasion', *British Journal of Cancer* 2010 102:4. Nature Publishing Group, 102(4), pp. 639–644. doi: 10.1038/sj.bjc.6605530.

- Yamada, T. *et al.* (2011) 'RANKL Expression Specifically Observed in Vivo Promotes Epithelial Mesenchymal Transition and Tumor Progression', *The American Journal of Pathology*. American Society for Investigative Pathology, 178(6), p. 2845. doi: 10.1016/J.AJPATH.2011.02.003.
- Yang, S. and Li, Y. P. (2007) 'RGS10-null mutation impairs osteoclast differentiation resulting from the loss of [Ca²⁺]_i oscillation regulation', *Genes and Development*. Genes Dev, 21(14), pp. 1803–1816. doi: 10.1101/gad.1544107.
- Yang, X. *et al.* (2018) 'Rnf126 as a biomarker of a poor prognosis in invasive breast cancer and chek1 inhibitor efficacy in breast cancer cells', *Clinical Cancer Research*. American Association for Cancer Research Inc., 24(7), pp. 1629–1643. doi: 10.1158/1078-0432.CCR-17-2242.
- Yang, X. and Lippman, M. E. (1999) 'BRCA1 and BRCA2 in breast cancer', *Breast Cancer Research and Treatment*. Breast Cancer Res Treat, pp. 1–10. doi: 10.1023/A:1006189906896.
- Yao, S. *et al.* (2017) 'Bone remodeling and regulating biomarkers in women at the time of breast cancer diagnosis', *Breast Cancer Research and Treatment*. Springer New York LLC, 161(3), pp. 501–513. doi: 10.1007/s10549-016-4068-5.
- Yasuda, H. *et al.* (1998) 'Osteoclast differentiation factor is a ligand for osteoprotegerin/osteoclastogenesis-inhibitory factor and is identical to TRANCE/RANKL', *Proceedings of the National Academy of Sciences of the United States of America*. National Academy of Sciences, 95(7), pp. 3597–3602. doi: 10.1073/pnas.95.7.3597.
- Yersal, O. and Barutca, S. (2014) 'Biological subtypes of breast cancer: Prognostic and therapeutic implications', *World Journal of Clinical Oncology*. Baishideng Publishing Group Co., Limited, pp. 412–424. doi: 10.5306/wjco.v5.i3.412.
- Yi, T. *et al.* (2008) 'Epidermal growth factor receptor regulates osteoclast differentiation and survival through cross-talking with RANK signaling', *Journal of Cellular Physiology*. J Cell Physiol, 217(2), pp. 409–422. doi: 10.1002/jcp.21511.
- Yi, Z. *et al.* (2020) 'Clinical spectrum and prognostic value of TP53 mutations in circulating tumor DNA from breast cancer patients in China', *Cancer Communications*. John Wiley and Sons Inc., 40(6), pp. 260–269. doi: 10.1002/cac2.12032.
- Yin, L. *et al.* (2020) 'Triple-negative breast cancer molecular subtyping and treatment

progress', *Breast Cancer Research*. BioMed Central Ltd. doi: 10.1186/s13058-020-01296-5.

Yiu, S. *et al.* (2014) 'Lessons from patient-derived xenografts for better in vitro modeling of human cancer ☆ , ☆☆☆'. doi: 10.1016/j.addr.2014.09.009.

Yoldi, G. *et al.* (2016) 'RANK signaling blockade reduces breast cancer recurrence by inducing tumor cell differentiation', *Cancer Research*. American Association for Cancer Research Inc., 76(19), pp. 5857–5869. doi: 10.1158/0008-5472.CAN-15-2745.

Yoshida, H. *et al.* (2002) 'Different Cytokines Induce Surface Lymphotoxin- $\alpha\beta$ on IL-7 Receptor- α Cells that Differentially Engender Lymph Nodes and Peyer's Patches', *Immunity*. Cell Press, 17(6), pp. 823–833. doi: 10.1016/S1074-7613(02)00479-X.

Youlden, D. R. *et al.* (2012) 'The descriptive epidemiology of female breast cancer: An international comparison of screening, incidence, survival and mortality', *Cancer Epidemiology*. *Cancer Epidemiol*, pp. 237–248. doi: 10.1016/j.canep.2012.02.007.

Zhang, L. *et al.* (2012) 'Receptor activator for nuclear factor κ B expression predicts poor prognosis in breast cancer patients with bone metastasis but not in patients with visceral metastasis', *Journal of Clinical Pathology*. BMJ Publishing Group, 65(1), pp. 36–40. doi: 10.1136/JCLINPATH-2011-200312.

Zhang, X. and Lewis, M. T. (2013) 'Establishment of Patient-Derived Xenograft (PDX) Models of Human Breast Cancer', *Current Protocols in Mouse Biology*. Wiley, 3(1), pp. 21–29. doi: 10.1002/9780470942390.mo120140.

Zhao, H. *et al.* (2016) 'Aromatase expression and regulation in breast and endometrial cancer', *Journal of Molecular Endocrinology*. BioScientifica Ltd., pp. R19–R33. doi: 10.1530/JME-15-0310.

Zheng, H. *et al.* (2006) 'RANKL stimulates inducible nitric-oxide synthase expression and nitric oxide production in developing osteoclasts: An autocrine negative feedback mechanism triggered by RANKL-induced interferon- β via NF- κ B that restrains osteoclastogenesis and bone resorption', *Journal of Biological Chemistry*. *J Biol Chem*, 281(23), pp. 15809–15820. doi: 10.1074/jbc.M513225200.

LIST OF FIGURES

INTRODUCTION	
Figure 1. Members and classification of the TNFR superfamily.....	33
Figure 2. Human RANKL isoforms	35
Figure 3. Schematic diagram of the RANKL-RANK-induced signaling cascades..	36
Figure 4. Schematic of RANKL reverse signaling activation	38
Figure 5. The mammary gland development stages.....	44
Figure 6. The approvals in clinics for denosumab by FDA.....	48
RESULTS.....	
Figure 1.1. RANK is expressed in tumor and stromal cells of human BC and its expression in tumor cells associates with poor survival in postmenopausal patients	71
Figure 1.2. RANK tumor expression is not associated with survival in ER ⁺ BC.....	72
Figure 1.3. RANK tumor expression is associated with reduced survival in postmenopausal patients with ER ⁻ tumors and poor response to chemotherapy ..	74
Figure 1.4. RANK is expressed and functional in BC PDXs	77
Figure 1.5. RANK signaling regulates tumor cell proliferation, stemness, and chemotherapy response in BC PDXs	79
Figure 1.6. RANK signaling regulates proliferation, stemness, adhesion metabolism, and immunity in BC PDXs	81
Supplementary figure 1.1. Tumor tmRANKL expression is not associated with clinic-pathological factors in human breast adenocarcinomas	84
Supplementary figure 1.2. RANK tumor expression is not related to any clinic-pathologic factor and RANKL associates with younger patients in ER ⁺ BC	86
Supplementary figure 1.3. RANK or RANKL tumor expression are not related to any clinic-pathologic factor in ER ⁻ BC but RANK associates with poor response to chemotherapy including taxanes	87
Supplementary figure 1.4. Distinct biology of RANK signaling according to ER expression and menopausal status	89
Supplementary figure 1.5. RANK signaling is active in a subset of BC PDXs.....	91
Supplementary figure 1.6. Modulation of RANK signaling in BC PDXs.....	93

Supplementary figure 1.7. RANK inhibition regulates proliferation and oncogenic pathways mainly in BC PDXs.....	95
Figure 2.1. icRANKL is expressed in human BC and its expression in tumor cells associates with ER ⁻ subtype	99
Figure 2.2. From non-canonical RANKL isoforms, only RANKL3 is conserved in mammals, birds, and reptiles	101
Figure 2.3. RANKL3 is trapped in the intracellular compartment	103
Figure 2.4. Characterization of RANKL-OE human cell lines	105
Figure 2.5. RANKL overexpression in BC cells does not regulate proliferation <i>in vitro</i>	106
Figure 2.6. Human RL1- and RL3-OE MDA-MB-468 tumors led to tumor development in nude mice	107
Figure 2.7. RANKL1 and RANKL3 overexpression in KPL1 cells triggered earlier tumor onset	107
Figure 2.8. Human RL1-OE aKPL1 tumors showed a shorter tumor onset	108
Figure 2.9. RL1-OE aKPL1 tumors show higher TAMs infiltration	109
Figure 2.10. DNS treatment attenuated the growth of RL1-OE tumors implanted in nude mice	110
Figure 2.11. DNS treatment decreased the infiltration of TAMs in RL1-OE aKPL1 tumors	112
Figure 2.12. RANKL inhibitors attenuated the growth of HCI-001 tumors.....	113
Figure 2.13. The overexpression of Rankl1 did not increase the growth of E0771 cells <i>in vitro</i>	115
Figure 2.14. RL1-OE E0771 tumors showed a shorter latency and faster tumor growth in immune-deficient and immune-competent mice	117
Figure 2.15. Constitutive genetic RANK deletion contributed to the initiation of RL1-OE E0771 tumors	118
Figure 2.16. RL1-OE E0771 tumors promoted shorter tumor onset and faster growth than control tumors in RANK ^{LysMΔ/Δ} mice.....	119
Figure 2.17. Pharmacological systemic inhibition of RANKL reduced the aggressiveness of RL1-OE E0771 tumors	120
Figure 2.18. Expression profile in RL1- and RL3-OE human cell lines	123

Figure 2.19. Expression profile in RL1-OE murine E0771 cell line 125

LIST OF TABLES

INTRODUCTION	
Table 1. Main subtypes of invasive breast carcinomas.....	20
Table 2. Representative BC genomic tests	26
Table 3. Classification of BC molecular subtypes, prognosis and therapies	26
Table 4. Classification of the chemotherapeutic agents and their mechanism of action.....	30
Table 5. Subgroups of patients enrolled in the D-CARE clinical trial.....	50
METHODS.....	
Table 1. Antibodies employed for flow cytometry	61
Table 2. Human and mouse primers employed for Q-RT-PCR.....	63
Table 3. Primary and secondary antibodies used for western blot.....	64
RESULTS.....	
Supplementary tables chapter 1.....	97
Table 2.1. Survival data of patients (whole cohort) from <i>NPS</i> dataset	128
Table 2.2. Survival data of patients (whole cohort) from <i>METABRIC</i> dataset	129
Table 2.3. Survival data of patients (ER ⁺ cohort) from <i>NPS</i> dataset	130
Table 2.4. Survival data of patients (ER ⁺ cohort) from <i>METABRIC</i> dataset	131
Table 2.5. Survival data of patients (ER ⁻ cohort) from <i>NPS</i> dataset.....	132
Table 2.6. Survival data of patients (ER ⁻ cohort) from <i>METABRIC</i> dataset.....	133
Table 2.7. Survival data of patients from <i>ER-NEGATIVE ONLY</i> dataset	134
Table 2.8. GSEA between RANK-Fc vs. mock treatments in the HCI-001 PDX implanted in NSG hosts.....	135
Table 2.9. Up-regulated and down-regulated genes in a single or shared between different human cell lines.....	137
Table 2.10. Up-regulated and down-regulated pathways in RL1-OE MDA-MB-468 cells (vs. pwpi-OE MDA-MB-468 cells)	138
Table 2.11. Up-regulated and down-regulated pathways in RL3-OE MDA-MB-468 cells (vs. pwpi-OE MDA-MB-468 cells)	139

Table 2.12. Up-regulated and down-regulated pathways in RL1-OE aKPL1 cells (vs. pwpi-OE aKPL1 cells)	140
Table 2.13. Up-regulated and down-regulated pathways in RL3-OE aKPL1 cells (vs. pwpi-OE aKPL1 cells)	141
Table 2.14. Up-regulated and down-regulated pathways in a single or shared between different human cell lines	142
Table 2.15. Up-regulated and down-regulated pathways in RL1-OE aKPL1 cells treated with DNS (vs. RL1-OE aKPL1 cells treated with IgG)	143
Table 2.16. Up-regulated and down-regulated pathways in a single or shared between different cell lines	144

APPENDIX

ARTICLE



<https://doi.org/10.1038/s41467-020-20138-8>

OPEN

Inhibition of RANK signaling in breast cancer induces an anti-tumor immune response orchestrated by CD8⁺ T cells

Clara Gómez-Aleza  et al.[#]

Most breast cancers exhibit low immune infiltration and are unresponsive to immunotherapy. We hypothesized that inhibition of the receptor activator of nuclear factor- κ B (RANK) signaling pathway may enhance immune activation. Here we report that loss of RANK signaling in mouse tumor cells increases leukocytes, lymphocytes, and CD8⁺ T cells, and reduces macrophage and neutrophil infiltration. CD8⁺ T cells mediate the attenuated tumor phenotype observed upon RANK loss, whereas neutrophils, supported by RANK-expressing tumor cells, induce immunosuppression. RANKL inhibition increases the anti-tumor effect of immunotherapies in breast cancer through a tumor cell mediated effect. Comparably, pre-operative single-agent denosumab in premenopausal early-stage breast cancer patients from the Phase-II D-BEYOND clinical trial (NCT01864798) is well tolerated, inhibits RANK pathway and increases tumor infiltrating lymphocytes and CD8⁺ T cells. Higher RANK signaling activation in tumors and serum RANKL levels at baseline predict these immunomodulatory effects. No changes in tumor cell proliferation (primary endpoint) or other secondary endpoints are observed. Overall, our preclinical and clinical findings reveal that tumor cells exploit RANK pathway as a mechanism to evade immune surveillance and support the use of RANK pathway inhibitors to prime luminal breast cancer for immunotherapy.

[#]A list of authors and their affiliations appears at the end of the paper.

Breast cancer (BC) in young women has a unique biology and is associated with poor prognosis. Previous results support a role for the receptor activator of nuclear factor- κ B (RANK) signaling pathway in these tumors¹. RANK pathway plays a crucial role in bone remodeling and mammary gland development^{2,3}, acting as a paracrine mediator of progesterone for the expansion of mammary stem/progenitor cells, and mediates the early steps of progesterone-driven mammary tumorigenesis^{4–7}. Denosumab is a human monoclonal antibody against RANK ligand (RL), approved for the prevention of skeletal morbidity associated with metastatic bone disease and the management of treatment-induced bone loss in early postmenopausal BC. Preclinical data reinforce the potential role of RL inhibitors such as denosumab in BC prevention^{4,5,8,9} and treatment due to its ability to reduce recurrence and metastasis¹⁰. We previously found that RANK loss in the oncogene-driven mammary tumor model MMTV-PyMT (PyMT) significantly reduced tumor incidence and lung metastases¹⁰. Tumor cells lacking RANK showed delayed tumor onset and a reduced ability to initiate tumors and metastasis. Pharmacological inhibition of RL also reduced tumor-initiating ability and led to the lactogenic differentiation of tumor cells¹⁰.

RANK and RL are expressed in a wide variety of immune cells¹¹ and are involved in various immune processes, including lymph node development¹², the activation of dendritic cells, monocytes and T cells, and the establishment of central and peripheral tolerance^{11–19}. Thus, RANK pathway regulates innate and adaptive immune responses, and may promote or suppress immunity, depending on the context.

Tumor cells develop several strategies to evade immune surveillance: reducing infiltration by cytotoxic T lymphocytes or natural killer (NK) cells and increasing recruitment of immunosuppressive cells, such as regulatory T cells (Tregs) and different myeloid populations, such as tumor-associated macrophages (TAMs) and tumor-associated neutrophils (TANs)²⁰. Immune-checkpoint inhibitors (mainly antibodies against cytotoxic T-lymphocyte-associated protein 4 (CTLA4) and programmed cell death protein-1 (PD-1) and its ligand (PD-L1)) have emerged as potent therapies against some solid tumors such as melanoma and advanced non-small cell lung cancer (NSCLC)^{21,22}. Nevertheless, in BC the efficacy of immunotherapy remains limited even after the inclusion of radiotherapy or chemotherapy²³, in particular in the immune “cold” luminal tumors.

Here, exploiting complementary genetic and pharmacological approaches in the PyMT tumor model²⁴, we investigate the effects of RANK pathway inhibition on mammary tumor immune surveillance. RANK and RL expression patterns in PyMT tumors resemble those found in human breast adenocarcinomas, with RANK being expressed in tumor cells and myeloid cells, and RL in tumor-infiltrating lymphocytes (TILs)^{4,10,25,26}. RANK deletion in tumor cells, but not in myeloid cells, leads to an increase in immune, lymphocyte, and CD8⁺ T-lymphocyte infiltration, and a reduction in the infiltration of myeloid cells. TANs and CD8⁺ T lymphocytes modulate the anti-tumor immune response driven by loss of RANK expression in tumor cells. Systemic RL inhibition also increases CD8⁺ T-cell infiltration and reinforces the anti-tumor benefits of checkpoint inhibitors in RANK-positive tumors. Importantly, the immunomodulatory effect of RANK signaling is confirmed in the D-BEYOND (denosumab, a RANK-ligand (RANKL) inhibitor and its Biological Effects in YOUNG premenopausal women Diagnosed with early breast cancer) clinical trial (NCT01864798), a prospective, pre-operative study evaluating denosumab and its biological effects in premenopausal early-stage BC. Two courses of denosumab induce an increase in TILs and CD8⁺ T-cell infiltration. Increased activation of RANK signaling pathway in

the tumors and circulating serum RL at baseline are identified as predictive biomarkers for the denosumab-driven increase in TILs. Together, these results demonstrate the key role of RANK pathway in the tumor-immune crosstalk and support the use of RL inhibitors, such as denosumab, for enhancing the immune response in poorly immunogenic luminal BC.

Results

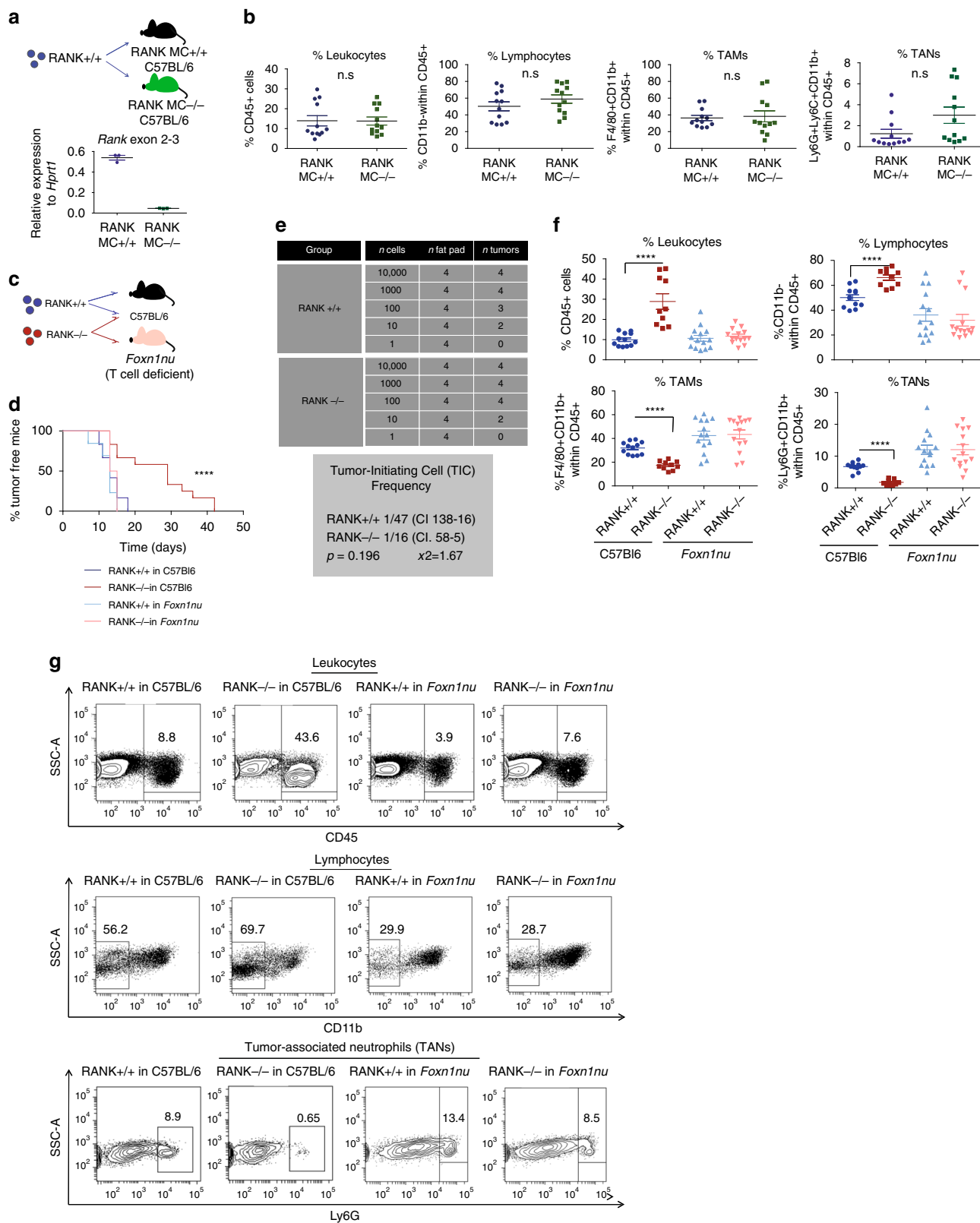
Loss of RANK in tumor cells leads to increased lymphocyte infiltration. We hypothesized that, beyond its tumor cell-intrinsic effects¹⁰, inhibition of RANK signaling pathway may enhance immune activation in BC. To test this hypothesis, we undertook genetic approaches using the PyMT luminal tumor mouse model. First, we tested whether loss of RANK signaling in myeloid cells could induce changes in immune infiltration, by using LysM-cre/RANK^{lox/lox} mice. Expression of Cre driven by LysM deletes RANK in the myeloid compartment (RANK MC^{-/-})²⁷. As expected, lower levels of *Rank* mRNA were found in peritoneal macrophages from RANK MC^{-/-} mice (Fig. 1a). PyMT RANK^{+/+} (RANK^{+/+}) tumors were orthotopically transplanted in RANK MC^{-/-} mice and corresponding controls (RANK MC^{+/+}) (Fig. 1a). Analyses of the tumor immune infiltrates revealed no changes in immune infiltration, leukocytes (CD45⁺), lymphocytes (CD11b⁻ within CD45⁺), TAMs (F4/80⁺CD11b⁺ within CD45⁺), or TANs (Ly6G⁺CD11b⁺ within CD45⁺) between genotypes (Fig. 1b and Supplementary Fig. 1a, b). The frequencies of infiltrating CD8⁺ T cells (CD11b⁻CD3⁺CD8⁺), CD4⁺ T cells (CD11b⁻CD3⁺CD8⁻), and the CD4/CD8 ratio were also similar in RANK^{+/+} tumors growing in RANK MC^{-/-} or RANK MC^{+/+} mice (Supplementary Fig. 1a, b).

We next tested whether RANK loss exclusively in tumor cells could alter tumor immune infiltration: tumors derived from PyMT/RANK^{-/-} mice (RANK^{-/-} tumors) were orthotopically transplanted in syngeneic C57Bl6 mice and compared with RANK^{+/+} tumor transplants. RANK^{-/-} tumors showed greater infiltration by leukocytes, lymphocytes, and CD8⁺ T cells compared with RANK^{+/+} tumors of similar size (Supplementary Fig. 1a, c). Together, these results demonstrate that loss of RANK in tumor cells, but not in myeloid cells, induces an increase in tumor-immune infiltrates, TILs, and CD8⁺ T cells.

T cells mediate the longer tumor latency of RANK^{-/-} tumors.

The increase in TILs observed after loss of RANK in tumor cells, prompted us to investigate the functional contribution of this immune population. To this end, RANK^{+/+} and RANK^{-/-} tumor cells were transplanted in parallel in syngeneic mice and in T-cell-deficient *Fox1^{mu}* mice (Fig. 1c). We had previously demonstrated that, compared with RANK^{+/+}, RANK^{-/-} tumor cells display prolonged latency to tumor formation, increased apoptosis, and a lower frequency of tumor-initiating cells when transplanted in syngeneic mice¹⁰.

Strikingly, when transplanted in T-cell-deficient *Foxn1^{mu}* mice, no differences in latency to tumor onset were observed between RANK^{+/+} and RANK^{-/-} tumor transplants, whereas the same tumors transplanted in syngeneic C57BL/6 mice corroborated previous results (Fig. 1d and Supplementary Fig. 2a)¹⁰. In addition, limiting dilution assays in *Foxn1^{mu}* mice showed no differences in the ability of RANK^{+/+} and RANK^{-/-} tumor cells to initiate tumors (Fig. 1e). Further characterization of the tumors revealed that RANK^{-/-} tumor transplants growing in syngeneic hosts contained more apoptotic and necrotic cells than did their RANK^{+/+} counterparts (Supplementary Fig. 2b), corroborating previous findings¹⁰. However, the frequency of apoptotic cells was similar in RANK^{-/-} and RANK^{+/+} tumor cells growing in



Foxn1^{nu} mice. Differences in late apoptosis/necrosis (7AAD⁺/Annexin V⁺ cells) between RANK^{+/+} and RANK^{-/-} tumor cells were observed in both syngeneic and *Foxn1^{nu}* recipients, but were less marked in T-cell-deficient mice (Supplementary Fig. 2b). These observations suggest that the increased tumor cell death rate in the absence of RANK is due to a combination of tumor

cell-intrinsic and T-cell-mediated effects, whereas T cells are responsible for the delayed tumor onset and the reduced tumor-initiating ability of RANK-null tumor cells.

Analyses of RANK^{+/+} and RANK^{-/-} tumors confirmed the higher frequency of leukocytes and the enrichment in TILs in RANK^{-/-} compared with RANK^{+/+} tumors (Fig. 1f, g and

Fig. 1 Loss of RANK in tumor cells, but not in myeloid cells, leads to increased TIL frequency, and T cells drive the delayed tumor formation and the reduced tumor-initiating ability of RANK-null tumor cells. **a** Top panel: injection scheme showing the implantation of PyMT RANK^{+/+} (RANK^{+/+}) tumors in LysM-Cre RANK^{fl/fl} mice (RANK MC^{-/-}) and WT (RANK MC^{+/+}) (C57BL/6). Bottom panel: *Rank* mRNA expression levels relative to *Hprt1* in peritoneal macrophages of RANK MC^{-/-} and RANK MC^{+/+} mice ($n = 3$). Mean \pm SEM is shown. **b** Graphs showing the percentages of tumor-infiltrating leukocytes (CD45⁺), lymphocytes (CD11b⁻ within CD45⁺), tumor-associated macrophages (TAMs) (F4/80⁺CD11b⁺ within CD45⁺) and tumor-associated neutrophils (TANs) (Ly6G⁺Ly6C⁻CD11b⁺ within CD45⁺) in RANK^{+/+} tumor transplants in RANK MC^{-/-} and RANK MC^{+/+} mice ($n = 12$ tumors). Mean, SEM shown. *t*-test and *p*-values were calculated. **c** Injection scheme showing the implantation of PyMT RANK^{+/+} and PyMT RANK^{-/-} tumors in C57BL/6 WT animals and *Foxn1*^{tmu} mice. **d** Kinetics of palpable tumor onset (left) after tumor transplantation of RANK^{+/+} and RANK^{-/-} tumor cells in syngeneic C57BL/6 ($n = 6$) and *Foxn1*^{tmu} mice ($n = 7$). Log-rank test performed with two-tailed *p*-value (**** $p = 0.005$). One representative experiment out of two is shown. **e** Tumor-initiating frequencies as calculated by ELDA. Cells isolated from RANK^{+/+} and RANK^{-/-} tumors were injected in *Foxn1*^{tmu} mice in limiting dilutions. WEHI's online ELDA-software (<http://bioinf.wehi.edu.au/software/elda/>) was used to calculate the χ^2 -values with 95% confidence interval. **f** Graphs showing the percentages tumor-infiltrating leukocytes (CD45⁺; **** $p < 0.0001$), lymphocytes (CD11b⁻ within CD45⁺; **** $p < 0.0001$), TAMs (F4/80⁺CD11b⁺ within CD45⁺; **** $p < 0.0001$), TANs (Ly6G⁺CD11b⁺ within CD45⁺; **** $p < 0.0001$) in RANK^{+/+} or RANK^{-/-} tumor transplants in syngeneic C57BL/6 and *Foxn1*^{tmu} mice ($n = 12$ RANK^{+/+} tumors, $n = 10$ RANK^{-/-} tumors in C57BL/6 hosts; $n = 14$ RANK^{+/+} or RANK^{-/-} tumors in *Foxn1*^{tmu} hosts). Tumors were analyzed at endpoint (>0.2 cm²). Mean, SEM and *t*-test two-tailed *p*-values are shown. Two representative primary tumors were used in these experiments. **g** Representative dot blots of leukocytes (CD45⁺) gated in live cells (7AAD⁻) and lymphocytes (CD11b⁻) gated on CD45⁺.

Supplementary Fig. 1c). In contrast, the relative frequency of TAMs and TANs was higher in RANK^{+/+} than in RANK^{-/-} tumors (Fig. 1f, g and Supplementary Fig. 1c). These differences were no longer observed in *Foxn1*^{tmu} transplants (Fig. 1f, g).

To rule out the possibility that immune cells transplanted along with tumor cells were responsible for the observed changes, the CD45⁻ population (tumor cell-enriched) was sorted and transplanted into syngeneic hosts. The longer tumor latency observed in RANK^{-/-} was exacerbated when sorted CD45⁻ cells were injected, compared with whole tumor transplants (Supplementary Fig. 2c). Accordingly, differences in immune infiltration were also observed between tumors derived from sorted CD45⁻ RANK^{+/+} and CD45⁻ RANK^{-/-} cells and those derived from whole tumor transplants (Supplementary Fig. 2d).

To confirm that our findings are not affected by differences other than RANK status between RANK^{+/+} and RANK^{-/-} tumors, we infected PyMT/RANK^{fl/fl} tumors with pLVX-Cre-IRES-zsGreen or control lentivirus. Infected tumor populations were fluorescence-activated cell sorting (FACS)-sorted and orthotopically transplanted into C57BL/6 mice. RANK depletion was confirmed by reverse transcription PCR (RT-PCR) and immunohistochemistry (IHC) (Supplementary Fig. 2e). RANK-depleted tumors showed lower tumor growth rate (Supplementary Fig. 2f) and greater infiltration of leukocytes, lymphocytes, and T cells (CD3⁺ CD11b⁻CD45⁺), corroborating previous findings (Supplementary Fig. 2g). CD8⁺ T cells were more abundant and TANs were reduced in RANK-depleted tumors, although the differences were not significant (Supplementary Fig. 2g). Thus, RANK loss in tumor cells leads to a significant increase in TILs.

Together, these results demonstrate that RANK loss in tumor cells leads to a significant increase in TILs that restrict RANK^{-/-} tumor cell growth. Reciprocally, they indicate that RANK expression in tumor cells induces an immunosuppressive microenvironment enriched in TAMs and TANs, allowing tumor cells to escape T-cell immune surveillance.

CD8⁺ T cell depletion rescues the delay in tumor onset of RANK^{-/-} tumors. Further characterization of TIL subsets from syngeneic transplants (Supplementary Fig. 1a), revealed a significant increase in the percentage of CD3⁺ T lymphocytes and CD8⁺ T cells in RANK^{-/-} tumors and a lower CD4⁺/CD8⁺ ratio in RANK^{-/-} compared with the RANK^{+/+} tumors (Fig. 2a). There were no significant differences between the two groups in the frequencies of NK cells (NK1.1⁺ CD3⁻), B cells (CD19⁺ CD3⁻CD11b⁻), or levels of interferon- γ (IFN γ)

production by tumor-infiltrating CD4⁺ and CD8⁺ T cells (Supplementary Fig. 3a). However, TAMs that infiltrated RANK^{-/-} tumors expressed higher levels of IL-12/IL23, indicative of an anti-tumor M1 response (Supplementary Fig. 3a). Increased CD3⁺ T-lymphocyte and CD8⁺ T-cell tumor infiltration in RANK^{-/-} tumors compared with RANK^{+/+} was confirmed by IHC (Fig. 2b, c) and the mRNA levels of the cytotoxicity markers, namely *Irfy* and perforin (*Prf1*) were higher in RANK^{-/-} tumors (Fig. 2d). Gene expression analysis comparing sorted CD45⁻ cells (tumor cell-enriched) isolated from RANK^{+/+} vs. RANK^{-/-} tumor transplants revealed 604 differentially expressed genes (Supplementary Data 1). Gene Ontology (GO) and Generally Applicable Gene Set Enrichment (GAGE) analyses revealed that RANK^{-/-} tumor cells overexpressed a subset of genes related to the “intrinsic apoptotic signaling pathway,” “antigen processing and presentation,” and “positive regulation of T-cell-mediated cytotoxicity” (Supplementary Data 2–4). Similar frequencies of CD3⁺, CD4⁺, and CD8⁺ T cells were found in draining lymph nodes from RANK^{+/+} and RANK^{-/-} tumor transplants, but a moderate increase in IFN γ production in the lymph node T cells was observed in the RANK^{-/-} tumor transplants (Supplementary Fig. 3b).

Next, we investigated the effects on the tumor immune infiltrates after systemic pharmacological inhibition of RL (RANK-Fc treatment 10 mg/kg three times per week, for 4 weeks) in serial tumor transplants from PyMT mice (Supplementary Fig. 3c)¹⁰. No significant changes in the total number of TILs upon RL inhibition were observed (Supplementary Fig. 3d, e). However, after RL inhibition, the frequency of infiltrating CD8⁺ T cells increased (Supplementary Fig. 3d) and CD4⁺ T cells decreased (Supplementary Fig. 3e), leading to a lower CD4⁺/CD8⁺ ratio (Supplementary Fig. 3d, e). An increased infiltration by CD8⁺ T cells in tumors continuously treated with RL inhibitor was also observed by IHC (Fig. 2e, f). Together, these evidences demonstrate that genetic or pharmacologic inhibition of RANK signaling increases CD8⁺ T-cell tumor infiltration.

CD8⁺ T and NK cells have been shown to drive tumor cell cytotoxicity²⁰; therefore, depletion experiments were performed in RANK^{+/+} and RANK^{-/-} tumor transplants to confirm their involvement (Fig. 2g). Depletion of CD8⁺ T cells, but not of NK cells, rescued the delayed tumor formation observed in RANK^{-/-} transplants with minor effects on RANK^{+/+} transplants (Fig. 2h). CD8⁺ T- and NK-cell depletions were corroborated in blood samples and tumor infiltrates (Supplementary Fig. 4a, b). CD8⁺ T-cell depletion resulted in increased NK-cell frequency in tumors and, conversely, NK-cell depletion led to increased CD8⁺ T-cell

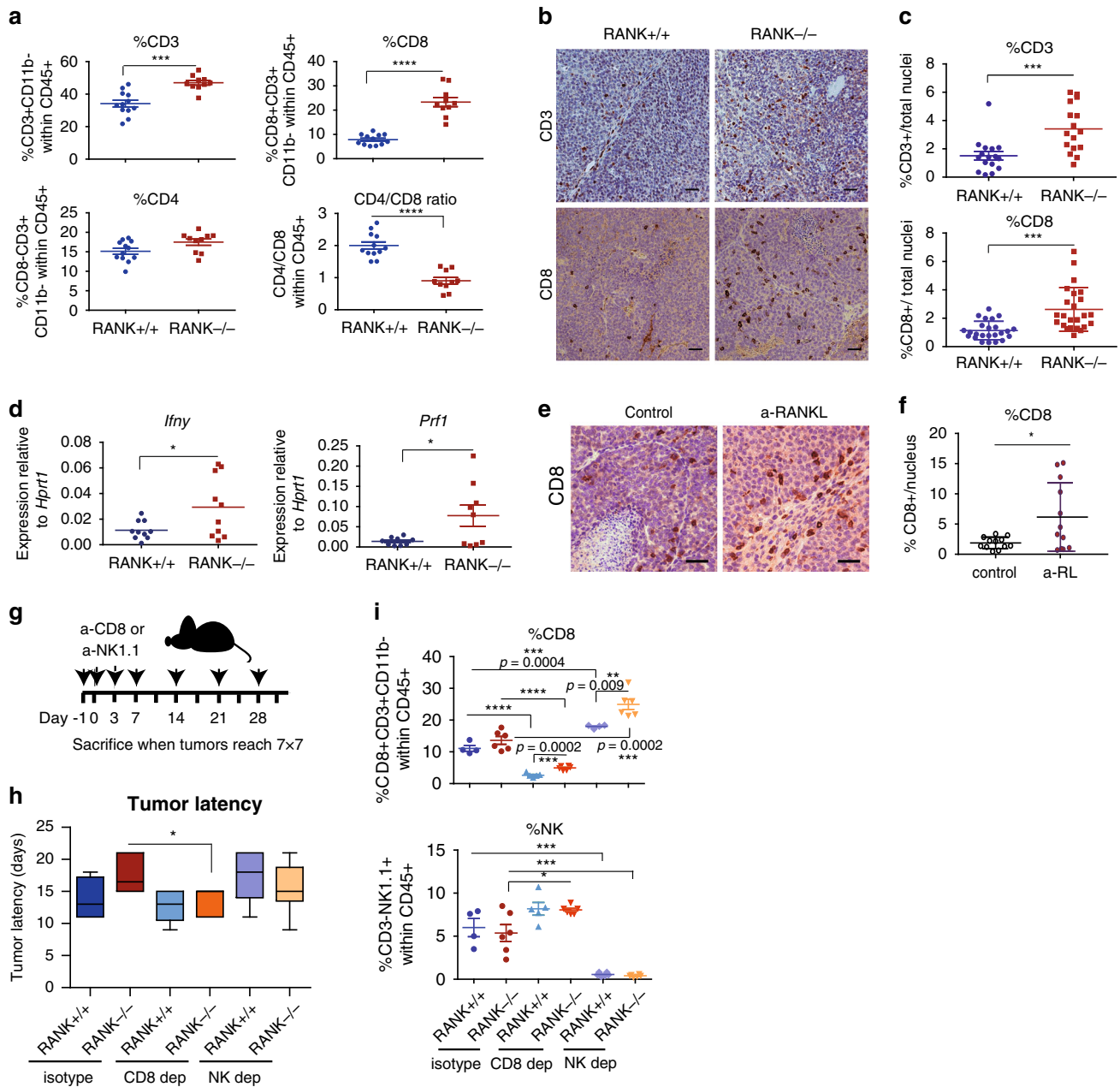


Fig. 2 RANK loss in tumor cells leads to increased CD8⁺ T cell tumor infiltration that mediates the delayed tumor latency of RANK^{-/-} tumors. a Graphs showing the percentage of T cells (CD3+CD11b⁻ within CD45⁺; ****p* = 0.0001), CD8 (CD8+CD3+CD11b⁻ within CD45⁺; *****p* < 0.0001), CD4 (CD8-CD3+CD11b⁻ within CD45⁺; *p* = 0.0503), and the CD4/CD8 ratio (*****p* < 0.0001) in RANK^{+/+} (*n* = 12) or RANK^{-/-} (*n* = 10) tumor cells injected in syngeneic C57BL/6 mice[#]. Representative images (b) and quantification (c) of CD3⁺ (*n* = 4 tumors, ****p* = 0.0009) and CD8⁺ cells (*n* = 6 tumors, ****p* = 0.0001) in RANK^{+/+} and RANK^{-/-} tumor transplants as assessed by IHC. Scale = 25 μm. Tumors derived from three independent primary tumors were used. Each dot represents one picture[#]. **d** *Prf1* and *Ifny* mRNA levels relative to *Hprt1* of whole tumors from RANK^{+/+} and RANK^{-/-} transplants in syngeneic C57BL/6 mice (*n* = 10; *Prf1* **p* = 0.0286, *Ifny* **p* = 0.0360)[#]. **e, f** Representative images (e) and quantification (f) of CD8⁺ cells in RANK^{+/+} control and anti-RANKL-treated tumors from second transplants as assessed by IHC. Scale = 25 μm. Each dot represents one picture (*n* = 12 pictures, *n* = 3 tumors, **p* = 0.0168)[#]. **g** Schematic overview of CD8 (300 μg, clone 53-5.8) and NK1.1 (200 μg, clone PK136) treatments in orthotopic RANK^{+/+} and RANK^{-/-} tumor transplants. Animals were treated i.p. on days -1, 0, 3, and 7 after tumor cell injection and then once per week until the day of killing, when tumors were >0.5 cm². **h** Latency to tumor onset of RANK^{+/+} and RANK^{-/-} tumor cells implanted in syngeneic C57BL/6 animals and treated with anti-CD8 or anti-NK1.1 depletion antibodies (*n* = 6) or corresponding isotype control (*n* = 4 for RANK^{+/+} and *n* = 6 for RANK^{-/-}). Box and whisker plots (box represents the median and the 25th and 75th percentiles, whiskers show the largest and smallest values) and significant t-test two-tailed *p*-values are shown (**p* = 0.05). **i** Graphs showing the percentage of infiltrating CD8 T cells (CD8+CD3+CD11b⁻ within CD45⁺) and NK (NK1.1+CD3⁻ within CD45⁺). Each dot represents one tumor (*n* = 4 control and NK-depleted RANK^{+/+} tumors; *n* = 5 CD8-depleted RANK^{+/+} tumors; and *n* = 6 RANK^{-/-} control, NK- and CD8-depleted tumors)[#]. #Mean, SEM and t-test two-tailed *p*-values are shown (**p* < 0.05; **0.001 < *p* < 0.01; ***0.001 < *p* < 0.0001; *****p* < 0.0001). For **a** and **d**, each dot represents one tumor analyzed at the endpoint (>0.2 cm²). Data for tumor transplants derived from two representative primary tumors in two independent experiments.

infiltration (Fig. 2i). These results suggest that CD8⁺ T cells mediate the anti-tumorigenic response induced by RANK loss in tumor cells, and that the exacerbated T-cell response in RANK^{-/-} tumors is responsible for the delay in tumor formation.

RANK⁺ tumor cells promote immunosuppression through neutrophils. To clarify the intercellular crosstalk involved in the observed phenotypes we cultured three-dimensional (3D) tumor acini from RANK^{+/+} and RANK^{-/-} tumor transplants for 72 h, and measured the levels of cytokines and chemokines in the culture supernatants (Supplementary Data 5). Fewer cytokines/chemokines were more abundant in RANK^{-/-} than in RANK^{+/+} tumor supernatants and included the following: (i) eotaxin 1, which is involved in eosinophil recruitment; (ii) CD40, which enhances T-cell responses; and (iii) B lymphocyte chemoattractant (BLC), which controls B-cell trafficking²⁸ (Fig. 3a). However, no significant differences in the frequencies of eosinophils or B cells were found in RANK^{-/-} as compared to RANK^{+/+} tumor transplants (Supplementary Fig. 3a). In supernatants derived from RANK^{+/+} tumor acini, many cytokines were upregulated including stromal cell-derived factor-1 α , macrophage inflammatory protein-1 α , interleukin (IL)-1 α , stem cell factor, tumor necrosis factor- α , IL-13, macrophage colony-stimulating factor, IL-10, IL-4, IL-17, and IL-1 β (Supplementary Data 5 and Fig. 3a). These various cytokines/chemokines are characteristic of an immunosuppressive microenvironment and have a wide-range of actions, including myeloid cell recruitment²⁸. The mRNA expression levels of *Il-1 β* and *Caspase-4*, which mediates the activation of pre-IL1- β in the inflammasome²⁹, were also higher in RANK^{+/+} tumors, whereas *s100a9*, a gene related to neutrophil stimulation and migration, showed a tendency to increase³⁰ (Fig. 3b). These changes may contribute to the increased infiltration of TANs observed in RANK^{+/+} tumors (Fig. 1f, g and Supplementary Figs. 1c and 2d) and the suppression of T-cell immunity as previously reported^{31,32}. In fact, the percentage of TANs (Ly6G⁺) and that of CD8⁺ T cells were negatively correlated in the mouse tumors (Fig. 3c).

To confirm the crosstalk between RANK activation in BC cells and neutrophils, we adopted an independent experimental approach by modulating RANK expression levels in human BC cells and directly testing in co-culture assays whether this influenced neutrophil survival and activation. MCF7 luminal BC cells that had undetectable RANK expression and were unresponsive to RL stimulation, were infected with RANK-overexpressing vectors (Supplementary Fig. 4c). Conversely, HCC1954 basal-like HER2⁺ cells, which, despite the low levels of RANK expression, are responsive to RL stimulation, were infected with two different short hairpin RNAs to downregulate RANK (Supplementary Fig. 4c). Corresponding changes in RANK expression and downstream targets (*BIRC3*, *ICAM1*, *NFKB2*, and *RELB*) in these BC cells were confirmed by RT-PCR (Supplementary Fig. 4c).

BC cells were stimulated with RL for 1 h before co-culturing with neutrophils isolated from blood of healthy human donors (Supplementary Fig. 4d). MCF7-RANK tumor cells and HCC1954-shSCR cells increased neutrophil survival more than did their corresponding tumor cells lacking RANK (MCF7-GFP and HCC1954 shRANK, respectively) (Supplementary Fig. 4e). Conditioned medium (CM) from BC cells with higher level of RANK expression and activation was enough to increase the survival of neutrophils significantly more than CM from cells with low RANK (Fig. 3d). These neutrophils also presented a more mature/active phenotype based on the increased CD11b levels (Fig. 3e)³³.

Finally, to confirm whether neutrophils are involved in the observed differences in latency between RANK^{+/+} and RANK^{-/-} tumor transplants and the crosstalk with T cells, Ly6G depletion

assays were performed (Fig. 3f). Neutrophil depletion significantly delayed tumor appearance in RANK^{+/+} transplants with no effects in RANK^{-/-} transplants (Fig. 3g). Neutrophil depletion was confirmed in blood samples (Supplementary Fig. 4f, g). The frequency of TANs after depletion was reduced in RANK^{+/+} but not in RANK^{-/-} tumor transplants, in which TAN infiltration was much lower (Fig. 3h). Neutrophil depletion led to a significant increase in TILs, CD4⁺, and CD8⁺ T cells, and to a decrease in the frequency of TAMs infiltrating RANK^{+/+} transplants to levels comparable with those found in RANK^{-/-} transplants (Fig. 3h). A trend to increased levels of total leukocyte infiltration was also observed after neutrophil depletion ($p = 0.06$, Fig. 3h).

Altogether, these results suggest that RANK activation in tumor cells induces an immunosuppressive microenvironment that favors neutrophil survival, thus restricting T-cell immunity.

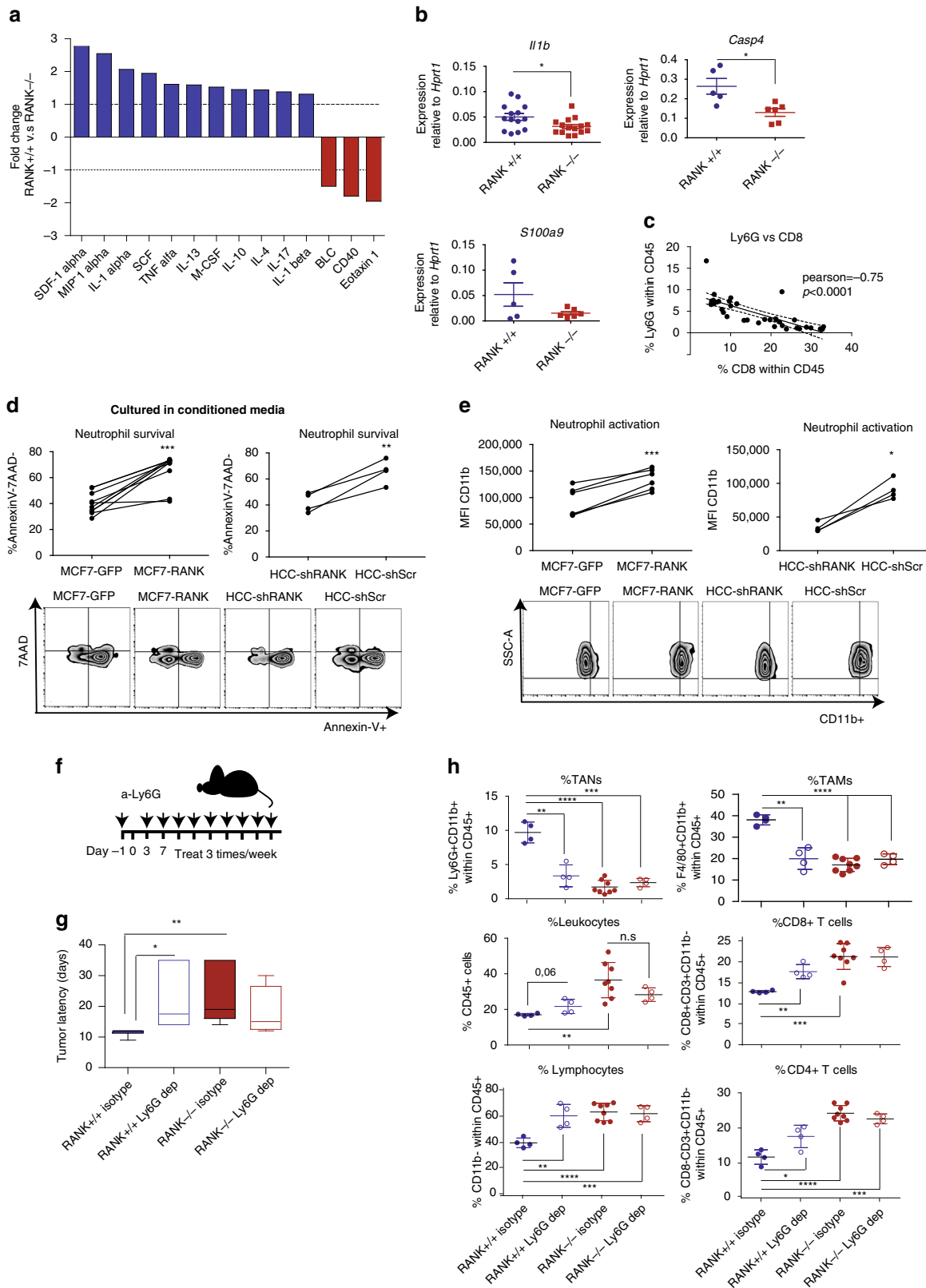
RL inhibition in tumor cells increases responsiveness to immunotherapy. Despite the stronger anti-tumor immune response, RANK^{-/-} tumors eventually evade the immune response and grow. Increased expression of checkpoint regulators such as PD-1 in lymphoid cells and CTLA4 in CD4⁺ T cells was found in RANK^{-/-} relative to RANK^{+/+} tumors (Fig. 4a). The level of PD-L1 expression in RANK^{-/-} tumor cells was also higher than in RANK^{+/+} tumors (Fig. 4a). Tregs (FoxP3⁺ CD25⁺ CD4⁺ CD11b⁻) were more frequent in RANK^{-/-} than in RANK^{+/+} tumors, possibly as a result of the enhanced cytotoxic response, as reported elsewhere³⁴ (Fig. 4a). These results suggest that the exacerbated T-cell response in RANK^{-/-} tumors may facilitate the induction of negative immune-checkpoint regulators and Tregs, evading immune surveillance and allowing tumor growth. This prompted us to investigate the effects of anti-PD-L1 and/or anti-CTLA4 checkpoints inhibitors in combination with the loss of RANK signaling. In RANK^{+/+} tumors early treatment (72 h after tumor implantation) with anti-RL did not affect tumor growth; however, anti-CTLA4 combined with anti-RL reduced tumor growth to a greater extent than did single anti-CTLA4 treatment (28.5% of implanted tumors did not even grow) (Fig. 4b, c). No benefit of combining anti-RL and anti-PD-L1 compared to anti-PD-L1 alone was observed in RANK^{+/+} tumors in the early setting (Fig. 4b, c).

Early treatment with anti-CTLA4, but not with anti-PD-L1 or anti-RL, significantly attenuated RANK^{-/-} tumor growth (66.7% of implanted tumors did not grow) compared with the isotype-treated control (Fig. 4d). Addition of anti-RL did not improve the response to anti-CTLA4 (or anti-PD-L1) in RANK^{-/-} tumors as did in RANK^{+/+} tumors, suggesting that the augmented benefit of the anti-RL/anti-CTLA4 combination was driven by inhibition of RANK signaling in tumor cells (Fig. 4d).

Next, we tested the effect of checkpoint inhibitors on the growth of already palpable, actively growing tumors (Fig. 4e). None of the RANK^{+/+} tumors responded to anti-PD-L1 or anti-RL as single agents but their combination significantly reduced tumor growth in 50% of the tumors (Fig. 4f). Anti-RL did not improve the response to anti-CTLA4 (Fig. 4f). In tumors lacking RANK, anti-PD-L1 treatment was more efficient than anti-CTLA4, but no improvement was observed after the addition of anti-RL (Fig. 4g), in contrast with the observations on RANK^{+/+} tumors.

Collectively, these results demonstrate that in this luminal-like BC, RL inhibition improves the anti-tumor response to anti-CTLA4 (in the early setting) and anti-PD-L1 (for established tumors) through inhibition of RANK signaling in the tumor cells.

A short course of denosumab treatment in early-stage BC increased TILs. To confirm the immunomodulatory role of RANK pathway inhibition in the clinical setting, we analyzed



denosumab-treated BC clinical samples from the D-BEYOND study (NCT01864798): a prospective, pre-operative window-of-opportunity, single-arm, multi-center trial assessing the effect of denosumab in premenopausal women with early-stage BC. Twenty-seven patients were included in this study and received two doses of denosumab 120 mg subcutaneously 1 week apart,

followed by surgery. The median time interval between the first administration of denosumab and surgery was 13 days. No serious adverse events (AEs) were reported. All non-serious AEs are summarized in Supplementary Data 6, the most frequent being arthralgia (4/27 patients, 14.8%). Table 1 summarizes the clinicopathological features of the 24 patients subsequently analyzed.

Fig. 3 Neutrophils recruited by the proinflammatory cytokine/chemokine milieu driven by RANK restrict T-cell immunity. **a** Cytokines/chemokines in the supernatant of RANK^{+/+} and RANK^{-/-} tumor 3D acini cultured during 72 h, expressed as the magnitude of change between RANK^{+/+} and RANK^{-/-} tumor acini (pool of 3 tumors, $n = 1$). See also Supplementary Data 5. **b** *Il1b*, *Casp4*, and *S100a9* mRNA levels relative to *Hprt1* of whole tumors from RANK^{+/+} and RANK^{-/-} transplants in syngeneic C57BL/6 mice ($n = 14$ for *Il1b*, $*p = 0.005$; $n = 5$ RANK^{+/+} tumors, $n = 6$ RANK^{-/-} tumors for *Casp4*, $p = 0.011$; and *S100a9*, $p = 0.12$). Two representative primary tumors of two independent experiments were used[#]. **c** Correlation between the frequency of TANs (Ly6G⁺ Ly6C⁺ CD11b⁺) and CD8⁺ T cells (CD8⁺ CD3⁺ CD11b⁻) infiltrates in tumor transplants. Pearson's correlation coefficients (r) associated probabilities are shown ($p < 0.0001$). **d** Percentage of Annexin V-7AAD⁻ neutrophils ($n = 5$, 2 healthy donors) cultured with conditioned media (CM) from the indicated RL-treated tumor cells. CM was added (1:1) to human neutrophil cultures for 24 h. Paired t -test with one-tailed p -value is shown ($***p = 0.0002$, $**p = 0.009$). **e** Mean fluorescence intensity (MFI) of CD11b⁺ neutrophils ($n = 4$, 2 healthy donors) cultured in CM from the indicated RL-treated tumor cells. CM was added (1:1) to human neutrophils cultures for 24 h. Paired t -test with one-tailed p -value is shown ($***p = 0.0004$, $*p = 0.01$). **f** Schematic overview of TAN (Ly6G⁺) depletion experiments in orthotopic RANK^{+/+} and RANK^{-/-} tumor transplants. Anti-Ly6G (clone 1A8) was administered i.p. before tumor cell injection (400 μ g) and then once per week (100 μ g) until the day of killing. **g** Latency to tumor formation of RANK^{+/+} and RANK^{-/-} tumor cells orthotopically implanted in syngeneic C57BL/6 animals and treated with anti-Ly6G depletion antibody or isotype control ($n = 4$ control and neutrophil-depleted RANK^{+/+} tumors, $n = 8$ control RANK^{-/-} tumors, $n = 4$ neutrophil-depleted RANK^{-/-} tumors). Box and whisker plots (box represents the median and the 25th and 75th percentiles, whiskers show the largest and smallest values) and t -test two-tailed p -values are shown. ($*p = 0.028$; $**p = 0.007$). **h** Graphs showing the percentage of TANs (Ly6G⁺ CD11b⁺, $**p = 0.0012$; $***p = 0.0003$; $****p < 0.0001$), leukocytes (CD45⁺; $**p = 0.034$), lymphocytes (CD11b⁻; $**p = 0.048$; $***p = 0.0008$; $****p < 0.0001$), TAMs (F4/80⁺ CD11b⁺, $**p = 0.0019$; $****p < 0.0001$), CD8⁺ T cells (CD8⁺ CD3⁺ CD11b⁻, $***p = 0.0003$, $**p = 0.0014$), and CD4⁺ T cells (CD8⁻ CD3⁺ CD11b⁻, $*p = 0.0213$, $***p = 0.001$; $****p < 0.0001$) ($n = 4$ control and neutrophil-depleted RANK^{+/+} tumors, $n = 8$ control RANK^{-/-} tumors, $n = 4$ neutrophil-depleted RANK^{-/-} tumors)[#]. #Each dot represents one tumor. Mean, SEM, and t -test two-tailed p -values are shown ($*p < 0.05$; $**p < 0.01$; $***p < 0.001$; $****p < 0.0001$). Tumors of similar size were analyzed at endpoint (>0.2 cm²). For **d**, **e**, each dot represents a technical replicate from healthy donors. Representative dot blots are shown below.

In brief, the median age at diagnosis was 45 years (range, 35–51 years); tumors of 19 patients were hormone receptor positive (79.2%), 4 were HER2⁺ (16.7%), and 1 was triple negative (4.2%). After treatment, serum levels of soluble homotrimeric form of RL (sRL) (unbound to denosumab) and C-terminal telopeptide (CTX), a surrogate marker for denosumab activity, decreased in all patients evaluated ($P < 0.001$, Fig. 5a), confirming the target inhibition. Given its correlation with clinical response in luminal BC^{35–37}, the primary study endpoint was a geometric mean (GM) decrease in the percentage of Ki-67-positive cells. Secondary endpoints included tumor cell survival assessed by cleaved caspase-3, as well as tumor immune infiltration. There was no significant reduction in the percentage of Ki-67-positive cells (GM change from baseline: 1.07, 95% confidence interval (95% CI) 0.87–1.33, $P = 0.485$, Fig. 5a) and no absolute Ki-67 or cleaved caspase-3 responders were identified (Fig. 5a and Supplementary Fig. 5a).

Collectively, these data confirm that a short course of denosumab was associated with effective systemic RL inhibition, but not with a reduction in tumor proliferation or survival.

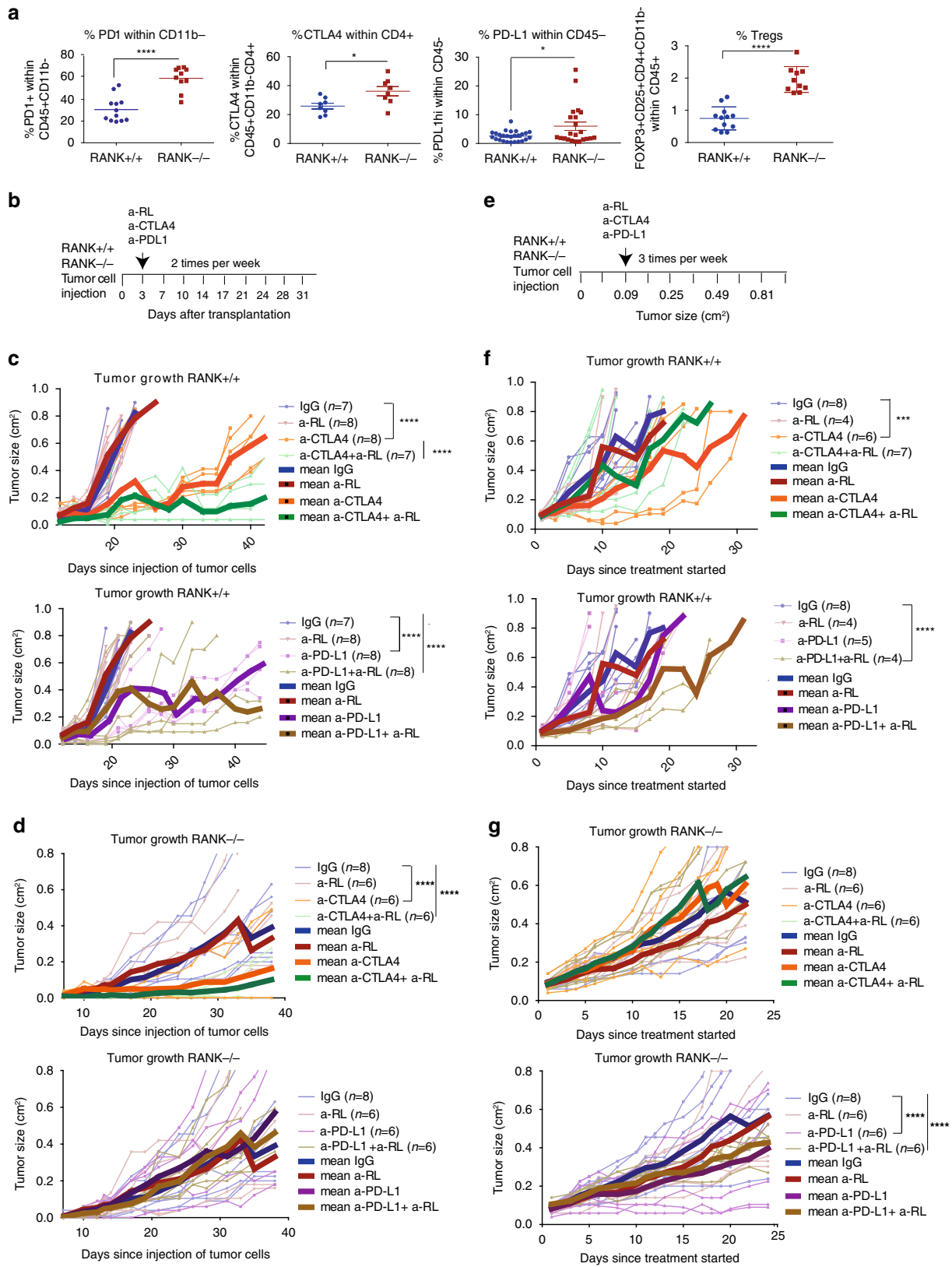
Next, we assessed the effect of denosumab on tumor immune infiltration in 24 available paired samples. Of note, similar to our preclinical model, we observed a significant increase in stromal and intratumoral lymphocyte levels after short exposure to denosumab (GM change from baseline: 1.75, 95% CI 1.28–2.39, $P = 0.006$ and 1.59, 95% CI 1.14–2.21, $P = 0.008$, respectively, Fig. 5b, c and Supplementary Fig. 5a). In particular, 11/24 patients (45.8%), including 6/14 luminal A, 3/5 luminal B, and 2/4 HER2⁺ cases, showed an immunomodulatory response defined as a ≥ 10 percent increase in stromal TILs (sTILs) in tumor samples, and therefore they were considered responders. Analyses of the percentage of Ki-67⁺ TILs suggested a trend to increase after denosumab treatment, particularly in responders (7/11) (Fig. 5b).

The composition of the immune infiltrate associated with denosumab treatment was analyzed by IHC in 23 available pairs of pre- and post-denosumab treatment tumor tissues (Fig. 5b and Supplementary Fig. 5a, b). These analyses revealed a significant increase in the percentage of T (CD3⁺) and B (CD20⁺) cells after denosumab treatment (GM change from baseline: 1.68, 95% CI 1.18–2.40, $P = 0.006$ and 1.62, 95% CI 1.09–2.40, $P = 0.019$, respectively) and increased levels of CD8⁺ T cells, validating our

preclinical observations (GM change from baseline: 1.59, 95% CI 1.14–2.21, $P = 0.008$). Moreover, there was a significant decrease in FOXP3⁺/CD4⁺ Tregs cell frequency (GM change from baseline: 0.63, 95% CI 0.49–0.83, $P = 0.002$, Fig. 5b), even in patients with no increase in TILs. No significant differences in macrophage infiltration (CD68⁺ or CD163⁺) were observed (Fig. 5b and Supplementary Fig. 5a). Intratumoral immune population abundance was also quantified, and an increase of TILs and CD3⁺ T cells was observed (Supplementary Fig. 5a). These findings were illustrated using multiplex IHC of the top four tumors associated with the highest TIL increase (Fig. 5c).

To investigate the biological effect of denosumab in early BC further, we performed RNA sequencing (RNA-seq) on 22 available pre- and posttreatment tumor samples and identified 379 genes that were differentially expressed (Supplementary Data 7). In addition, we performed RNA-seq on 11 available pre- and post-treatment normal mammary samples. Only ten genes were differentially expressed between pre- and posttreatment normal samples (Supplementary Data 8) and all of them were also differentially expressed in the tumor tissue (Supplementary Data 7). Pathway analysis using GO and GAGE in the tumor-derived RNA-seq data revealed the enrichment of several genes related to immune activation, immune cell migration, and cytokine-mediated signaling pathways (Fig. 5d and Supplementary Data 9 and 10). In line with these findings, the expression levels of several chemokines were increased after treatment, including that of the well-known CD8⁺ T-cell chemoattractants CCL4 and CXCL10^{38,39} (Supplementary Fig. 5c). No significant changes in RANK/RL at the protein (IHC) (Supplementary Fig. 5d, e) or at the gene expression levels (RNA-seq) (Supplementary Data 7 and 8) were found. Of note, no differences in genes related to immature mammary epithelial cell (MEC) populations (*ALDH1*) or related to estrogen receptor (ER) pathway (*ESR1*, *PR*, *BCL2*) both in tumor and normal samples, were observed (D-BEYOND secondary endpoints) (Supplementary Data 7 and 8).

To further explore the impact of denosumab treatment on the immune cell landscape of BC we used CIBERSORT⁴⁰, a deconvolution method for inferring immune cell content from gene expression data. Consistent with the IHC results, this analysis confirmed the increase in the relative frequencies of CD8⁺ T cells, B cells, and CD4⁺ T cells, and the decrease in the



frequencies of Tregs after denosumab treatment (Supplementary Fig. 5f). Despite the overall increase in immune infiltration, the relative frequency of macrophage infiltration was reduced after denosumab, particularly in responders (8/11) (Supplementary Fig. 5f), as observed in the mouse models. No significant changes

in NK cells, dendritic cells, mast cells, neutrophils, and eosinophils were noted, because these populations may be too scarce to be captured properly by this method (Supplementary Fig. 5f). Of note, after denosumab treatment, neutrophils correlated negatively with sTILs (Supplementary Fig. 5g), and

Fig. 4 RANKL pharmacological inhibition reinforces anti-CTLA4 and anti-PD-L1 anti-tumor response in RANK^{+/+} but not in RANK^{-/-} tumors. a Graphs showing the percentage of PD-1⁺ cells within CD11b⁻ lymphocytes ($n = 12$ RANK^{+/+} tumors, $n = 10$ RANK^{-/-} tumors; PD-1⁺ within CD11b⁻ CD45⁺; **** $p < 0.0001$), CTLA4 within CD4⁺ T cells ($n = 8$; CTLA4 within CD3⁺ CD8⁻ CD11b⁻ CD45⁺; * $p = 0.0166$), PD-L1 within tumor CD45⁻ cells ($n = 26$ RANK^{+/+} tumors, $n = 22$ RANK^{-/-} tumors; * $p = 0.017$), and Tregs ($n = 12$ RANK^{+/+} tumors, $n = 10$ RANK^{-/-} tumors; FoxP3⁺ CD25⁺ CD4⁺ CD11b⁻ within CD45⁺; **** $p < 0.0001$) in RANK^{+/+} and RANK^{-/-} transplants in syngeneic C57BL/6 mice. Each dot represents an individual tumor transplant derived from two to five different primary tumors. Mean, SEM, and t-test two-tailed p -values are shown (* $p < 0.05$; **** $p < 0.0001$). **b** Experimental scheme for early treatments with anti-RANKL (a-RL), anti-CTLA4, anti-PD-L1, or their respective isotype controls (rat IgG2A and mouse IgG2b). All treatments were administered i.p., two times/week, and started 3 days after injection of RANK^{+/+} and RANK^{-/-} tumor cells into the mammary gland of syngeneic C57BL/6 mice. **c, d** Tumor growth curves for early treatments (scheduled as in Fig. 4b) of RANK^{+/+} (**c**) and RANK^{-/-} (**d**) tumor cells injected in syngeneic C57BL/6. Each thin curve represents one single tumor. Each thick curve represents the mean of all the tumors that received the specific treatment. Linear regression analysis was performed and a two-tailed p -value was calculated to compare the tumor growth slopes after the specified treatments (**** $p < 0.0001$). **e** Experimental scheme for late treatments with anti-RL, anti-CTLA4, anti-PD-L1, or their respective isotype controls (rat IgG2A and mouse IgG2b). All treatments were administered i.p., three times/week, and started when transplanted tumors reached a size of 0.09 cm². **f, g** Tumor growth curves for late treatments (scheduled as in Fig. 4e) of RANK^{+/+} (**f**) and RANK^{-/-} (**g**) tumor cells injected in syngeneic C57BL/6. Each thin curve represents one single tumor. Each thick curve represents the mean of all the tumors that received the specific treatment. Linear regression analysis was performed and a two-tailed p -value was calculated to compare the tumor growth slopes after the specified treatments *** $p = 0.0002$; **** $p < 0.0001$).

Table 1 Clinicopathological features of the 24 evaluable patients.

N		24
Interval surgery-Denosumab	Median days (range)	13 (9–21)
Age	Median years (range)	44 (35–51)
Size	>2 cm	11 (45.8%)
Nodal status	Positive	4 (16.7%)
Histological grade	High	8 (33.3%)
Molecular subtypes	LumA	10 (41.7%)
	LumB	9 (37.5%)
	HER2	4 (16.7%)
	TNBC	1 (4.2%)
Immune response	Percentage of patients	11 (45.8%)

the neutrophil chemotaxis and migration pathways were modulated after denosumab treatment (Supplementary Data 9), supporting the preclinical findings.

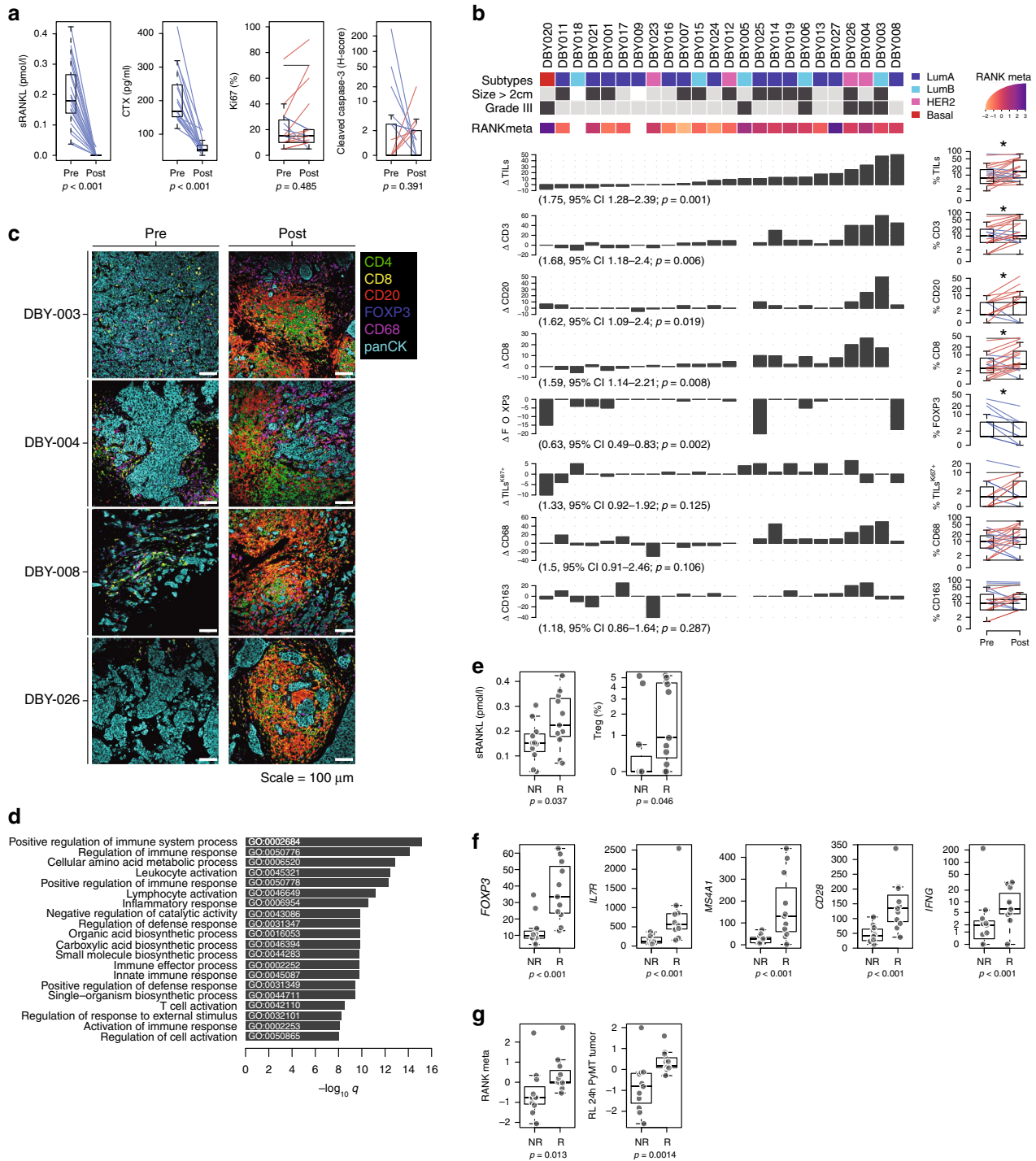
To ensure that these changes are specific to denosumab treatment and not a consequence of the presurgical biopsy procedure, we interrogated the publicly available gene expression data of patients from the control arm (untreated) of the Peri Operative Endocrine Therapy - Individualizing Care (POETIC) study, a large BC window-of-opportunity study evaluating the role of perioperative aromatase inhibitor, for which gene expression data were obtained from presurgical biopsies and surgical specimens. Similar to the D-BEYOND study, biopsies were taken at diagnosis and 2 weeks later, at the time of surgery. The comparison of surgery and biopsy samples from the POETIC study did not reveal any enrichment of immune cells assessed by CIBERSORT or an immune pathway, as assessed by GAGE analyses (Supplementary Fig. 5h and Supplementary Data 11). Together, our results indicate that a short course of denosumab enhances immune infiltration as determined by the increased levels of TILs, B and T lymphocytes, and CD4⁺ and CD8⁺ T cells in luminal and HER2⁺ breast tumors, validating the clinical relevance of the findings in the preclinical models.

RANK pathway activation in tumors and circulating sRL levels predict denosumab's immune effect. Finally, we investigated the baseline features associated with the immunomodulatory effect of denosumab. We identified 11 responder (R) cases, defined by a $\geq 10\%$ increase in TIL infiltration after denosumab treatment and 13 non-responder (NR) cases. No associations were found between any baseline clinicopathological features and the

immune modulation induced by denosumab (Supplementary Data 12). Of the characteristics compared between R and NR patients, high sRL serum levels, a high percentage of Tregs measured by CIBERSORT, and the presence of intratumoral FOXP3⁺ cells measured by IHC, were significantly associated with increased TIL infiltration after denosumab treatment (Fig. 5e and Supplementary Data 12). CD20 IHC staining at baseline was also associated with response, but this finding was not corroborated by CIBERSORT (Supplementary Data 12). A differential gene expression analysis using RNA-seq data from biopsy samples evidenced 42 genes expressed at higher levels in R than in NR, including *FOXP3*, *IL7R*, *MS4A1* (CD20), *CD28*, and *IFNG* (Fig. 5f and Supplementary Data 13), and the enrichment of genes involved in lymphocyte activation and immunoglobulin production in R patients (Supplementary Data 14), which may be indicative of an enhanced immune response.

RANK and RL expression determined by IHC was not predictive of the immunomodulatory effects of denosumab (Supplementary Fig. 6a). However, as it has been reported that RANK IHC is an unreliable tool to detect RANK protein on breast tumor samples⁴¹, we computed RANK and RL metagenes to increase the potency and reliability of RANK and RL detection. These metagenes included the expression levels of the top 100 genes that are co-expressed at baseline with RANK and RANKL mRNA, respectively (see “Methods” and Supplementary Data 15). Importantly, high expression level of RANK metagene in the tumors at baseline (Fig. 5g), but neither RL metagene nor individual gene expression of RANK or RANKL, is predictive of denosumab-induced immune response (Supplementary Fig. 6b).

GO analyses showed that the RANK metagene includes genes associated with nuclear factor- κ B (NF- κ B) pathway activation, as well as with immune response (Supplementary Fig. 6c). Indeed, the RANK metagene strongly correlated with several public signatures of the RANK and NF- κ B pathways, as well as with RL-induced genes in mouse MECs (wild type (WT) and Rank overexpressing) and PyMT tumor cells (Supplementary Fig. 6d and Supplementary Data 16). These results demonstrate that RANK metagene captures RANK pathway activation and support the relevance of the PyMT model. Accordingly, tumors responding to denosumab presented at baseline higher scores for these RL-driven genes in mouse MECs and PyMT tumor cells (Fig. 5g and Supplementary Fig. 6e), and RANK and NF- κ B pathway gene signatures (Supplementary Fig. 6f). Thus, tumors with increased RANK pathway activation at baseline are more likely to show increased TILs after RL inhibition, corroborating the preclinical findings: inhibition of RANK signaling in tumor cells contributes to the immunomodulatory effect of denosumab in BC.



Together, these results indicate that higher RANK pathway activation, soluble RL, and the presence of Tregs at baseline are predictive biomarkers of the immunomodulatory response induced by denosumab in BC patients.

Discussion

Several studies have shown the prognostic and predictive value of TILs, especially in HER2⁺ and triple-negative BC^{42,43}. However, TILs continue to be infrequent in most luminal breast tumors. The identification of a therapy that could convert immune “cold” tumors into “hot” ones would represent a major step towards the development of immune-related therapies. Based on our clinical

and preclinical findings, denosumab appears to be just this type of promising therapeutic agent. This question is particularly relevant for luminal BC, which is poorly infiltrated and insensitive to immunotherapies.

The results of the D-BEYOND clinical trial provide strong evidence of the immunomodulatory effect of denosumab in luminal early BC and identify predictive biomarkers of response. The mouse genetic studies demonstrate that inhibition of RANK signaling in the tumor cells increases TILs and CD8⁺ T-cell infiltration, and attenuates tumor growth. Mechanistically we found that activation of RANK signaling in tumor cells induces a proinflammatory microenvironment that favors survival of TANs and restricts T-cell anti-tumor response.

Fig. 5 The immunomodulatory role of anti-RANKL in BC. **a** Change from baseline in serum levels of free-sRANKL ($n = 23$, $p = 2.384e-07$) and CTX ($n = 17$, $p = 1.526e-05$) (significance assessed by the two-tailed sign test), the percentage of Ki-67-positive cells ($p = 0.485$) and the staining of activated caspase-3 ($p = 0.391$) (H-score) ($n = 24$) (significance assessed by two-tailed paired t -tests). Boxplots display median line, IQR boxes, $1.5 \times$ IQR whiskers, and data points. **b** Each bar plot shows the change from baseline (Δ ; post- minus pretreatment values) of the immune parameters assessed using HE (TILs) and IHC (CD3, CD20, CD8, FOXP3, proliferative TILs (TILs^{Ki67+}), CD68, and CD163). Each bar represents one patient, which are ranked by their increase in stromal TIL levels. Geometric mean changes, 95% CIs, and p -values are shown below each bar plot. For each measured parameter, the corresponding boxplot is displayed on the right-hand side. Boxplots display median line, IQR boxes, $1.5 \times$ IQR whiskers, and data points. Tumor characteristics and tumor RANK metagene expression at baseline are shown above. p ; p -values derived from two-tailed paired t -tests ($*p < 0.05$)[#]. **c** Representative micrographs of multiplex IHC of pre- and posttreatment tumor sections from the four patients with the highest immunomodulatory response. White scale bar, 100 μ m. **d** Top 20 significantly enriched pathways after denosumab treatment, identified by GAGE. **e** Comparison of baseline serum levels of sRANKL between non-responders (NR; $n = 13$) vs. responders (R; $n = 11$) and comparison of baseline percentage of regulatory T cells (Tregs) as inferred from CIBERSORT. Boxplots display median line, IQR boxes, $1.5 \times$ IQR whiskers, and data points. Significance determined by the two-tailed Mann-Whitney U -test. **f** Comparison of baseline mRNA expression levels of indicated genes (normalized counts) between non-responder (NR; $n = 11$) and responder (R; $n = 11$) groups. Boxplots display median line, IQR boxes, $1.5 \times$ IQR whiskers, and data points. Significance determined by the two-tailed Mann-Whitney U -test. p -values: *FOXP3* ($p = 1.61e - 05$), *IL7R* ($p = 1.53e - 07$), *MS4A1* ($p = 1.00E - 06$), *CD28* ($p = 5.63e - 06$), *IFNG* ($p = 4.15e - 05$). **g** Comparison of baseline RANK metagene and RANKL-treated PyMT tumor acini-derived gene signature between non-responder (NR; $n = 11$) and responder (R; $n = 11$) patients. Significance determined by the two-tailed Mann-Whitney U -test. For **a**, **b**: each colored line represents one patient and indicates increase (red), decrease (blue), or no change (black) relative to baseline. Note that all variables were analyzed for all patients, but values for some lines overlap or the indicated population was not detected. Boxplots display median line, IQR boxes, $1.5 \times$ IQR whiskers, and data points. [#]Responder patients are those with $\geq 10\%$ increase in TIL infiltration after denosumab treatment. Significance determined by the two-tailed Mann-Whitney U -test.

The strength of our work resides in the fact that two independent studies, a clinical trial and preclinical research on tumor-prone mouse models, equally conclude that the inhibition of RANK signaling increases the anti-tumor immune response and set the basis for additional trials combining denosumab with immunotherapy in presumably immune “cold” luminal BC.

Although the clinical trial primary efficacy endpoint was not met, as tumor cell proliferation was not reduced, a short course of denosumab did induce an increase in the levels of TILs, T and B cells, and CD8⁺ T-cell infiltration. In contrast with the increased levels of T cells and CD8⁺ T cells, which were associated with enhanced TIL infiltration, the reduction of Tregs was observed equally in R and NR cases, indicating that it may be driven by additional systemic effects of denosumab, rather than by the loss of RANK signaling in the tumor cells, as suggested by the different results seen in RANK^{-/-} tumors.

Importantly, preclinical genetic mouse approaches evidence that the main immunomodulatory changes induced by denosumab in D-BEYOND—increased in TILs and CD8⁺ T cells—are replicated when RANK is lost specifically in the tumor compartment. In addition, they add functional relevance to the changes in immune infiltration, as T lymphocytes and CD8⁺ T cells are responsible for the delayed tumor onset and reduction of tumor-initiating ability observed in RANK-null tumors. In contrast, RANK loss in myeloid cells does not change the tumor immune infiltration. In the PyMT mouse model, the frequency CD8⁺ T cells also increases after systemic anti-RL treatment and the CD4/CD8 ratio was reduced, but no differences in total leukocyte or lymphocyte infiltration were observed. Differences with the D-BEYOND results might be due to drug-specific aspects, treatment schedule, or tumor divergences.

RANK expression in tumor cells led to a significant increase in the levels of several cytokines and chemokines involved in macrophage and neutrophil recruitment and polarization^{28,44,45}, in line with the increased infiltration of TAMs and TANs in RANK^{+/+} tumors. Indeed, we found that RANK-expressing human BC cells promote survival of inflammatory neutrophils. Neutrophil depletion significantly delayed tumor appearance in RANK^{+/+}, but not in RANK^{-/-} models, supporting a pro-tumorigenic role for neutrophils recruited by RANK^{+/+} tumor cells. Neutrophils have different polarization states and can promote tumorigenesis and metastasis⁴⁶. Our mouse and human data are consistent with the previously reported negative

correlation of TANs and CD8⁺ T-cell infiltration in NSCLC⁴⁷. Neutrophils have a well-defined role in the suppression of the action of CD8⁺ T cells⁴⁸. Our results demonstrate that RANK activation in tumor cells increases neutrophil survival and activation inducing an immunosuppressive environment, which could restrict the cytotoxic T-cell response. These findings support the connection between RANK activation in tumor cells, neutrophils, and CD8⁺ T cells (see Fig. 6).

A critical aspect of current and future clinical trials is the selection of BC patients who may benefit from denosumab treatment, considering the limitations of the RANK IHC. We demonstrate that the RANK metagene we generated, captures RANK activation and predicts the denosumab-driven increase in TILs in BC. Higher RANK metagene, RANK/NF- κ B activation in the tumors, and soluble RL at baseline could be better biomarkers than the individual expression levels of RANK or RL for the selection of BC patients who might benefit from denosumab treatment.

The D-BEYOND trial has some limitations, such as the small sample size, the inclusion of only premenopausal patients, and the limited number of triple-negative and HER2⁺ cases. Whether the immunomodulatory response associated with RL inhibition could also be effective in postmenopausal patients will be addressed in the ongoing trial: D-BIOMARK (NCT03691311). It will be also worth reassessing the clinical outcome of two recent large phase III trials of adjuvant denosumab in early BC, D-CARE, and ABCSG-18, according to the predictive biomarkers we defined as follows: baseline RANK metagene, sRL levels, and the presence of Tregs. The D-CARE study reported no differences in disease-free survival (DFS), whereas the ABCSG-18 trial showed DFS improvement in postmenopausal patients^{49–51}.

Results in the RANK^{-/-} mouse tumors suggest that up-regulation of negative checkpoints and Tregs occurs as a consequence of a proinflammatory, anti-tumor IFN γ -enriched microenvironment^{34,52}, and may allow RANK^{-/-} tumor cells to evade immune surveillance and grow. The blockade of CTLA4 and PD-1/PD-L1 has revolutionized treatment of highly immunogenic tumors such as melanoma and NSCLC^{21,22} but, so far, results in BC have been restricted to basal-like tumors in combination with radiotherapy or chemotherapy²³.

CTLA4 blockade affects mainly the priming phase of the immune response, whereas PD-L1 inhibition works mostly during the effector phase to restore the immune function of previously activated T cells⁵³. In both scenarios, we have shown an

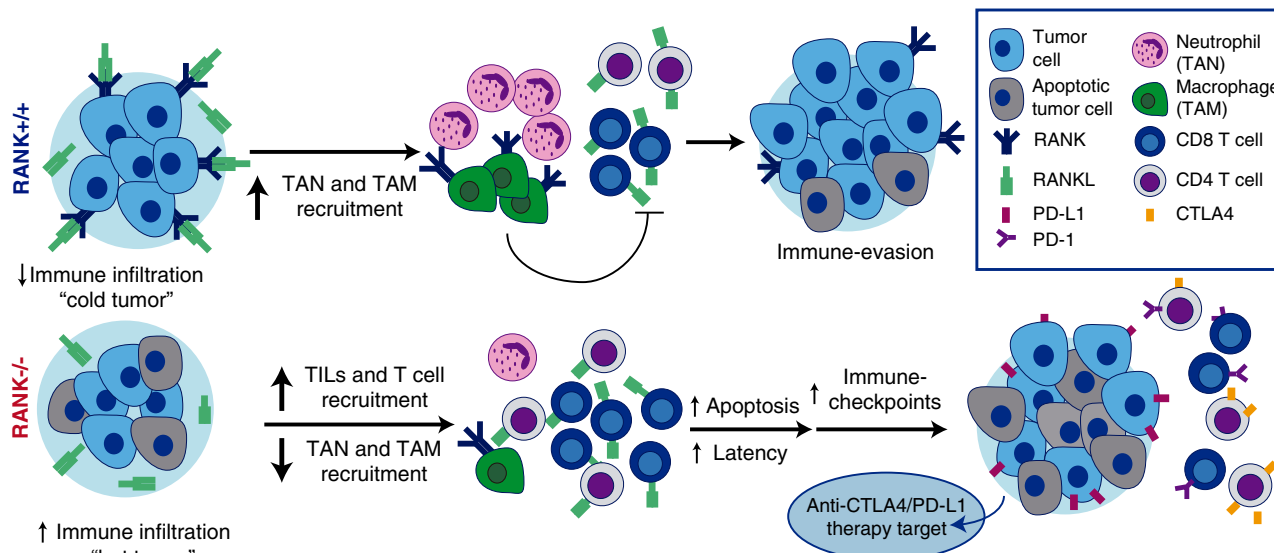


Fig. 6 The RANK pathway as immune modulator in breast cancer. RANK expression in luminal breast cancer cells leads to the expression of proinflammatory cytokines/chemokines favoring recruitment of TAMs and TANS, immunosuppressive population that interfere with lymphocyte T-cell recruitment and/or activity. Denosumab (anti-RANKL) or RANK signaling inhibition results in increased TILs, lymphocytes, and CD8+ T-cell infiltration, transforming immune “cold” tumors into “hot” ones and attenuating tumor growth. Eventually, the exacerbated immune response driven by RANK inhibition will induce the expression of immune checkpoints evading immune surveillance and allowing tumor growth. These results support the benefit of combining RANKL and immune-checkpoint inhibitors in luminal breast cancer.

increased benefit after the addition of RL inhibitors to immune checkpoints in RANK^{+/+} tumors, which is highly relevant in poorly immunogenic tumors such as luminal BC. Importantly, the combined treatments show no increased benefit in RANK^{-/-} tumors, indicating that it is driven by the inhibition of RANK signaling in tumor cells. This is a novel mechanism of action, as previous preclinical studies reporting the benefit of the combination were done in melanoma and colon cancer cell lines highly responsive to immunotherapy but lacking RANK expression^{54,55}. Although we cannot rule out that denosumab may have additional systemic effects, our findings support that a tumor cell-driven effect contributes to the immunomodulatory effect of denosumab in BC.

The benefit of the combined effect of anti-RL and immune-checkpoint inhibitors will be investigated in the CHARLI trial (NCT03161756), a phase I/II study of the effect of denosumab in combination with nivolumab (an anti-PD-1), with or without ipilimumab (anti-CTLA4), in metastatic melanoma patients, and in the POPCORN trial (ACTRN12618001121257), which will evaluate immune changes in NSCLC patients treated with nivolumab alone or in combination with denosumab. Clinical and preclinical evidence shown in this work encourage the initiation of similar trials in BC.

In summary, compelling clinical and preclinical data reveal an unexpected immunomodulatory role for RANK pathway in luminal early-stage BC and demonstrate denosumab to be a promising agent for enhancing the immune response in luminal BC alone or in combination with immune-checkpoint inhibitors.

Methods

Animals and in vivo treatments. All research involving animals was performed at the IDIBELL animal facility in compliance with protocols approved by the IDIBELL Committee on Animal Care and following national and European Union regulations. MMTV-PyMT (FVB/N-Tg(MMTV-PyVT)634Mul) were acquired from the Jackson Laboratory²⁴ and RANK^{+/+} (C57Bl/6) mice from Amgen, Inc.¹². MMTV-PyMT; RANK^{-/-} mice were obtained by backcrossing the MMTV-PyMT (FVB/N) strain with RANK^{+/+} mice into the C57Bl/6 background for at least ten generations. RANK^{fl/fl} (RANK^{fl/fl}) were provided by Dr. Joseph Penninger⁵⁶ and crossed with either MMTV-PyMT^{-/-} or LysM-cre mice (MGI: 1934631) all in

C57Bl/6 background. The athymic nude *Foxn1*^{tmu} mice were obtained from Envigo. For RANK depletion in the MMTV-PyMT^{-/-} RANK^{fl/fl} tumors, cells were plated in vitro and infected with lentivirus produced in HEK293T cells. Lentiviral packaging plasmids psPAX2 (Addgene, 12260) and pMD2.G (Addgene, 12259), with either control pLVX-IRES-ZsGreen1 vector (Addgene, 632187), or pLVX-Cre-IRES-ZsGreen1, kindly provided by Dr. Alejandro Vaquero, were used, following Addgene’s recommended protocol for lentiviral production. Tumor cells were cultured for 16 h with 1:3 virus-containing medium and, 72 h later, infected cells were FACS-sorted for zsGreen expression before being injected into syngeneic hosts.

RANK-Fc (10 mg/kg, Amgen) was injected subcutaneously three times a week^{3,4}. Therapeutic anti-RL (clone IK22/5), anti-CTLA4 (clone 9D9), anti-PD-L1 (clone 10 F.9G2), and isotype control rat IgG2A (clone 2A3) and mouse IgG2b (clone MCP-11) were obtained from BioXCell, and 200 µg were administered intraperitoneally twice per week for treatments starting 72 h after tumor cell injection or three times per week for treatments of established tumors (size > 0.09 cm²). For depletion experiments, anti-CD8 (300 µg, clone 53-5.8), anti-NK1.1 (200 µg, clone PK136), anti-Ly6G (first injection 400 µg, 100 µg thereafter, clone 1A8), and isotype controls mouse IgG2a (clone C1.18.4) and rat IgG1 (clone TNP6A7) were injected intraperitoneally. Treatment was administered on days -1, 0, 3, and 7 after tumor cell injection, and then once per week until experimental endpoint for CD8 and NK depletion. For neutrophil depletion, aLy6G was injected on day -1 and thereafter three times weekly. In all cases, mice were euthanized before tumors exceeded 10 mm in any dimension. Euthanasia was performed by CO₂ inhalation. Blood samples were taken flow cytometry analyses to check the depletion 7–10 days and 14–20 days after the first injection. Animals were randomized before beginning the treatment schedule. Mice were kept in individually ventilated and open cages and food and water were provided ad libitum.

Mouse tumor-cell isolation and tumor-initiation assays. Draining lymph nodes were removed and fresh tissues were mechanically dissected with a McIlwain tissue chopper and enzymatically digested with appropriate medium (Dulbecco’s modified Eagle’s medium (DMEM) F-12, 0.3% collagenase A, 2.5 U/mL dispase, 20 mM HEPES, and penicillin–streptomycin 1×) for 40 min at 37 °C. Samples were washed with Leibowitz L15 medium containing 10% fetal bovine serum (FBS) between each step. Erythrocytes were eliminated by treating samples with hypotonic lysis buffer (Lonza Iberica). Single cells were isolated by treating with trypsin (PAA Laboratories) for 2 min at 37 °C. Cell aggregates were removed by filtering the cell suspension with a 70 µm filter and counted. For orthotopic transplants and tumor-limiting dilution assays tumor cells isolated from PyMT;RANK^{+/+} or PyMT; RANK^{-/-} (C57Bl/6) mice were mixed 1:1 with Matrigel matrix (BD Biosciences) and orthotopically implanted in the inguinal mammary gland of 6–10-week-old syngeneic females or *Foxn1*^{tmu} females. Mammary tumor growth was monitored by palpation and caliper measurements three times per week. Lymph nodes were

treated with hypotonic lysis buffer and then mashed through a 70 μm cell strainer to isolate single cells.

Flow cytometry. Single cells from tumors or lymph nodes were resuspended and blocked with phosphate-buffered saline 2% FBS and blocked with FcR blocking reagent (Miltenyi Biotec) for 10 min on ice and incubated for 30 min on ice with the corresponding surface antibodies as follows: CD45-APCCy7 (0.125 $\mu\text{g}/\text{mL}$; 30-F11), CD11b-APC (2.5 $\mu\text{g}/\text{mL}$; M1/70), CD11b-PECy7 (2.5 $\mu\text{g}/\text{mL}$; M1/70), CD8-PE (1 $\mu\text{g}/\text{mL}$; 53-6.7), CD8-FITC (8 $\mu\text{g}/\text{mL}$; 53-6.7), CD4-PE-Cy7 (2 $\mu\text{g}/\text{mL}$; RM4-5), CD25-APC (2 $\mu\text{g}/\text{mL}$; PC61), Ly6C-FITC (1.25 $\mu\text{g}/\text{mL}$; HK1.4), Gr1-FITC (2 $\mu\text{g}/\text{mL}$; RB6-8C5), Ly6G-PECy7 (1.25 $\mu\text{g}/\text{mL}$; 1A8), F4/80-PE (1.25 $\mu\text{g}/\text{mL}$; BM8), CD3-PerCPCy5.5 (3.2 $\mu\text{g}/\text{mL}$; 145-2C11), CD3-APC (3.2 $\mu\text{g}/\text{mL}$; 145-2C11), Siglec-F-PerCP-Cy5.5 (4 $\mu\text{g}/\text{mL}$; E50-2440), CD19-PE (2.5 $\mu\text{g}/\text{mL}$; 6D5), NK1.1-PE (2.5 $\mu\text{g}/\text{mL}$; PK136), PD-1-PE (10 $\mu\text{g}/\text{mL}$; 29 F.1A12), PD-L1-PECy7 (1.25 $\mu\text{g}/\text{mL}$; 10 F.9G2), and anti-human CD11b-PECy7 (0.8 $\mu\text{g}/\text{mL}$; M1/70) from BioLegend. Apoptosis and necrosis were evaluated using the Annexin V Apoptosis Detection Kit (640930, BioLegend). 7AAD or LIVE/DEAD[™] Fixable Green Dead Cell Stain Kit (488 nm) from ThermoFisher was added in the various antibody combinations to remove dead cells. The following antibodies were used for intracellular staining: IFN γ -PE (2 $\mu\text{g}/\text{mL}$; XMG1.2); CTLA4-PerCPCy5.5 (10 $\mu\text{g}/\text{mL}$; UC10-4B9) and CTLA4-PECy7 (5 $\mu\text{g}/\text{mL}$; UC10-4B9) from BioLegend; and FOXP3-FITC (10 $\mu\text{g}/\text{mL}$; FJK-16s) and IL-12-FITC (2 $\mu\text{g}/\text{mL}$; C17.8) from eBioscience. Single-cell suspensions were stimulated in Leibowitz L15 medium containing 10% FBS, 10 ng/mL phorbol 12-myristate 13-acetate (PMA), 1 $\mu\text{g}/\text{mL}$ ionomycin, and 5 $\mu\text{g}/\text{mL}$ brefeldin A (for IFN γ and CTLA4) or just 5 $\mu\text{g}/\text{mL}$ brefeldin A (for IL-12) for 4 h at 37 °C. Surface antibodies were stained first, then fixed with paraformaldehyde (PFA) 4% (in the case of cytokines) or Fixation Reagent of the Foxp3/Transcription Factor Staining Buffer Set from eBioscience (in the case of FOXP3), and permeabilized using Permeabilization Buffer of the Foxp3/Transcription Factor Staining Buffer Set from eBioscience. The intracellular proteins were then stained. FACS analysis was performed using FACS Canto and Diva software. Cells were sorted using MoFlo (Beckman Coulter) at 25 psi with a 100 μm tip.

Blood samples were collected in tubes containing heparin and stained with CD45-APC-Cy7 (0.125 $\mu\text{g}/\text{mL}$; 30-F11), CD11b-APC (2.5 $\mu\text{g}/\text{mL}$; M1/70), CD3-PerCPCy5.5 (3.2 $\mu\text{g}/\text{mL}$; 145-2C11), CD8-PE (1 $\mu\text{g}/\text{mL}$; 53-6.7), NK1.1-PE (2.5 $\mu\text{g}/\text{mL}$; PK136), Ly6G-PECy7 (1.25 $\mu\text{g}/\text{mL}$; 1A8), and Gr1-FITC (2 $\mu\text{g}/\text{mL}$; RB6-8C5) for 30 min at room temperature (RT) in the dark. Versalyse (Beckman Coulter) containing 0.1% PFA was added to the samples and incubated for 10 min at RT in the dark before passing them through the cytometer.

IHC in mouse tumor tissues. Mouse tissue samples were fixed in formalin and embedded in paraffin. Three-micrometer sections were cut for histological analysis and stained with hematoxylin and eosin (HE). Three-micrometer tissue sections were used for immunostaining. Primary antibody was incubated overnight at 4 °C, detected with biotinylated secondary antibodies and streptavidin horseradish peroxidase (Vector), and revealed with DAB substrate (DAKO). CD3 and CD8 immunostaining was performed in the Histopathology Core Unit of the Spanish National Cancer Research Centre (CNIO, Madrid, Spain), using antibodies CD3 (clone M20 from Santa Cruz Biotechnology) and CD8 (clone 94 A from the Monoclonal Antibodies Core Unit of the CNIO). For RANK IHC, antigen retrieval was performed with Protease XXIV at 5 U/ml for 5 min (P8038, Sigma) and the anti-RANK (R&D AF692, 1:200).

Real-time PCR. Total RNA was extracted with Tripure Isolation Reagent (Roche) or Maxwell RSC Simply RNA Tissue kit (AS1340, Promega). Frozen tumor tissues were fractionated using glass beads (Sigma-Aldrich) and the Precellys[®] 24 tissue homogenizer (Berting Technologies), and Polytron PT 1200e (Kinematica). cDNA was produced by reverse transcription using 1 μg of RNA in a 35 μl reaction with random hexamers following the kit instructions (Applied Biosystems). In the case of sorted cells, RNA was retrotranscribed with Superscript II Reverse Transcriptase in a 20 μl reaction carried out according to the manufacturer's instructions (ThermoFisher). cDNA (20 ng/well) for whole tumors were analyzed by SYBR green real-time PCR with 10 μM primers using a LightCycler[®] 480 thermocycler (Roche). Analyses were performed in triplicate. *Hprt1* was used as the reference gene. The following primer pairs were used for each gene: *Hprt1*, 5'-TCAGT-CAACGGGGACATAAA-3', 5'-GGGGCTGTACTGCTTAACCAG-3'; *Prfl*, 5'-CTGGATGTGAACCTTAGGCC-3', 5'-GCGAAACCTGTACATCGCAG-3'; *Ifm1*, 5'-CACGGCACAGTCATTGAAAG-3', 5'-CATCCCTTTGGCAGTTCCCTC-3'; *Il-1 β* , 5'-CAACCAACAAGTGATATTCTCCATG-3', 5'-GATCCACACTCTCCAGTGC-3'; *Casp4*, 5'-AATTGCCACTGTCCAGGTCT-3', 5'-CTCTGCACACTGGGTTT-3'; *S100a9*, 5'-TCAGACAAATGGTGAAGCA-3', 5'-GCTCCTGGTTTGTGTCAGGT-3'.

For human cell line samples, the following primer sequences were used: *PPIA*, 5'-GGGCCTGGATACCAAGAAGT-3', 5'-TCTGTCTCTTTGGGACCTT-3'; *BIRC3*, 5'-GGTAACAGTGTATGTCAAATG-3', 5'-TAACTGGCTTGAAGTGTGACG-3'; *ICAM1*, 5'-AACTGACACCTTTGTAGCCACCTC-3', 5'-CCCAGTGAATGCAAACAGGAC-3'; *Nf κ B2*, 5'-

GGCGGGCGTCTAAAATTCTG-3', 5'-CCAGACCTGGGTTGTAGCA-3'; *RELB*, 5'-TGTGGTGAGGATCTGCTCCAG-3', 5'-TCGGCAATCCGCAGCTCTGAT-3'.

Mouse RNA labeling and hybridization to Agilent microarrays. Hybridization to the SurePrint G3 Mouse Gene Expression Microarray (ID G4852A, Agilent Technologies) was conducted following the manufacturer's two-color protocol (Two-Color Microarray-Based Gene Expression Analysis v. 6.5, Agilent Technologies). Dye swaps (Cy3 and Cy5) were performed on RNA amplified from each sample. Microarray chips were then washed and immediately scanned using a DNA Microarray Scanner (Model G2505C, Agilent Technologies).

Tumor acinar cultures and cytokine array. Isolated tumor cells coming from RANK^{+/+} or RANK^{-/-} transplants were seeded on top of growth factor-reduced matrigel (one million cells/well in six-well plates) in growth medium (DMEM-F-12, 5% FBS, 10 ng/mL of epidermal growth factor (EGF), 100 ng/mL cholera toxin, 5 $\mu\text{g}/\text{mL}$ insulin and 1x penicillin/streptomycin).

For cytokine arrays, tumor supernatants were collected 72 h after plating. A pool of three supernatants derived from three independent tumor transplants and primary tumors was used for the analyses. Multiplex quantification of cytokines and chemokines of supernatants collected from 3D acinar cultures was performed using the Mouse Cytokine Array C1000 (RayBiotech) following the manufacturer's instruction and using the recommended ImageJ plug-in. To detect genes affected by RANK activation, 1 $\mu\text{g}/\text{mL}$ RL was added 24 h after tumor plating. RNA was extracted 24 h after RL stimulation for hybridization to a gene expression microarray, as previously described.

Cell line culture and lentiviral transduction. The human BC cell lines MCF7 and HCC1954 were purchased from the American Type Culture Collection (ATCC). ATCC provides molecular authentication in support of their collection through their genomics, immunology, and proteomic cores, as described, by using DNA barcoding and species identification, quantitative gene expression, and transcriptomic analyses (ATCC Bulletin, 2010). Cells were grown in DMEM and RPMI 1640 medium, respectively, supplemented with 10% FBS and 1% penicillin-streptomycin solution (all from Gibco). The cells were grown at 37 °C in the presence of 5% CO₂ in humidified incubators and were tested for the absence of mycoplasma.

To ectopically express green fluorescent protein (control) or RANK (*TNFRSF11A*), the corresponding genes were cloned in the lentiviral vector pSD-69 (PGK promoter, generously donated by S Duss and M Bentires-Alj) following Gateway cloning protocols. To knock down the expression of endogenous RANK, we used the lentiviral vector pGIPZ clones V3LHS_307325 and V3LHS_400741 with RANK-specific short hairpin RNA expression (Dharmacon). As a control (ctrl), we used a verified non-targeting clone (Dharmacon). Lentiviruses were prepared in HEK293T cells with packaging and envelope plasmids psPAX2 and pMD2.G (AddGene). Transduced cells were selected with 1.5 $\mu\text{g}/\text{ml}$ puromycin, starting 3 days after infection.

Human neutrophil and T-cell isolation and culture. Peripheral blood was provided by the "Banc de Sang I Teixits" (Hospital Universitari de Bellvitge). Mononuclear cells were isolated from buffy coats using Ficoll-plus gradient (GE Healthcare Bio-Sciences). Neutrophils were isolated from the red fraction, then purified by dextran sedimentation. Purified cells were resuspended at 5×10^6 cells/mL in RPMI supplemented with 10% of FBS and 50 U/mL streptomycin and penicillin. FACS analysis was performed to detect CD66b (G10F5, BD Bioscience) to confirm purity (98% average).

Neutrophil apoptosis and activation were analyzed culturing 10⁴ neutrophils per well in 96-well plates over 24 h in the indicated medium or CM. Apoptosis was measured using the Annexin AV Apoptosis Detection Kit (640930, BioLegend) and activation was detected by staining for CD11b following the previously described flow cytometry staining protocol.

Clinical trial design and patient characteristics. Twenty-seven patients were enrolled in the D-BEYOND trial: the first patient enrolled on 2 October 2013 and the last patient enrolled on 9 June 2016. D-BEYOND was a prospective, single-arm, multi-center, open label, pre-operative "window-of-opportunity" phase IIa trial (NCT01864798). All patients received two injections of denosumab 120 mg subcutaneously, administered 7–12 days apart, prior to surgical intervention. Surgery was performed 10–21 days after the first dose of denosumab (median, 13 days). Post-study treatment was at the discretion of the investigator. Snap-frozen and formalin-fixed, paraffin-embedded (FFPE) tumor and normal tissues were collected at baseline (pretreatment) and at surgery (posttreatment). Normal tissues (snap-frozen and FFPE) were defined as being at least 1 cm away from tumor, another quadrant, or contralateral breast biopsies. All samples (including normal) were reviewed by a pathologist to assess epithelial content. Eligible patients were premenopausal women with histologically confirmed newly diagnosed operable primary invasive carcinoma of the breast, who had not undergone previous treatment for invasive BC. Other key eligibility criteria included a tumor size > 1.5 cm, any nodal status, and known ER, progesterone receptor (PR), and human epidermal

growth factor receptor 2 (HER2) status. Key exclusion criteria included bilateral invasive tumors, current or previous osteonecrosis, or osteomyelitis of the jaw, and known hypersensitivity to denosumab. Evaluation of conventional BC markers including ER, PR, HER2, and Ki-67 were centrally performed at the Institut Jules Bordet (IJB). ER and PR status were defined according to the American Society of Clinical Oncology and the College of American Pathologists (ASCO-CAP) guidelines. BC subtypes were defined according to the St Gallen 2015 Consensus Meetings⁵⁷ using immunohistochemical surrogates as follows: Luminal A: ER and/or PR(+), HER2(-), Ki-67 < 20%; Luminal B: ER and/or PR(+), HER2(-), Ki-67 ≥ 20; Basal: ER(-), PR(-), and HER2(-), irrespective of Ki-67 score; and HER2: HER2(+), irrespective of ER, PR, or Ki-67. All 4 HER2+ patients included in the study were ER+ PR+. The full study protocol is available as Supplementary Note 1 in the Supplementary Information file.

Serious and non-serious AEs were collected from the day of signed informed consent until one month after the final administration of the study drug, except for the project-specific AEs, for which the reporting was extended to 3 months after the final dose of denosumab. Safety data were evaluated using the National Cancer Institute Common Terminology Criteria for Adverse Events (NCI-CTCAE v 4.0). AEs were coded according to the Medical Dictionary for Regulatory Activities (version 20.1). All non-serious AEs are summarized in Supplementary Data 6, the most frequent one being arthralgia (4/27, 14.8%). This study was approved by the Ethics Committee of the trial sponsor; the Medical Ethics Committee of the Institut Jules Bordet (IJB No.: 2064) and the Melbourne Health Human Research Ethics Committee. All patients provided written informed consent prior to study entry.

One patient was excluded because she had a ductal in situ carcinoma and two patients were excluded because of lack of available tumor tissue. Another patient was excluded from TIL evaluation due to tissue exhaustion. The primary study endpoint was a GM decrease in the percentage of Ki-67-positive cells assessed by IHC. Key secondary endpoints included absolute Ki-67 responders (defined as <2.7% Ki-67 IHC staining in the posttreatment tumor tissue), decrease in serum C-terminal telopeptide (CTX) levels measured by enzyme-linked immunosorbent assay (ELISA), increase in apoptosis as detected by cleaved caspase-3 or terminal deoxynucleotidyl transferase dUTP nick end labeling assays, evaluate the tolerability of a short course of denosumab, and observe changes in TIL percentage in tumor tissue evaluated on HE slides. Changes in the infiltration of immune populations as measured by IHC were also performed. Paired samples of breast tumor and normal tissue at baseline and at surgery were required. The limited epithelial content precluded analyses of changes in the paired normal tissues. Gene expression analyses in paired tumor and normal tissue at baseline and at surgery was performed for patients with enough epithelial content. Additional secondary endpoints include: change in RANK/RL gene expression and signaling, change in tumor proliferation rates using gene expression, change in expression levels from genes corresponding to mammary progenitor populations, estrogen pathways, immune pathways, and gene expression changes in the paired samples of surrounding normal tissue when available. All primary, secondary, and exploratory endpoints performed are summarized in Supplementary Data 17.

Enzyme-linked immunosorbent assay. Serum concentrations of human sRL were centrally assessed at IJB in triplicate, using an ELISA according to the manufacturer's instructions (Biomedica, Austria). sRL bound to denosumab is not detected by this assay. Serum CTX levels were routinely evaluated in each center by ELISA.

Pathological assessment and immunohistochemical staining of human tumor samples. Tumor cellularity was centrally assessed on HE-stained tissue sections from FFPE and frozen human tumor samples. For patients with multiple samples, the sample with the highest tumor content was chosen for further analyses. The percentage of intratumoral and sTILs was independently evaluated by two trained pathologists (R.S. and G.V.D.E.) who were blinded to the clinical and experimental data on the HE slides, following the International TIL Working Group 2014 methodology, as described elsewhere⁵⁸. Median tumor cellularity ranged between 35% and 90%. TIL proliferation was assessed as the percentage of Ki-67+ TILs among all TILs.

Tissue sections (4 μm) from FFPE tissues of human primary breast tissue were used to assess RANK and RL. For each patient, representative unstained slides of the primary tumor were shipped to NeoGenomics Laboratories (California, USA) for immunohistochemical staining of RANK (N1H8, Amgen), RL (M366, Amgen), blinded to clinical information. The percentage of stained cells and their intensity (0, negative; 1+, weak; 2+, moderate; and 3+, strong) were recorded as described previously²³.

An H-score was calculated using the following formula: H = (% of cells of weak intensity × 1) + (% of cells with moderate staining × 2) + (% of cells of strong staining × 3). The maximum possible H-score is 300, corresponding to 100% of cells with strong intensity.

Serial FFPE tissue sections (4 μm) were immunohistochemically stained for CD3/CD20, CD4/CD8, and FOXP3/CD4 dual staining, as well as single Ki-67 and cleaved caspase-3 staining on a Ventana Benchmark XT automated staining instrument (Ventana Medical Systems)⁵⁹. The antibodies used for dual IHC are as follows: CD3 (IR503, polyclonal), CD8 (C8/144B, IR623), and CD20 (L26, IR604

from Dako; CD4 (RBT-CD4, BSB5150) from BioSB; FOXP3 (236 A/E7, 14-4777-82) from E-Bioscience; Ki-67 (Clone MIB-1) from Dako; and cleaved caspase-3 (ab2302) from Abcam. T cells were quantified by CD3 protein expression, B cells by CD20 protein expression, cytotoxic T cells by CD4-negative and CD8-positive expression, and Treg cells by simultaneous CD4 and FOXP3 expression. Scoring was defined as the percentage of immune-positive cells among stromal and tumoral area.

For multiplex IHC, FFPE tissue sections (4 μm) were processed manually. Briefly, slides were heated at 37 °C overnight, deparaffinized, and then fixed in neutral-buffered 10% formalin. The presence of helper T cells (CD4), cytotoxic T cells (CD8), B cells (CD20), Tregs (FOXP3), macrophages (CD68), cancer cells (pan-cytokeratin), and cell nuclei (4',6-diamidino-2-phenylindole) was assessed using a serial same-species fluorescence-labeling approach that employs tyramide signal amplification and microwave-based antigen retrieval and antibody stripping in accordance with the manufacturer's instructions (Opal Multiplex IHC, Perkin Elmer). Staining was visualized on a Zeiss LSM 710 confocal microscope equipped with PMT spectral 34-Channel QUASAR (Carl Zeiss). All IHC slides were centrally reviewed by a breast pathologist (R.S.).

RNA extraction from human samples and RNA-seq. RNA was extracted from frozen tumor and normal tissue using the AllPrep DNA/RNA Mini kit (Qiagen, Germany) according to the manufacturer's instructions. RNA quality was assessed using a Bioanalyzer 2100 (Agilent Technologies). A total of 22 patients had sufficient tumor RNA quantity from both pre- and posttreatment timepoints. A total of 11 patients had sufficient RNA quantity in normal tissue samples from both pre- and posttreatment timepoints. Among the patients without enough RNA quantity in normal tissue, six had biopsies containing mainly fatty tissue without any epithelial cell. Indexed cDNA libraries were obtained using the TruSeq Stranded Total RNA Kit (Illumina) following the manufacturer's recommendations. The multiplexed libraries were loaded onto a NovaSeq 6000 apparatus (Illumina) using a S2 flow cell and sequences were produced using a 200 Cycle Kit (Illumina).

Bioinformatic analyses. RNA-seq read pairs from the D-BEYOND samples were trimmed using Trimmomatic⁶⁰. Alignment was performed using STAR¹⁰. The number of reads mapping to each gene was assessed with the Rsamtools package in the R environment. As gene expression profiles of tissues taken at biopsy and surgery are known to be sensitive to differences in tissue-handling procedures⁶¹, we used a publicly available dataset from the no-treatment arm of POETIC study to filter-out differentially expressed genes. This study included 57 pairs of samples from untreated patients taken at diagnosis (baseline) and surgery (GEO ID: GSE73235⁶¹). We filtered out 3270/21,931 (14.9%) genes that were differentially expressed between diagnosis and surgery by using a strict cutoff of a raw value of $P < 0.05$ from a non-parametric Mann-Whitney U -test. Differential expression was analyzed with DESeq2 v.1.14.1R/Bioconductor package⁶² using raw count data. Significantly differentially expressed genes were selected if they had a q val of < 0.05 and an absolute log₂-fold change of > 0.5 . We used the GAGE v.2.24.0 R/Bioconductor package⁶³ to identify significantly enriched biological processes from the Biological Process from GO database. CIBERSORT software was used⁴⁰ to refine the subsets of immune cells present in each sample. Reads per kilobase of transcript, per million mapped reads expression data were uploaded to www.cibersort.stanford.edu and CIBERSORT was run using LM22 as a reference matrix and, as recommended for RNA-seq data, quantile normalization was disabled.

All other parameters were set to default values. Output files were downloaded as tab-delimited text files and immune cell subsets that were present in fewer than ten samples were discarded.

We reported the ten aggregates as described before [PMID: 29628290]:

T.cells.CD8 = T.cells.CD8,
T.cells.CD4 = T..CD4.naive + T..CD4.memory.resting + T..CD4.memory.activated,

T.reg = T.cells.regulatory..Tregs.
B.cells = B.cells.naive + B.cells.memory,
NK.cells = NK.cells.resting + NK.cells.activated,
Macrophage = Macrophages.M0 + Macrophages.M1 + Macrophages.M2,
Dendritic.cells = Dendritic.cells.resting + Dendritic.cells.activated,
Mast.cells = Mast.cells.restin + Mast.cells.activated,
Neutrophils = Neutrophils,
Eosinophils = Eosinophils

RNA-seq data have been deposited under EGA accession number EGAS00001003252 as a fastq file (available on request from the IJB Data Access Committee).

The prototype-based co-expression module score for *TNFRSF11A* (RANK metagene) and *TNFSF11* (RL metagene) was computed for each sample as $\text{ModuleScore} = \sum_{i=1}^{100} w_i x_i$. Where x_i is the expression of the top 100 genes positively correlated with *TNFRSF11A* or *TNFSF11* at baseline (before treatment) and w_i is the Pearson's correlation coefficient between x_i and *TNFRSF11A* or *TNFSF11*.

The public signatures of RANK/NFκB were retrieved from MSigDB⁶⁴ (Cell Systems, PMID:26771021) and computed using the GM and then scaling. RL-induced genes in mouse MECs (WT and Rank overexpression) were retrieved from publicly available GEO dataset: GSE66174.

Mouse microarray data were feature-extracted using Agilent's Feature Extraction Software (v. 10.7), using the default variable values.

Outlier features in the arrays were flagged by the same software package. Data were analyzed using the *Bioconductor* package in the R environment. Data preprocessing and differential expression analysis were performed using the *limma* and *RankProd* packages, and the most recently available gene annotations were used. Raw feature intensities were background-corrected using the *normexp* background-correction algorithm. Within-array normalization was done using spatial and intensity-dependent *loess*. *Aquantile* normalization was used to normalize between arrays. The expression of each gene was reported as the base 2 logarithm of the ratio of the value obtained for each condition relative to the control condition. A gene was considered differentially expressed if it displayed a *pp* (proportion of false positives) < 0.05, as determined by a non-parametric test.

Statistical analyses. All statistical tests comparing pre- and posttreatment paired values were done using the sign test or Student's paired samples *t*-test. All IHC values were log-transformed to give values of $\log_{10}(x + 1)$, thereby overcoming the problem of some raw variable values being zero. To compare NRs and responders, the Mann-Whitney *U* and Fisher's exact tests were used for continuous and categorical variables, respectively. All correlations were measured using the Spearman's non-parametric *rho* coefficient. All reported *P*-values were two-tailed. All analyses were performed using R version 3.3.3 (available at www.r-project.org) and Bioconductor version 3.6. No correction was made for multiple testing for exploratory analyses, except for the gene expression analysis, for which the false discovery rate was used.

Mouse experimental data were analyzed using GraphPad Prism version 5. Differences were analyzed with a two-tailed Student's *t*-test, an F-test, or an unpaired-samples *t*-test against a reference value of 1. Tumor growth curves were compared using two-way analysis of variance. Frequency of tumor initiation was estimated using the extreme limiting dilution assay (<http://bioinf.wehi.edu.au/software/elda/>). Regression analysis of the growth curves' mean for the anti-CTLA4, anti-RL, and anti-PD-L1 treatments was performed, and 2 × 2 χ^2 -contingency tables (two-tailed probabilities) were used to evaluate responses. The statistical significance of group differences is expressed by asterisks: **p* < 0.05; ***p* < 0.01; ****p* < 0.0001; *****p* < 0.0001).

Data availability

Raw microarray data from preclinical samples have been deposited in GEO, access number [GSE119464](https://www.ncbi.nlm.nih.gov/geo/query/acc.cgi?acc=GSE119464), and are publicly available. Patients' RNA-seq data have been deposited under EGA accession number [EGAS00001003252](https://ega-archive.org/studies/EGAS00001003252). Access can be obtained by contacting the Institute Jules Bordet Data Access committee or Christos Sotiriou (christos.sotiriou@bordet.be). Raw clinical data are available as Supplementary Data 18. The full study protocol is available in the Supplementary Information file. The POETIC clinical trial gene expression data used in this study are available in the GEO database under accession code [GSE73235](https://www.ncbi.nlm.nih.gov/geo/query/acc.cgi?acc=GSE73235). MECsWT and Rank overexpression microarray data used in this study are available in the GEO database under accession code [GSE66174](https://www.ncbi.nlm.nih.gov/geo/query/acc.cgi?acc=GSE66174). The remaining data are available within the Article, Supplementary Information, or available from the authors upon request.

Received: 9 June 2020; Accepted: 12 November 2020;

Published online: 10 December 2020

References

- Azim, H. A. et al. RANKL-ligand (RANKL) expression in young breast cancer patients and during pregnancy. *Breast Cancer Research*. **17**, 24 (2015).
- Fata, J. E. et al. The osteoclast differentiation factor osteoprotegerin-ligand is essential for mammary gland development. *Cell* **103**, 41–50 (2000).
- Gonzalez-Suarez, E. et al. RANK overexpression in transgenic mice with mouse mammary tumor virus promoter-controlled RANK increases proliferation and impairs alveolar differentiation in the mammary epithelia and disrupts lumen formation in cultured epithelial acini. *Mol. Cell. Biol.* **27**, 1442–1454 (2007).
- Gonzalez-Suarez, E. et al. RANK ligand mediates progesterin-induced mammary epithelial proliferation and carcinogenesis. *Nature* **468**, 103–107 (2010).
- Schramek, D. et al. Osteoclast differentiation factor RANKL controls development of progesterin-driven mammary cancer. *Nature* **468**, 98–102 (2010).
- Asselin-Labat, M.-L. et al. Control of mammary stem cell function by steroid hormone signalling. *Nature* **465**, 798–802 (2010).
- Joshi, P. A. et al. Progesterone induces adult mammary stem cell expansion. *Nature* **465**, 803–807 (2010).
- Nolan, E. et al. RANK ligand as a potential target for breast cancer prevention in BRCA1-mutation carriers. *Nat. Med.* **22**, 933–939 (2016).
- Sigl, V. et al. RANKL/RANK control Brca1 mutation-driven mammary tumors. *Cell Res.* **26**, 761–774 (2016).

- Yoldi, G. et al. RANK signaling blockade reduces breast cancer recurrence by inducing tumor cell differentiation. *Cancer Res.* **76**, 5857–5869 (2016).
- González-Suárez, E. & Sanz-Moreno, A. RANK as a therapeutic target in cancer. *FEBS J.* **283**, 2018–2033 (2016).
- Dougall, W. C. et al. RANK is essential for osteoclast and lymph node development. *Genes Dev.* **13**, 2412–24 (1999).
- Walsh, M. C. & Choi, Y. Biology of the RANKL-RANK-OPG system in immunity, bone, and beyond. *Front. Immunol.* **5**, 511 (2014).
- Anderson, D. M. et al. A homologue of the TNF receptor and its ligand enhance T-cell growth and dendritic-cell function. *Nature* **390**, 175–179 (1997).
- Green, E. A., Choi, Y. & Flavell, R. A. Pancreatic lymph node-derived CD4(+) CD25(+) Treg cells: highly potent regulators of diabetes that require TRANCE-RANK signals. *Immunity* **16**, 183–91 (2002).
- Seshasayee, D. et al. A novel in vivo role for osteoprotegerin ligand in activation of monocyte effector function and inflammatory response. *J. Biol. Chem.* **279**, 30202–30209 (2004).
- Walsh, N. C. et al. Activated human T cells express alternative mRNA transcripts encoding a secreted form of RANKL. *Genes Immunol.* **14**, 336–345 (2013).
- Biswas, S. K. & Lewis, C. E. NF- κ B as a central regulator of macrophage function in tumors. *J. Leukoc. Biol.* **88**, 877–884 (2010).
- Green, E. A., Choi, Y. & Flavell, R. A. Pancreatic lymph node-derived CD4 +CD25+ Treg cells: highly potent regulators of diabetes that require TRANCE-RANK signals. *Immunity* **16**, 183–191 (2002).
- DeNardo, D. G. & Coussens, L. M. Inflammation and breast cancer. Balancing immune response: crosstalk between adaptive and innate immune cells during breast cancer progression. *Breast Cancer Res.* **9**, 212 (2007).
- Hodi, F. S. et al. Improved survival with ipilimumab in patients with metastatic melanoma. *N. Engl. J. Med.* **363**, 711–723 (2010).
- Owen, D. & Chaft, J. E. Immunotherapy in surgically resectable non-small cell lung cancer. *J. Thorac. Dis.* **10**, S404–S411 (2018).
- Adams, S. et al. Current landscape of immunotherapy in breast cancer: a review. *JAMA Oncol.* **5**, 1205–1214 (2019).
- Guy, C. T., Cardiff, R. D. & Mülle, W. J. Induction of mammary tumors by expression of polyomavirus middle T oncogene: a transgenic mouse model for metastatic disease. *Mol. Cell. Biol.* **12**, 954–961 (1992).
- Palafox, M. et al. RANK induces epithelial-mesenchymal transition and stemness in human mammary epithelial cells and promotes tumorigenesis and metastasis. *Cancer Res.* **72**, 2879–2888 (2012).
- Pfützner, B. M. et al. RANK expression as a prognostic and predictive marker in breast cancer. *Breast Cancer Res. Treat.* **145**, 307–315 (2014).
- Clausen, B. E., Burkhardt, C., Reith, W., Renkawitz, R. & Förster, I. Conditional gene targeting in macrophages and granulocytes using LysMcre mice. *Transgenic Res.* **8**, 265–277 (1999).
- Griffith, J. W., Sokol, C. L. & Luster, A. D. Chemokines and chemokine receptors: positioning cells for host defense and immunity. *Annu. Rev. Immunol.* **32**, 659–702 (2014).
- Guo, H., Callaway, J. B. & Ting, J. P. Y. Inflammasomes: mechanism of action, role in disease, and therapeutics. *Nat. Med.* **21**, 677–687 (2015).
- Ryckman, C., Vandal, K., Rouleau, P., Talbot, M. & Tessier, P. A. Proinflammatory activities of S100: proteins S100A8, S100A9, and S100A8/A9 induce neutrophil chemotaxis and adhesion. *J. Immunol.* **170**, 3233–3242 (2003).
- Coffelt, S. B., Wellenstein, M. D. & De Visser, K. E. Neutrophils in cancer: neutral no more. *Nat. Rev. Cancer* **16**, 431–446 (2016).
- Youn, J.-I., Nagaraj, S., Collazo, M. & Gabrilovich, D. I. Subsets of myeloid-derived suppressor cells in tumor-bearing mice. *J. Immunol.* **181**, 5791–5802 (2008).
- Shaul, M. E. & Fridlender, Z. G. Cancer-related circulating and tumor-associated neutrophils – subtypes, sources and function. *FEBS J.* **285**, 4316–4342 (2018).
- Spranger, S. et al. Up-regulation of PD-L1, IDO, and T(regs) in the melanoma tumor microenvironment is driven by CD8(+) T cells. *Sci. Transl. Med.* **5**, 200ra116 (2013).
- Ellis, M. J. et al. Randomized phase II neoadjuvant comparison between letrozole, anastrozole, and exemestane for postmenopausal women with estrogen receptor-rich stage 2 to 3 breast cancer: clinical and biomarker outcomes and predictive value of the baseline PAM50-based intrinsic subtype - ACOSOG Z1031. *J. Clin. Oncol.* **29**, 2342–2349 (2011).
- Horimoto, Y. et al. Ki67 expression and the effect of neo-adjunct chemotherapy on luminal HER2-negative breast cancer. *BMC Cancer* **14**, 550 (2014).
- Yoshioka, T. et al. Prognostic significance of pathologic complete response and Ki67 expression after neoadjuvant chemotherapy in breast cancer. *Breast Cancer* **22**, 185–191 (2015).
- Dufour, J. H. et al. IFN-inducible protein 10 (IP-10; CXCL10)-deficient mice reveal a role for IP-10 in effector T cell generation and trafficking. *J. Immunol.* **168**, 3195–3204 (2002).
- Honey, K. CCL3 and CCL4 actively recruit CD8+ T cells. *Nat. Rev. Immunol.* **6**, 427–427 (2006).

40. Newman, A. M. et al. Robust enumeration of cell subsets from tissue expression profiles. *Nat. Methods* **12**, 453–457 (2015).
41. Taylor, C. R. et al. Distribution of RANK and RANK ligand in normal human tissues as determined by an optimized immunohistochemical method. *Appl. Immunohistochem. Mol. Morphol.* **25**, 299–307 (2017).
42. Salgado, R. & Loi, S. Tumour infiltrating lymphocytes in breast cancer: increasing clinical relevance. *Lancet Oncol.* **19**, 3–5 (2018).
43. Savas, P. et al. Clinical relevance of host immunity in breast cancer: from TILs to the clinic. *Nat. Rev. Clin. Oncol.* **13**, 228–241 (2016).
44. Ramos, C. D. L. MIP-1 [CCL3] acting on the CCR1 receptor mediates neutrophil migration in immune inflammation via sequential release of TNF- and LTB4. *J. Leukoc. Biol.* **78**, 167–177 (2005).
45. Oliveira, S. H. P., Canetti, C., Ribeiro, R. A. & Cunha, F. Q. Neutrophil migration induced by IL-1 β depends upon LTB4 released by macrophages and upon TNF- α and IL-1 β released by mast cells. *Inflammation* **31**, 36–46 (2008).
46. Fridlender, Z. G. et al. Polarization of tumor-associated neutrophil phenotype by TGF- β : ‘N1’ versus ‘N2’ TAN. *Cancer Cell* **16**, 183–194 (2009).
47. Kargl, J. et al. Neutrophils dominate the immune cell composition in non-small cell lung cancer. *Nat. Commun.* **8**, 14381 (2017).
48. Michaeli, J. et al. Tumor-associated neutrophils induce apoptosis of non-activated CD8 T-cells in a TNF α and NO-dependent mechanism, promoting a tumor-supportive environment. *Oncoimmunology* **6**, e1356965 (2017).
49. Coleman, R. et al. Adjuvant denosumab in early breast cancer (D-CARE): an international, multicentre, randomised, controlled, phase 3 trial. *Lancet Oncol.* **21**, 60–72 (2020).
50. Coleman, R. E. et al. Adjuvant denosumab in early breast cancer: First results from the international multicenter randomized phase III placebo controlled D-CARE study. *J. Clin. Oncol.* **36**, 501–501 (2018).
51. Gnant, M. et al. Adjuvant denosumab in postmenopausal patients with hormone receptor-positive breast cancer (ABCSG-18): disease-free survival results from a randomised, double-blind, placebo-controlled, phase 3 trial. *Lancet Oncol.* **20**, 339–351 (2019).
52. Taube, J. M. et al. Colocalization of inflammatory response with B7-H1 expression in human melanocytic lesions supports an adaptive resistance mechanism of immune escape. *Sci. Transl. Med.* **4**, 127ra37–127ra37 (2012).
53. Buchbinder, E. I. & Desai, A. CTLA-4 and PD-1 pathways similarities, differences, and implications of their inhibition. *Am. J. Clin. Oncol.* **39**, 98–106 (2016).
54. Ahern, E. et al. Co-administration of RANKL and CTLA4 antibodies enhances lymphocyte-mediated antitumor immunity in mice. *Clin. Cancer Res.* **23**, 5789–5801 (2017).
55. Ahern, E. et al. RANKL blockade improves efficacy of PD1-PD-L1 blockade or dual PD1-PD-L1 and CTLA4 blockade in mouse models of cancer. *Oncoimmunology* **7**, e1431088 (2018).
56. Hanada, R. et al. Central control of fever and female body temperature by RANKL/RANK. *Nature* **462**, 505–509 (2009).
57. Coates, A. S. et al. Tailoring therapies—improving the management of early breast cancer: St Gallen International Expert Consensus on the Primary Therapy of Early Breast Cancer 2015. *Ann. Oncol.* **26**, 1533–1546 (2015).
58. Salgado, R. et al. The evaluation of tumor-infiltrating lymphocytes (TILs) in breast cancer: recommendations by an International TILs Working Group 2014. *Ann. Oncol.* **26**, 259–271 (2015).
59. Buisseret, L. et al. Tumor-infiltrating lymphocyte composition, organization and PD-1/PD-L1 expression are linked in breast cancer. *Oncoimmunology* **6**, e1257452 (2017).
60. Bolger, A. M., Lohse, M. & Usadel, B. Trimmomatic: a flexible trimmer for Illumina sequence data. *Bioinformatics* **30**, 2114–2120 (2014).
61. López-Knowles, E. et al. Heterogeneity in global gene expression profiles between biopsy specimens taken peri-surgically from primary ER-positive breast carcinomas. *Breast Cancer Res.* **18**, 39 (2016).
62. Love, M. I., Huber, W. & Anders, S. Moderated estimation of fold change and dispersion for RNA-seq data with DESeq2. *Genome Biol.* **15**, 550 (2014).
63. Luo, W., Friedman, M. S., Shedden, K., Hankenson, K. D. & Woolf, P. J. GAGE: generally applicable gene set enrichment for pathway analysis. *BMC Bioinformatics* **10**, 161 (2009).
64. Liberzon, A. et al. The molecular signatures database hallmark gene set collection. *Cell Syst.* **1**, 417–425 (2015).

Acknowledgements

We thank the patients who contributed to this study and acknowledge the clinical staff for their dedication. The D-BEYOND clinical trial was sponsored by Jules Bordet Institute, which was responsible for the management of the study. This work was supported by grants to E. González-Suárez by MICINN (SAF2014-55997-R, SAF2017-86117-R) co-funded by FEDER funds/European Regional Development Fund (ERDF)—a way to build Europe), the European Research Council (ERC) under the European Union’s Horizon 2020 research and innovation program (grant agreement No 682935),

and Fundació La Marató de TV3. We thank CERCA Programme/Generalitat de Catalunya for institutional support. P.P. and S.B. were and A.B. is recipient of a predoctoral grant from the MICINN. We are grateful to William C. Dougall and AMGEN, Inc. for supporting the design of the D-BEYOND trial and providing RANKL, RANK-Fc reagents, and RANK^{-/-} mice. We thank the IDIBELL Animal Facility for their assistance with mouse colonies, Esther Castaño and the scientific services of the University of Barcelona for their assistance with FACS analyses, and P. Gonzalez-Santamaria, G Perez-Chacon, and M Jimenez for critical reading of the manuscript. C.S. and B.N. are supported by the National Fund for Research (FNRS) and Televie. R.S. is supported by a grant from the Breast Cancer Research Foundation (BCRF), grant number 17-194. This work was also supported in part by the Cancer Center Support Grant of the National Institutes of Health (Grant Number P30CA008748). We thank Samira Majjaj and Delphine Vincent for technical assistance. We extend gratitude to the patients who participated in the D-BEYOND study. This clinical study has been supported by research funding from Amgen.

Author contributions

G.Y. and C.G.A.: Collection and/or assembly of data, data analysis and interpretation, and manuscript writing. M.Z., P.P., E.M.T., S.B., M.C., A.B., and E.H.: Collection and/or assembly of data, and data analysis and interpretation. T.W. and L.P.: Conception and design, and data analysis and interpretation. P.M.: data analysis and interpretation. E.G.-S.: Conception and design of the preclinical study, financial support, collection and/or assembly of data, data analysis and interpretation, and manuscript writing. M.P., C.S., S.L., and H.A.A.: Conception and design of the D-BEYOND clinical trial. B.N.: Collection and/or assembly of clinical trial and biological samples data, data analysis, and manuscript writing. F.R.: Experiments on patients’ samples supervision, data analysis and interpretation, and final approval of manuscript. S.M. and D.V.: Statistical design and clinical trial data analysis. M.M.: collection and/or assembly of the clinical trial data and biological samples. R.S., D.L., and G.V.E.: Pathology assessment of the biological samples. P.V., L.P., H.W., P.S., G.L., and J.P.: Patient consent and recruitment. S.G. and K.W.-G.: Immunological assessment of the biological samples. C.V.: Clinical trial project management. All: interpretation of the data analysis and final approval of the manuscript.

Competing interests

R.S. reports non-financial support from Merck and Bristol Myers Squibb; research support from Merck, Puma Biotechnology, and Roche; and personal fees from BMS for an advisory board meeting and from Roche for an advisory board related to a trial-research project. H.A.A. is advisory board at Roche and current employee of Innate Pharma. E.G.S. and G.J.L. have served on advisory boards for Amgen and has received honoraria and research funding from Amgen. S.L. receives research funding from Novartis, Merck, BMS, Roche-Genentech, Puma Biotechnology, Pfizer, and uncompensated advisory board of Novartis, Merck, BMS, Roche-Genentech, Puma Biotechnology, Pfizer, and Seattle Genetics. The remaining authors declare no competing interests.

Additional information

Supplementary information is available for this paper at <https://doi.org/10.1038/s41467-020-20138-8>.

Correspondence and requests for materials should be addressed to C.S. or E.G.-S.

Peer review information: *Nature Communications* thanks Dung-Tsa Chen, Connie Eaves, and the other, anonymous, reviewer(s) for their contribution to the peer review of this work. Peer review reports are available.

Reprints and permission information is available at <http://www.nature.com/reprints>

Publisher’s note Springer Nature remains neutral with regard to jurisdictional claims in published maps and institutional affiliations.



Open Access This article is licensed under a Creative Commons Attribution 4.0 International License, which permits use, sharing, adaptation, distribution and reproduction in any medium or format, as long as you give appropriate credit to the original author(s) and the source, provide a link to the Creative Commons license, and indicate if changes were made. The images or other third party material in this article are included in the article’s Creative Commons license, unless indicated otherwise in a credit line to the material. If material is not included in the article’s Creative Commons license and your intended use is not permitted by statutory regulation or exceeds the permitted use, you will need to obtain permission directly from the copyright holder. To view a copy of this license, visit <http://creativecommons.org/licenses/by/4.0/>.

© The Author(s) 2020

Clara Gómez-Aleza ^{1,20}, Bastien Nguyen ^{2,3,20}, Guillermo Yoldi^{1,20}, Marina Ciscar^{1,4}, Alexandra Barranco^{1,4}, Enrique Hernández-Jiménez ¹, Marion Maetens², Roberto Salgado^{2,5}, Maria Zafeirolou¹, Pasquale Pellegrini¹, David Venet², Soizic Garaud⁶, Eva M. Trinidad ¹, Sandra Benítez ¹, Peter Vuylsteke⁷, Laura Polastro⁸, Hans Wildiers ⁹, Philippe Simon¹⁰, Geoffrey Lindeman ¹¹, Denis Larsimont¹², Gert Van den Eynden⁶, Chloé Velghe¹³, Françoise Rothé², Karen Willard-Gallo ⁶, Stefan Michiels ¹⁴, Purificación Muñoz¹, Thierry Walzer¹⁵, Lourdes Planelles¹⁶, Josef Penninger^{17,18}, Hatem A. Azim Jr¹⁹, Sherene Loi ¹¹, Martine Piccart⁸, Christos Sotiriou ^{2,8,21✉} & Eva González-Suárez ^{1,4,21✉}

¹Oncobell, Bellvitge Biomedical Research Institute, IDIBELL, Barcelona, Spain. ²Breast Cancer Translational Research Laboratory J.-C. Heuson, Institut Jules Bordet, Université Libre de Bruxelles, Brussels, Belgium. ³Marie-Josée and Henry R. Kravis Center for Molecular Oncology, Memorial Sloan Kettering Cancer Center, New York, NY 10065, USA. ⁴Molecular Oncology, Spanish National Cancer Research Centre (CNIO), Madrid, Spain. ⁵Department of Pathology, GZA-ZNA Ziekenhuizen, Antwerp, Belgium. ⁶Molecular Immunology Unit, Institut Jules Bordet, Université Libre de Bruxelles, Brussels, Belgium. ⁷Department of Medical Oncology, Université Catholique de Louvain, CHU UCL, Namur, site Sainte-Elisabeth, Namur, Belgium. ⁸Department of Medical Oncology, Institut Jules Bordet, Université Libre de Bruxelles, Brussels, Belgium. ⁹Department of Oncology, KU Leuven-University of Leuven, Leuven, Belgium. ¹⁰Department of Obstetrics and Gynaecology, Erasme, Université Libre de Bruxelles, Brussels, Belgium. ¹¹Peter MacCallum Cancer Centre, The Walter and Eliza Hall Institute of Medical Research and The Royal Melbourne Hospital, Melbourne, VIC, Australia. ¹²Department of Pathology, Institut Jules Bordet, Université Libre de Bruxelles, Brussels, Belgium. ¹³Clinical Trial Supporting Unit, Institut Jules Bordet, Université Libre de Bruxelles, Brussels, Belgium. ¹⁴Service de Biostatistique et D'Epidémiologie, Gustave Roussy, CESP, U1018, Université Paris-Sud, Faculté de Médecine, Université Paris-Saclay, Villejuif, France. ¹⁵Centre International de Recherche en Infectiologie, CIRI, Inserm U1111, CNRS, Université Claude Bernard, Lyon, France. ¹⁶BiOncotech Therapeutics, Parc Científic Universitat, Valencia, Spain. ¹⁷Life Sciences Institute, University of British Columbia, Vancouver, BC, Canada. ¹⁸IMBA, Institute of Molecular Biotechnology of the Austrian Academy of Sciences, Vienna, Austria. ¹⁹Division of Hematology/Oncology, Department of Medicine, American University of Beirut, Beirut, Lebanon. ²⁰These authors contributed equally: Clara Gómez Aleza, Bastien Nguyen, Guillermo Yoldi. ²¹These authors jointly supervised this work: Christos Sotiriou, Eva González-Suárez. ✉email: christos.sotiriou@bordet.be; egonzalez@cnio.es

RESEARCH ARTICLE

Open Access



RANK signaling increases after anti-HER2 therapy contributing to the emergence of resistance in HER2-positive breast cancer

Adrián Sanz-Moreno^{1,2†}, Sonia Palomer^{3†}, Kim Pedersen^{1†}, Beatriz Morancho^{4,5}, Tomas Pascual^{6,7,8}, Patricia Galván⁶, Sandra Benítez¹, Jorge Gomez-Miragaya^{1,9}, Marina Ciscar^{1,10}, Maria Jimenez¹⁰, Sonia Pernas^{7,11}, Anna Petit^{11,12}, María Teresa Soler-Monso^{11,12}, Gemma Viñas^{3,13}, Mansour Alsaleem¹⁴, Emad A. Rakha¹⁴, Andrew R. Green¹⁴, Patricia G. Santamaria^{5,10}, Celine Mulder¹⁵, Simone Lemeer¹⁵, Joaquin Arribas^{4,5}, Aleix Prat^{6,7,8,16}, Teresa Puig^{3*} and Eva Gonzalez-Suarez^{1,10*}

Abstract

Background: Around 15–20% of primary breast cancers are characterized by HER2 protein overexpression and/or *HER2* gene amplification. Despite the successful development of anti-HER2 drugs, intrinsic and acquired resistance represents a major hurdle. This study was performed to analyze the RANK pathway contribution in HER2-positive breast cancer and anti-HER2 therapy resistance.

Methods: RANK and RANKL protein expression was assessed in samples from HER2-positive breast cancer patients resistant to anti-HER2 therapy and treatment-naïve patients. RANK and RANKL gene expression was analyzed in paired samples from patients treated with neoadjuvant dual HER2-blockade (lapatinib and trastuzumab) from the SOLTI-1114 PAMELA trial. Additionally, HER2-positive breast cancer cell lines were used to modulate RANK expression and analyze in vitro the contribution of RANK signaling to anti-HER2 resistance and downstream signaling.

(Continued on next page)

* Correspondence: teresa.puig@udg.edu; egsuarez@idibell.cat; egonzalez@cni.es

[†]Adrian Sanz-Moreno, Sonia Palomer and Kim Pedersen contributed equally to this work.

³New Therapeutics Targets Lab (TargetsLab), Department of Medical Sciences, University of Girona, Girona, Spain

¹Oncobell, Bellvitge Biomedical Research Institute (IDIBELL), L'Hospitalet de Llobregat, Barcelona, Spain

Full list of author information is available at the end of the article



© The Author(s). 2021 **Open Access** This article is licensed under a Creative Commons Attribution 4.0 International License, which permits use, sharing, adaptation, distribution and reproduction in any medium or format, as long as you give appropriate credit to the original author(s) and the source, provide a link to the Creative Commons licence, and indicate if changes were made. The images or other third party material in this article are included in the article's Creative Commons licence, unless indicated otherwise in a credit line to the material. If material is not included in the article's Creative Commons licence and your intended use is not permitted by statutory regulation or exceeds the permitted use, you will need to obtain permission directly from the copyright holder. To view a copy of this licence, visit <http://creativecommons.org/licenses/by/4.0/>. The Creative Commons Public Domain Dedication waiver (<http://creativecommons.org/publicdomain/zero/1.0/>) applies to the data made available in this article, unless otherwise stated in a credit line to the data.

(Continued from previous page)

Results: RANK and RANKL proteins are more frequently detected in HER2-positive tumors that have acquired resistance to anti-HER2 therapies than in treatment-naïve ones. *RANK* (but not *RANKL*) gene expression increased after dual anti-HER2 neoadjuvant therapy in the cohort from the SOLTI-1114 PAMELA trial. Results in HER2-positive breast cancer cell lines recapitulate the clinical observations, with increased RANK expression observed after short-term treatment with the HER2 inhibitor lapatinib or dual anti-HER2 therapy and in lapatinib-resistant cells. After RANKL stimulation, lapatinib-resistant cells show increased NF- κ B activation compared to their sensitive counterparts, confirming the enhanced functionality of the RANK pathway in anti-HER2-resistant breast cancer. Overactivation of the RANK signaling pathway enhances ERK and NF- κ B signaling and increases lapatinib resistance in different HER2-positive breast cancer cell lines, whereas RANK loss sensitizes lapatinib-resistant cells to the drug. Our results indicate that ErbB signaling is required for RANK/RANKL-driven activation of ERK in several HER2-positive cell lines. In contrast, lapatinib is not able to counteract the NF- κ B activation elicited after RANKL treatment in RANK-overexpressing cells. Finally, we show that RANK binds to HER2 in breast cancer cells and that enhanced RANK pathway activation alters HER2 phosphorylation status.

Conclusions: Our data support a physical and functional link between RANK and HER2 signaling in breast cancer and demonstrate that increased RANK signaling may contribute to the development of lapatinib resistance through NF- κ B activation. Whether HER2-positive breast cancer patients with tumoral RANK expression might benefit from dual HER2 and RANK inhibition therapy remains to be elucidated.

Keywords: Breast cancer, HER2, Lapatinib, NF- κ B, RANK, RANKL, Resistance, Trastuzumab

Background

The human epidermal growth factor receptor 2 (HER2), known as ErbB2 or Neu, is a tyrosine kinase receptor protein encoded by the *ERBB2* (*HER2*) gene [1]. HER2 is a member of the epidermal growth factor (EGF) receptor family along with EGFR/HER1, ERBB3/HER3, and ERBB4/HER4. The four receptors are transmembrane proteins with an intracellular tyrosine kinase domain (although ERBB3/HER3 is considered kinase impaired). While HER2 is the only family member that does not bind to a ligand, it forms heterodimers with the other EGF receptor protein members and shows strong catalytic kinase activity, efficiently triggering downstream signaling through phosphatidylinositol-3 kinase (PI3K) and mitogen-activated protein kinase (MAPK) [1]. Approximately 15–20% of primary breast cancers show HER2 protein overexpression and/or *HER2* gene amplification [2], which is associated with poor prognosis. The development of humanized monoclonal antibodies binding the extracellular domain of HER2 (e.g., trastuzumab, pertuzumab), EGFR-HER2 small molecule kinase inhibitors (e.g., lapatinib, neratinib, or tucatinib), and antibody-drug conjugates (e.g., T-DM1 or DS-8201) has revolutionized HER2-positive breast cancer treatment [3]. Still, most patients with metastatic disease eventually progress on anti-HER2 therapy due to de novo or acquired resistance, and 20–30% of patients with early HER2+ breast cancer relapse [4–6]. Therefore, elucidating the mechanisms of resistance to anti-HER2 drugs is pivotal to further improve patients' survival outcomes.

Receptor activator of nuclear factor kappa-B ligand (RANKL) and its receptor (RANK) belong to the TNF superfamily. The fundamental role of RANK signaling in osteoporosis and bone metastasis inspired the

development of denosumab, a monoclonal antibody against RANKL, for the treatment of skeletal-related events (SREs) linked to osteoporosis and cancer [7]. RANK signaling activation in the breast epithelium promotes tumor initiation, progression, and metastatic spread. Thus, RANK and RANKL have emerged as promising targets for breast cancer prevention and treatment [8]. RANKL is expressed in progesterone receptor-positive cells and acts as a paracrine mediator of progesterone in the mammary epithelia [9, 10]. Increased RANK receptor expression is more frequent in hormone receptor-negative tumors and high-grade breast cancer, but it is also found in a subset of luminal tumors [11, 12]. RANK signaling controls proliferation and stemness in BRCA1-mutant and oncogene-driven mammary tumors [13, 14]. Interestingly, RANK signaling inhibition has been shown to reduce HER2 tumorigenesis in pre-clinical studies [9, 15]. In human tumors, RANKL and HER2 levels predict metastasis to the bone in breast cancer better than RANKL alone [16].

Some of the common (intrinsic or acquired) resistance mechanisms to trastuzumab and/or lapatinib treatment are impaired HER2 binding, parallel/downstream pathway activation, ER signaling, cell cycle de-regulation, or escape from antibody-dependent cellular cytotoxicity (ADCC) [17]. Personalized treatment of HER2-positive breast cancer and better predictive biomarkers to anticipate therapy resistance will contribute to the identification of patients that will benefit from new combinatorial therapies, paving the way for HER2-positive breast cancer precision medicine [18].

In this study, we unveiled a functional relationship between RANK and HER2 signaling using HER2-positive

breast cancer patient samples and cell lines. Upon analyses of HER2-positive breast cancer samples from treatment-naïve patients and residual disease at surgery after neoadjuvant anti-HER2 therapy, including paired samples from the phase II SOLTI-1114 PAMELA trial, we observed that anti-HER2 treatment or resistance to anti-HER2 therapy both resulted in increased RANK expression. Additionally, when we analyzed the effects of RANK modulation on anti-HER2 treatment in HER2-positive breast cancer cell lines, we observed that enhanced RANK signaling led to increased lapatinib resistance.

Methods

Patient samples

RANK and RANKL expression was assessed in tumor samples from three different cohorts of patients with HER2-positive breast cancer.

Treatment-naïve cohort

Patients with primary and operable HER2-positive breast cancer ($n = 197$) diagnosed from 2003 to 2010 at the Nottingham City Hospital, Nottingham, UK. Tumor samples were collected at surgery prior to any neoadjuvant treatment. Histological grade was assessed by the Nottingham Grading System [19] and other clinicopathological factors such as tumor size, lymph node (LN) status, estrogen receptor (ER), progesterone receptor (PR), and HER2 expression, as well as patient age and disease progression, were analyzed before including the samples into the TMAs, prepared as previously described [20].

Anti-HER2-resistant cohort

Patients treated with trastuzumab-based primary chemotherapy and residual disease at surgery ($n = 43$) diagnosed at the Catalan Institute of Oncology (ICO), Bellvitge University Hospital in l'Hospitalet de Llobregat, and Dr. Josep Trueta University Hospital in Girona (Spain) between 2005 and 2014 and described in [21]. The selection criterion included patients with early or locally advanced HER2-positive breast cancer (including inflammatory breast cancer) who had received neoadjuvant treatment with trastuzumab-based chemotherapy and had residual invasive disease following surgery (i.e., who had not achieved a pathological complete response at surgery). Neoadjuvant chemotherapy was based on anthracyclines and taxanes given concurrently with weekly trastuzumab for 24 weeks followed by surgery. For all patients, hematoxylin and eosin (H&E)-stained slides from formalin-fixed paraffin-embedded (FFPE) tumor blocks were examined to determine representative areas of the invasive tumor. ER, PR, and HER2 positivity were assessed in the initial tumor core biopsies as

well as in the residual disease. For each patient, different clinical and histopathological features such as age, and histological grade (Nottingham Grading System) were obtained.

SOLTI-1114 PAMELA cohort

Patients treated with neoadjuvant dual-blockade trastuzumab and lapatinib ($n = 151$) and in which biopsy paired samples were prospectively obtained. The main results of the PAMELA neoadjuvant phase II study have been previously reported [22] and the completed study is registered in ClinicalTrials.gov (number NCT01973660). In this trial, patients with early HER2-positive breast cancer were treated with neoadjuvant lapatinib (1000 mg daily) and trastuzumab (8 mg/kg i.v. loading dose followed by 6 mg/kg) for 18 weeks. Patients with hormonal receptor-positive breast cancer received letrozole or tamoxifen according to menopausal status. FFPE tumor samples at baseline, at day 14 of treatment, and at surgery were collected according to standard protocols.

Gene expression analyses

RNA samples of the PAMELA trial from tumors at baseline ($n = 151$) were previously analyzed [22]. Here, the nCounter platform (NanoString Technologies, Seattle, WA, USA) analyzed RNA of 101 residual tumors from surgical samples of the PAMELA trial. A minimum of 100 ng of total RNA was used to measure the expression of 550 genes, including *RANK* and *RANKL*, and 5 housekeeping genes (*ACTB*, *MRPL19*, *PSMC4*, *RPLP0*, and *SF3A1*). Expression counts were then normalized using the nSolver 4.0 software and custom scripts in R 3.4.3. For each sample, we calculated the PAM50 signature scores (basal-like, HER2-E, luminal A and B, normal-like) and the risk of recurrence score [23]. Intrinsic molecular subtypes were identified using the research-based PAM50 predictor as previously described [22, 24].

Immunohistochemistry and tissue microarray scoring

Immunohistochemistry (IHC) in TMAs was performed using anti-human mouse monoclonal RANK (N-1H8 Amgen) and human RANKL (M366 Amgen) as described in [9]. RANK or RANKL staining was scored on a scale of 0 to 3 for intensity (0 = no staining, 1 = weak, 2 = moderate, 3 = intense) and for the percentage of positively stained tumor cells (0–100) as previously reported [25]. The result of multiplying staining intensity by positive cell percentage is the *H*-score value, ranging from 0 to 300. TMA cores were scored for RANK and RANKL with the assistance of the breast cancer pathologists from the Bellvitge Hospital, if tumor cells represented > 15% of the total TMA core area. Patients were stratified according to RANK or RANKL *H*-scores as

being protein-positive (H -score ≥ 1) or protein-negative (H -score = 0). Breast tumors from patient-derived xenografts were used as positive and negative controls. Experimental data from our laboratory in breast cancer cells and patients' samples [26] confirmed that cells in which RANK protein expression is not detected by IHC/western blot may still respond to RANKL stimulation or denosumab inhibition [11, 26, 27]. This is probably due to the "fragility" of the RANK epitope and the limited sensitivity of the current tools to detect RANK protein expression. Thus, even with an H -score ≥ 1 , we are likely underestimating samples with a functional RANK signaling pathway.

Statistical analyses were performed with the support of IDIBELL and Nottingham University Statistical Assessment Services. The ER/PR/HER2 status, grade, and tumor stage were known for each case included in the TMAs. Associations between IHC scores and clinicopathological parameters were evaluated using Pearson's chi-squared test.

Cell lines and cell culture

The cell lines BT474 parental (BT474) and BT474 with lapatinib resistance (BTLR) were described in [28]. SKBR3 parental (SKBR3) and SKBR3 lapatinib resistant (SKLR) lines were described in [29]. The cell line HCC1954 was obtained from ATCC (CRL-2338). BT474 cells were grown in DMEM + GlutaMAX (Gibco) supplemented with 2 mM L-glutamine (HyClone), 1× penicillin-streptomycin solution (P/S, Gibco), and 7.5% fetal bovine serum (FBS, Gibco). SKBR3 cells were grown in McCoy's 5A + GlutaMAX supplemented with 2 mM L-glutamine, 1 mM sodium pyruvate (HyClone), 1× P/S, and 5% FBS. HCC1954 cells were grown in RPMI medium 1640 + GlutaMAX supplemented with 2 mM L-glutamine, 1× P/S, and 5% FBS. The cells were grown at 37 °C in 5% CO₂ humidified incubators. For RANKL treatments, cells were incubated in the presence of 100–300 ng/ml of RANKL. Cell lines were routinely tested for mycoplasma contamination.

Viral transduction

To ectopically express RANK, the *RANK* gene (*TNFR SF11A*) was cloned into the lentiviral vector pSD-69 (kindly provided by S. Duss and M. Bentires-Alj) under the control of hPGK promoter. As a control (ctrl), we used an empty pSD-69 plasmid generated by removing the BamHI-SalI fragment containing CcdB and CmR genes. Knockdown of *RANK* endogenous expression was achieved by shRNA lentiviral delivery using pGIPZ vectors containing shRNAs against human *RANK* (RHS4531, Dharmacon), and shRNAs sequences #3 (TATCTTCTTC ATTCCAGCT) and #4 (ATTCTTCCTTGAAGTTCCC) were selected based on their ability to silence *RANK*

expression. As a control, we used pGIPZ expressing a verified non-targeting sequence (RHS4346 Dharmacon). Lentiviruses were prepared in HEK293T cells transfected with psPAX2 (Addgene #12260) and pMD2.G (Addgene #12259) by the calcium phosphate method. Virus-containing supernatants were centrifuged at 1500 rpm for 5 min and filtered with 0.45- μ m filters (Millipore). The medium from 1-cm² production cells was used to infect 2-cm² recipient cells at roughly 33% confluence, adding fresh medium (1:1) and 8 μ g/ml polybrene (Millipore). Approximately 90% infection efficiency was verified 3 days after transduction by detection of GFP expressed from pGIPZ plasmids. Transduced cells were selected with 1.5 μ g/ml puromycin (Sigma), starting 3 days after infection, and subsequently maintained with 1 μ g/ml puromycin in the growth media.

Cell proliferation

To determine cell proliferation, 1000–4000 cells per well in 100 μ l were seeded in 96-well plates. After 24 h, 100 μ l of medium with or without the indicated concentrations of lapatinib (0–16 μ M) was added, and cells were incubated for 4 days. The relative number of viable cells each day was determined by adding 50 μ l of diluted CCK-8 reagent according to the manufacturer's protocol (Sigma).

Western blot

Cells were seeded at approximately 33% confluence in 6-well plates. The following day, they were washed and incubated in a medium without FBS. The next day, the medium was changed to 1.8 ml medium with or without 1 μ M lapatinib followed by a 2-h incubation. Subsequently, 0.2 ml of medium with or without 300 ng/ml of RANKL (RANKL-LZ Amgen) was added to the wells. Ten minutes later, the extracts for immunoblots were prepared with modified RIPA buffer (50 mM Tris pH 7.4, 150 mM NaCl, 1% NP-40, 0.25% sodium deoxycholate) containing 1× PhosSTOP and complete protease inhibitor cocktail (Roche), and protein concentrations determined with DC protein assay reagents (BIO-RAD). Fifteen micrograms of protein were resolved by SDS-PAGE and blotted into Immobilon-P 0.45 μ m membranes (Millipore). Antibodies against the following proteins were used for probing: RANK (R&D Systems AF683), p-HER2 (#2249), HER2 (#2165), p-EGFR (#3777), EGFR (#4267), p-ERK1/2 (#9101), ERK1/2 (#9102), p-AKT (#4051), AKT (#9272), p-p65 (#3033), p65 (#8242), p-I κ B (#9246), I κ B (#9242) (from Cell Signaling), β -actin (sc-47778), and tubulin (Abcam ab21058).

Immunoprecipitation

Upon transiently transfecting HEK293 cells with affinity-tagged versions of full-length RANK (RANK-V5 in

pLenti6/V5-DEST, Invitrogen), full-length HER2 (FLAG-HER2 [30]), an amino (742-NTF) [30], or carboxy-terminal fragment of HER2 (611-CTF) [31], cells were washed twice with ice-cold PBS and proteins were extracted with 20 mM Tris-HCl pH 7.4, 137 mM NaCl, 2 mM EDTA, 10% glycerol, 1% NP-40 supplemented with 50 µg/ml leupeptin, 50 µg/ml aprotinin, 0.5 mM sodium orthovanadate, and 1 mM phenylmethylsulfonyl fluoride. Equal amounts of extracts were incubated for 3 h with immunoglobulin G (Abcam ab171870), FLAG (Sigma F3165), HA (Abcam ab9110), V5 (Thermo Scientific #R961-25), HER2 (32H2 in house antibody described in [32]), or trastuzumab (Hoffmann-La Roche) antibodies. Then, protein A agarose beads (Calbiochem IP02) were added for 2 h. Immunoprecipitates were washed thoroughly with lysis buffer and boiled in reducing SDS loading buffer to be analyzed by Western blot.

RNA isolation and RT-qPCR

Cells were seeded at approximately 33% confluence in 6-well plates. The next day, the medium was changed to medium with or without 100 ng/ml RANKL followed by an additional 24 h incubation period. To analyze mRNA expression levels, total RNA was purified with Maxwell RSC simplyRNA Tissue kit (AS1340 Promega). For each sample, cDNA was retrotranscribed from 1 µg of RNA using 200 U SuperScript II plus random hexamer oligos following the manufacturer's protocol (Invitrogen); cDNA from 20 ng RNA for each sample was analyzed by SYBR green real-time PCR (Applied Biosystems) with 10 µM primers using a LightCycler[®] 480 thermocycler (Roche). Analyses were performed in triplicates using the LightCycler[®] 480 software (Roche). Peptidylprolyl isomerase A, *PPIA*, was used as the reference gene. The primer sequences used in the analyses are as follows: *PPIA* (fw ATGGTCAACCCACCGTT, rev TCTGCTGTCTTTGGGACCTTG), *RANK* (fw GCAGGTGGCTTTGCAGAT, rev 5'GCATTTAGAAACATGTACTTTTCCTG), *BIRC3* (fw GGTAACAGTGATGATGTCAAATG, rev TAACTGCTTGAACCTTGACG), *ICAM1* (fw AACTGACACCTTTGTTAGCCACCTC, rev CCCAGTGAAATGCAAA CAGGAC), *TNFα* (fw AAGCTGTAGCCCATGTTGT, rev TGAGGTAACAGGCCCTCTGAT), and *IL8* (fw CTGCGC CAACACAGAAATTA, rev CATCTGGCAACCCTACAA CA).

Results

RANK is expressed in HER2-positive and anti-HER2-resistant breast cancer patients

The expression of RANK and RANKL in HER2-positive breast cancer patients was analyzed by immunohistochemistry (IHC) in two independent sets of tissue microarrays (TMAs): a collection of HER2-positive tumor samples from treatment-naive patients ($n = 197$) and a cohort with tumors resistant to neoadjuvant trastuzumab-

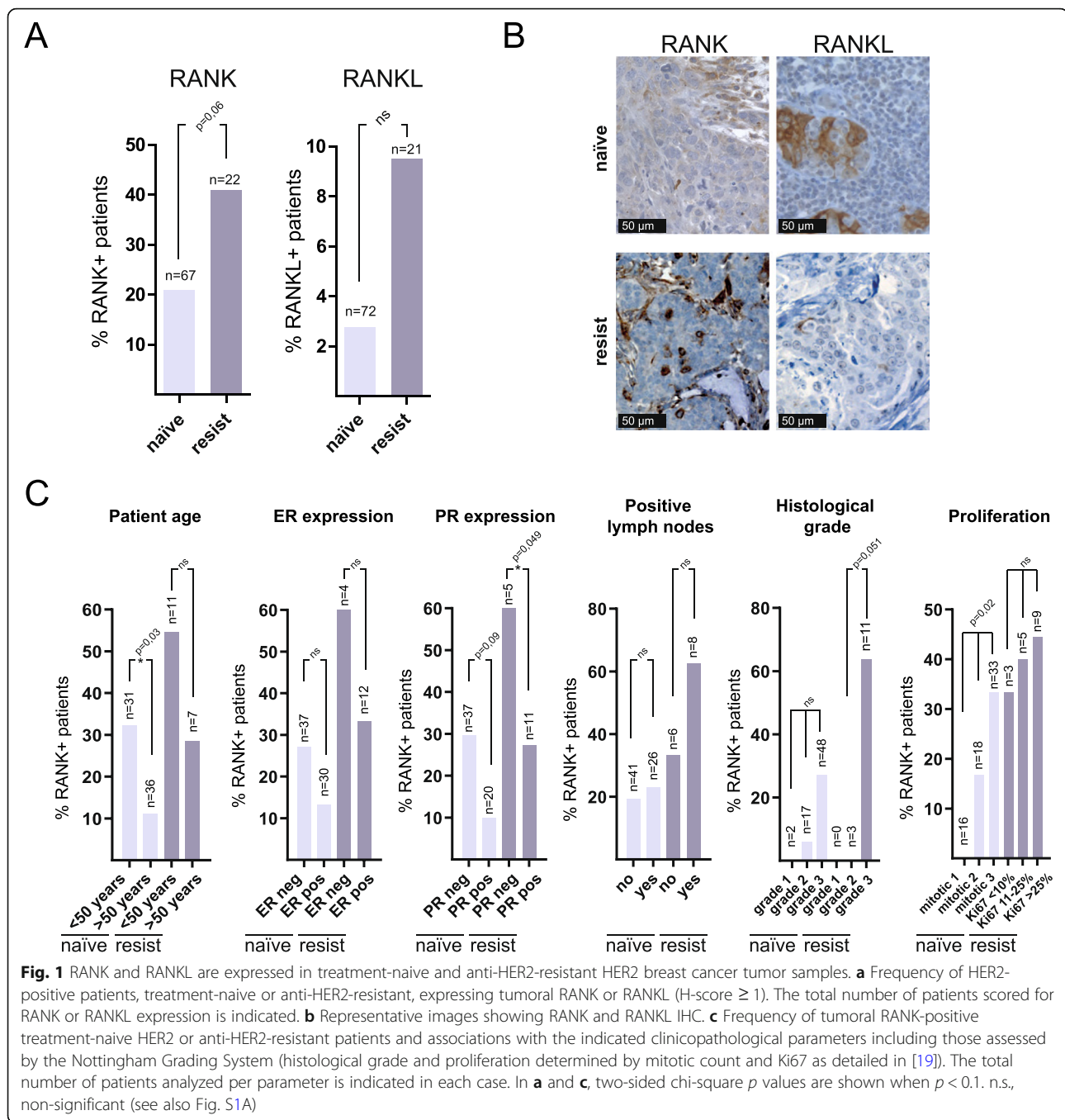
based chemotherapy ($n = 43$) from patients with residual invasive disease at surgery.

In the first collection, the integrity of the tissue allowed scoring of 67 and 72 patients for RANK and RANKL expression, respectively. Considering positive those with H -score ≥ 1 for the tumor cells, RANK expression was found in 14/67 (20.9%) cases and transmembrane RANKL staining in just 2/72 (2.8%) of the samples (Fig. 1a). In the anti-HER2-resistant tumor samples, we could score 22 patients for RANK and 21 for RANKL (Fig. 1a). In these, 9/22 (40.9%) were positive for RANK and 2/21 (9.5%) for transmembrane RANKL in tumor cells (Fig. 1a). Representative pictures of RANK and RANKL positive samples are shown in Fig. 1b, and H -scores for the whole tumor core from all samples (excluding those with integrity issues) and controls are presented in Fig. S1A and B. Pictures of the whole TMA core area in both collections are shown in Fig. S2.

Next, we evaluated the clinico-pathological factors associated with RANK expression in treatment-naive HER2-positive tumors (Fig. 1c). RANK expression was significantly associated with tumors from younger patients (less than 50 years old; $p = 0.034$) and tumors with a higher Ki67 proliferation index ($p = 0.02$). A trend of increased frequency of RANK expression was found in ER/PR negative tumors ($p = 0.170$ and $p = 0.090$, respectively), and higher histological grade ($p = 0.138$) (Fig. 1c). Similar patterns were observed in tumors resistant to anti-HER2 treatment (Fig. 1c). In both series, the limited number of samples prevented additional statistically significant associations, but general patterns coincided with those reported in previous studies of RANK/RANKL expression in human breast cancer samples [11, 12, 33]. Importantly, the frequency of RANK/RANKL-positive samples was higher in anti-HER2-resistant compared to treatment-naive HER2-positive tumors.

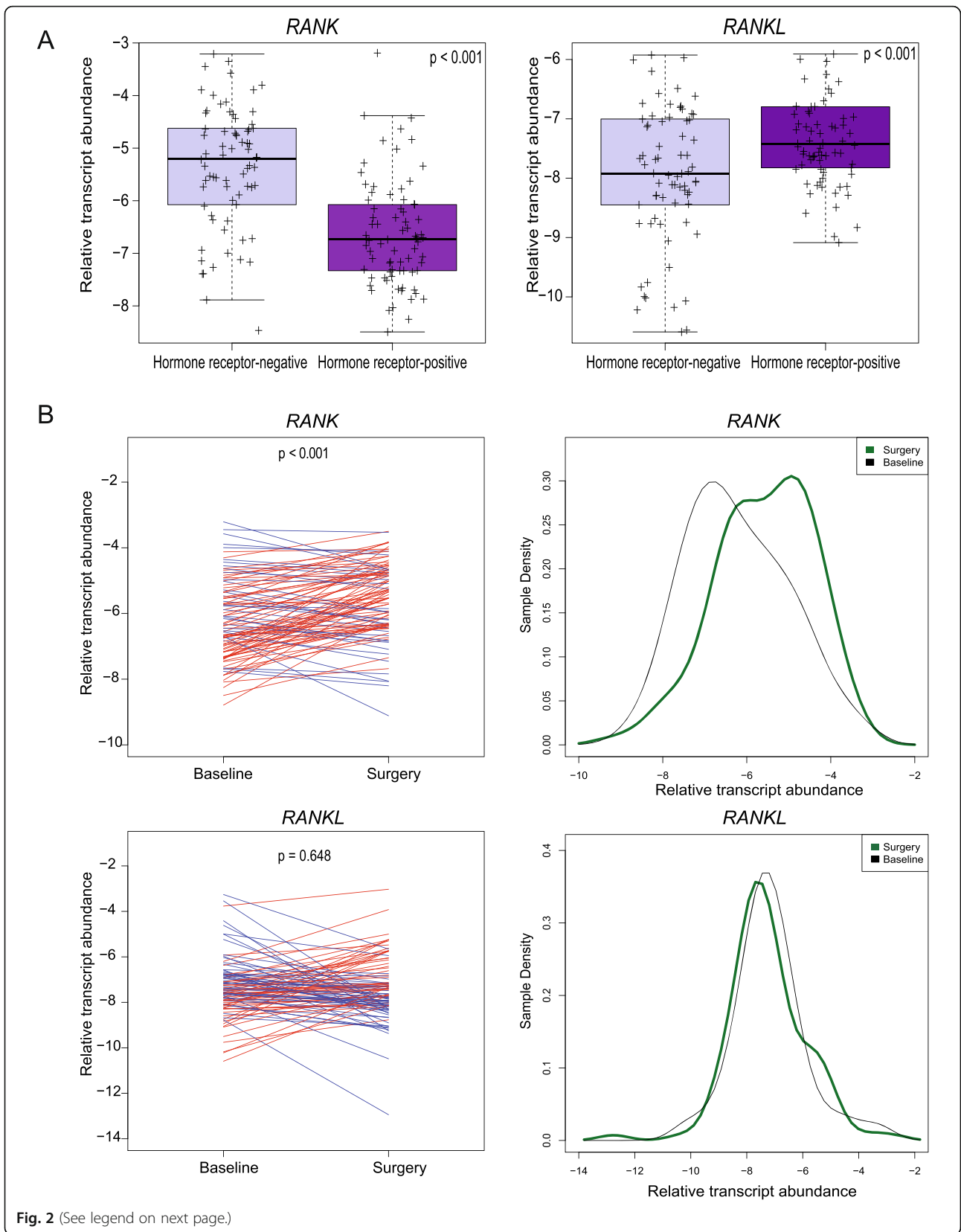
RANK expression increases after anti-HER2 treatment in HER2-positive breast cancer patients (PAMELA clinical trial)

Our previous results suggested that RANK and RANKL expression may increase upon acquisition of anti-HER2 treatment resistance (Fig. 1a). To determine the possible changes in RANK and RANKL expression induced by dual HER2 blockade, gene expression profiling was performed in paired surgical tumor samples obtained before and following treatment with lapatinib and trastuzumab (and endocrine therapy if the tumor was hormone receptor-positive) from the PAMELA phase II clinical trial [22]. At baseline, the expression of *RANK* was significantly associated with the PAM50 intrinsic subtypes (Fig. S3A; $p < 0.001$); non-luminal subtypes (Basal-like and HER2-enriched) had the highest *RANK* expression. No significant differences in *RANKL* gene expression



across PAM50 intrinsic subtypes were observed, although *RANKL* levels were slightly increased in the luminal A subtype (Fig. S3A), as previously reported [33]. Moreover, *RANK* gene expression was higher in hormone receptor-negative tumor samples ($p < 0.001$) while *RANKL* showed the opposite trend (Fig. 2a) confirming previous findings [12, 34]. *ERBB2* gene expression at baseline had a weak positive correlation ($r = 0.16$) with *RANK* and the opposite trend ($r = -0.21$) with

RANKL expression (Fig. S3B and C). *RANK* gene expression increased (Fig. 2b, denoted by red lines in the left graph and a green line in the right graph) following dual treatment with lapatinib and trastuzumab ($p < 0.001$), while *RANKL* expression did not significantly change when analyzing residual disease samples at surgery (Supplementary Table 1). Specifically, the mean *RANK* expression in baseline samples was -6.22 (standard deviation (SD) = 1.22) versus -5.58 (SD = 1.14) in the



(See figure on previous page.)

Fig. 2 *RANK*, but not *RANKL*, expression increased after dual anti-HER2 therapy in patient samples ($n = 151$) from the PAMELA trial. **a** Box plots of *RANK* and *RANKL* gene expression in HER2-positive tumors at baseline classified by hormone receptor expression. **b** Ladder plots (on the left) show the *RANK* and *RANKL* gene expression in PAMELA HER2-positive tumors before (baseline) and after (surgery) dual anti-HER2 treatment. An increase in gene expression is represented in red and a decrease in blue. Each line represents a tumor sample from one patient. p values in **a** were calculated by comparing the mean values between both groups and in **b** were determined by paired two-tailed t tests. Density plots (on the right) showing the *RANK* and *RANKL* gene expression in PAMELA HER2-positive tumors before (baseline) and after (surgery) treatment (see Fig. S3, S4, and Supplementary Table 1 for further analyses)

paired surgical samples. In contrast, the mean *RANKL* expression in the baseline samples was -7.36 ($SD = 1.28$) versus -7.44 ($SD = 1.33$) in the surgical samples. When populations were studied separately according to hormone receptor expression, the same findings were observed, an increase in *RANK* mRNA expression in both hormone receptor positive and negative HER2+ tumors after HER2 inhibition (Fig. S4A and B).

These results confirmed that *RANK* expression increases in HER2-positive breast tumors after dual HER2 blockade. The increased levels of *RANK* observed in patients upon anti-HER2 treatment suggest that activation of *RANK* signaling may allow survival of HER2-positive tumor cells and contribute to resistance to anti-HER2 therapies.

RANK signaling is upregulated after short-term lapatinib treatment and in HER2-resistant cell lines

As *RANK* expression increased after dual lapatinib/trastuzumab treatment in HER2-positive breast cancer patients, we decided to test whether in vitro short-term treatment with both anti-HER2 drugs, alone or in combination, would influence *RANK* expression in three different HER2-positive breast cancer cell lines. While SKBR3 and BT474 cells are sensitive to lapatinib and trastuzumab, HCC1954 cells are less sensitive to lapatinib and resistant to trastuzumab [35].

Lapatinib treatment, alone or in combination with trastuzumab, resulted in higher *RANK* mRNA expression in SKBR3 when compared with non-treated cells (Fig. 3a). Lapatinib or trastuzumab treatment, as well as their combination, also increased *RANK* expression levels in BT474 cells. In HCC1954 cells, *RANK* expression increased with lapatinib alone or in combination treatment after 12 h, whereas trastuzumab alone did not alter *RANK* expression levels. Also, we analyzed *RANK* expression in SKBR3 cells, either parental (sensitive to lapatinib and trastuzumab) or resistant to trastuzumab (SKTR), to lapatinib (SKLR), or to both (SKTLR and SKLTR; derived from SKTR and SKLR, respectively) [29]. *RANK* gene and protein expression levels were significantly higher in lapatinib-resistant SKLR and dual lapatinib/trastuzumab-resistant SKLTR cells when compared to SKBR3 parental cells (Fig. 3b, c). Increased *RANK* mRNA expression was also observed in BT474

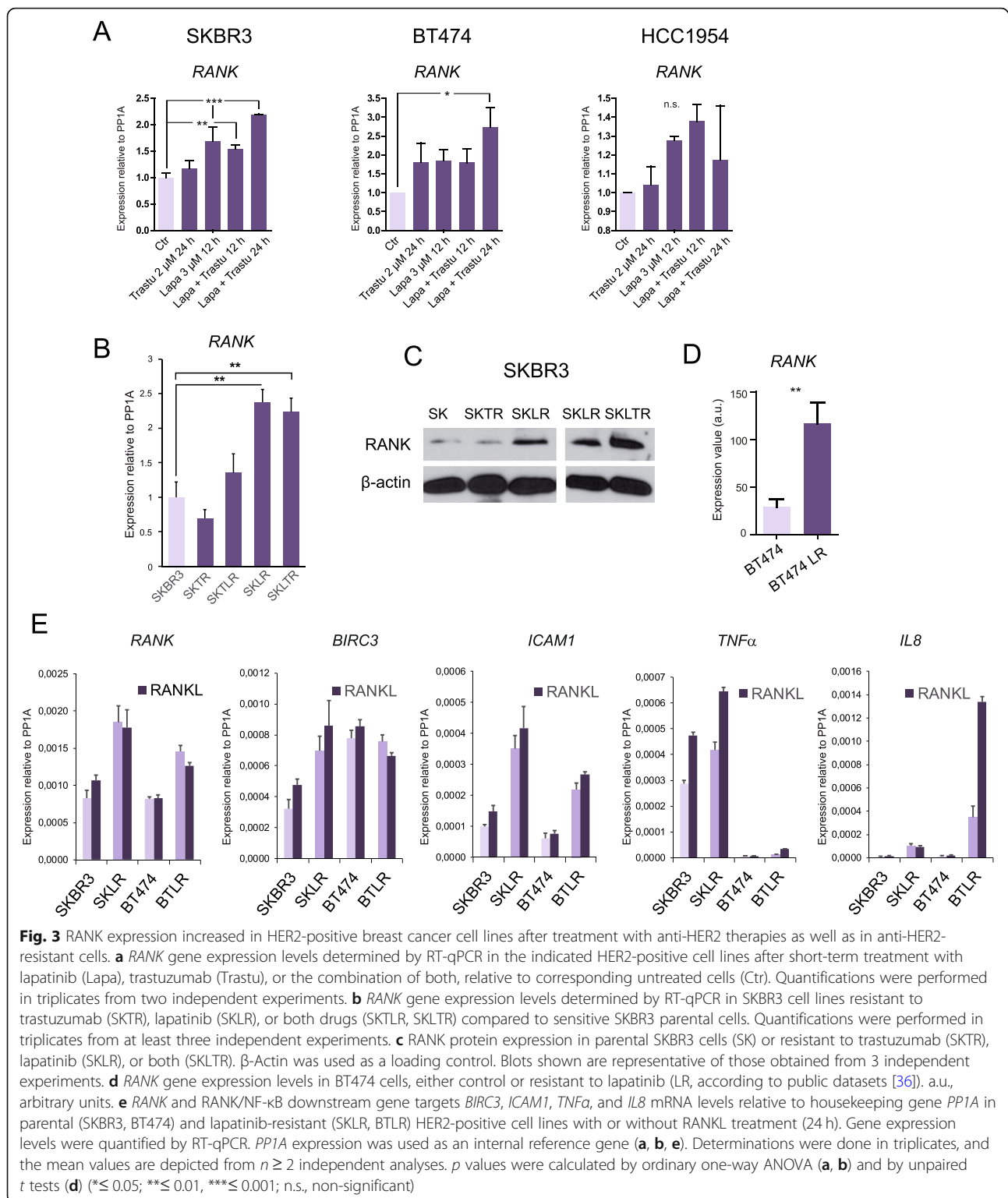
cells with acquired lapatinib resistance (LR) when compared to lapatinib-sensitive parental cells according to public datasets, platform ID: GPL570 [36]; (Fig. 3d), an increase we verified by RT-qPCR (Fig. 3e).

To confirm that the elevated *RANK* expression levels were accompanied by increased activation of the *RANK* signaling pathway, the expression of *RANK* downstream gene targets *BIRC3*, *ICAM1*, *TNF α* , and *IL8*, indicative of NF- κ B pathway activation [37, 38], was analyzed in sensitive and lapatinib-resistant (LR) cells treated with or without *RANKL*. Lapatinib-resistant SKLR cells showed higher gene expression levels of *RANK*, *BIRC3*, *ICAM1*, *TNF α* , and *IL8* compared with control SKBR3 cells, and their levels were further increased after pathway stimulation with *RANKL*, except for *IL8* (Fig. 3e). In lapatinib-resistant BTLR, increased expression of *RANK* and its downstream targets *ICAM1* and *IL8* was detected, and their levels increased further upon *RANKL* stimulation compared to sensitive BT474 cells. In these cells, *BIRC3* expression did not change whereas *TNF α* was barely expressed (Fig. 3e).

Taken together, *RANK* expression increased after dual treatment with lapatinib and trastuzumab in HER2-positive human breast cancer cell lines, mimicking the results seen in breast cancer samples from the PAMELA trial (Fig. 2b). Additionally, two HER2-positive cell lines (SKBR3 and BT474) with acquired resistance to lapatinib (SKLR and BTLR) showed increased expression of *RANK* and several downstream targets, when compared to their respective parental controls (Fig. 3b–e).

RANK overactivation increases NF- κ B signaling and resistance to lapatinib

To verify that *RANK* plays a direct role in the cellular response to lapatinib, we studied the consequences of *RANKL* stimulation and *RANK* loss in control and lapatinib-resistant SKBR3 cell lines. A small increase in lapatinib tolerance was observed in SKLR but not SKBR3 cells in the presence of *RANKL* (Fig. S5A). *RANK* silencing with two specific shRNAs reduced lapatinib resistance in SKLR cells, although sensitivity was not fully restored to the levels observed in WT cells (Fig. 4a, b). These results indicate that the activation of *RANK* signaling contributes to lapatinib resistance; however, it is not the only mechanism responsible for the emergence



of resistance in SKLR cells. This is in line with the multiple anti-HER2 resistance mechanisms reported for these cells [39–41].

Increased I κ B and p65 phosphorylation was observed in lapatinib-resistant SKLR compared to SKBR3 cells

upon RANKL stimulation (Fig. 4c, Fig. S5B and C), confirming the elevated NF- κ B signaling in lapatinib-resistant cells. As expected, RANKL-induced NF- κ B activation was abrogated upon RANK silencing in SKLR cells. RANKL treatment did not significantly alter the

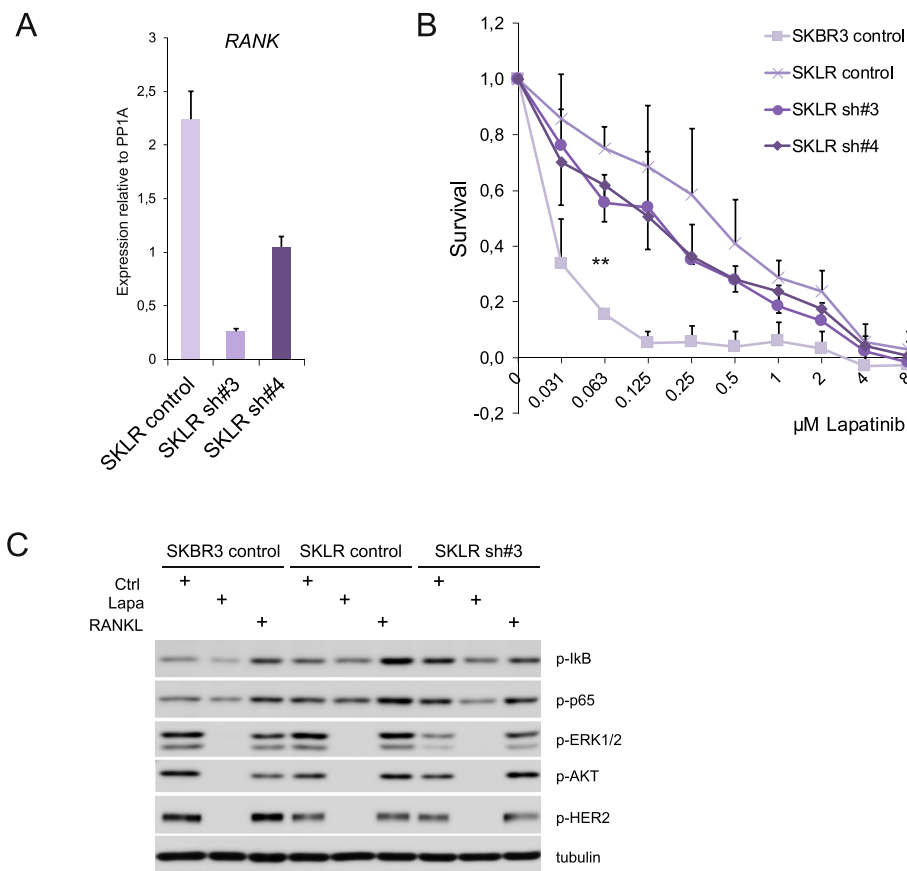


Fig. 4 RANK knockdown slightly resensitizes SKLR cells to lapatinib. **a** The expression levels of *RANK* mRNA in lapatinib-resistant SKLR cells stably transduced with non-targeting (control) or two independent RANK knock-down (sh#3 and #4) vectors. *RANK* expression values were quantified by RT-qPCR relative to *PP1A* gene expression. Quantifications were performed in triplicates. **b** Relative number of living (relative survival) cells stably transduced with control (SKBR3 and SKLR), sh#3 or sh#4 (SKLR) and incubated for 4 days with the indicated concentrations of lapatinib. Cells were seeded in growth media; 24 h later lapatinib was added and cells were analyzed with CCK8 as detailed in the “Methods” section. The mean values and SD of four independent experiments are shown. For each experiment, data was obtained from quintuplicates. Paired *t* tests were done between the groups, and the two-tailed *p* value is depicted (**). In accordance with the lower expression of RANK achieved, sh#3 significantly reduced survival compared to SKLR control cells at 0.063 ($p = 0.0097$), 0.125 ($p = 0.0055$), and 0.25 ($p = 0.0003$) μM of lapatinib. For sh#4, a significant reduction in survival was observed at 0.125 μM of lapatinib ($p = 0.014$). The significance of relative survival was calculated for each concentration using two-tailed *p* values for one sample *t* test. **c** Western blot showing the levels of NF- κB (p-p65, p-I κB) and HER2 (p-HER2, p-ERK1/2, p-AKT) pathway activation in control SKBR3, lapatinib-resistant SKLR, and sh#3 SKLR cells treated with RANKL or lapatinib. Cells were serum-starved for 12 h and then treated with lapatinib (2 h) or RANKL (10 min) before processing them. Tubulin was used as a loading control (see Fig. S5B for total protein levels and Fig. S5C for relative quantifications)

phosphorylation status of AKT nor ERK in SKBR3, SKLR, and the RANK-silenced cells (Fig. 4c, S5B and C). After lapatinib treatment, HER2, AKT, and ERK1/2 protein phosphorylation levels were undetectable in all cell lines, but baseline phosphorylation of p65 and I κB was maintained (Fig. 4c, S5B and C), demonstrating that NF- κB activation is not dependent on ErbB signaling and may support the survival of HER2-positive breast cancer cells in the presence of lapatinib.

To test if RANK signaling and enhanced NF- κB activation may directly contribute to resistance, we stably transduced HER2-positive cell lines with RANK overexpressing (psD69-RANK) and empty control (psD69-

empty) vectors. RANK overexpression was confirmed by increased *RANK* mRNA levels (Fig. 5a) and induction of NF- κB downstream targets (*BIRC3*, *ICAM1*, *TNF α* , and *IL8*) in SKBR3, BT474, and HCC1954 cells (Fig. 5b). These RANK-overexpressing cell lines showed enhanced expression of all NF- κB targets analyzed after RANKL treatment compared to the corresponding parental cells (Fig. 5b). Next, we tested whether increased activation of RANK signaling would alter the cell response to lapatinib; RANKL stimulation of control cells (empty) did not alter lapatinib sensitivity (Fig. 5c). In contrast, RANK overexpression coupled with RANKL treatment resulted in an increased resistance to lapatinib in all HER2-

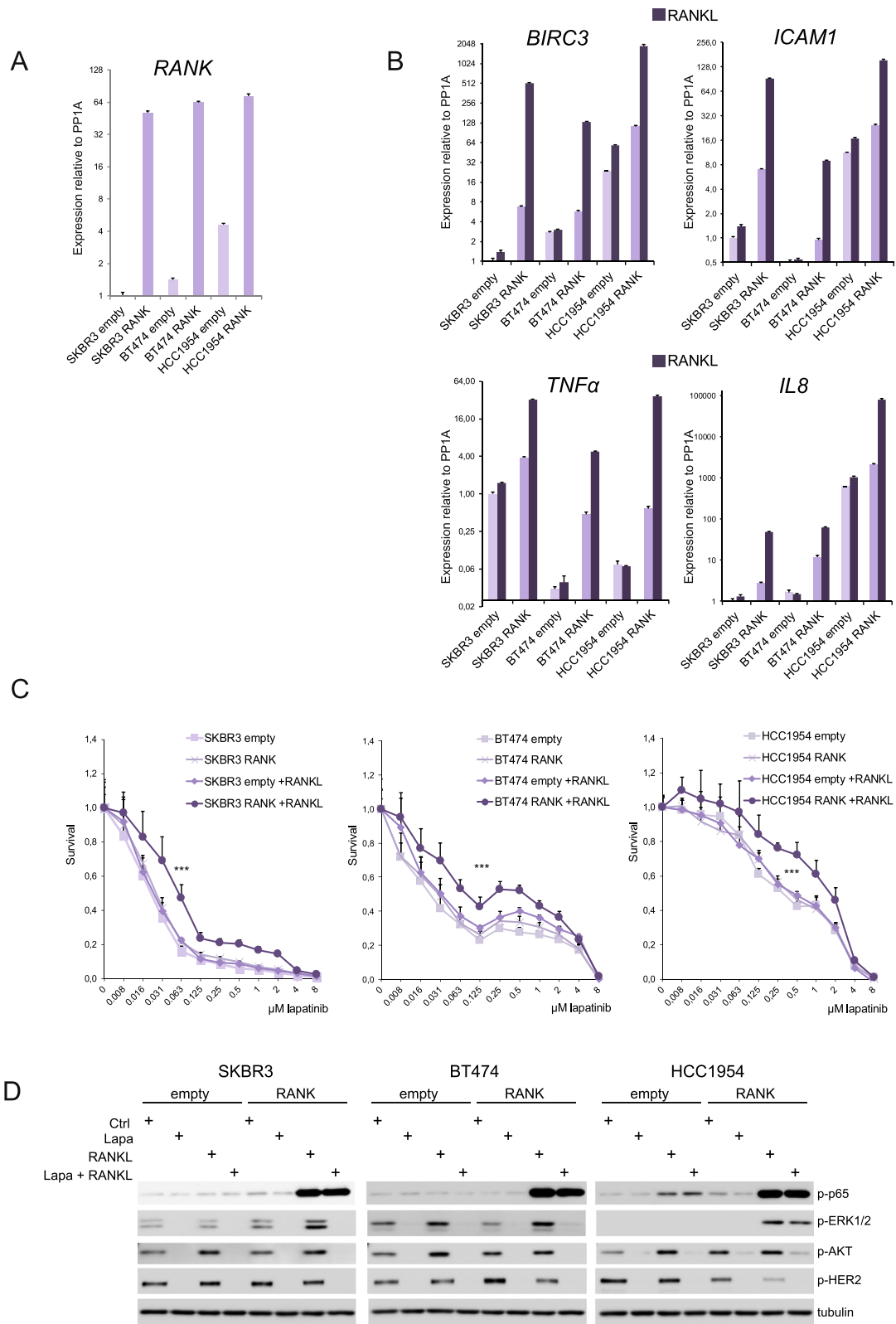


Fig. 5 (See legend on next page.)

(See figure on previous page.)

Fig. 5 Overactivation of RANK signaling in HER2-positive cell lines increased NF- κ B activation and lapatinib resistance. **a** Expression levels of *RANK* mRNA in HER2-positive SKBR3, BT474, and HCC1954 cells stably transduced with control (empty) or RANK-overexpressing (RANK) vectors. *RANK* expression values were quantified by RT-qPCR relative to *PP1A* gene expression. Experiments were performed in triplicates and standard error is depicted. **b** Expression levels of RANK/NF- κ B downstream gene targets *BIRC3*, *ICAM1*, *TNFA*, and *IL8* relative to *PP1A* gene expression in cells described in **a**, with and without RANKL treatment (24 h). Experiments were performed in triplicates and standard error is depicted. **c** Relative number of living (relative survival) SKBR3, BT474, and HCC1954 cells stably transduced with control (empty) or RANK-overexpressing (RANK) vectors incubated for 4 days with the indicated concentrations of lapatinib and/or stimulated with RANKL. Cells were seeded in growth media with/without 100 ng/ml RANKL; 24 h later, lapatinib was added and cells were analyzed with CCK8 after 4 days as detailed in the “Methods” section. A representative experiment out of three independent experiments is shown. For each experiment, data was obtained from triplicates and SD, and a two-way ANOVA *p* value is included. **d** Western blot analyses of NF- κ B (p-p65) and HER2 (p-HER2, p-ERK1/2, and p-AKT) pathway activation in cells depicted in **c**. Before collecting the cells, they were cultured in media without FBS for 12 h and pretreated with/without lapatinib for 2 h followed by 10 min stimulation with RANKL. Representative blots from three independent experiments are shown. Tubulin was used as a loading control (see Fig. S6B for total protein levels, Fig. S6C for quantifications and Fig. S7 for EGF/HRG stimulations)

positive cell lines tested (Fig. 5c), and this effect was abrogated by the RANKL inhibitor denosumab as expected (Fig. S6A).

We then analyzed RANK downstream signaling in these cell lines after treatment with lapatinib and/or RANKL. p65 was strongly phosphorylated in RANK-overexpressing cell lines upon RANKL treatment and in parental HCC1954 cells fitting with the higher RANK expression levels of these cells (Fig. 5d, Fig. S6B and C). Phosphorylation of p65 was not affected by lapatinib treatment. ERK1/2 phosphorylation levels increased after RANKL treatment to a greater extent in the RANK-overexpressing cells compared to control ones (Fig. 5d, Fig. S6B and C). AKT phosphorylation increased after RANKL stimulation in all cells irrespectively of RANK levels. Interestingly, RANKL-mediated activation of ERK1/2 and AKT in SKBR3 and BT474 cells overexpressing RANK was completely abrogated in the presence of lapatinib, meaning that ErbB signaling is required for RANK/RANKL-driven activation of ERK and AKT in these cells. In HCC1954 cells, AKT phosphorylation was also abolished by lapatinib. In contrast, the increased p-ERK levels upon RANKL stimulation in HCC1954 RANK-overexpressing cells were not affected by lapatinib (Fig. 5d, Fig. S6B and C).

In summary, enhanced RANK signaling in HER2-positive cells led to higher NF- κ B activation and increased lapatinib resistance.

RANK and HER2 physically and functionally interact

To investigate whether RANK/RANKL activation of ERK and AKT might take place, at least partially, via direct crosstalk with ErbB receptors, we compared the phosphorylation levels of HER2 in cells with and without RANK overexpression upon RANKL stimulation. RANK overexpression led to higher levels of p-HER2 in SKBR3 and BT474, but not in HCC1954 cells, compared with the corresponding controls (Fig. 5d, Fig. S6B and C). Importantly, in all HER2-positive cell lines, concomitant

RANK overexpression and stimulation with RANKL resulted in decreased HER2 phosphorylation, indicating that RANKL might impinge on the HER2/ErbB signaling pathway (Fig. 5d).

To further study the putative crosstalk between RANK and ErbB signaling, we analyzed NF- κ B and ErbB signaling after stimulation with ErbB ligands in RANK-overexpressing HER2-positive cell lines and corresponding controls at different time points. A slight increase in p65 phosphorylation was observed in SKBR3 and BT474 RANK-overexpressing cells compared with control cells (Fig. S7). EGF stimulation faintly increased p-p65 levels in HER2-positive cell lines, but this was not observed after heregulin (HRG) treatment (Fig. S7). As extensively reported [42], treatment with EGF and HRG efficiently induces ERK phosphorylation in all HER2-positive cell lines (Fig. S7), but no clear differences were observed between RANK-overexpressing cells and corresponding controls. Of note, 5 min after ErbB ligand stimulation, pERK levels are higher but a decrease in HER2 phosphorylation was observed, accompanied by less pERK and pHER2 after 10 min of ErbB ligand stimulation (Fig. S7). Thus, the reduced HER2 phosphorylation observed in RANK-overexpressing cells 10 min after RANKL stimulation may reflect previous activation of HER2/ERK signaling.

Due to the change in HER2 phosphorylation upon activation of RANK signaling with RANKL, we hypothesized that the two receptors might physically interact. To enable efficient immunoprecipitation and detection, we transiently co-expressed affinity-tagged versions of the receptors in HEK293 cells, including an amino (742-NTF) [30] and a carboxy-terminal fragment of HER2 (611-CTF) [31]. As shown in Fig. 6a, RANK-V5 was detected after immunoprecipitation of HER2 or 611-CTF HER2, but not in 742-NTF or any of the control samples (IgG), indicating that RANK interacts with the carboxy-terminal region of HER2. The reverse immunoprecipitation of RANK-V5 corroborated these results (Fig. 6b). To confirm the interaction between the two receptors

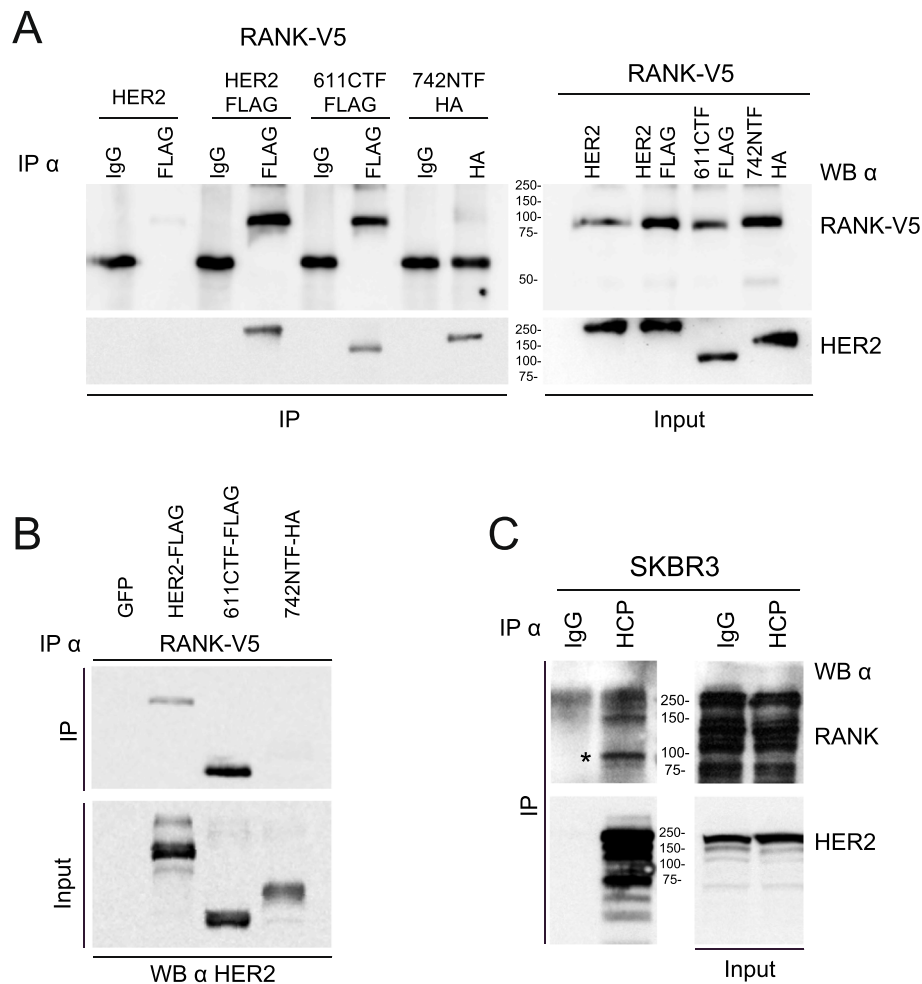


Fig. 6 Co-immunoprecipitation of RANK and HER2. **a** Immunoprecipitation (IP) against HER2 was performed in HEK293 cells transfected with RANK-V5 and HER2, HER2-FLAG, a carboxy-terminal fragment of HER2 (611-CTF) or an amino-terminal fragment of HER2 (742-NTF). IP was performed using anti-FLAG, anti-HA, or control IgG antibodies as indicated. RANK was detected by blotting the immunoprecipitates (IP, left upper panel) or the whole lysates (input, right upper panel) with the V5 antibody. HER2 was detected in IPs (left lower panel) and input (right lower panel) using the 32H2 antibody that detects all forms of HER2. **b** IP against RANK-V5 was performed in HEK293 cells transfected with RANK-V5 and GFP, HER2-FLAG, a carboxy-terminal fragment of HER2 (611-CTF) or an amino-terminal fragment of HER2 (742-NTF) using the V5 antibody. In the IP and input, HER2 was detected using the 32H2 antibody. **c** IP against endogenous HER2 was performed in SKBR3 cells using trastuzumab (Herceptin-HCP) or a control IgG. Endogenous RANK and HER2 were detected in IP (RANK immunoprecipitated by HER2 is indicated by an asterisk (*) in the upper panel) and input samples

under endogenous expression levels in the context of breast cancer, we chose SKBR3 cells that, compared to other breast cancer cell lines, express higher levels of HER2 and intermediate/lower levels of RANK and do not express EGFR [43]. HER2 was immunoprecipitated with the antibody trastuzumab (HCP) that binds to the HER2 extracellular domain, and the presence of RANK in the immunoprecipitate was tested by Western blotting. As seen in Fig. 6c, trastuzumab precipitated endogenous RANK demonstrating that the two receptors physically interact in breast cancer cells in an EGFR-independent manner.

Discussion

A crosstalk between RANK and EGFR signaling has been described in the context of osteoclast differentiation [44], as well as in breast cancer for a particular RANK truncated isoform [45]. In the mammary gland, we found that pharmacological inhibition of RANKL decreases tumorigenesis and lung metastases in the MMTV-ErbB (Neu) transgenic mouse model [9]. In the same line, MMTV-ErbB mice with a heterozygous RANK deletion showed decreased pulmonary metastasis than RANK WT MMTV-ErbB controls [15]. In addition, RANKL treatment increased lung metastases in both

FVB/N and MMTV-ErbB animals [15]. More recently, a review [46] followed by an article with experimental data [47], suggested the combination of RANK and HER2 signaling inhibition as a new strategy for the treatment of HER2-positive breast carcinomas.

In this study, we have shown that *RANK* gene expression increased after dual treatment with lapatinib and trastuzumab in HER2-positive tumor samples from the PAMELA clinical trial [22] and in HER2-positive breast cancer cell lines. These observations would point to increased RANK signaling in patients treated with anti-HER2 drugs. We also observed that the percentage of patients with RANK tumor expression doubled in the context of HER2 resistance when compared to treatment-naïve HER2-positive breast tumors. Furthermore, both SKBR3- and BT474 HER2-positive cell lines with acquired lapatinib resistance displayed increased RANK expression and pathway activation compared to their respective lapatinib-sensitive controls. Thus, our combined analyses of HER2-positive breast cancer samples and cell lines demonstrate that RANK expression is higher in HER2-resistant breast cancer. RANK loss moderately sensitized lapatinib-resistant cells to the drug, and overactivation of RANK signaling increased lapatinib resistance in HER2-positive cell lines (SKBR3, BT474, and HCC1954). Based on these results, one could speculate that activation of RANK signaling may allow breast cancer cells to survive anti-HER2 therapies and the benefit of combining denosumab with HER2 inhibitors as postulated by [47].

NF- κ B signaling has been shown to enhance ErbB2-induced tumor growth both in vitro and in immune-competent mice [48, 49]. Increased NF- κ B activation downstream of RANK [50] may also contribute to lapatinib resistance. Hyperactive NF- κ B signaling has been proposed as a possible resistance mechanism after lapatinib treatment in HER2-positive [51] and triple-negative breast cancer [52, 53]. In HER2-positive breast cancer, lapatinib-resistant cells show increased NF- κ B levels and do not respond to single HER2 or NF- κ B inhibitors, but to a combination of both [51]. The NF- κ B expression is normally linked to invasive high-grade tumors, and several NF- κ B inhibitors are currently being investigated [54, 55]. Chen and colleagues showed that lapatinib treatment induced a constitutive activation of NF- κ B through Src-dependent p65 and I κ B α phosphorylation, sensitizing the cells to proteasome inhibitors [52]; our data suggest that increased RANK being a well-known regulator of NF- κ B may also play a role, although we cannot discard the contribution of other RANK-driven downstream pathways. The phosphorylation of I κ B α , leading to its degradation and resulting in p50/p65 heterodimer nuclear translocation, is mediated by the IKK complex (comprising IKK α , IKK β , and IKK γ /NEMO)

[56, 57]. HER2 itself was shown to activate NF- κ B via the canonical pathway involving IKK α in HER2-positive and ER-negative breast cancer cells [58]. IKK α also mediates NF- κ B activation in mammary cells during pregnancy and after RANKL stimulation [59]. In our study, we did not observe clear changes in p65 phosphorylation after stimulation with ErbB ligands and the treatment with lapatinib could not counteract p65 phosphorylation driven by RANKL treatment in RANK-overexpressing HER2-positive cell lines, providing an alternative survival path for these cells.

Importantly, we have shown RANK binding to HER2 by co-immunoprecipitation experiments. Accordingly, Zoi et al. recently showed the interaction of RANK with ErbB family members by proximity ligation assays [47]. In this publication, the authors claim that the number of RANK/HER2 dimers in cells correlates with HER2 expression levels. Also, denosumab, trastuzumab, and/or pertuzumab treatment reduces the number of RANK/HER2 dimers whereas RANKL stimulation leads to an increased number of RANK/HER2 dimers [47]. Finally, their data show that RANKL addition decreases the efficacy of HER2 inhibitors [47]. In our hands, a direct interaction between RANK and HER2, independent of EGF, was observed. RANKL stimulation of HER2-positive breast cancer cells overexpressing RANK decreases HER2 phosphorylation, indicating that RANKL influences ErbB2 signaling.

RANKL was shown to promote migration in breast cancer cells after activation of the ERK and AKT pathways [60]. We have also found increased phosphorylation of ERK1/2 and AKT after RANKL treatment in SKBR3 and BT474 cell lines, with either physiological or increased RANK levels by receptor overexpression. Interestingly, we observed that RANKL-mediated induction of ERK1/2 and AKT phosphorylation was completely abrogated after lapatinib treatment in SKBR3 and BT474 cells, again independently of RANK receptor expression levels. These observations and the fact that RANK and HER2 interact suggest that lapatinib inhibits not only EGFR/HER2 tyrosine phosphorylation but also RANK signaling driven by RANKL (e.g., ERK1/2 and AKT). Importantly, in addition to the direct interaction between RANK and HER2, we observed that RANK signaling is functionally linked to the ErbB2 pathway. Additional research is required to address whether the direct RANK/HER2 interaction contributes to the enhanced resistance to lapatinib observed after activation of RANK signaling.

Taken together, we showed that anti-HER2 treatment and resistance acquisition both raised RANK expression levels in HER2-positive clinical breast tumors and cell lines. Also, enhanced RANK signaling increased lapatinib resistance in HER2 breast cancer cells. We found

that RANK and HER2 physically and functionally interact. Altogether, these results hint to a dual RANK and HER2 inhibition therapy for RANK-expressing HER2-positive breast cancer patients, whose benefit remains to be tested.

Conclusions

In summary, we showed that RANK is expressed in HER2-positive breast cancer samples, particularly in patients resistant to anti-HER2 blocking therapy. The RANK expression is often associated with younger age, hormone receptor-negative status, and higher histological grade and proliferation index. Moreover, in HER2-positive breast cancer samples from the PAMELA trial, RANK expression increased upon treatment with lapatinib and trastuzumab. This was confirmed in vitro in several HER2-positive human breast cancer cell lines suggesting that RANK signaling may contribute to the development of lapatinib resistance. Indeed, RANK-overexpressing HER2-positive cell lines showed increased resistance to lapatinib and higher NF- κ B pathway activation. Finally, we demonstrated that RANK physically and functionally interacted with HER2 suggesting a RANK/HER2 crosstalk. Together, these results suggest that inhibition of RANK signaling may improve the response to anti-HER2 therapies in RANK-positive, HER2-positive breast cancer patients.

Supplementary Information

The online version contains supplementary material available at <https://doi.org/10.1186/s13058-021-01390-2>.

Additional file 1: Figure S1. TMA H-scores and controls. A. RANK and RANKL H-scores in HER2-positive breast cancer samples, treatment-naïve (left panels) or anti-HER2-resistant (right panels). In treatment-naïve TMAs, each number represents a "core" from a single patient. In anti-HER2-resistant TMAs, scored independent tumor cores are numbered for each patient (after the symbol #). B. Representative pictures of human breast tumors from patient-derived xenografts used as positive and negative controls for RANK and RANKL IHC.

Additional file 2: Figure S2. RANK and RANKL staining in TMAs. A. Pictures of RANK and RANKL protein expression analyzed by IHC in the TMA cores from the treatment-naïve cohort. B. Pictures of RANK and RANKL protein expression analyzed by IHC in the TMA cores from the anti-HER2 resistant cohort.

Additional file 3: Figure S3. RANK and RANKL expression in breast cancer samples from the PAMELA clinical trial. A. Expression of RANK and RANKL across the intrinsic molecular subtypes from the PAMELA study. P values were calculated by comparing mean values across all groups. B. Scatter plots of RANK and RANKL expression versus ERBB2 expression for baseline samples in the PAMELA study. Solid line in each figure represents the regression line. Pearson correlation coefficient (r) with significance (p value) is presented in each figure. C. Pearson correlation between single genes and gene expression signatures evaluated in baseline samples from the PAMELA study.

Additional file 4: Figure S4. RANK but not RANKL expression increased after dual anti-HER2 therapy in HR+ and HR- patient samples ($n = 151$) from the PAMELA trial. A and B. Ladder plots (left panels) showing RANK and RANKL gene expression in PAMELA HER2-positive HR+ (A) and HR- (B) tumors before (baseline) and after (surgery) dual anti-HER2 treatment.

An increase in gene expression is represented in red and a decrease in blue. Each line represents a tumor sample from one patient. P values in A were calculated by comparing mean values between both groups and in B were determined by paired two-tailed t-tests. Density plots (right panels) showing RANK and RANKL gene expression in PAMELA HER2-positive HR+ (A) and HR- (B) tumors before (baseline) and after (surgery) treatment.

Additional file 5: Figure S5. A. Relative number of living (relative survival) SKBR3 and SKLR control cells incubated for 4 days with the indicated concentrations of lapatinib and stimulated with RANKL. Cells were seeded in growth media, 100 ng/ml RANKL were added 24h after seeding, lapatinib was added 24 h later and cells were analyzed with CCK8 as detailed in methods. Determinations were done in triplicates, mean values are depicted from $n = 5$ independent experiments and SD and p -value (**) calculated by one-way ANOVA is depicted ($p \leq 0.05$ for SKBR3 vs SKLR and SKLR +RANKL, SKBR3 +RANKL vs SKLR and SKLR +RANKL; n.s. for SKBR3 vs SKBR3 +RANKL and SKLR vs SKLR +RANKL). Significance of relative survival was calculated for each concentration using two-tailed p values for one sample t test. RANKL significantly increased survival of SKLR cells at 0.018 μ M of lapatinib ($p = 0.019$). **B.** Western blot showing the total levels of κ B, p65, ERK1/2, AKT and HER2 in SKBR3 control, SKLR control and SKLR sh#3 cells treated with RANKL or lapatinib as depicted in Fig. 4c. Cells were serum starved for 12 h and then treated with lapatinib (2 h) or RANKL (10 min) before processing them. Tubulin was used as a loading control. **C.** Table depicting the relative phospho-protein levels of the indicated proteins from the western blots shown in Fig. 4c and Fig. S5B determined by densitometry analyses with Image J.

Additional file 6: Figure S6. A. Relative number of living (relative survival) SKBR3 RANK cells stimulated with RANKL in the presence or absence of denosumab (DNS) and incubated for 4 days with the indicated concentrations of lapatinib. Cells were seeded in growth media with/without denosumab (1 μ g/ml), lapatinib was added after 24 h stimulation with 100 ng/ml RANKL, and cell viability was analyzed with CCK8 as detailed in methods. Determinations were done in triplicates, mean values from $n \geq 2$ independent experiments and SD are depicted. **B.** Western blot analyses of total levels of p65, ERK1/2 and HER2 in whole lysates from SKBR3, BT474 and HCC1954 cells stably transduced with control (empty) or RANK overexpressing (RANK) vectors as depicted in Fig. 5d. Before collecting the cells, they were cultured in media without FBS for 12 h, pretreated with/without lapatinib for 2 h followed by 10 min stimulation with RANKL. Tubulin was used as a loading control. **C.** Table depicting the relative phospho-protein levels of the indicated proteins from the western blots shown in Fig. 5d and Fig. S6B determined by densitometry analyses with Image J.

Additional file 7: Figure S7. Western blot analyses of HER2 (p-HER2, p-ERK1/2) and NF- κ B (p-p65) pathway activation in SKBR3, BT474 and HCC1954 cells stably transduced with empty or RANK overexpressing (RANK) vectors. Cells were cultured in media without FBS for 12 h, followed by stimulation with EGF (100 ng/ml) (upper panels) or heregulin (HRG 10 ng/ml) (lower panels) for the indicated times. Tubulin was used as a loading control.

Additional file 8: Supplementary Table 1.

Abbreviations

EGFR: Epidermal growth factor receptor; ER: Estrogen receptor; HER2: Epidermal growth factor receptor 2; IHC: Immunohistochemistry; IP: Immunoprecipitation; NF- κ B: Nuclear factor kappa B; PR: Progesterone receptor; RANK: Receptor activator of NF- κ B; RANKL: Receptor activator of NF- κ B ligand; RT-qPCR: Reverse transcriptase quantitative PCR; TMA: Tissue microarray

Acknowledgements

We thank all the patients who contributed to this study. We would like to thank Maria Subijana and Elba López for their contributions, Dr. E. López (Pathology Department Director, Hospital Josep Trueta, Girona, Spain), and the Xarxa de Bancs de Tumors de Catalunya sponsored by Pla Director d'Oncologia de Catalunya (XBTC).

Authors' contributions

EGS and TP designed the study. ASM, SPa, KM, BM, TP, PG, SB, JGM, MC, MJ, SP, AP, MTSM, GV, MA, EAR, ARG, PGS, CM, SL, JA, and AP collected the data. ASM, SPa, KM, BM, TP, MC, SP, GV, MA, PGS, and EGS assembled the data. All authors analyzed the data. ASM, PGS, and EGS wrote the manuscript. All authors critically reviewed the drafts of the manuscript and read and approved the final manuscript.

Funding

Work in the laboratory of Eva González Suárez is supported by the Spanish Ministerio de Ciencia, Innovación y Universidades, which is part of Agencia Estatal de Investigación (AEI) (SAF2017-86117-R), a Career Catalyst Grant from the Susan Komen Foundation (CCR13262449), the European Research Council (ERC) under the European Union's Horizon 2020 research and innovation programme ERC Consolidator grant (grant agreement No682935), and the Catalan Government 2017SGR00665. We thank IDIBELL and CERCA Programme/Generalitat de Catalunya for institutional support. This work was in part supported by a grant from La Marató de TV3 20131530, to Eva González Suárez and Teresa Puig. The work was in part supported by grants to Teresa Puig from the Spanish Instituto de Salud Carlos III (ISCIII; FIS PI11/00692 and PI14/00329) and the Catalan Government (2017SGR00385). Work in the laboratory of Joaquín Arribas was supported by the ISCIII (PI19/01181 and CB16/12/00449), the Breast Cancer Research Foundation (BCRF-19-008), and the Asociación Española Contra el Cáncer (GCAEC19017ARRI). BM was a recipient of a PERIS fellowship (Departament de Salut, Generalitat de Catalunya). The work in the group of Aleix Prat is supported by GlaxoSmithKline (to SOLTI), the ISCIII (PI16/00904), a Career Catalyst Grant from the Susan Komen Foundation, Banco Bilbao Vizcaya Argentaria (BBVA) Foundation, Pas a Pas, Save the Mama, and Breast Cancer Research Foundation. Emad A Rakha and Andrew R Green are part of the PathLAKE digital pathology consortium supported by a £50m investment from the Data to Early Diagnosis and Precision Medicine strand of the UK Government's Industrial Strategy Challenge Fund (UKRI).

Availability of data and materials

Data generated during this study are included in this published article (and its supplementary information files), and datasets generated and analyzed supporting the findings of this study are available from the corresponding authors upon reasonable request.

Ethics approval and consent to participate

This work obtained ethics approval to use the human tissue samples by the North West – Greater Manchester Central Research Ethics Committee under the title; Nottingham Health Science Biobank (NHSB), reference number 15/NW/0685. Informed consent was obtained from all individuals prior to surgery to use their tissue materials in research. This study was performed in compliance with the clinical research guidelines established by the Dr. Josep Trueta University Hospital Ethics Committee. This study was approved by the Institutional Review Board of Hospital Vall d'Hebron (Barcelona) AC/R (AG)110/2013(3755). All patients provided written informed consent.

Consent for publication

Not applicable.

Competing interests

EGS has served on advisory boards for Amgen and has received research funding from Amgen. AP has declared personal honoraria from Pfizer, Novartis, Roche, MSD Oncology, Lilly, and Daiichi Sankyo; travel, accommodations, and expenses paid by Daiichi Sankyo; and research funding from Roche and Novartis; consulting/advisory role for NanoString Technologies, Amgen, Roche, Novartis, Pfizer, and Bristol-Myers Squibb. SP has received travel and accommodation grants from Roche and Novartis and holds consulting/advisory roles for Polyphor and Roche.

Author details

¹Oncobell, Bellvitge Biomedical Research Institute (IDIBELL), L'Hospitalet de Llobregat, Barcelona, Spain. ²Present Address: German Mouse Clinic, Institute of Experimental Genetics, HMGU, Neuherberg 85764, Germany. ³New Therapeutics Targets Lab (TargetsLab), Department of Medical Sciences, University of Girona, Girona, Spain. ⁴Preclinical Research Program, Vall d'Hebron Institute of Oncology (VHIO), Barcelona, Spain. ⁵Centro de

Investigación Biomédica en Red de Cáncer (CIBERONC), Madrid, Spain.

⁶Translational Genomics and Targeted Therapeutics in Solid Tumors, August Pi i Sunyer Biomedical Research Institute (IDIBAPS), Barcelona, Spain. ⁷SOLTI Breast Cancer Research Group, Barcelona, Spain. ⁸Department of Medical Oncology, Hospital Clinic, Barcelona, Spain. ⁹Present Address: Department of Biomedicine, Department of Surgery, University Hospital Basel, University of Basel, Basel, Switzerland. ¹⁰Molecular Oncology, Spanish National Cancer Research Centre (CNIO), Madrid, Spain. ¹¹Department of Medical Oncology, Breast Unit, Catalan Institute of Oncology (ICO), University Hospital of Bellvitge IDIBELL, L'Hospitalet de Llobregat, Barcelona, Spain. ¹²Pathology Department, University Hospital of Bellvitge, IDIBELL, Barcelona, Spain. ¹³Medical Oncology Department, Catalan Institute of Oncology (ICO), Girona, Spain. ¹⁴Division of Cancer and Stem Cells, School of Medicine, University of Nottingham Biodiscovery Institute, University Park, Nottingham NG7 2RD, UK. ¹⁵Biomolecular Mass Spectrometry and Proteomics Bijvoet Center, Utrecht University, Utrecht, The Netherlands. ¹⁶Medicine Department, University of Barcelona, Barcelona, Spain.

Received: 24 April 2020 Accepted: 11 January 2021

Published online: 30 March 2021

References

- Moasser MM. The oncogene HER2: its signaling and transforming functions and its role in human cancer pathogenesis. *Oncogene*. 2007; 26(45):6469–87.
- Slamon DJ, Clark GM, Wong SG, Levin WJ, Ullrich A, McGuire WL. Human breast cancer: correlation of relapse and survival with amplification of the HER-2/neu oncogene. *Science*. 1987;235(4785):177–82.
- Pernas S, Tolane SM. HER2-positive breast cancer: new therapeutic frontiers and overcoming resistance. *Ther Adv Med Oncol*. 2019;11:1758835919833519.
- Chumsri S, Li Z, Serie DJ, Mashadi-Hossein A, Colon-Otero G, Song N, et al. Incidence of late relapses in patients with HER2-positive breast cancer receiving adjuvant trastuzumab: combined analysis of NCCTG N9831 (Alliance) and NRG oncology/NSABP B-31. *J Clin Oncol*. 2019; 37(35):3425–35.
- von Minckwitz G, Huang CS, Mano MS, Loibl S, Mamounas EP, Untch M, et al. Trastuzumab emtansine for residual invasive HER2-positive breast cancer. *N Engl J Med*. 2019;380(7):617–28.
- Braso-Maristany F, Griguolo G, Pascual T, Pare L, Nuciforo P, Llombart-Cussac A, et al. Phenotypic changes of HER2-positive breast cancer during and after dual HER2 blockade. *Nat Commun*. 2020;11(1):385.
- Lacey DL, Boyle WJ, Simonet WS, Kostenuik PJ, Dougall WC, Sullivan JK, et al. Bench to bedside: elucidation of the OPG-RANK-RANKL pathway and the development of denosumab. *Nat Rev Drug Discov*. 2012;11(5):401–19.
- Yoldi G, Pellegrini P, Trinidad EM, Cordero A, Gomez-Miragaya J, Serra-Musach J, et al. RANK signaling blockade reduces breast cancer recurrence by inducing tumor cell differentiation. *Cancer Res*. 2016; 76(19):5857–69.
- Gonzalez-Suarez E, Jacob AP, Jones J, Miller R, Roudier-Meyer MP, Erwert R, et al. RANK ligand mediates progesterin-induced mammary epithelial proliferation and carcinogenesis. *Nature*. 2010;468(7320):103–7.
- Schramek D, Leibbrandt A, Sigl V, Kenner L, Pospisilik JA, Lee HJ, et al. Osteoclast differentiation factor RANKL controls development of progesterin-driven mammary cancer. *Nature*. 2010;468(7320):98–102.
- Palafox M, Ferrer I, Pellegrini P, Vila S, Hernandez-Ortega S, Urruticoechea A, et al. RANK induces epithelial-mesenchymal transition and stemness in human mammary epithelial cells and promotes tumorigenesis and metastasis. *Cancer Res*. 2012;72(11):2879–88.
- Pfritznier BM, Branstetter D, Loibl S, Denkert C, Lederer B, Schmitt WD, et al. RANK expression as a prognostic and predictive marker in breast cancer. *Breast Cancer Res Treat*. 2014;145(2):307–15.
- Nolan E, Vaillant F, Branstetter D, Pal B, Giner G, Whitehead L, et al. RANK ligand as a potential target for breast cancer prevention in BRCA1-mutation carriers. *Nat Med*. 2016;22(8):933–9.
- Sigl V, Owusu-Boaitey K, Joshi PA, Kavirayani A, Wirmsberger G, Novatchkova M, et al. RANKL/RANK control Brca1 mutation. *Cell Res*. 2016;26(7):761–74.
- Tan W, Zhang W, Strasner A, Grivennikov S, Cheng JQ, Hoffman RM, et al. Tumour-infiltrating regulatory T cells stimulate mammary cancer metastasis through RANKL-RANK signalling. *Nature*. 2011;470(7335):548–53.

16. Shaker OG, Helmy HS. Circulating bone-related markers and YKL-40 versus HER2 and TOPO2a in bone metastatic and nonmetastatic breast cancer: diagnostic implications. *Clin Breast Cancer*. 2018;18(3):e321–e8.
17. Vernieri C, Milano M, Brambilla M, Mennitto A, Maggi C, Cona MS, et al. Resistance mechanisms to anti-HER2 therapies in HER2-positive breast cancer: current knowledge, new research directions and therapeutic perspectives. *Crit Rev Oncol Hematol*. 2019;139:53–66.
18. Goutsouliak K, Veeraraghavan J, Sethunath V, De Angelis C, Osborne CK, Rimawi MF, et al. Towards personalized treatment for early stage HER2-positive breast cancer. *Nat Rev Clin Oncol*. 2019. *Nat Rev Clin Oncol*. 2020;17(4):233–250.
19. Elston CW, Ellis IO. Pathological prognostic factors in breast cancer. I. The value of histological grade in breast cancer: experience from a large study with long-term follow-up. *Histopathology*. 1991;19(5):403–10.
20. Abd El-Rehim DM, Ball G, Pinder SE, Rakha E, Paish C, Robertson JF, et al. High-throughput protein expression analysis using tissue microarray technology of a large well-characterised series identifies biologically distinct classes of breast cancer confirming recent cDNA expression analyses. *Int J Cancer*. 2005;116(3):340–50.
21. Pernas S, Gil-Gil M, de Olza MO, Guma A, Climent F, Petit A, et al. Efficacy and safety of concurrent trastuzumab plus weekly paclitaxel-FEC as primary therapy for HER2-positive breast cancer in everyday clinical practice. *Breast Cancer Res Treat*. 2012;134(3):1161–8.
22. Llombart-Cussac A, Cortes J, Pare L, Galvan P, Bermejo B, Martinez N, et al. HER2-enriched subtype as a predictor of pathological complete response following trastuzumab and lapatinib without chemotherapy in early-stage HER2-positive breast cancer (PAMELA): an open-label, single-group, multicentre, phase 2 trial. *Lancet Oncol*. 2017;18(4):545–54.
23. Parker JS, Mullins M, Cheang MC, Leung S, Voduc D, Vickery T, et al. Supervised risk predictor of breast cancer based on intrinsic subtypes. *J Clin Oncol*. 2009;27(8):1160–7.
24. Prat A, Cheang MC, Galvan P, Nuciforo P, Pare L, Adamo B, et al. Prognostic value of intrinsic subtypes in hormone receptor-positive metastatic breast cancer treated with letrozole with or without lapatinib. *JAMA Oncol*. 2016;2(10):1287–94.
25. McCarty KS Jr, Miller LS, Cox EB, Konrath J, McCarty KS Sr. Estrogen receptor analyses. Correlation of biochemical and immunohistochemical methods using monoclonal anti-receptor antibodies. *Arch Pathol Lab Med*. 1985;109(8):716–21.
26. Gomez-Aleza C, Nguyen B, Yoldi G, Ciscar M, Barranco A, Hernandez-Jimenez E, et al. Inhibition of RANK signaling in breast cancer induces an anti-tumor immune response orchestrated by CD8+ T cells. *Nat Commun*. 2020;11(1):6335.
27. Gonzalez-Suarez E, Branstetter D, Armstrong A, Dinh H, Blumberg H, Dougal WC. RANK overexpression in transgenic mice with mouse mammary tumor virus promoter-controlled RANK increases proliferation and impairs alveolar differentiation in the mammary epithelia and disrupts lumen formation in cultured epithelial acini. *Mol Cell Biol*. 2007;27(4):1442–54.
28. Ruprecht B, Zaal EA, Zecha J, Wu W, Berkers CR, Kuster B, et al. Lapatinib resistance in breast cancer cells is accompanied by phosphorylation-mediated reprogramming of glycolysis. *Cancer Res*. 2017;77(8):1842–53.
29. Blancafort A, Giro-Perafita A, Oliveras G, Palomeras S, Turrado C, Campuzano O, et al. Dual fatty acid synthase and HER2 signaling blockade shows marked antitumor activity against breast cancer models resistant to anti-HER2 drugs. *PLoS One*. 2015;10(6):e0131241.
30. Morancho B, Parra-Palau JL, Ibrahim YH, Bernado Morales C, Peg V, Bech-Serra JJ, et al. A dominant-negative N-terminal fragment of HER2 frequently expressed in breast cancers. *Oncogene*. 2013;32(11):1452–9.
31. Parra-Palau JL, Morancho B, Peg V, Escorihuela M, Scaltriti M, Vicario R, et al. Effect of p95HER2/611CTF on the response to trastuzumab and chemotherapy. *J Natl Cancer Inst*. 2014;106(11):dju291.
32. Parra-Palau JL, Pedersen K, Peg V, Scaltriti M, Angelini PD, Escorihuela M, et al. A major role of p95/611-CTF, a carboxy-terminal fragment of HER2, in the down-modulation of the estrogen receptor in HER2-positive breast cancers. *Cancer Res*. 2010;70(21):8537–46.
33. Azim HA Jr, Peccatori FA, Brohee S, Branstetter D, Loi S, Viale G, et al. RANKL ligand (RANKL) expression in young breast cancer patients and during pregnancy. *Breast Cancer Res*. 2015;17:24.
34. Santini D, Schiavon G, Vincenzi B, Gaeta L, Pantano F, Russo A, et al. Receptor activator of NF- κ B (RANK) expression in primary tumors associates with bone metastasis occurrence in breast cancer patients. *PLoS One*. 2011;6(4):e19234.
35. Jernstrom S, Hongisto V, Leivonen SK, Due EU, Tadele DS, Edgren H, et al. Drug-screening and genomic analyses of HER2-positive breast cancer cell lines reveal predictors for treatment response. *Breast Cancer* (Dove Med Press). 2017;9:185–98.
36. Liu L, Greger J, Shi H, Liu Y, Greshock J, Annan R, et al. Novel mechanism of lapatinib resistance in HER2-positive breast tumor cells: activation of AXL. *Cancer Res*. 2009;69(17):6871–8.
37. Pahl HL. Activators and target genes of Rel/NF-kappaB transcription factors. *Oncogene*. 1999;18(49):6853–66.
38. Yamaguchi N, Yokota M, Taguchi Y, Gohda J, Inoue J. cIAP1/2 negatively regulate RANKL-induced osteoclastogenesis through the inhibition of NFATc1 expression. *Genes Cells*. 2012;17(12):971–81.
39. Chang Y, Park KH, Lee JE, Han KC. Phosphoproteomic analysis reveals PAK2 as a therapeutic target for lapatinib resistance in HER2-positive breast cancer cells. *Biochem Biophys Res Commun*. 2018;505(1):187–93.
40. Feng WW, Wilkins O, Bang S, Ung M, Li J, An J, et al. CD36-mediated metabolic rewiring of breast cancer cells promotes resistance to HER2-targeted therapies. *Cell Rep*. 2019;29(11):3405–20 e5.
41. Tracey N, Creedon H, Kemp AJ, Culley J, Muir M, Klinowska T, et al. HO-1 drives autophagy as a mechanism of resistance against HER2-targeted therapies. *Breast Cancer Res Treat*. 2020;179(3):543–55.
42. Arteaga CL, Engelman JA. ERBB receptors: from oncogene discovery to basic science to mechanism-based cancer therapeutics. *Cancer Cell*. 2014;25(3):282–303.
43. Ostrander JH, Daniel AR, Lofgren K, Kleer CG, Lange CA. Breast tumor kinase (protein tyrosine kinase 6) regulates heregulin-induced activation of ERK5 and p38 MAP kinases in breast cancer cells. *Cancer Res*. 2007;67(9):4199–209.
44. Yi T, Lee HL, Cha JH, Ko SI, Kim HJ, Shin HI, et al. Epidermal growth factor receptor regulates osteoclast differentiation and survival through cross-talking with RANK signaling. *J Cell Physiol*. 2008;217(2):409–22.
45. Sirinian C, Papanastasiou AD, Schizas M, Spella M, Stathopoulos GT, Repanti M, et al. RANK-c attenuates aggressive properties of ER-negative breast cancer by inhibiting NF-kappaB activation and EGFR signaling. *Oncogene*. 2018;37(37):5101–14.
46. Zoi I, Karamouzis MV, Adamopoulos C, Papavassiliou AG. RANKL signaling and ErbB receptors in breast carcinogenesis. *Trends Mol Med*. 2016;22(10):839–50.
47. Zoi I, Karamouzis MV, Xingi E, Sarantis P, Thomaidou D, Lembessis P, et al. Combining RANK/RANKL and ERBB-2 targeting as a novel strategy in ERBB-2-positive breast carcinomas. *Breast Cancer Res*. 2019;21(1):132.
48. Liu M, Ju X, Willmarth NE, Casimiro MC, Ojeifo J, Sakamaki T, et al. Nuclear factor-kappaB enhances ErbB2-induced mammary tumorigenesis and neoangiogenesis in vivo. *Am J Pathol*. 2009;174(5):1910–20.
49. Liu M, Sakamaki T, Casimiro MC, Willmarth NE, Quong AA, Ju X, et al. The canonical NF-kappaB pathway governs mammary tumorigenesis in transgenic mice and tumor stem cell expansion. *Cancer Res*. 2010;70(24):10464–73.
50. Anderson DM, Maraskovsky E, Billingsley WL, Douglall W, Tometsko ME, Roux ER, et al. A homologue of the TNF receptor and its ligand enhance T-cell growth and dendritic-cell function. *Nature*. 1997;390(6656):175–9.
51. Bailey ST, Miron PL, Choi YJ, Kochupurakkal B, Maulik G, Rodig SJ, et al. NF-kappaB activation-induced anti-apoptosis renders HER2-positive cells drug resistant and accelerates tumor growth. *Mol Cancer Res*. 2014;12(3):408–20.
52. Chen YJ, Yeh MH, Yu MC, Wei YL, Chen WS, Chen JY, et al. Lapatinib-induced NF-kappaB activation sensitizes triple-negative breast cancer cells to proteasome inhibitors. *Breast Cancer Res*. 2013;15(6):R108.
53. Darvishi B, Farahmand L, Eslami SZ, Majidzadeh AK. NF-kappaB as the main node of resistance to receptor tyrosine kinase inhibitors in triple-negative breast cancer. *Tumour Biol*. 2017;39(6):1010428317706919.
54. Jiang Z, Liu JC, Chung PE, Egan SE, Zacksenhaus E. Targeting HER2(+) breast cancer: the TBK1/IKKepsilon axis. *Oncoscience*. 2014;1(2):180–2.
55. Wang W, Nag SA, Zhang R. Targeting the NFkappaB signaling pathways for breast cancer prevention and therapy. *Curr Med Chem*. 2015;22(2):264–89.
56. Israel A. The IKK complex, a central regulator of NF-kappaB activation. *Cold Spring Harb Perspect Biol*. 2010;2(3):a000158.
57. Rothwarf DM, Karin M. The NF-kappa B activation pathway: a paradigm in information transfer from membrane to nucleus. *Sci STKE*. 1999;1999(5):Re1.

58. Merkhofer EC, Cogswell P, Baldwin AS. Her2 activates NF-kappaB and induces invasion through the canonical pathway involving IKKalpha. *Oncogene*. 2010;29(8):1238–48.
59. Cao Y, Bonizzi G, Seagroves TN, Greten FR, Johnson R, Schmidt EV, et al. IKKalpha provides an essential link between RANK signaling and cyclin D1 expression during mammary gland development. *Cell*. 2001; 107(6):763–75.
60. Zhang L, Teng Y, Zhang Y, Liu J, Xu L, Qu J, et al. C-Src-mediated RANKL-induced breast cancer cell migration by activation of the ERK and Akt pathway. *Oncol Lett*. 2012;3(2):395–400.

Publisher's Note

Springer Nature remains neutral with regard to jurisdictional claims in published maps and institutional affiliations.

Ready to submit your research? Choose BMC and benefit from:

- fast, convenient online submission
- thorough peer review by experienced researchers in your field
- rapid publication on acceptance
- support for research data, including large and complex data types
- gold Open Access which fosters wider collaboration and increased citations
- maximum visibility for your research: over 100M website views per year

At BMC, research is always in progress.

Learn more biomedcentral.com/submissions

